Wind power integration into weak power systems

Abulanwar, El-Saye Mohamed

DOI (link to publication from Publisher):
10.5278/vbn.phd.engsci.00110

Publication date:
2016

Document Version
Publisher's PDF, also known as Version of record

WIND POWER INTEGRATION INTO WEAK POWER SYSTEMS

BY
ELSAYED MOHAMED MOHAMED ABULANWAR

DISSERTATION SUBMITTED 2016

AALBORG UNIVERSITY
DENMARK

WIND POWER INTEGRATION INTO WEAK POWER SYSTEMS

By

Elsayed Mohamed Mohamed Abulanwar

Department of Energy Technology

AALBORG UNIVERSITY
DENMARK

A Dissertation Submitted to

The Faculty of Engineering and Science, Aalborg University

In partial Fulfilment for the Degree of Doctor of Philosophy

January 2016

Aalborg, Denmark

Dissertation submitted: May 2016

PhD supervisor: Professor Zhe Chen
Aalborg University, Denmark

PhD committee: Associate Professor Filipe Miguel Faria Da Silva (chairman)
Aalborg University, Denmark

Professor Anouar Belahcen
Aalto University, Finland

Professor Gareth Taylor
Brunel University London, United Kingdom

PhD Series: Faculty of Engineering and Science, Aalborg University

ISSN (online): 2246-1248
ISBN (online): 978-87-7112-708-9

Published by:
Aalborg University Press
Skjernvej 4A, 2nd floor
DK – 9220 Aalborg Ø
Phone: +45 99407140
aauf@forlag.aau.dk
forlag.aau.dk

Printed in Denmark by Rosendahls, 2016

Mandatory Page

Thesis Title:

Wind Power Integration into Weak Power Systems

Name of PhD Student:

Elsayed Mohamed Mohamed Abulanwar

Name and title of supervisor and any other supervisors

Professor Zhe Chen

Associate Professor Florin Iov

Associate Professor Weihao Hu

List of Publications

Journal papers:

J1. **S. Abulanwar**, W. Hu, Z. Chen and F. Iov "Adaptive voltage control strategy for variable-speed wind turbine connected to a weak network*", IET Renewable Power Generation,* vol. 10, no. 2, pp. 238-249, 2016.

Conference papers:

C1. **S. Abulanwar**, W. Hu, F. Iov and Z. Chen, "Characterization and assessment of voltage and power constraints of DFIG WT connected to a weak network," in Proc. *IEEE PES General Meeting*, Washington, US, 2014, pp. 1-5.

C2. **S. Abulanwar**, Zhe Chen and Birgitte Bak-Jensen, "Study of DFIG wind turbine fault ride-through according to the Danish grid code" in Proc. *IEEE Power & Energy Society General Meeting*, Vancouver, Canada, 2013, pp. 1-5.

C3. **S. Abulanwar**, Zhe Chen and Florin Iov, "Enhanced LVRT control strategy for DFIG based WECS in weak grid", in Proc. *The International Conference on Renewable Energy Research and Applications, ICRERA, Madrid, Spain, 2013, pp. 476 – 481.*

C4. **S. Abulanwar**, Zhe Chen and Florin Iov, "Improved FRT control scheme for DFIG wind turbine connected to a weak grid", in Proc. *IEEE PES Asia-Pacific Power and Energy Engineering Conference (IEEE PES APPEEC), Hong Kong, 2013, pp. 1-6.*

This thesis has been submitted for assessment in partial fulfillment of the PhD degree. The thesis is based on the submitted or published scientific papers which are listed above. Parts of the papers are used directly or indirectly in the extended summary of the thesis. As part of the assessment, co-author statements have been made available to the assessment committee and are also available at the Faculty. The thesis is not in its present form acceptable for open publication but only in limited and closed circulation as copyright may not be ensured.

Acknowledgments

The research work carried out within this dissertation is supported by The Sino- Danish Centre for Education and Research, SDC. I would like to thank them for their financial support.

I would like to thank my supervisor Professor Zhen Chen for his endless support, kindness, valuable suggestions, and encouragement through this PhD course. His fruitful discussions and knowledge contributed markedly in the completeness of this research work. I would like to express my deepest appreciation to my co-supervisors, Associate professor Florin Iov and Associate professor Weihao Hu, for their constructive technical discussions and critical comments which directed me to the right path during my research.

I thank all the staff and colleagues in the Department of Energy Technology for their support and encouragement.

Last but not least, I wish to thank my family especially my wife, Ayat for their love and mental support.

Elsayed Abulanwar

December, 2015

Aalborg-Denmark

Abstract

Wind Farms (WFs) are geographically constructed in remotely located areas with favorable wind speed conditions. The structure of such locations is rather weak with lower short circuit power level due to long feeders' (high impedance) connections. Moreover, significant voltage fluctuations and power quality/stability challenges pose substantial constraints on the efficient integration of wind power into weak networks. Consequently, weak networks connections impose dramatic wind power limitations in terms of grid structure and wind turbine (WT) output power.

This dissertation addresses some of the technical challenges raised by the integration of wind power into weak power systems. The main objective is to investigate the dynamic interactions between the wind power generators and interconnected power systems, pinpoint the constraints and operational limitations and meanwhile propose potential solutions to maximize wind power penetration and improve the dynamic stability of the network.

First of all, this work investigates the characterization and assessment of voltage and power constraints raised by connecting a DFIG WT to a weak network. As a basis of investigation, a simplified system model is utilized and the respective PCC voltage, active and reactive power stability issues are evaluated and identified based on a steady-state study for DFIG WT system.

Secondly, a detailed megawatt-level variable speed wind turbine with partial scale converters connected to a weak network with widely varying parameters, i.e., short circuit capacity ratio SCR and X/R ratio is modeled in MATLAB/SIMULINK environment and investigated. An adaptive voltage control AVC scheme based network parameters and operating point is proposed to continually retain voltage constancy and smoothness at the point of connection POC in order to maximize the wind power penetration. Besides, a proposed reactive power dispatch to handle the reactive power sharing between the DFIG inherent stator reactive power and an oversized grid side converter is presented. The AVC showed pronounced mitigation capability with better damped performance particularly at very weak grid condition compared to traditional PI controllers.

Besides, the dissertation investigates the fault ride through FRT capability of WTs attached to weak networks. The study is firstly applied to stiff networks to realize the technical challenges of the different fault scenarios. A nonlinear feedback controller is proposed for the GSC control to suppress the DC voltage fluctuations and concurrently inject reactive power during contingencies to fulfil the reactive power support requirement.

Afterwards, the FRT of a megawatt-level variable speed wind turbine attached to a weak network is conducted. Owing to the poor dynamic performance of synchronous reference frame phase locked loop PLL under unbalanced utility conditions, two enhanced PLLs are investigated namely, decoupled double synchronous reference frame PLL (DDSRF-PLL) and Dual Second Order Generalized Integrator, DSOGI based Frequency Locked Loop, DSOGI-FLL. Additionally, decoupled double synchronous reference frame current controller is devoted for the GSC controller to counteract current ripples and tackle dc voltage fluctuations during unsymmetrical faults to improve the system performance and help fulfill the grid code requirements.

Danske Abstrakt

Vindmølleparker (WFS) er geografisk konstrueret i fjernt beliggende områder med gunstige betingelser vindhastighed. Strukturen af sådanne steder er temmelig svag med lavere kortslutning strøm på grund af lange foderautomater '(høj impedans) forbindelser. Desuden betydelige spændingsudsving og magt kvalitet / stabilitet udfordringer udgør betydelige begrænsninger i effektiv integration af vindkraft i svage netværk. Derfor svage netværk tilslutninger pålægge dramatiske vindkraft begrænsninger i form af gitter struktur og vindmølle (WT) udgangseffekt. Denne afhandling omhandler nogle af de tekniske udfordringer, som integrationen af vindkraft i svage elsystemer. Hovedformålet er at undersøge de dynamiske interaktioner mellem vindkraft generatorer og sammenkoblede kraftsystemer, lokalisere de begrænsninger og operationelle begrænsninger og i mellemtiden foreslå mulige løsninger for at maksimere vindkraft penetration og forbedre den dynamiske stabilitet af nettet.

Først og fremmest, dette værk undersøger karakterisering og vurdering af spænding og effekt begrænsninger rejst ved at tilslutte en DFIG WT til et svagt netværk. Som grundlag for undersøgelsen, er et forenklet system model udnyttet, og de respektive PCC spænding, er aktive og reaktive effekt stabilitetsproblemer evalueret og identificeret baseret på en steady state-undersøgelse for DFIG WT-systemet.

For det andet er en detaljeret megawatt-plan variabel hastighed vindmølle med partielle skala omformere tilsluttet et svagt netværk med vidt forskellige parametre, dvs. Kortslutningseffekten forhold SCR og X/R-forhold modelleret i MATLAB / SIMULINK miljø og undersøgt. En adaptiv spændingsregulering AVC der er baseret netværksparametre og driftspunkt foreslås til stadighed bevarer spænding konstans og glathed ved tilslutningspunktet POC med henblik på at maksimere vindkraft penetration. Desuden er en foreslået reaktiv effekt afsendelse til at håndtere den reaktive magtdeling mellem DFIG iboende stator reaktive effekt og en overdimensioneret gitter side konverter præsenteret. AVC viste udtalt afbødning kapacitet med bedre dæmpet ydeevne især ved meget svag gitter tilstand i forhold til traditionelle PI controllere.

Desuden afhandlingen undersøger fejlen turen gennem FRT evne WTS knyttet til svage netværk. Undersøgelsen er først anvendt på stive netværk til at realisere de tekniske udfordringer ved de forskellige fejl scenarier. Der foreslås en ikke-lineær feedback-controller til GSC-kontrol til at undertrykke DC spændingsudsving og samtidig tilføre reaktive effekt i løbet af uforudsete at opfylde den reaktive kravet effekt support.

Bagefter FRT en megawatt-plan variabel hastighed vindmølle knyttet til et svagt netværk udført. På grund af den dårlige dynamiske præstationer synkron referenceramme fase låst sløjfe PLL under ubalancerede nytteværdi betingelser, to forbedrede PLL'er undersøges nemlig afkoblet dobbelt synkron referenceramme PLL (DDSRF-PLL) og Dual Second Order Generaliseret Integrator, DSOGI baseret Frekvens Locked Loop, DSOGI-FLL. Derudover er afkoblet dobbelt synkron referenceramme nuværende controller afsat til GSC controller til at modvirke de nuværende krusninger og tackle dc spændingsudsving under usymmetriske fejl for at forbedre systemets ydeevne og hjælpe med at opfylde de netkode krav.

Abbreviations

RES	Renewable Energy Source
WT	Wind Turbine
WF	Wind Farm
WPP	Wind Power Plant
TSO	Transmission System Operator
CPP	Conventional Power Plant
SCC	Short Circuit Capacity
POC	Point of Connection
SCR	Short Circuit Capacity Ratio
GC	Grid Code
WTG	Wind Turbine Generator
LVRT	Low Voltage Ride-Through
WECS	Wind Energy Conversion Systems
FSWT	Fixed Speed Wind Turbines
VSWT	Variable Speed Wind Turbines
IG	Induction Generator
GB	Gear Box
WRIG	Wound Rotor Induction Generator
BPA	Blade Pitch Angle
DFIG	Doubly-Fed Induction Generator

PWM	Pulse Width Modulated
WRSG	Wound Rotor Synchronous Generator
PMSG	Permanent Magnet Synchronous Generator
PF	Power Factor
HVRT	High-Voltage Ride-Through
FRT	Fault Ride-Through
AVC	Adaptive Voltage Control
GSC	Grid Side Converter
RSC	Rotor Side Converter
DDSRF	Decoupled Double Synchronous Reference Frame
PLL	Phase Locked Loop
DG	Distributed Generation
EMT	Electromagnetic Transient
VSC	Voltage-Source Converter
RPC	Reactive Power Compensation
UPF	Unity Power Factor
VC	Voltage Control
CVC	Conventional Voltage Control
MPPT	Maximum Power Point Tracking
DC	Direct Current
DSOGI	Dual Second Order Generalized Integrator
FLL	Frequency Locked Loop

QSG	Quadrature Signal Generator
PIR	Proportional Integral Resonance

Table of Contents

Chapter 1

Introduction

This chapter provides the general background of the thesis, a brief review of the challenges of wind power plants operating in weak grids. The conventional, state-of-the-art of wind turbine configuration and details of modern grid code regulations are discussed. The research objectives, technical contributions and the thesis outline are also provided.

1.1 Background

With 282.5 GW installed capacity in 2012 compared to 94 GW in 2007, wind energy is potentially one of the fastest emerging renewable energy source (RES) worldwide [1]. Motivated by the desire to reduce fossil fuel emissions, policy makers continually implement incentives for increasing investment in wind energy worldwide [2]. By 2020, the total wind power generation is expected to supply about 12% of the gross world electricity demands [3]. According to the goal of the European Union, 20% of the energy should be via renewable sources by 2020. The contribution of renewable energy sources has to be over 30% to meet this target. Due to the limited potential growth of onshore wind farms (WFs) by human activities and sitting spaces, offshore WFs are more favorable because of better wind speed conditions and environmental concerns. A partly from being costly, offshore WFs are usually located at a distance from utilities which requires long feeders [4].

By the end of 2013, China possessed 91.4 GW cumulative capacity fostering its rank in the global wind market [1]. Typically, 95% of the wind energy resources in China are located in northern part, northwest and the eastern coast as demonstrated in Fig. 1.1 [5], [6]. However, about two-thirds of the Chinese electricity demand is concentrated in the middle and eastern territories. Due to the rapid growth of wind energy in the northern areas, the insufficient power grid supporting infrastructure issue is becoming severer. The installed capacity of wind energy in China which is out of grid access exceeded 30% compared to 10% in United States and Europe [5]. As a result, about 10 % of the net generated wind power in China is curtailed as a consequence to the limited transmission capacity to accommodate the harvested wind

power [4]. The latter resulted in $1.6 billion nationwide economic loss in the same year [6]. Additionally, voltage violations to some of the transmission networks have been detected in different territories due to the steady growth of wind power penetration [7].

Denmark has the highest wind power penetration worldwide, where wind power acquires about 40% of the installed generation capacity in Denmark [8]. Denmark looks forward at achieving 50% of the whole power consumption via wind energy by 2020 which is considered the highest compared to other countries [9]. At the end of September 2010, the total installed wind power capacity in Denmark was 3.73 GW, in which 868 MW supplied from offshore wind power plants (WPPs) [3]. The significant wind power penetration in Denmark exemplifies additional burdens on transmission as well as distribution networks. A significant portion of the Danish energy consumption is speculated via offshore WFs in the long-term.

With vast sum of funds invested in wind energy market, EU aims at supplying 14% of Europe's gross electricity demand by 2020 and 33% by 2030 including onshore as well as offshore WFs [10]. A steady growth in the net annual increase in offshore wind capacity is expected from 1.1 GW in 2011 to 6.5 GW in 2020. Europe plans for 40 GW offshore wind power installed capacity by 2020 and 150 GW by 2030 [10] - [12]. Figure 1.2 demonstrates the offshore wind power future development in the North Sea.

However, the integration of such significant wind power into power systems presents a major challenge to transmission system operators (TSOs). Thereby, operation of wind power into weak networks is seen as an expected operating scenario in the near future in Denmark and EU.

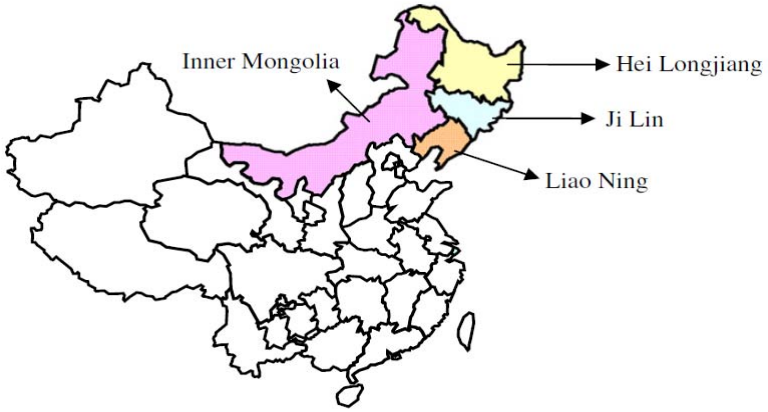

Figure 1.1 Main territories of wind energy resources in China.

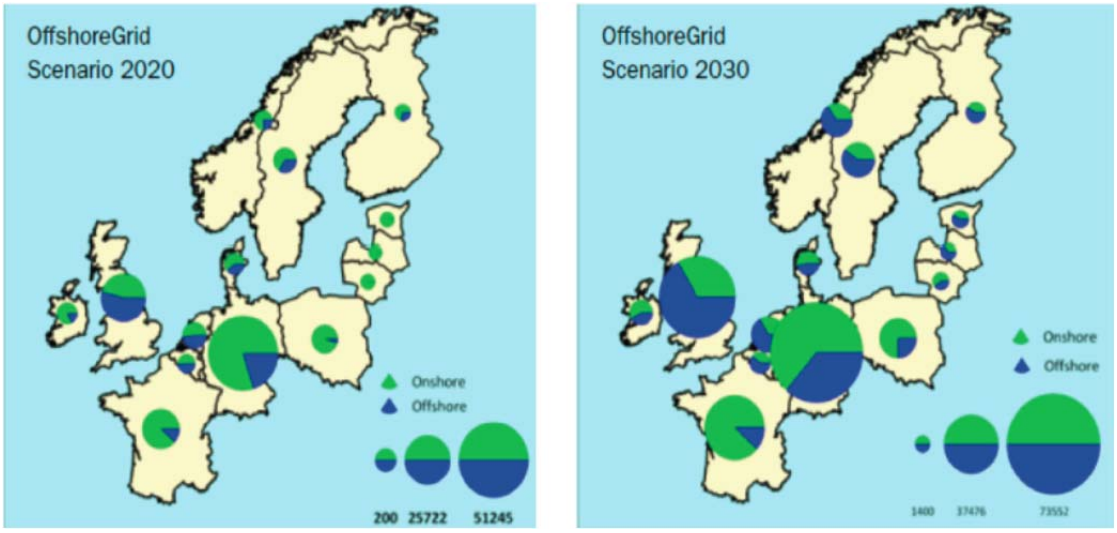

Figure 1.2 Offshore and onshore wind farm installations in Northern Europe in 2020 and 2030 [11].

1.2 Characteristics of Weak Grids

Owing to the rapid replacement of conventional power plants (CPPs) with renewable resources, power systems are becoming weak. Grid strength at a certain bus is usually represented by its short circuit capacity (SCC) which depends on the current flowing at this bus due to a solid fault. For a certain grid represented by its Thevenin equivalent seen from a bus as seen in Fig. 1.3, the SCC at the point of connection POC is calculated as below:

$$SCC=\frac{V_g^2}{Z_g} \tag{1.1}$$

Hence, the lower the Thevenin equivalent impedance, the stronger the grid is.

One of the key indicators of a weak grid is the short circuit capacity ratio (SCR). The SCR is the ratio between the point of connection (POC) short circuit capacity SCC to the maximum apparent power of the wind generator S_{WG}:

$$SCR=\frac{SCC}{S_{WG}} \tag{1.2}$$

According to the definition in [13], the strength of an ac system can be classified according to the SCR as:

- Strong system, if the ac system SCR is greater than 3.0.
- Weak system, if the ac system SCR is between 2.0 and 3.0.
- Very weak system, if the ac system SCR is lower than 2.0.

In the literature, SCR of 10 is perceived as a boundary below which the attached network is weak. In The German grid code [14], the related transmission system operators TSOs require a stiff network minimum SCR of 6 for the connection of the WPP. In the Danish grid code, an SCR of 10 is requested during system studies for WPPs [9]. However, the system SCR can vary widely depending on the system structure especially with the increasing installations of renewable resources which may result in very weak grid connections, i.e., SCR below 2.

Table 1.1 lists typical WPP projects in Australia with very weak grid connections [15].

Table 1.1

WPP	**Rating, MW**	**SCR**
Mussellroe	168	1.74
Collgar	250	2.56
Silverton (stage 1)	300	1.24

Virtually, a weak network can be also due to different reasons such as:

- A network with low SCC due to high impedance lines, and/or not connected to other strong neighboring networks.
- Due to significant replacement of conventional power plants CPPs with renewable sources, it follows that SCC gets lower at all system buses.
- The long distance connections of the remotely located WPPs which are typically found in areas with favorable wind speed conditions.

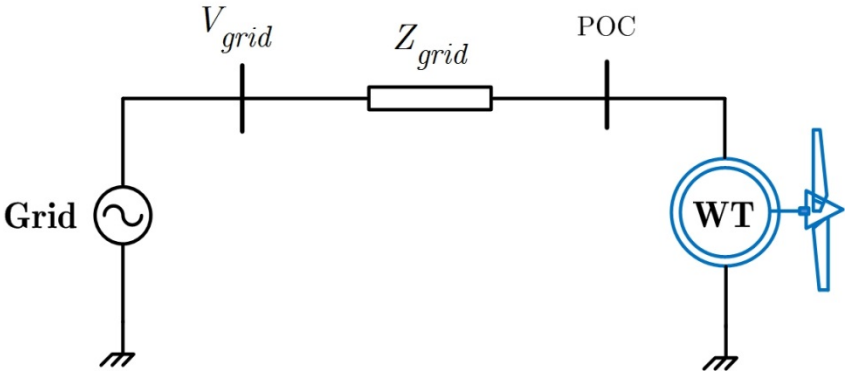

Figure 1.3 equivalent circuit of a WT connected to a weak grid.

1.3 Weak Grid Challenges

Weak grid connections can represent serious technical issues to WPP operational scenario. The following section provides a description to the likely challenges cause by weak grid connection and its impacts on WPPs operation.

1.3.1 Steady-state Issues

As Wind Farms (WFs) are geographically constructed in remotely located areas with favorable wind speed conditions as the case of offshore WPPs. The structure of such locations is rather weak with lower fault level due to long feeders' (high impedance) connections. Moreover, significant voltage fluctuations and power quality/stability challenges pose substantial constraints on the efficient integration of wind power into weak networks. On the other hand, even relatively strong networks might also encounter markedly grid impedance change owing to load variations and/or lines tripping [5].

One of the main challenges provoked by weak grid connections is voltage stability caused by the active and/or reactive power injection to/from the grid-connected WPP. As a consequence to the high ac system impedance, a weak network is liable to remarkable voltage deviations as a result of active and/or reactive power changes, worsening the point of connection (POC) voltage quality. Such POC voltage deviations are highly undesirable and can be harmful for power converters and adversely impact the quality of power supply. In addition, voltage fluctuations

provoke flicker emissions which represent a serious drawback impacting power quality and restrict the captured wind power [16]-[19].

Wind power curtailment is crucial to address the POC voltage fluctuations and maintain the system stability. Despite, active power curtailment can sustain normal operations, significant power loss is consequent. Besides, the reactive power capability of the WPP is also affected due to the change of the system voltage operating range during continuous operation. Several serious concerns regarding voltage, frequency and system stability manifested recently due to connecting WPPs to weak networks which irritated the proliferation of wind power [1].

Furthermore, wind power vagaries due to wind speed variations and 3p oscillations resulting from tower shadow and wind shear effects exacerbate voltage perturbations and power quality as well [6], [7].

1.3.2 Dynamic Issues

According the modern grid codes (GCs) commitments, WPPs must participate in reactive power support during a fault in order to retrieve the system voltage. As weak grid connection can dramatically affect the reactive power capacity of WPPs, the inability of power system to handle the necessary reactive power during faults may result in tripping of WPPs owing to transient overvoltage during recovery period.

Being highly distorted, accurate tracking of the system voltage angle becomes difficult due to fast and large voltage angle shifts which may result in instability of wind turbine generator (WTG) fast current control loops [15]. Consequently, retriggering of WTG low voltage ride through (LVRT) controller may incur reactive power swings and voltage instability if the WTG level and WPP controllers are not coordinated. Such coordination can be challenging because of significant voltage difference between the WPP and the POC.

Generally speaking, recent grid codes take into account only strong networks in their regulations. Therefore, for weak or even very weak grid connections, some technical regulations might be difficult to be fulfilled. For instance, enabling the WPP to operate at 0.93 leading/lagging power factor entails exceeding the normal system voltage range, $\pm 10\%$. Furthermore, achieving the rewarded PQ ramp rates might not be as fast as in a stiff network unless exceeding the voltage range, damping or setting

time of the respective grid code regulation [15]. Also, retrieving WPP active power production to pre-fault condition too fast can produce transient overvoltage which can cause retriggering LVRT and thus tripping the WPP.

Consequently, weak networks connections impose dramatic wind power limitations in terms of grid structure and wind turbine WT output power [18]-[20].

1.4 Wind Turbine Technology Development

Wind turbines have evolved significantly through the last decades due to the continuous efforts to improve the efficiency of the wind energy conversion systems (WECS). Wind turbines can be classified into two main groups, fixed speed wind turbines FSWTs (type A) and variable speed wind turbines VSWTs (type B,C and D) which predominate the today's wind global market. These types are based on horizontal axis, three-bladed upwind structure which differs in generator type and its respective control systems. These four types are explained below.

1.4.1 Type A: Fixed Speed Wind Turbine (FSWT)

This type is also known as the Danish concept which has been introduced in the early 1990. As the name suggests, FSWT operates at a constant rotor speed. As seen in Fig. 1.4, FSWT is comprised of a fixed speed induction (asynchronous) generator (IG) with its rotor coupled with the low speed WT through a fixed ratio gear box (GB) while its stator is directly coupled to the main grid via a step-up transformer. A soft electronic starter is usually included to render soft starting during grid connection. Despite the fact that this type is simple and robust structure with relatively low cost, it produces fluctuating output power as the wind speed variates due to operating at constant speed [21]. Besides, the maximum wind energy conversion efficiency can be only attained at a typical wind speed. Furthermore, a shunt capacitor bank is usually installed at its terminals as IG cannot control reactive power.

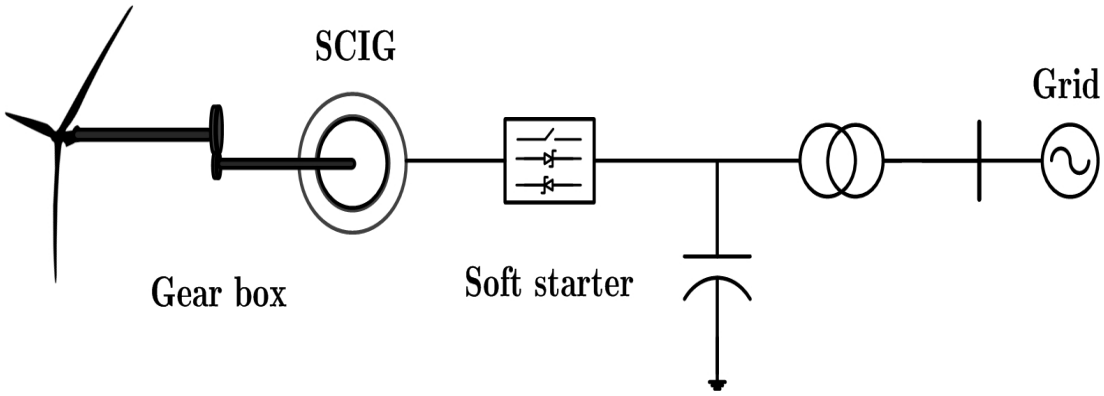

Figure 1.4 Configuration of FSWT (type A).

1.4.2 Type B: Limited Variable Speed Wind Turbine

In this type of WTs, a wound rotor induction generator (WRIG) directly coupled to the grid is existed. The configuration of this type is demonstrated in Fig. 1.5. Similar to type A, a soft starter, shunt capacitor and gear box are augmented and perform the same role. Compared to type A, a power electronic controlled variable resistor equipped with the rotor allows for slip control and therefor the generator can achieve 10% speed variation during wind gusts. Moreover, the construction of this type of WTs makes it aerodynamically more efficient with better power quality and lower mechanical drive-train stresses compared to type A. Also, this type of WTs usually employs an active blade pitch angle (BPA) control system.

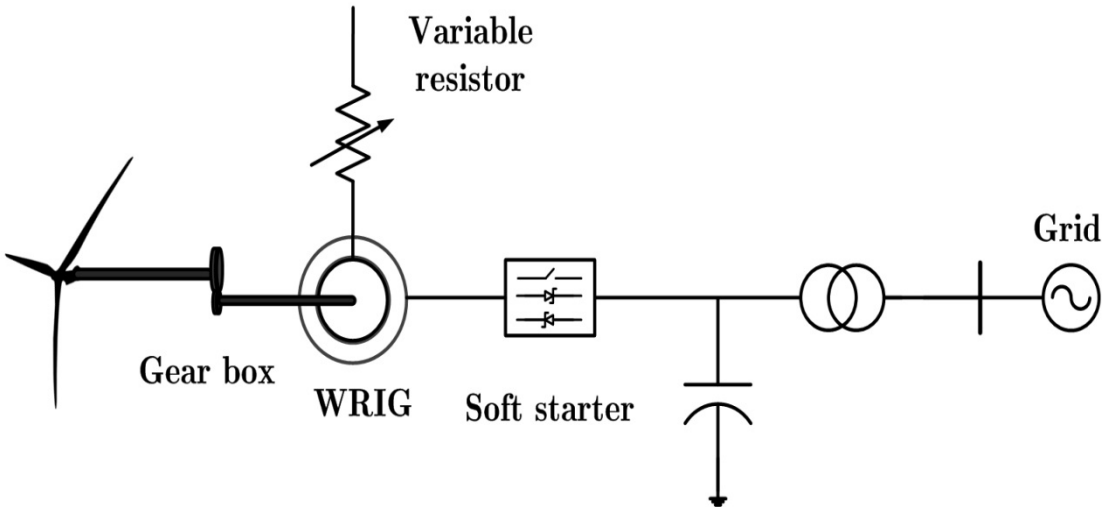

Figure 1.5 Configuration of limited variable speed wind turbine (type B).

1.4.3 Type C: VSWT with Double-Fed Induction Generator

The configuration of type C wind generator is illustrated in Fig. 1.6. In the doubly-fed induction generator (DFIG) pitch-controlled WT, the stator is directly connected to the grid whereas, the rotor side is connected to the grid via two two-level partial scale pulse width modulated (PWM) converters. Typically, the partial scale converters are rated at 25-30% of the generator rating. Using partial scale converters, DFIG WTs still dominate the global market as it acquires 50% of the current installed WPPs [22].

The main advantages of such wind generator are known as variable speed operation, smooth startup, small power fluctuations especially above rated wind speed and possibility for dynamic reactive power support during contingencies.

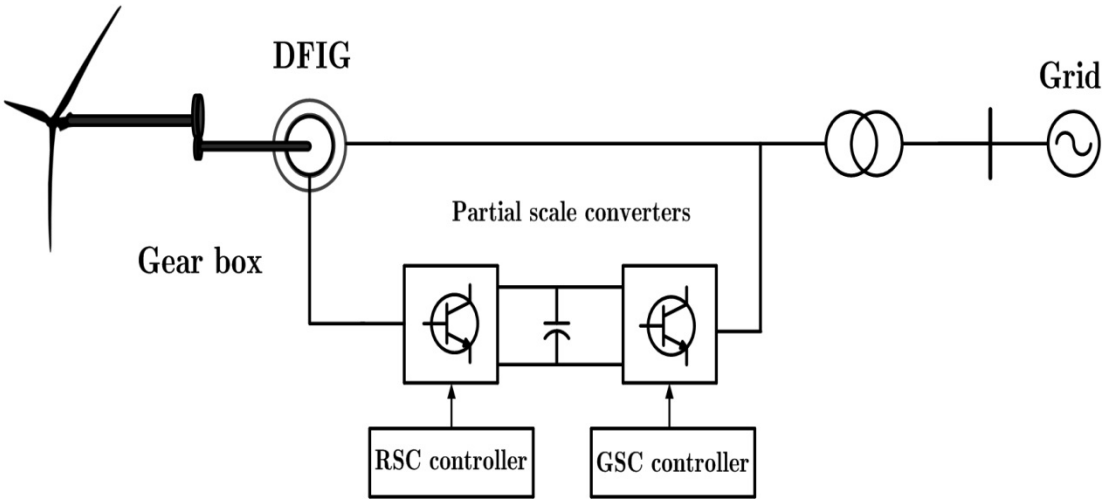

Figure 1.6 Configuration of DFIG-based wind turbine (type C).

1.4.4 Type D: VSWT with Full Power Converter

Figure 1.7 depicts the configuration of this concept. Typically, several generators can be utilized with this type such as wound rotor synchronous generator WRSG and permanent magnet synchronous generator (PMSG). In this configuration, gear box can be dispensed if a low speed multi-pole synchronous generator is used. The WTG is fully decoupled from the grid with virtue of two full scale power converters which ensures full range of variable speed operation, better controllability and dynamic grid support capability during emergencies. Due to its advantages, PMSG based WT is also widely used in the global market of wind power. However,

its cost is higher than that of DFIG based WTs due to the full scale converters which have the same rating as the generator.

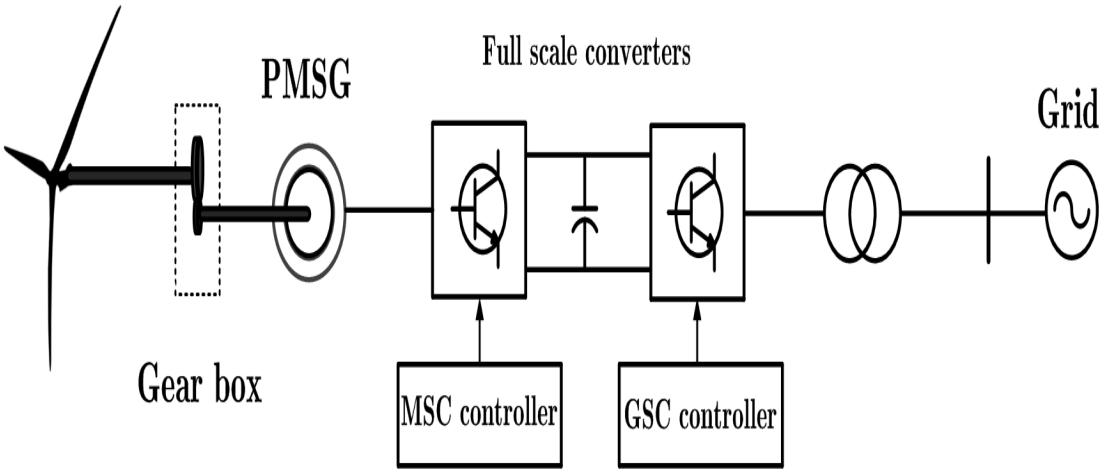

Figure 1.7 Configuration of PMSG-based wind turbine (type D).

Thanks to their power converters, VSWTs can readily control independently output active and reactive powers compared to FSWTs. Therefore, wind generator types C and D can potentially comply with the stringent grid code regulations with respect to reactive power control, active power curtailment and contribute to power system stability. However, the transient response under disturbances for these types is challenging and needs proper control strategies as will be handled later.

1.5 Grid Codes Requirements

Grid codes regulations are introduced by transmission system operators TSOs in order to outline the operational responsibilities of the generating units of the respective transmission/distribution networks [27]. In the past, as the share of the RES compared to CPPs was negligible, grid codes didn't stipulate regulations for WPPs. Yet, with the significant increase of wind power penetration in many countries, the situation has dramatically changed. Several serious concerns have been raised recently regarding the adverse impacts of wind energy as stochastic and intermittent power source. To maintain the system stability and reliability, TSOs stipulated stringent technical regulations on WPPs that are connected to the power system. According to the grid codes, WPPs not only have to withstand grid excursions but also provide

ancillary service regarding reactive power support as traditional generators to recover the ac voltage. Different international grid codes exist in many countries which differ according to the wind power penetration level, robustness of the power system and local utility practices [27]. Despite the technical differences between the various grid codes, common requirements exist among these grid codes which are:

- Low voltage ride-through LVRT
- Dynamic reactive power support
- Active power control
- Reactive power control
- Voltage and frequency operating ranges

Being one of the countries that has significant wind power share, the transmission system operators (Energinet.dk) in Denmark has introduced the Danish grid code which is a set of requirements that WPP has to satisfy in order to remain connected to the power system [9]. WPPs must be capable of constantly operating at a specific range of inductive/capacitive power factor in order to provide voltage regulation during normal operation. Figure 1.8 shows the reactive power regulations enforced by different grid codes. The Danish grid code requires a WPP with power output range of 1.5 MW to 25 MW to operate with a capacitive/inductive power factor PF of 0.975 when active power production represents more than 20% of nominal power. This operating range of reactive power/power factor relies on the SCC and configuration of the power system. Furthermore, WPP should be designed in such a way that the operating point lies somewhere within the hatched area.

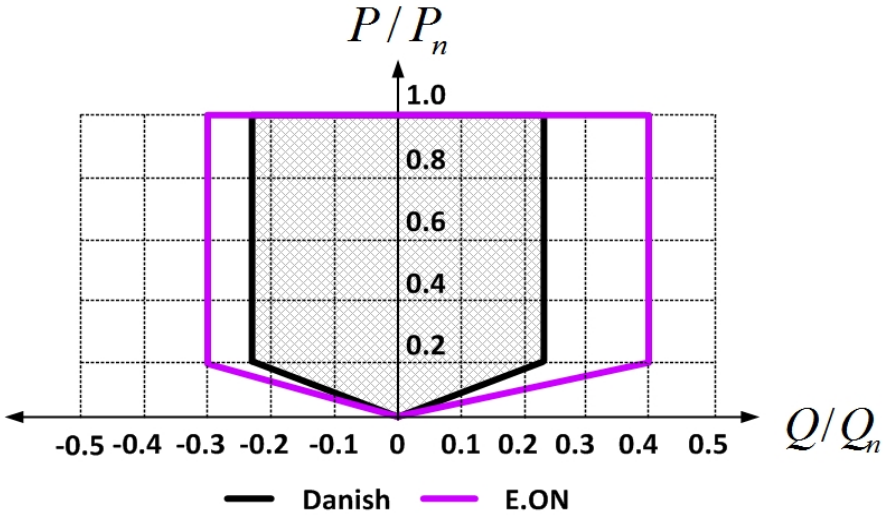

Figure 1.8 Reactive power requirements of different grid codes [9], [28].

Modern grid codes request WPPs to continue their uninterrupted supply under different fault scenarios based on a prescribed voltage–time profile. Such regulations are usually known as low voltage ride-through LVRT.

Figure 1.9-a shows the LVRT requirement imposed by the Danish grid code on the WPPs connected to the transmission system [9]. As seen, it implies three operational modes; (1) The WPP must remain connected to the power system in area A and uphold normal production without reactive power support if the system voltage higher than 0.9 p.u. (2) The WPP should not only remain connected to the power system in area B but also provides reactive power support to the grid as demanded in Fig. 1.9-b to help stabilize the voltage with full reactive current injection in the area B′. However, the free current capacity must also be dedicated to pursue active power production in proportion to the voltage dip magnitude as recommended by Danish and British grid codes which will be discussed later. (3) The disconnection of the WPP is allowed in area C. On the other hand, the Danish grid code has stipulated another requirement for high voltage operation known as high voltage ride-through, HVRT as depicted in Fig. 1.9-c. Such operating condition may arise due to disconnecting large load or a grid fault [27].

Fig. 1.10-a depicts the German E.ON, Scottish and Irish grid code low voltage ride-through, LVRT commitment which implies that the WTs, must remain connected if the terminal voltage within the shaded area [29]. As seen in Fig. 1.10-a, E.ON LVRT is onerous as it requests fault ride-through, FRT, capability for different faults accompanied with zero voltage dips for 150 ms duration. Irish grid code requires FRT against faults with remnant voltage of 0.15 p.u for more than 500 ms. Fig.1.10-b illustrates the Spanish and German reactive power support obligation. Typically, no reactive power support is demanded for voltage dips with remnant voltage of 0.9 p.u. Nevertheless, maximum reactive current support is required for voltage dips below 0.5 p.u.

In the European Network for Transmission System Operators for Electricity (ENTSO-E) grid code, it is implied that FRT response during asymmetrical faults and reactive power support is to be set by agreement between TSOs and WPP operators [14]. However, compared to symmetrical faults with only 5% occurrence, asymmetrical faults are reported more frequently occurring in transmission systems

with single line-to-ground faults 70%, line-to-line faults 15%, double line-to-ground faults 10% [30].

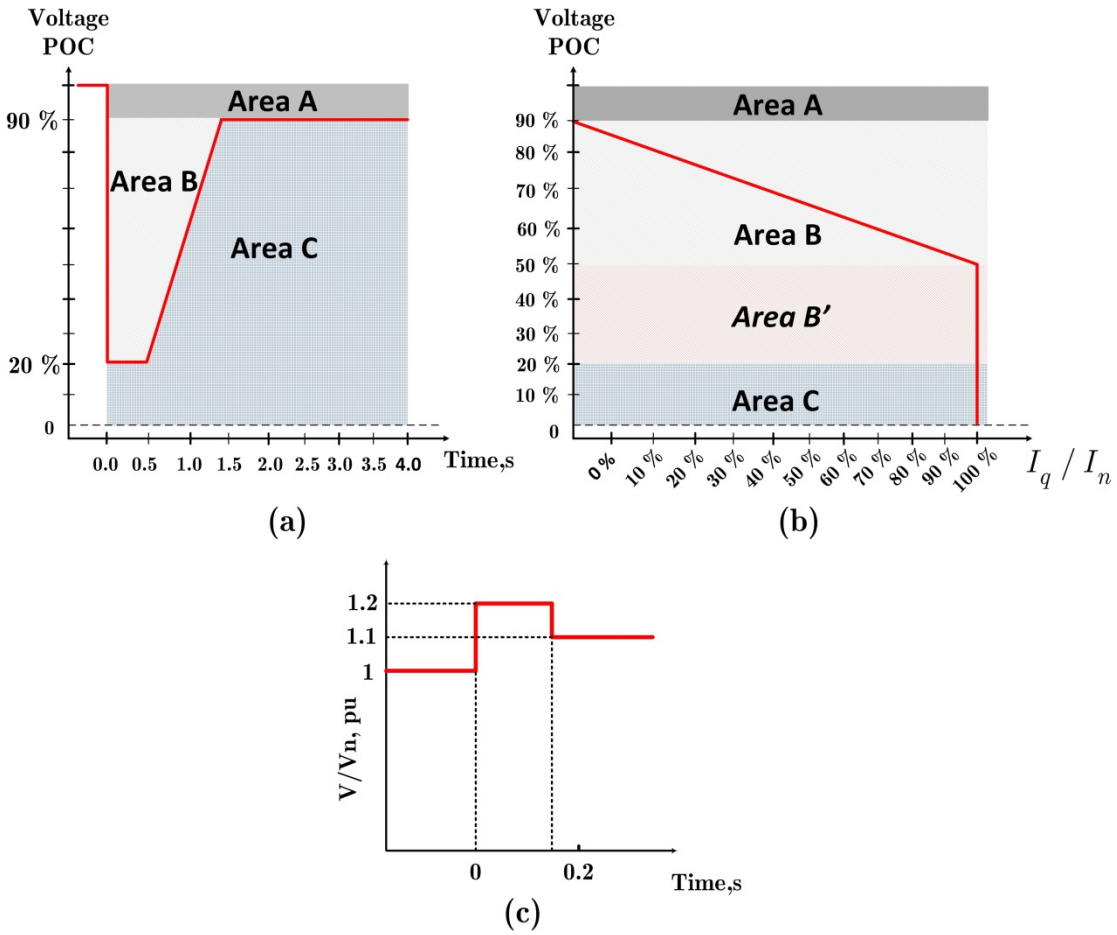

Figure 1.9 Danish grid code requirements: (a) LVRT, (b) Reactive power support criterion, (c) HVRT.

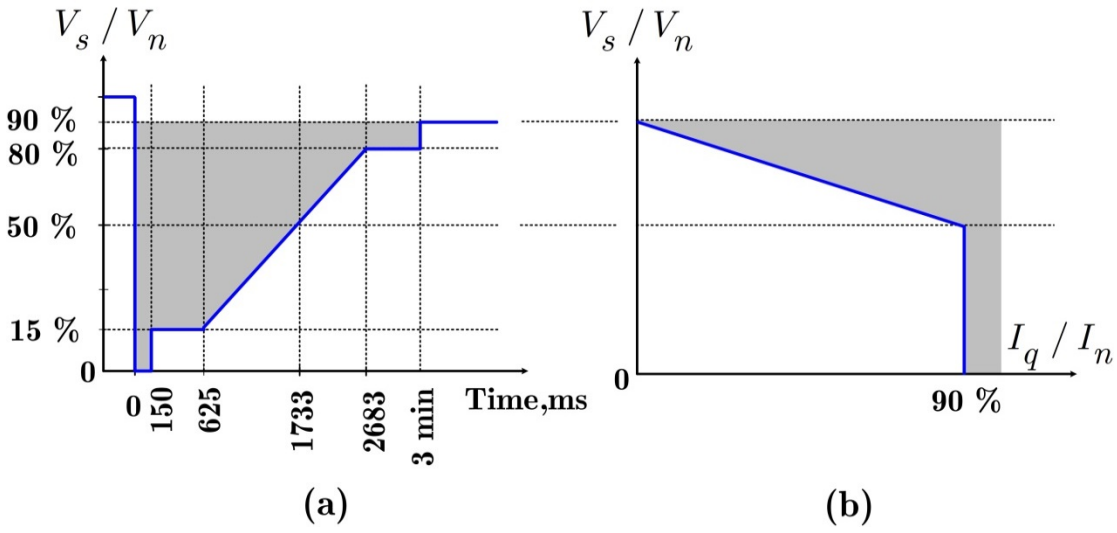

Figure 1.10 Typical WT Grid code requirements: (a) LVRT, (b) Reactive power Support.

1.6 Research Objective

This three-year PhD research project "wind power integration into weak power systems" was initiated by Department of Energy Technology at Aalborg University in collaboration with the Sino-Danish Center for Education and Research, SDC.

First of all, this dissertation investigates the characterization and assessment of voltage and power constraints raised by connecting a DFIG WT to a weak network. a detailed model of a megawatt-level DFIG WT connected to a weak network with widely varying parameters, i.e., short circuit capacity ratio SCR and X/R ratio is modeled in MATLAB/SIMULINK environment and investigated. An adaptive voltage control AVC scheme based network parameters and operating point is proposed to continually retain voltage constancy and smoothness at the point of connection POC in order to maximize the wind power penetration. Besides, the dissertation investigates the fault ride through FRT capability of WTs attached to weak networks. The study is firstly applied to stiff networks to realize the technical challenges of the different fault scenarios.

Specifically, the objectives of this research study are as follows:

1) To develop models to study the characterization of wind power connected to weak power systems.
2) To propose control methods for the purpose of continually improving of POC voltage in case of very weak conditions and variable wind speed.
3) To develop a dispatch strategy to handle the reactive power absorption/release between the DFIG WT and the host power system under widely varying system parameters.
4) To analyze the FRT behavior of WTs connected to stiff as well as weak networks and explore the compliance with the grid codes requirements.
5) To improve the performance of WTs operating in weak systems via proposing control systems.

1.7 Technical Contribution of the Thesis

The main technical contribution of the thesis is summarized as follows:

1) A simplified model is conducted to study the technical constraints raised by connecting a DFIG WT to a weak network. Besides, the respective POC voltage, active and reactive power stability issues are evaluated and identified based on the studied system.
2) A proposed AVC scheme reliant on network parameters to continually mitigate POC voltage variations for very weak networks with widely varying SCR as well as X/R ratios under different operating conditions.
3) A proposed reactive power dispatch strategy to manage the reactive power exchange between the wind generator WG and the host power system is presented and validated.
4) The overall system stability is investigated using AVC via identifying the safe operating regions for a wide range of system parameters.
5) The FRT of a DFIG WT connected to stiff and weak systems is studied and control techniques are proposed to ensure the compliance of the grid codes.

1.8 Outline of the Thesis

This PhD dissertation is divided into six chapters and appendixes. It is organized as follows:

Chapter 1 Introduction

This chapter gives the background and main objective of this thesis. Besides, presents an overview of the expansion of wind energy in the global market and the recent challenges and technical issues which are related to the integration of wind power into weak power systems. Also the technical contributions in the project are discussed.

Chapter 2 Assessment of Technical Constraints of DFIG Connected To a Weak Network

This chapter investigates the diverse technical challenges experienced by integrating a DFIG WT into a weak grid of widely changing parameters. Firstly, a simplified model is utilized to develop the assessment criterion to evaluate the impact of the active and reactive power feed-in on the POC voltage under different conditions. The active and reactive power limitations according to the capability limits of the WTG is also considered. Moreover, the impact of the POC voltage deviation on the in-feed active/reactive power and the power factor of the system is presented.

Chapter 3 Adaptive Voltage Control Strategy for VSWT Connected to a Weak Network

In this chapter, an adaptive voltage control (AVC) strategy is proposed to retain voltage constancy and smoothness at the point of connection (POC) in order to maximize the wind power penetration into weak networks. A proposed reactive power dispatch strategy to manage the reactive power flow from/to the wind generator WG is presented. Intensive simulation case studies under different network topology and wind speed ranges reveal the effectiveness of the AVC scheme to effectively suppress the POC voltage variations particularly at very weak grid conditions during normal operation.

Chapter 4 Fault Ride-Through FRT Response for DFIG WT Connected to a Stiff Network

This chapter presents a new decentralized control strategy for a Doubly-fed Induction generator wind turbine, DFIG WT connected to a stiff network considering the Danish grid code requirements. A nonlinear controller is adopted for the grid side converter, GSC, to ensure decoupled control of the DC link voltage and the reactive power, and counteract the DC link voltage run-away. Moreover, the GSC is dedicated to inject reactive power during voltage dips to satisfy the grid code reactive power support obligation. A conventional PI controller is devoted to control the rotor side converter, RSC, with additional compensation terms to reduce the rotor over-speed,

and limit the rotor and stator large transient currents. The simulation results assure the FRT capability of the proposed control strategy in compliance with the Danish grid code without additional hardware circuits.

Chapter 5 Fault Ride-Through FRT Response for DFIG WT Connected to a Weak Network

An enhanced coordinated low voltage ride-through, LVRT, control strategy for a Doubly-fed Induction generator (DFIG)-based wind energy conversion system, WECS, connected to a weak grid is presented in this chapter. The compliance with the grid code commitments is also considered. A proposed decoupled double synchronous reference frame (DDSRF) current controller is adopted for the design of grid side converter, GSC, controller to counteract current oscillations during asymmetrical faults and tackle the DC link voltage run-away. For a precise detection of the grid voltage position even under severe voltage dips/unbalanced conditions, A DDSRF-PLL is proposed and analyzed to extract clean synchronization signal in order to improve the overall system performance. Moreover, a fast decomposition based positive and negative sequence algorithm is utilized for rapid fault detection and to engage the LVRT protection scheme. Furthermore, additional compensation terms are incorporated with the traditional GSC and rotor side converter, RSC, controllers to effectively suppress rotor as well as stator currents and meanwhile regulate the rotor speed.

Chapter 6 Conclusions and Future Work

This chapter presents the main findings and conclusions of this thesis and also the topics for future work.

List of publications

The scientific articles published during the course of this dissertation are listed.

Appendix

Additional and detailed derivation of modeling equations and parameters are listed in the appendix section.

Bibliography

[1] S. Lo, and C. Wu, “Evaluating the performance of wind farms in China: An empirical review” Electrical Power and Energy Systems., vol. 69, no. 1, pp. 58–66, July. 2015.

[2] T. Ejdemo, and P. Söderholm, “Wind power, regional development and benefit-sharing: The case of Northern Sweden” Ren. Sus. Energy Rev., vol. 47, no. 7, pp. 476-485, July. 2015.

[3] W. Hu., “Operation of modern distribution power systems in competitive electricity markets” PhD thesis, Aalborg University, Denmark, Sep., 2012.

[4] G. Mokryani, P. Siano, A. Piccolo and Z. Chen, “Improving fault ride-through capability of variable speed wind turbines in distribution networks”, IEEE Sys. Journal., vol. 7, no. 4, pp. 713-722, Dec. 2013

[5] Z. Zhao, H. Yan, J. Zuo, Y. Tian, and G. Zillante, “A critical review of factors affecting the wind power generation industry in China” Ren. Sus. Energy Rev., vol. 19, no. 7, pp. 499-508, Mar. 2013.

[6] X. Chen, et.al., “Increasing the flexibility of combined heat and power for wind power integration in china: modeling and implications” IEEE Trans. Power Syst. vol. 30, no. 4, pp. 1848–1857, July. 2015.

[7] Z. Zhao, H. Yan, J. Zuo, Y. Tian, and G. Zillante, “A critical review of factors affecting the wind power generation industry in China” Ren. Sus. Energy Rev., vol. 19, no. 7, pp. 499-508, Mar. 2013.

[8] Denmark’s Energy Strategy 2050 - from coal, oil and gas to green energy, the Danish Government, February 2011.

[9] Strategy Plan Energinet.dk, 2012, [Online]. Available: http://www.energinet.dk/SiteCollectionDocuments/Engelske%20dokumenter/Om%20os/Strategy%20Plan%202012.pdf

[10] European Wind Energy Association, “EU energy policy to 2050,” March 2011. [online]. Available: http://www.ewea.org, accessed in July, 2015.

[11] European Wind Energy Association, "OffshoreGrid: offshore electricity infrastructure in Europe," August 2015. [online]. Available: http://www.ewea.org, accessed in August, 2015.

[12] European Wind Energy Association, "Pure Power – wind energy targets for 2020 and 2030, 2009 update" August 2015. [online]. Available: http://www.ewea.org, accessed in August, 2015.

[13] "IEEE guide for planning DC links terminating at AC locations having low short circuit capacities," IEEE Std. 1204-1997, Tech. Rep., 1997.

[14] Ö. Göksu., "Control of wind turbines during symmetrical and asymmetrical grid faults" PhD thesis, Aalborg University, Denmark, Dec., 2012.

[15] P. kjaer, M. Gupta, A. Martinez and S. Saylors, "Experiences with wind power plants with low SCR: Lessons learned from the analysis, design and connection of wind power plants to weak electrical grids," in proc 2015 IEEE Power and Energy Society General Meeting, Denver, July 2015.

[16] T. Ejdemo, and P. Söderholm, "Wind power, regional development and benefit-sharing: The case of Northern Sweden" Ren. Sus. Energy Rev., vol. 47, no. 7, pp. 476-485, July. 2015.

[17] W. Hu, Z. Chen, Y. Wang, and Z. Wang, "Flicker mitigation by active power control of variable-speed wind turbines with full-scale back-to-back power converters," IEEE Trans. Energy Convers., vol. 24, no. 3, pp. 640–649, Sep. 2009.

[18] M. Ammar, and G. Joos, "Impact of distributed wind generators reactive power behavior on flicker severity," IEEE Trans. Energy Convers., vol. 28, no. 2, pp. 425–433, June. 2013.

[19] Y. Zhang, W. Hu, Z. Chen, M. Cheng and Y. Hu, "Flicker mitigation strategy for a doubly fed induction generator by torque control", IET Renewable Power Generation, vol. 8, no. 2, pp. 91-99, Mar. 2014.

[20] N. P. W. Strachan, and D. Jovcic, "Stability of a variable-speed permanent magnet wind generator with weak AC grids", IEEE Trans. Power Del., vol. 25, no. 4, pp. 2779-2788, Oct. 2010.

[21] T. Ackermann (Editor), *Wind Power in Power Systems (First Edition)*. John Wiley & Sons, Ltd, 2005.

[22] S. Abulanwar, Zhe Chen and Birgitte Bak-Jensen, "Study of DFIG Wind Turbine Fault Ride-Through According to The Danish Grid Code" in Proc. IEEE Power & Energy Society General Meeting, Vancouver, Canada, 2013.

[23] M. Mohseni and S. M. Islam, "Transient Control of DFIG-Based Wind Power Plants in Compliance With the Australian Grid Code", IEEE Trans. Power Electron., vol. 27, no. 6, pp. 2813-2824, Jun. 2012.

[24] C. Wessels, F. Gebhardt, and F. W. Fuchs, "Fault ride-through of a DFIG wind turbine using a dynamic voltage restorer during symmetrical and asymmetrical grid faults", IEEE Trans. Power Electron., vol. 26, no. 3, pp. 807-815, Mar. 2011.

[25] L. Yang, Z. Xu, J. Østergaard, Z. Y. Dong, and K. P. Wong, "Advanced control strategy of DFIG wind turbines for power system fault ride through", IEEE Trans. Power Syst., vol. 27, no. 2, pp. 713-722, Jul. 2012.

[26] A. E. Leon, J. M. Mauricio, and J. A. Solsona, "Fault ride-through enhancement of DFIG-based wind generation considering unbalanced and distorted conditions", IEEE Trans. Energy Convers., vol. 27, no. 3, pp. 775-783, Sept. 2012.

[27] M. Mohseni and S. M. Islam, "Review of international grid codes for wind power integration: diversity, technology and a case for global standard", Ren. Sustain. Energy Rev., vol. 16, no. 6, pp. 3876-3890, Aug. 2012.

[28] H. Liu., "Grid integration of offshore wind farms via VSC-HVDC – dynamic stability study" PhD thesis, Aalborg University, Denmark, 2014.

[29] S. Abulanwar, Zhe Chen and Florin Iov, "Enhanced LVRT Control Strategy for DFIG Based WECS in Weak Grid", in Proc. The International Conference on Renewable Energy Research and Applications, ICRERA 2013, Madrid, Spain, 2013.

[30] P. M. Anderson, "Analysis of Faulted Power Systems", IEEE Press, 1995.

Chapter 2

Assessment of Technical Constraints of DFIG Connected To a Weak Network

This chapter is dedicated to investigate the diverse technical challenges experienced by integrating a DFIG WT into a weak grid of widely changing parameters. First of all, a simplified model is utilized to develop the assessment criterion to evaluate the impact of the active and reactive power feed-in on the POC voltage under different conditions. The active and reactive power limitations according to the capability limits of the DFIG WT is also considered. Moreover, the impact of the PCC voltage deviation on the in-feed active and reactive power and also on the power factor of the system is presented. Finally, simulations investigations to verify the obtained results at different network strength are carried out.

2.1 Introduction

Distributed generation (DG) has a limited impact on local bus voltage and therefore power quality/stability in case of strong (low impedance) networks at the point of connection POC. In the literature, it has been found that the grid short circuit capacity ratio SCR and the X/R ratio have a great influence on the operation of WPPs connected to weak power systems. Wind farms, WFs, are geographically suited in areas with rich wind resources which is typically distant from the main grid [1]. The infrastructure of such remote areas is rather weak which poses serious constraints on the effective utilization of the available wind energy [2].

Despite the fact that weak ac networks can cause power quality/stability issues, this phenomenon has been challenging to studies over the last decades [3]. Detailed electromagnetic transient (EMT) simulations environments have been employed for the study of the inherent interactions between modern WPPs and the host power system. As such software tools only support time-domain trial and error simulations, insufficient qualitative conclusions are obtained for these multidimensional systems.

Though analytical models and the application of stability analysis criteria, is extensively reported in recent decades in various electrical power engineering fields,

the stability and control analytical studies applied to modern WPPs are not widely reported yet. The use of stability analysis approaches such as eigenvalues or frequency domain analytical techniques for modern WECS operated in weak networks provides insights into the latent system dynamics and its stability features [3]. However, such analytical models especially for complex nonlinear systems require detailed mathematical analysis. Besides, the accuracy of the resulting models is accurate only around steady-state operating points and EMT verification is always essential.

The purpose of this chapter is to thoroughly investigate the challenges and constraints raised by the integration of WPPs into an ac network of extensively varying parameters and very weak conditions. Therefore, a simplified model is utilized to develop the assessment criterion to evaluate the impact of the in-feed active and reactive power on the POC voltage under different conditions. The active and reactive power limitations according to the capability limits of the WTG is also considered. Moreover, the impact of the POC voltage deviation on the in-feed active and reactive power and also on the power factor of the system is presented. The methodology adopted here can be also applied to other wind generator system. Finally, simulations investigations to verify the obtained results at different network strength are carried out.

2.2 System Description

Figure 2.1 illustrates a typical representation of a wind generator of type C (DFIG WT) installation. The system comprises a 2 MW variable speed DFIG WT. The WT represented with the rotor as a two mass model is operated according to the well-known maximum power point tracking (MPPT) to extract the maximum available power at each wind speed below the rated value and holds a constant power over the rated wind speed [4]. The DFIG rotor speed is controlled via a blade pitch angle BPA controller in order to limit the WT rotational speed above rated wind speed. The DFIG is connected to the ac system through two two-level PWM back-to-back voltage-source converters (VSC) namely, RSC and GSC and a coupling transformer.

For sake of simplicity, the Thevenin equivalent circuit of the detailed system

of Fig 2.1 is used to represent the electrical network. This simplified system depicted in Fig. 2.2 is devoted to provide an insight into the different impacts posed by integrating a DFIG WT to a weak network, i.e., voltage-quality and active and reactive power constraints.

The system comprises a DFIG WT connected at the POC to the host "stiff" power system with constant voltage, V_n. The WG is modeled as a controllable current source with active and reactive power control. The equivalent impedance of the connection line and the coupling transformer is denoted by Z_{eq}. Large WPPs are usually connected to highly inductive transmission networks with X/R ratios between 1.4 to 11.4 whereas, it can be around 0.5 in case of small WTs attached to distribution networks [5] ,[9].

The POC bus voltage, V_{poc} can vary depending on the SCR and X/R seen at this bus. In addition, another key indicator that denotes the grid impedance angle or the ratio between the grid reactance to its resistance is the X/R. In the literature, inconsistency about a conclusive definition for a weak grid exists. However, a grid with SCR below 10 and X/R < 5 is considered as a weak grid [3].

For a certain SCR, the POC voltage can encounter increment or decrement based on the X/R value [5]. To develop the analytical model that represents the system dynamics, the DFIG active and reactive power capacity limits are first identified.

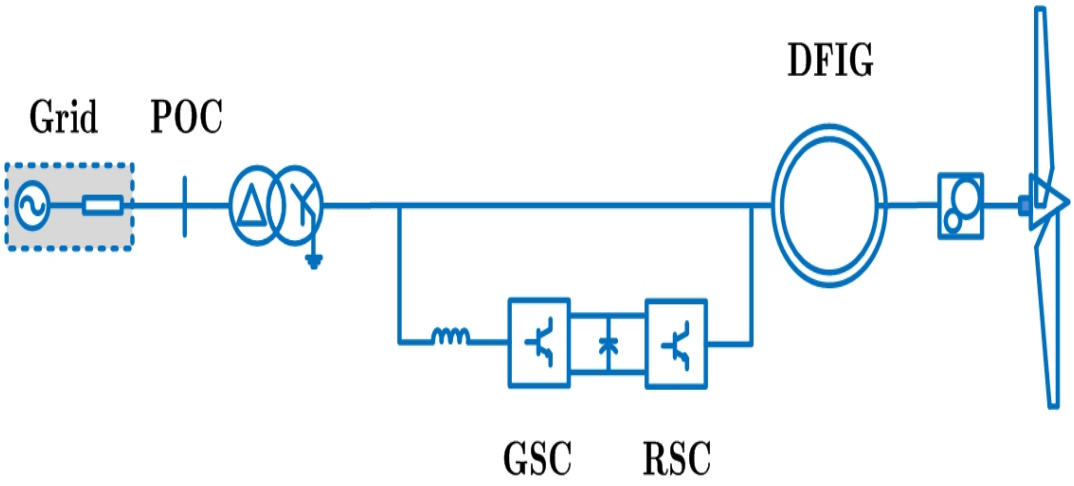

Figure 2.1 Schematic representation of DFIG wind generator model.

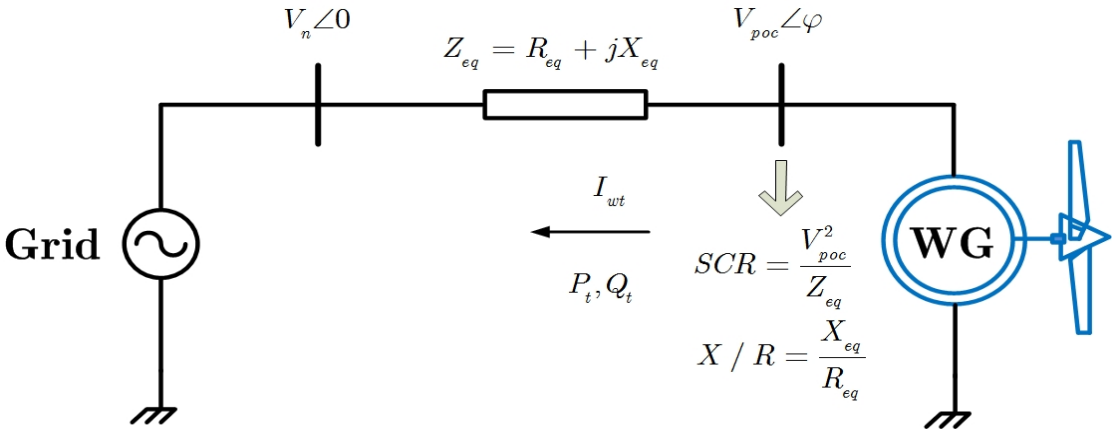

Figure 2.2 Grid-connected DFIG WT equivalent system.

2.3 System Modeling

Nowadays, WPPs are enforced to spontaneously manage reactive power to render a stable grid voltage and maintain grid connection in order to satisfy the onerous grid code commitments [6], [7]. Nevertheless, connecting an intermittent and stochastic WG to a weak power system with widely varying parameters aggravates the reactive power compensation (RPC). POC Voltage perturbations are directly related to different aspects, among which is the typology of the WT with the respective generator and embedded supervisory system [8]. Wind speed turbulences and profile also represents an important factor. Moreover, network characteristic, i.e., short circuit capacity ratio, SCR and feeders X/R ratio is a major aspect.

For the below analysis, reactive power at the POC is handled by the DFIG stator side only. Besides, the symbols, *V,P,Q,I*, signify voltage, active power, reactive power and current respectively. Subscripts, *t,s,r,w,m* refer to total, stator, rotor, wind and magnetizing respectively. *R,X,s* refer to resistance, reactance and slip respectively.

Assuming that the WT produces line current I_{wt}, an expression for the POC voltage magnitude can be described by the following equation:

$$\bar{V}_{poc} = \bar{V}_n + \bar{I}_{wt}\left(R_{eq} + jX_{eq}\right) \tag{2.1}$$

$$\bar{V}_{poc} = \bar{V}_n + \frac{P_t - jQ_t}{\bar{V}_{poc}^*}\left(R_{eq} + jX_{eq}\right) \tag{2.2}$$

Where:

$$\bar{V}_{poc} = V_{poc} e^{j\varphi} \tag{2.3}$$

Equation (2.2) can be rearranged and solved for V_{poc} as:

$$V_{poc}^4 - V_{poc}^2 \left(V_n^2 + 2\left[P_t R_{eq} + Q_t X_{eq} \right] \right) + \left(R_{eq}^2 + X_{eq}^2 \right) \left(P_t^2 + Q_t^2 \right) \Big) = 0 \tag{2.4}$$

After solving (2.4), the POC voltage can be expressed as:

$$V_{poc} = \sqrt{0.5\, V_n^2 + A} \tag{2.5}$$

Where,

$$A = P_t R_{eq} + Q_t X_{eq} + \sqrt{0.25\, V_n^4 + \left(P_t R_{eq} + Q_t X_{eq} \right) V_n^2 - \left(P_t X_{eq} - Q_t R_{eq} \right)^2} \tag{2.6}$$

The detailed derivation of (2.4), (2.5) can be found in Appendix A .The relation between the POC voltage, WT total delivered active and reactive powers, P_t, Q_t as well as equivalent impedance parameters, R_{eq},X_{eq} which directly influence SCR and X/R ratio is described by (2.5)-(2.6). It is worth mentioning that some studies suppose that the POC voltage magnitude is mostly determined by the real term contribution of (2.2) which yields [10]:

$$V_{poc} = V_n + \frac{P_t R_{eq} + Q_t X_{eq}}{V_{poc}^*} \tag{2.7}$$

Figure 2.3 compares actual and approximate POC voltage profile obtained using (2.5), (2.7) corresponding to rated WT output active power and 0.975 leading power factor. Clearly, it can be seen that (2.7) can be fair only for stiff distribution networks characterized by SCR>10. Nevertheless, for weak networks of lower SCRs, (2.5) is essential to accurately represent system behavior. Thereafter, (2.5) is used to characterize the POC voltage.

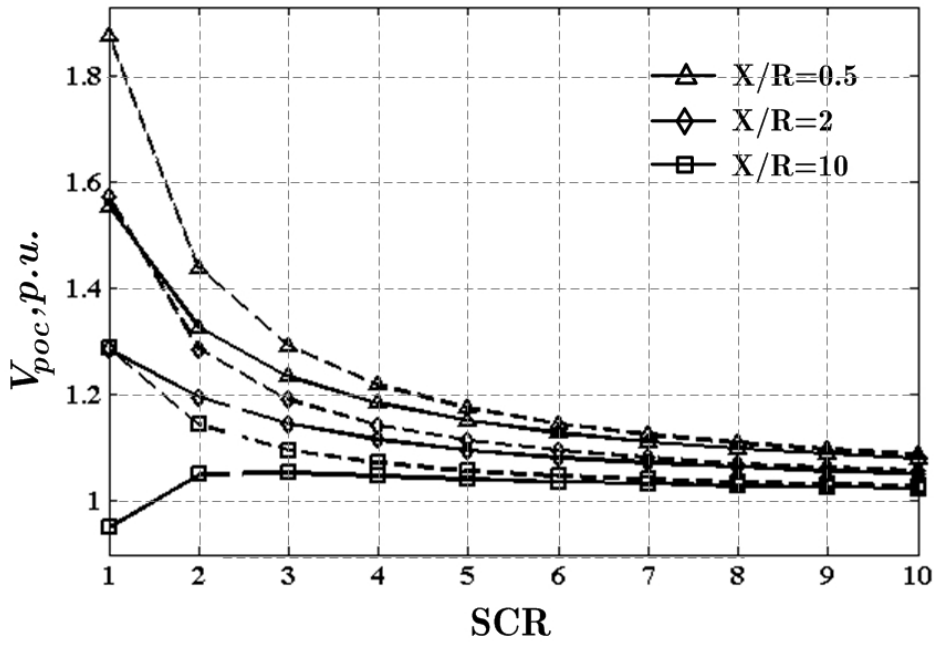

Figure 2.3 Actual (solid) and approximate (dashed) POC voltage versus SCR.

2.4 DFIG Capability Limits

The capability limits of a 2 MW DFIG of which parameters are listed in Appendix C considering stator and rotor currents heating constraints due to Joule's losses, maximum and minimum active and reactive power are shown in Fig. 2.4 [2], [11]. Identifying the control abilities of the WG aims at optimally design the DFIG control system in order to improve the system operation. The following sub-sections elaborate the diverse limiting factors that influence the DFIG active and reactive power capacity.

2.4.1 Stator Current Limit

When the stator rated voltage and rated current (base values) are expressed in p.u., the limit due to stator current can be expressed as:

$$P_s^2 + Q_s^2 = \left(V_{poc} I_s\right)^2 \qquad (2.8)$$

Equation (2.8) shows the maximum stator current in the PQ plane as a circle centered at the origin with a radius equal to the stator apparent power as shown in Fig 2.4.

2.4.2 Rotor Current Limit

The rotor current limit is obtained considering the heating owing to the rotor winding Joule's losses. Assuming that the DFIG stator resistance, R_s is neglected, then the stator active and reactive powers at rated stator voltage can be respectively expressed as [11]:

$$P_s = \frac{X_m}{X_s} V_{poc} I_r \sin\delta \tag{2.9}$$

$$Q_s = \frac{X_m}{X_s} V_{poc} I_r \cos\delta - \frac{V_{poc}^2}{X_s} \tag{2.10}$$

Combining (2.8) and (2.9)-(2.10), yields:

$$\left(P_s\right)^2 + \left(Q_s + \frac{V_{poc}^2}{X_s}\right)^2 = \left(\frac{X_m}{X_s} V_{poc} I_r\right)^2 \tag{2.11}$$

Equation (2.11) is depicted as a circle centered at $\left(-V_{poc}^2 / X_s, 0\right)$ in the considered PQ plane. The reactive power axis offset shows the DFIG magnetizing effect via a constant reactive power absorption which varies with the grid voltage (see Fig 2.4).

2.4.3 Total Capability Limit

The total DFIG active power is the sum of stator and rotor active power

$$P_t = P_s + P_r \tag{2.12}$$

Neglecting stator and rotor resistances, the rotor active power is given as

$$P_r = -sP_s \tag{2.13}$$

Hence, the DFIG total active power generation limit is expressed as

$$P_{t-\max} = \left(1-s\right)P_s \tag{2.14}$$

Figure 2.5 shows that the DFIG total capacity limit increases the stator capacity limit with the proportion of the rotor fed power. Thereby, Fig. 2.5 depicts the feasible operating zone of the DFIG including the total active power limit.

2.4.4 Maximum and Minimum Reactive Power Limits

The DFIG maximum and minimum reactive power limit considers the total capacity limit as well as the steady state stability limit. After solving (2.11), the maximum generation and absorption limits of DFIG reactive power can be obtained as:

$$Q_{sg-\max} = \sqrt{\left((X_m/X_s)V_{poc}I_r\right)^2 - P_t^2} - V_{poc}^2/X_s \qquad (2.15)$$

$$Q_{sa-\max} = -V_{poc}^2/X_s \qquad (2.16)$$

The detailed derivation of (2.11) is elaborated in Appendix B. The final capability area of the considered 2 MW DFIG based WT is shown in Fig. 2.5 the obtained capacity limits will be used for the design of the system controllers and evaluating the surplus reactive power required by the WG in order to maintain the voltage constancy for the range of SCR and X/R variations.

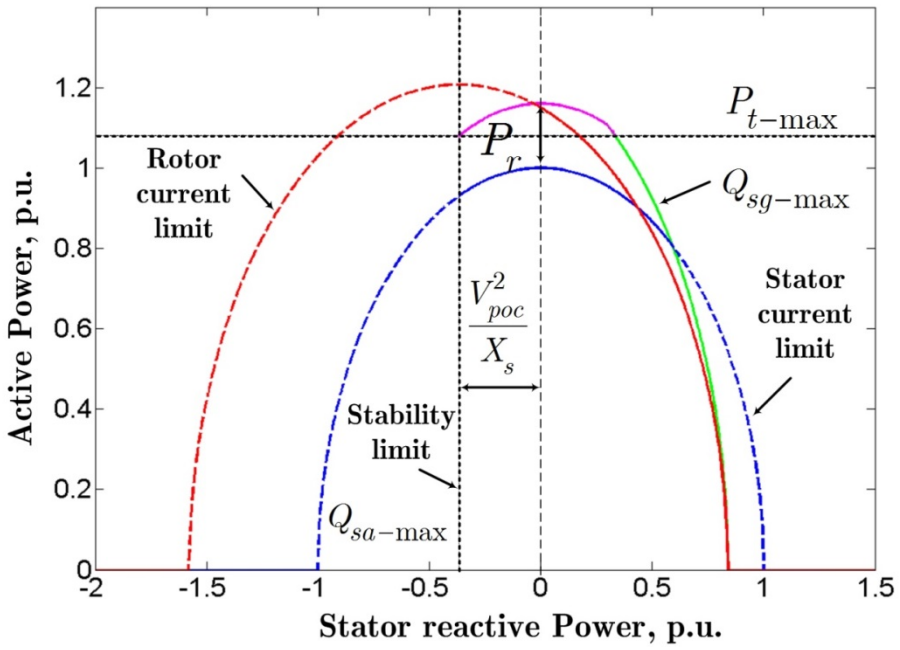

Figure 2.4 DFIG capability limits due to several limiting factors.

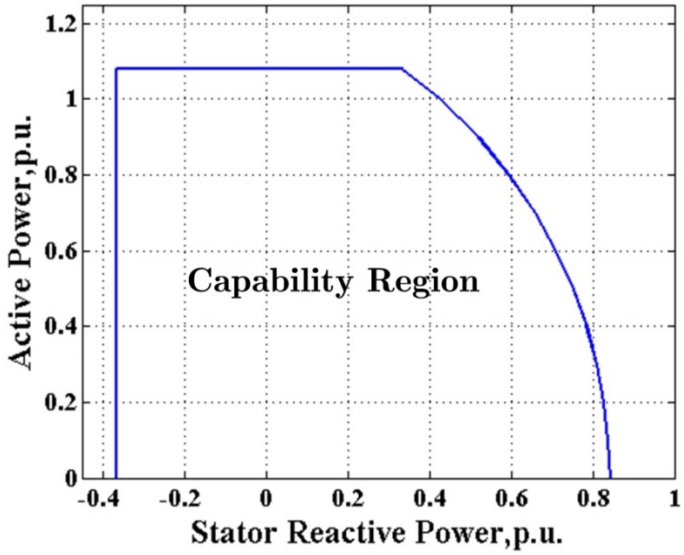

Figure 2.5 DFIG capability final working area.

2.5 DFIG Technical Constraints

In the following section, the conceivable impacts of the DFIG generated power on the PCC voltage profile under a wide range of SCR and X/R and also at different power factor scenarios are discussed.

2.5.1 Voltage Constraints

The European Standard EN 50160 has been issued to limit the voltage variations and maintain voltage quality by imposing statistical limits in such a way that a time limited deviation of exceeding them is allowable [12].

The POC voltage behavior in response to SCR and X/R ratio variations is depicted in Fig. 2.6. The WT is presumed to deliver the rated output power. In addition, different power factor PF scenarios are investigated to evaluate the impact of reactive power exchange on the POC voltage. The considered power factor PF operating scenarios are 0.975 leading, 0.975 lagging and unity power factor UPF as recommended by the Danish grid code for WPPs with output power greater than 1.5 MW [13]. As implied from Fig. 2.6, the POC voltage evokes dramatic perturbations as a consequence to the system parameters change. At a certain SCR, the POC voltage can overtake the nominal value or even decreases according to the X/R ratio or alternatively, the network impedance angle. Also, it is worth noting that for 1≤SCR≤4

and X/R≤2, higher voltage spikes unfolded which indicates for very weak condition. In particular, weak grids suffer significant parameters change with the SCR and/or X/R ratio variations. Besides, the grid features a resistive characteristic the lower the X/R ratio, specially below 2 as indicated above which can readily induce considerable voltage fluctuations as illustrated in Fig.2.6.

Additionally, the recorded POC voltage spikes vary according to reactive power flow or the power factor operating scenario. The leading PF scenario resulted in the maximum voltage increment as the WT releases reactive power rather than absorbing to regulate the voltage. Owing to the intermittence of wind speed, the variability of WT output power provokes POC voltage deviations [8].

Figure 2.7 shows the POC voltage behavior in response to the WT delivered output power and SCR change at different feeder X/R ratios calculated using (2.4). The WT reactive power Q_t corresponds to 0.975 leading PF. With higher SCR and X/R ratio "stiff network", the POC voltage is slightly influenced by the active power growth. Compared to X/R ratio of 10, the voltage rises quickly at X/R ratio of 0.5 particularly at very lower SCRs and thereby exceeds the acceptable limits, which is chosen as −5% ~ +5% in this study [1]. The result emphasizes on the impact of the feeder X/R ratio and the associated effect on the voltage-quality even at relatively higher SCRs.

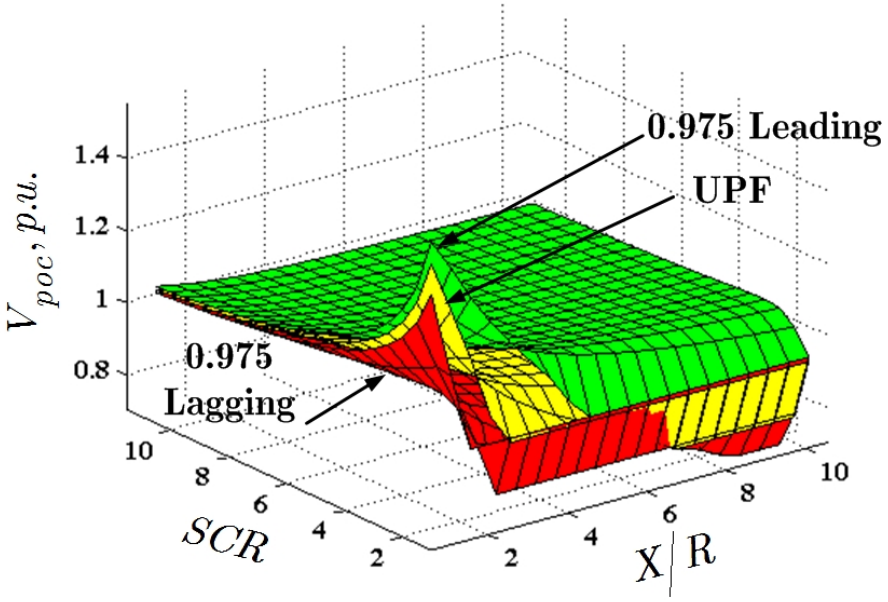

Figure 2.6 POC voltage behavior in response to SCR and X/R ratio variations.

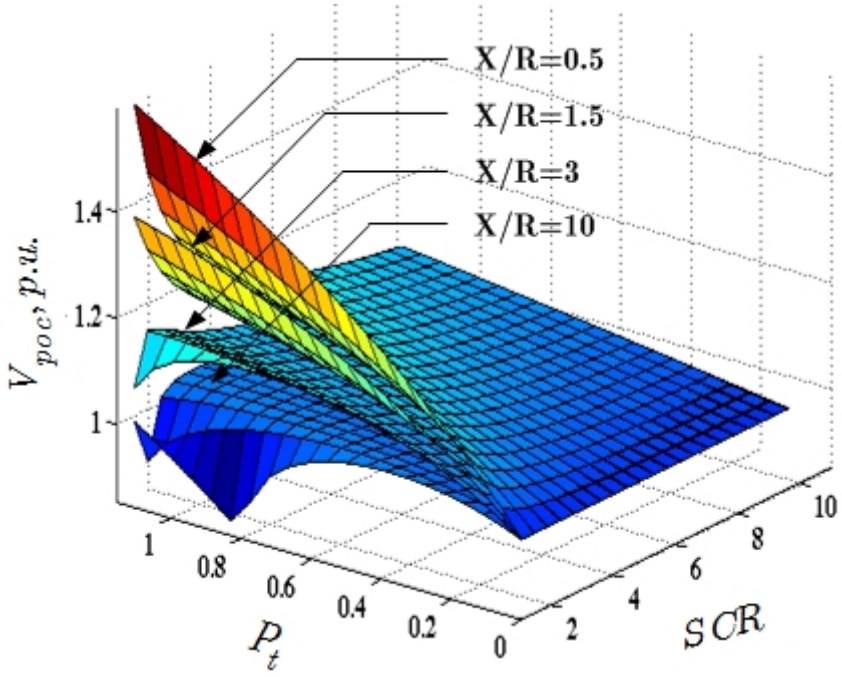

Figure 2.7 POC voltage response against in-feed wind power and grid parameters.

2.5.2 Active/Reactive Power Constrains

In order to quantify the reactive power required to retain rated POC voltage for the entire range of delivered active power and network parameters, (2.4) is solved for Q_t which results in:

$$Q_t = \frac{1}{R_{eq}^2 + X_{eq}^2}\left(V_{poc}^2 X_{eq} - \sqrt{B}\right) \tag{2.17}$$

Where,

$$B = V_{poc}^2\left(V_n^2 + 2P_t R_{eq}\right)\left(R_{eq}^2 + X_{eq}^2\right) - P_t^2\left(R_{eq}^2 + X_{eq}^2\right)^2 - V_{poc}^4 R_{eq}^2 \tag{2.18}$$

Figure 2.8 demonstrates the desired reactive power targeted at obtaining zero voltage deviation at the POC bus. It can be obviously seen that due to the DFIG capacity/stability limitations (discussed in section 2.4), infeasible operation in the entire active power range is depicted in Fig. 2.8 either for consumption or injection aspects especially at very low SCR and X/R ratio. Although wind power curtailment can sustain system normal operation, significant power loss is consequent. In an attempt to address the aforementioned shortcomings and allow for higher wind power expansion, exogenous reactive power reinforcement is imperative.

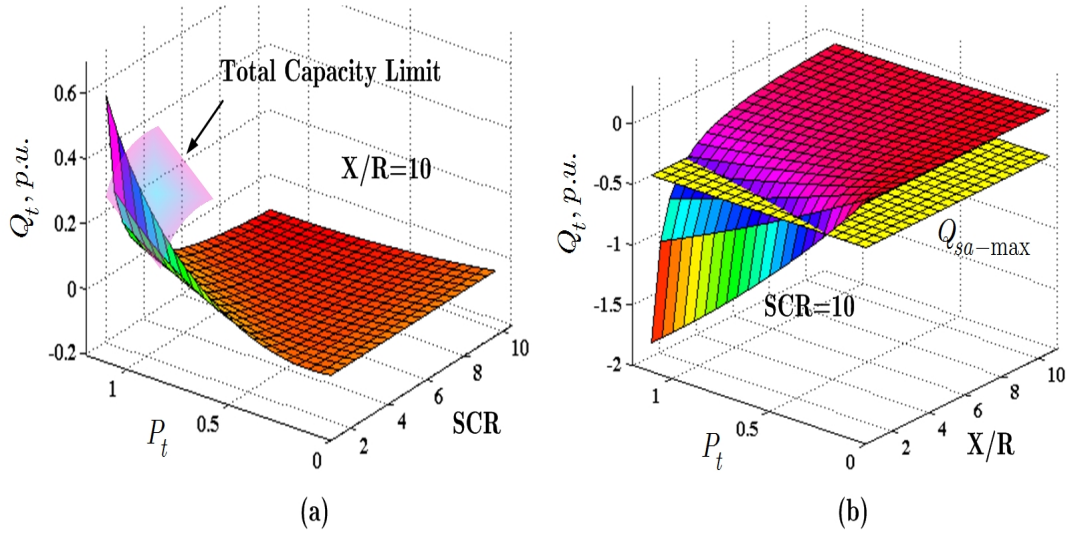

Figure 2.8 DFIG active/reactive power limitations due to SCR and X/R variation.

2.5.3 Reactive Power Regulation

Reactive power compensation RPC is a key factor to maintain the voltage quality of weak grid-connected DFIG WT systems [14]. Nonetheless, the effectiveness of RPC varies according to the network characteristics. Equation (2.17) can be used to explore the in-feed reactive power desired for maintaining POC voltage deviation within permissible levels ΔV_{poc} = ±5%, under various system strengths. The relevant results for the demanded reactive power and power factor are depicted in Fig. 2.9.a-f. Generally speaking, reactive power and power factor dramatically vary with the magnitude of voltage deviation, SCR and X/R ranges. Also, the reactive power consumed/supplied via DFIG can be a cost-effective option to handle the POC voltage deviation at certain SCR and X/R ranges. Yet, at very low SCR and X/R ratios, the DFIG cannot be solely utilized to regulate the POC voltage due to the imposed reactive power/power factor operational limits. Furthermore, higher reactive power demand is requested to attain voltage constancy the higher the SCR. This is because Q_t is more sensitive to the voltage deviation at the higher SCR value which can be also recognized from (2.17) [15].

Figure 2.10 shows the sensitivity of Q_t to the voltage deviation versus ±5% POC voltage variation at different network parameters. The Q_t surface area is getting

steeper the higher the SCR with higher demand the lower the X/R ratio 'resistive network'. Therewith, it is worth mentioning that a network with higher SCR is improbably evoke such significant voltage deviations [15] ,[16]. Therefore, minimal reactive power can readily adjust the POC voltage at higher SCRs.

To sum up, significant voltage fluctuations are induced owing to weak networks with lower SCR and/or X/R ratio that WTs are connected to which impose remarkable limitation on effective integration of WT generated output power. Besides, wind speed variations worsen voltage fluctuations which entails accurate voltage control VC to constantly regulate voltage waveform to address the aforementioned shortcomings which is presented in the next section.

2.5.4 Grid Codes Compliance

In addition to complying with the general GC requirements, wind power plants, WPPs, must be controlled in such a way that the operating point lies somewhere in the operating area to retain a specific range of power factor operation [13]. Assuming that the DFIG WT in Fig. 2.1 is attached to the host grid with SCR=2, hence, the active and reactive capacity limits can be obtained following the same procedure in section 2.4. Three distinct DFIG capacity limits are depicted in Fig. 2.11 as a result of three bus voltages, V_{poc} of 0.9, 1.0 and 1.1 p.u (which correspond to the maximum allowable voltage margin) along with the respective Energinet and E.ON grid codes requirements [7]. Obviously, from Fig. 2.11 it can be seen that subsequent to the POC voltage deviation, the DFIG WT is no longer capable of fulfilling the grid code requirements - set by either Energinet or E.ON - regarding reactive power/power factor regulation particularly when delivering the rated real power. In other words, reactive power support is necessary to maintain voltage constancy and thus drives the operating point into the operating area.

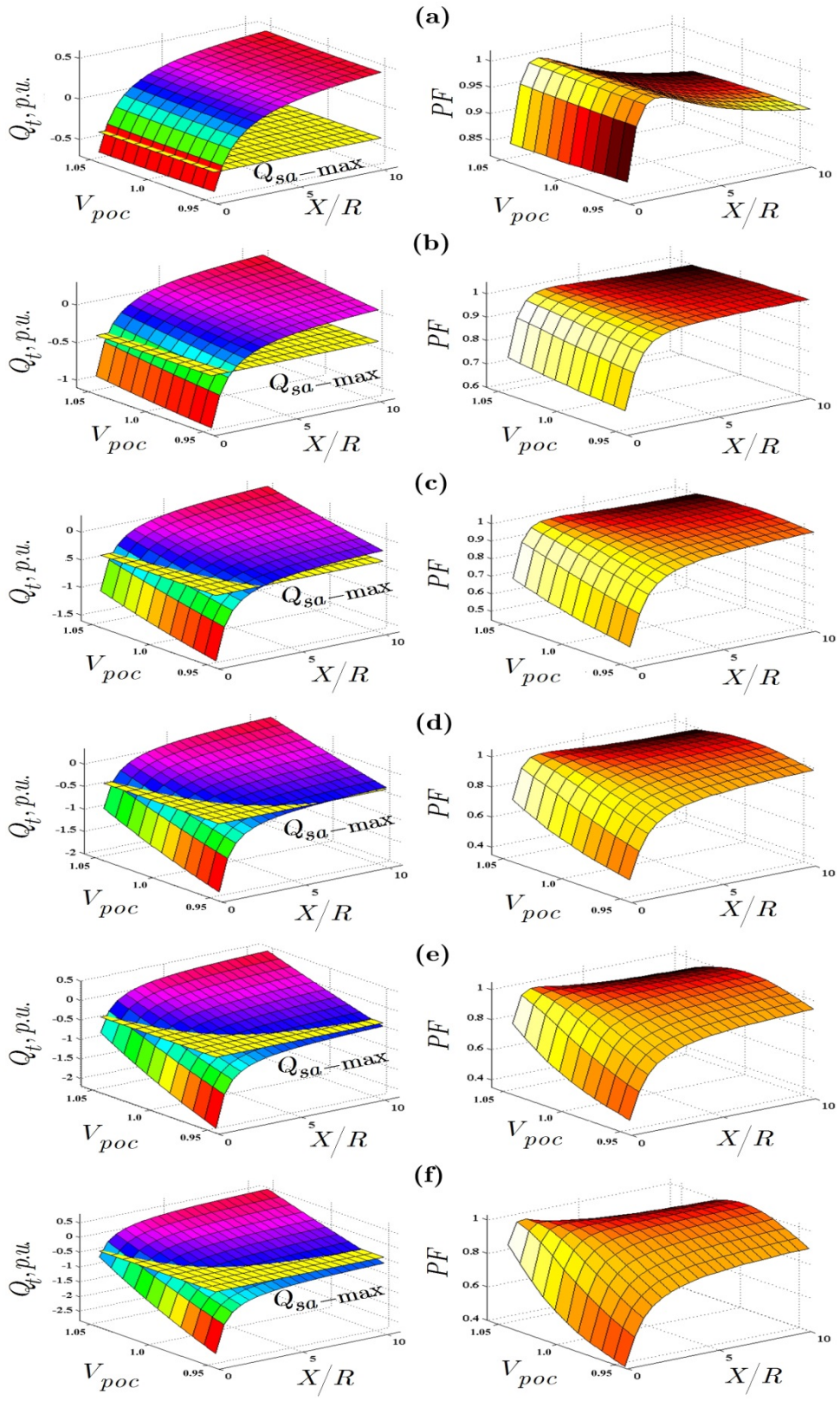

Figure 2.9 Reactive power and power factor regulation for ±5% POC voltage deviation. (a) SCR=1 (b) SCR=2 (c) SCR=4 (d) SCR=6 (e) SCR=8 (f) SCR=10.

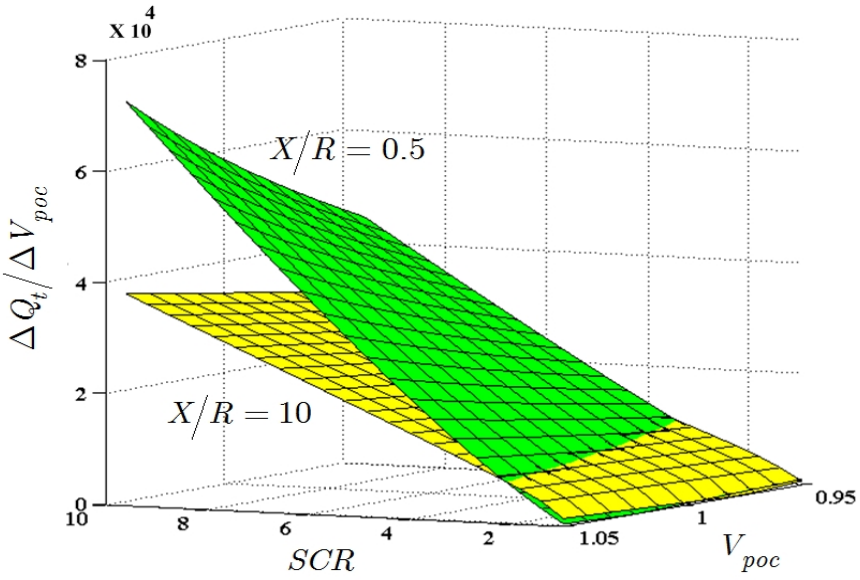

Figure 2.10 Rate of change of Q_t under different network parameters.

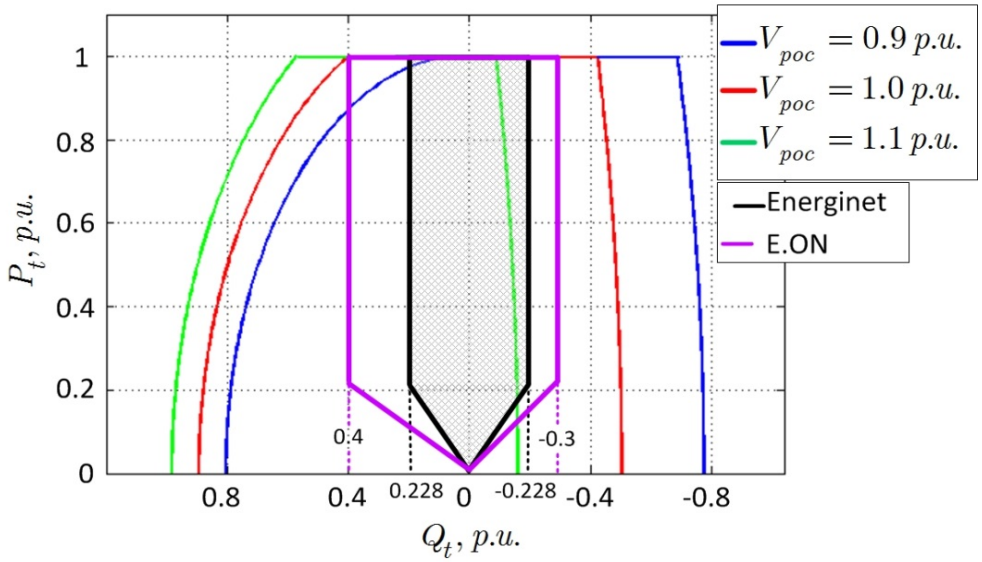

Figure 2.11 Grid codes compliance under PCC voltage deviation.

2.6 Results and Discussions

A set of simulation test cases is carried out to verify the aforementioned steady-state study. The equivalent system shown in Fig. 2.2 is used to conduct the test cases. A 2 MW DFIG WT is connected to a strong network with constant voltage, V_n, 690 V, via a long feeder which mimics a weak network. The DFIG WT is modeled as a controllable current source with outer active and reactive power controllers and inner current controllers [1]. The active power outer controller regulates the WT

output power according to the available wind speed. The rated wind speed is considered as 11.4 m/s. The reactive power control ensures that system power factor operating range is ± 0.975 lagging/leading as recommended by the Danish grid code [7]. The employed power factor control of the DFIG is devoted to assess the impact of the reactive power flow through the system under weak conditions. The investigations will be performed at different network strength, i.e., different SCR and X/R ratios. Throughout the simulations, the system is subjected to a realistic wind speed profile to evaluate the POC voltage response and the obtained results are depicted in Figs. 2.12-2.15.

From the results, it can be deduced that the POC voltage is significantly influenced by the real power feed-in especially at worst weak conditions with SCR=1 and X/R=0.5 (Fig. 2.12) where the PCC voltage exceeds the safe boundaries set by grid codes which is typically ±10%. Also, maximum voltage deviation is detected while the WG delivers the rated output power. Additionally, the reactive power flow (power factor) can contribute to further impact on the POC voltage according to the system strength. Throughout the test cases (Figs. 2.12-2.15), the leading power factor scenario results in higher voltage increment. The lagging power factor operating case showed the minimum voltage increment as in such range of network strength, the WG should absorb more reactive power to maintain the voltage constancy at the POC. However, due to the imposed reactive power limitation, the DFIG is solely incapable of handling the reactive power exchange with the weak grid.

Except for a network strength with SCR=10 and X/R=10, a relatively strong network encounters minimal voltage excursion within the allowable margins as in Fig 2.13. Despite, the wind power curtailment can contribute to enhancing the POC voltage, it represents a cost-ineffective action that results in huge wind power loss and misuse of the wind energy resources. Moreover, the results emphasize that additional compensation techniques are to be embedded to mitigate the POC voltage fluctuations and facilitate higher wind power penetration into such weak networks.

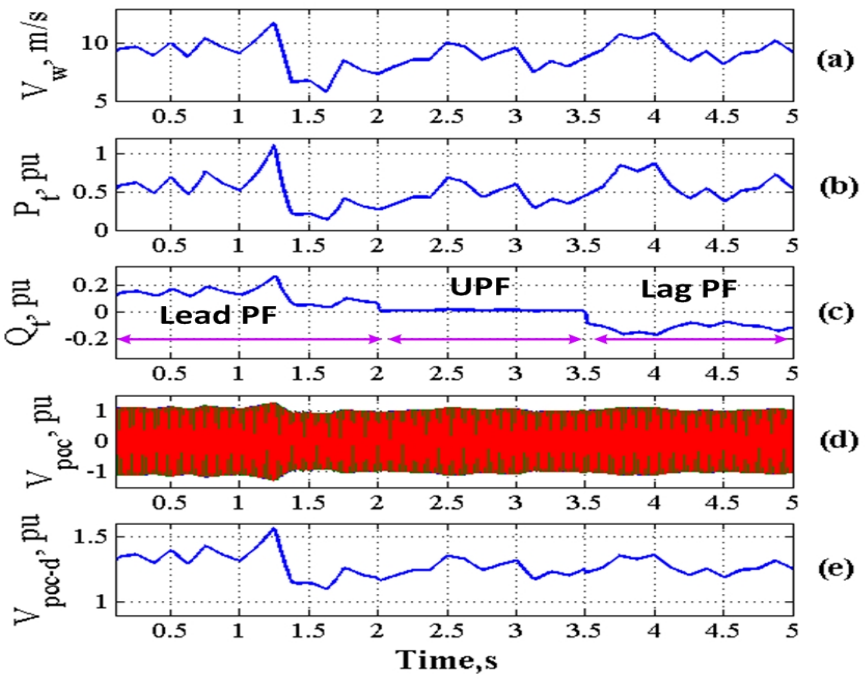

Figure 2.12 System response to different network strength SCR=1, X/R=0.5. (a) Wind speed Wind speed, V_w (b) Delivered active power, P_t (c) Exchanged reactive power,Q_t (d) POC voltage, V_{poc} (e) POC voltage d-axis component, V_{poc-d}.

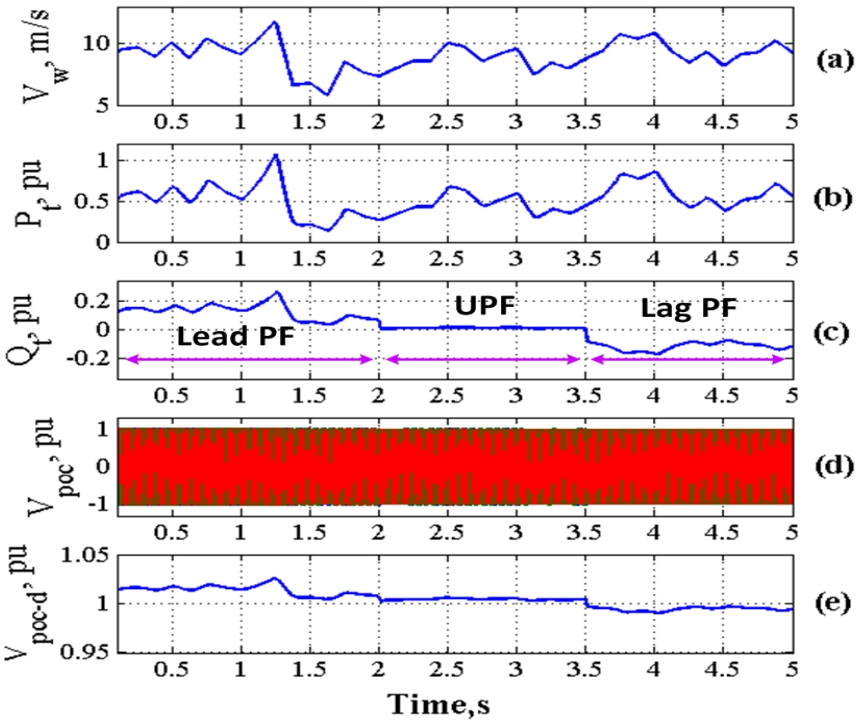

Figure 2.13 System response to different network strength SCR=10, X/R=10. (a) Wind speed Wind speed, V_w (b) Delivered active power, P_t (c) Exchanged reactive power,Q_t (d) POC voltage, V_{poc} (e) POC voltage d-axis component, V_{poc-d}.

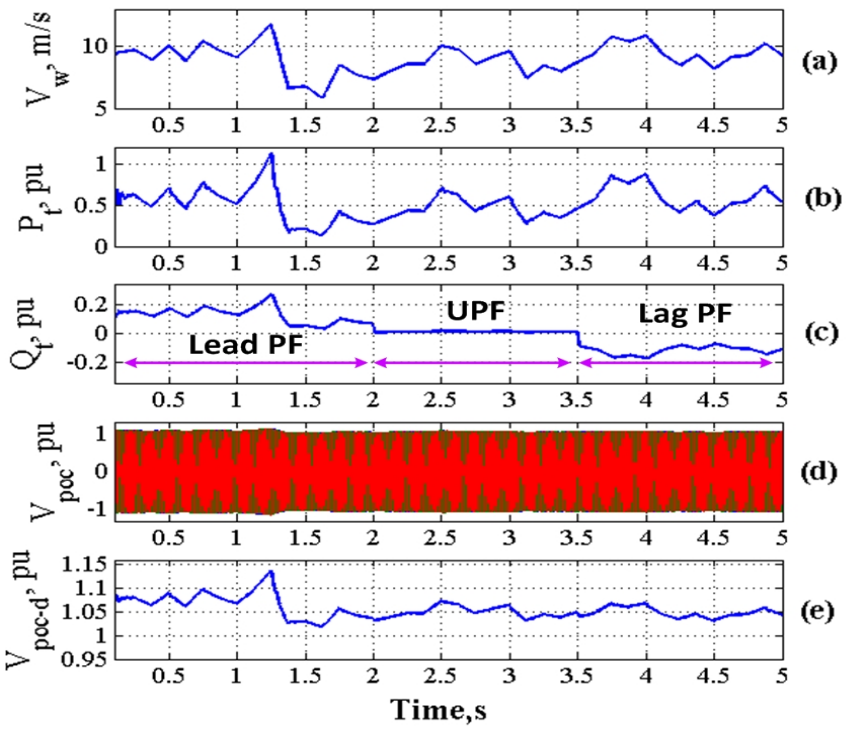

Figure 2.14 System response to different network strength SCR=5, X/R=1. (a) Wind speed Wind speed, V_w (b) Delivered active power, P_t (c) Exchanged reactive power,Q_t (d) POC voltage, V_{poc} (e) POC voltage d-axis component, V_{poc-d}.

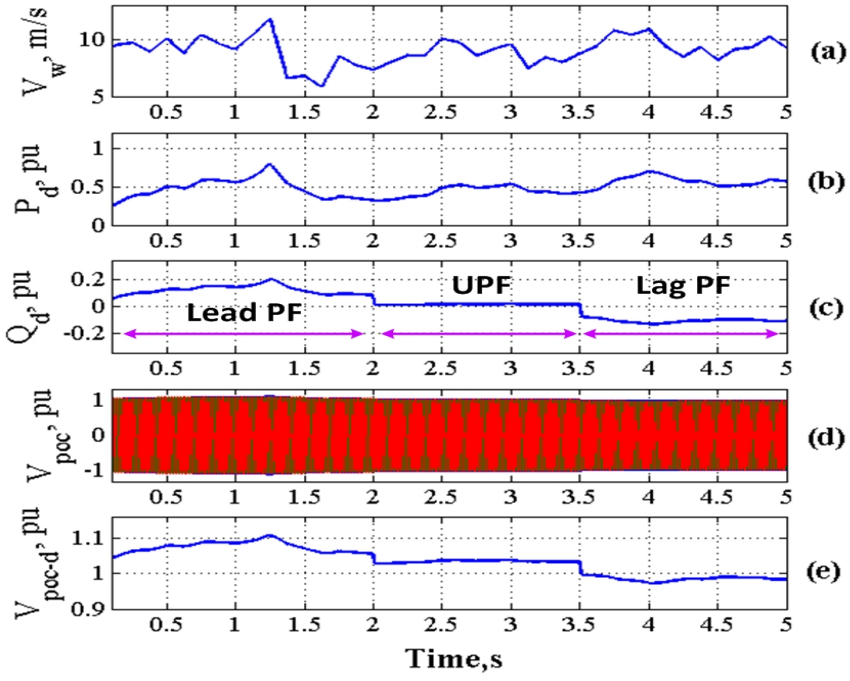

Figure 2.15 System response to different network strength SCR=2, X/R=4 (a) Wind speed Wind speed, V_w (b) Delivered active power, P_t (c) Exchanged reactive power,Q_t (d) POC voltage, V_{poc} (e) POC voltage d-axis component, V_{poc-d}.

2.7 Summary

A steady-state study for a DFIG WT attached to a weak ac network under different network strength has been presented in this chapter. The various technical aspects and constraints imposed on the POC voltage, real and reactive power have been assessed and discussed. The reactive power consumption/generation demanded to regulate the POC voltage under different operating conditions has been investigated. Simulation verification was conducted to verify the obtained steady-state results.

Furthermore, the simulations results assure the analytical study and emphasize the requirement for extra compensation reinforcements to foster more wind power penetration, effective usage of wind energy resources and attain satisfactorily POC voltage for weak network connections.

Bibliography

[1] S. Abulanwar, W. Hu, F. Iov and Z. Chen, "Characterization and assessment of voltage and power constraints of DFIG WT connected to a weak network," in Proc. IEEE PES General Meeting 2014, Washington, US, 2014.

[2] G. Mokryani, P. Siano, A. Piccolo and Z. Chen, "Improving fault ride-through capability of variable speed wind turbines in distribution networks", IEEE Sys. Journal., vol. 7, no. 4, pp. 713-722, Dec. 2013.

[3] N. P. W. Strachan, and D. Jovcic, "Stability of a variable-speed permanent magnet wind generator with weak AC grids", IEEE Trans. Power Del., vol. 25, no. 4, pp. 2779-2788, Oct. 2010.

[4] W. Hu, Z. Chen, Y. Wang, and Z. Wang, "Flicker mitigation by active power control of variable-speed wind turbines with full-scale back-to-back power converters", *IEEE Trans. Energy Conv*.,vol. 24, no. 3,pp. 640-649, Sep. 2009.

[5] J. O. Tande, G. Di Marzio, and K. Uhlen, "System requirements for wind power plants," SINTEF Energy Res., 2007. [Online]. Available: http://www.sintef.no/upload/ENERGI/pdf/Vind/TR%20A6586.pdf

[6] M. Kayıkcı, and J. V. Milanovic, "Reactive Power Control Strategies for DFIG-Based Plants," IEEE Trans. Energy Convers., vol. 22, no. 2, pp. 389–396, June. 2007.

[7] M. Mohseni and S. M. Islam, "Review of international grid codes for wind power integration: diversity, technology and a case for global standard", Ren. Sustain. Energy Rev., vol. 16, no. 6, pp. 3876-3890, Aug. 2012.

[8] F. Girbau-Llistuella, A. Sumper, F. Díaz-González, and S. Galceran-Arellano, "Flicker mitigation by reactive power control in wind farm with doubly fed induction generators," Electrical Power and Energy Systems., vol. 55, no. 1, pp. 285–296, Feb. 2014.

[9] J. O. Tande, G. Di Marzio, and K. Uhlen, "System requirements for wind power plants," SINTEF Energy Res., 2007. [Online]. Available: http://www.sintef.no/upload/ENERGI/pdf/Vind/TR%20A6586.pdf.

[10] M. Ammar, and G. Joos, "Impact of distributed wind generators reactive power behavior on flicker severity," IEEE Trans. Energy Convers., vol. 28, no. 2, pp. 425–433, June. 2013.

[11] M. E. Montilla-DJesus, D. Santos-Martin, S. Arnaltes, and E. D., Castronuovo, "Optimal operation of offshore wind farms with line-commutated HVDC link connection," IEEE Trans. Energy Convers., vol. 25, no. 2, pp. 504513–28, June. 2010.

[12] European Standard. EN 50160, voltage characteristics of electricity supplied by public electricity networks; 2011.

[13] Energinet. Technical regulation 3.2.5 for wind power plants with a power output greater than 11 kW; September 2010. Available at: http://www.energinet.dk.

[14] C. Han, A. Q. Huang, M. E. Baran, S. Bhattacharya, W. Litzenberger, L. Anderson, A. L. Johnson, and A. Edris, , "STATCOM impact study on the integration of a large wind farm into a weak loop power system," IEEE Trans. Energy Convers., vol. 23, no. 1, pp. 226–133, Mar. 2008.

[15] S. Abulanwar, W. Hu, Z. Chen and F. Iov "Adaptive Voltage Control Strategy for Variable-Speed Wind Turbine Connected to a weak network", Accepted by IET Renewable Power Generation Journal, 2015.

[16] J. Olav and G. Tande, "Exploitation of wind-energy resources in proximity to weak electric grids," Applied Energy., vol. 65, no. 1-4, pp. 395-401, April. 2000.

Chapter 3

Adaptive Voltage Control Strategy for VSWT Connected to a Weak Network

Significant voltage fluctuations and power quality issues pose considerable constraints on the efficient integration of remotely located wind turbines into weak networks. Besides, 3p oscillations arising from the wind shear and tower shadow effects induce further voltage perturbations during continuous operation. In this chapter, an adaptive voltage control (AVC) strategy is proposed to retain voltage constancy and smoothness at the point of connection (POC) in order to maximize the wind power penetration into weak networks. A proposed reactive power dispatch strategy to manage the reactive power flow from/to the wind generator WG is presented. Intensive simulation case studies under different network topology and wind speed ranges reveal the effectiveness of the AVC scheme to effectively suppress the POC voltage variations particularly at very weak grid conditions during normal operation.

3.1 Introduction

Traditionally, variable-speed wind turbines VSWTs are operated under fixed power factor control mode as stipulated by enforced grid codes. However, such operational mode shows pronounced limitation in case of weak grid scenario [1]. Fixed reactive power and voltage control (VC) are two favorable operational modes in the literature for the control of VSWTs [2], [3-6]. Apart from entailing active/reactive power dispatch [1], reactive power control mode becomes insignificant when adopted for very weak networks. Virtually, VC is increasingly desirable for weak networks to alleviate the POC voltage/power quality issues [6], [7]. Besides, with the prominent wind power penetration development, ancillary services such as VC provided by VSWTs become exigent [8] - [12]. Furthermore, VC allows for maximum reactive power compensation during utility contingencies.

In the literature, other authors have investigated weak networks in terms of short circuit capacity ratio SCR but with fixed feeder X/R ratio [6]. Besides, the design of the relevant VC relies on fixed gains to improve the POC voltage performance. The novelty of this study lies in a proposed adaptive voltage control (AVC) scheme reliant on network parameters to continually mitigate POC voltage variations for very weak networks with widely varying SCR as well as X/R ratios under different operating conditions. A reactive power dispatch strategy to manage the reactive power flow from/to the wind generator WG is proposed. Additionally, the study not only quantifies the system reactive power associated with the network parameters change but also the reactive power sharing within the WG and identifies the proper GSC rating to tackle the voltage perturbations at the conceivable system strengths and operating point.

Furthermore, the overall system stability is investigated using AVC via identifying the safe operating regions for a range of system parameters. In a broader context, the proposed AVC aims at facilitating wind power penetration into weak power systems. The reactive power compensation is realized primarily via the DFIG inherent stator reactive power as well as an over-sized grid side converter (GSC) which manipulates the reactive power deficit to address voltage disturbances. Moreover, a reactive power dispatch strategy to manage the reactive power coordination between the DFIG and the GSC is also presented.

3.2 System Description and Modeling

Figure 3.1 illustrates a schematic representation of the DFIG WT test system model. The model comprises a VSWT, mechanical drive-train, gear box, DFIG and two back-to-back AC-DC-AC partial converters, namely, grid side converter GSC and rotor side converter RSC. The WT is connected at the POC to the host network by means of an interface transformer and transmission line. A typical two level control scheme is devoted to control the DFIG WT system. A WT control is utilized to regulate WT mechanical output power through appropriate adjusting both pitch angle and the rotor speed according to the maximum power point tracking MPPT tracking.

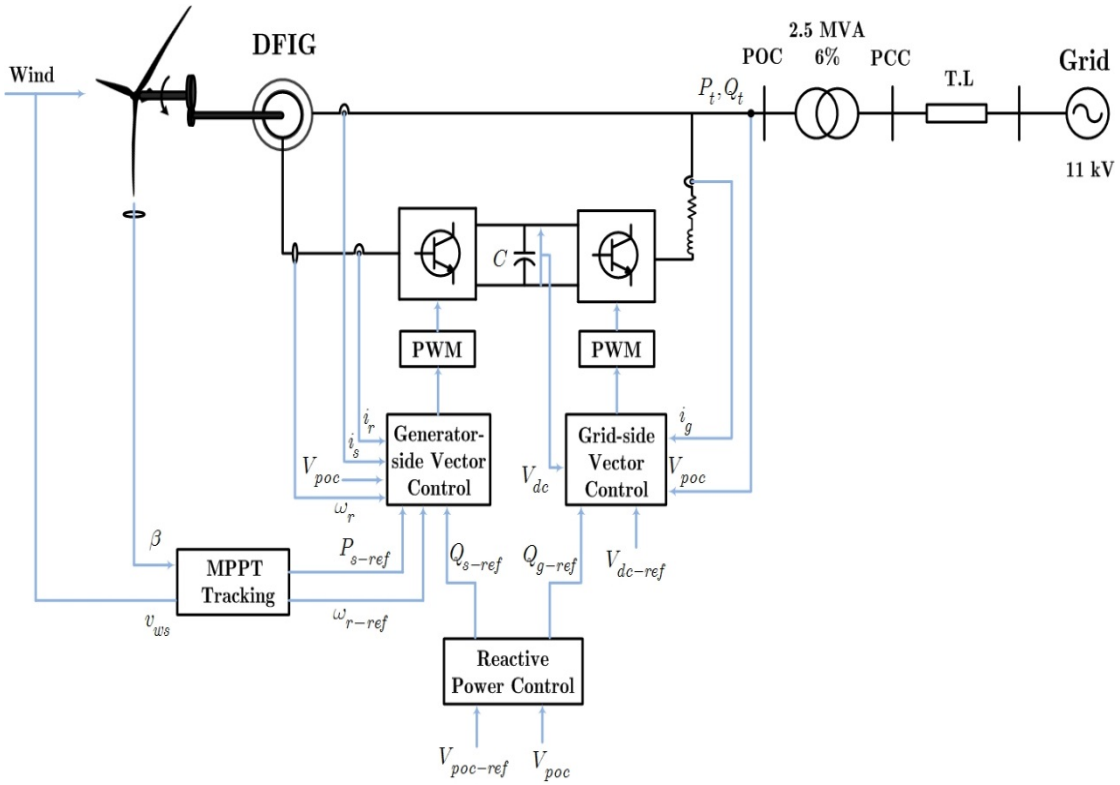

Figure 3.1 Block diagram of a grid-connected DFIG WT test system.

3.2.1 WT Aerodynamic Model

The WT extracts the kinetic energy from the wind and converts it into mechanical power to drive the wind generator. As the aim of this study is to investigate the interaction between the WG and the host power system, a simplified aerodynamic model can therefore be sufficient to reflect the behavior of the wind turbine [2]. The DFIG WT aerodynamic torque can be expressed by the following formula:

$$P_w = \frac{1}{2}\rho\pi R^2 v_{ws}^3 C_p(\beta,\lambda) \tag{3.1}$$

Where P_w is the WT extracted mechanical power from the wind in W, ρ is the air density in kg/m3, R is the wind turbine rotor radius in m, v_{ws} is the equivalent wind speed in m/s, β is the rotor pitch angle (°) , $\lambda = \omega_r R/v_{ws}$ is the tip speed ratio, and C_p is the rotor aerodynamic efficiency. The relation between C_p and the pitch angle β and the tip speed ratio λ is given as [10]:

$$C_p(\lambda,\beta) = 0.73\left(151/\lambda_i - 0.58\beta - 0.002\beta^{2.14} - 13.2\right)e^{-18.4/\lambda_i} \qquad (3.2)$$

With:

$$\lambda_i = 1\Big/\left(\frac{1}{\lambda - 0.02\beta} - \frac{0.003}{\beta^3 + 1}\right) \qquad (3.3)$$

Equation (3.2) implies that pitching the WT blades out of the wind direction reduces the efficiency of the WT system. Besides, for a given pitch angle, the maximum WT efficiency C_{pmax} is achieved at a specific tip speed ratio, which is known as the optimal tip speed ratio λ_{opt}. Consequently, for maximizing the WT output power at a specific pitch angle, the WT rotor speed is continually adjusted in proportion to the wind speed for maintaining the tip speed ratio equal to λ_{opt}, [8].

Figure 3.2-a illustrates the C_p coefficient variation versus the tip speed ratio and the blade pitch angle, whereas the WT power-speed characteristics calculated at different wind speeds using the WT parameters listed in Table 3.1 is shown in Figure 3.2-b. The maximum WT power trajectory can be obtained by rearranging (3.1) as:

$$P_{t\_\max} = k_t(\beta)\omega_r^3 \qquad (3.4)$$

Where,

$$k_t(\beta) = \frac{\rho A_r R C_{p\max}(\beta)}{2\lambda_{opt}^3} \qquad (3.5)$$

Where,

ω_r is the WT rotor speed in rad/s and A_r is the swept area of the WT in m^2.

3p torque oscillations are essential parts in the WT aerodynamic model. A comprehensive yet pragmatic model of 3p torque oscillations owing to wind shear and tower shadow effects for a three-blade WT has been developed in [2], [13] is applied in this study.

Figure 3.3 illustrates the dimensions used for the tower shadow model. According to this model, the equivalent wind speed v_{ws} is composed of three components, namely, the hub height v_H, the wind shear $v_{eq\text{-}WS}$, and the tower shadow

$v_{\text{eq-TS}}$ wind speeds. Thus, the equivalent wind speed v_{ws} is expressed as:

$$v_{ws} = v_H + v_{eq-WS} + v_{eq-TS} \tag{3.6}$$

$$v_{eq-WS} = v_H \left[\frac{(\alpha)(\alpha-1)}{8} (R/H)^2 + \frac{(\alpha)(\alpha-1)(\alpha-2)}{60} (R/H)^3 \cos 3\gamma \right] \tag{3.7}$$

$$v_{eq-TS} = \frac{m v_H}{3R^2} \sum_{b=1}^{3} \left[\frac{a^2}{\sin^2 \gamma_b} \ln\left(\frac{R^2 \sin^2 \gamma_b}{x^2} + 1 \right) - \frac{2a^2 R^2}{R^2 \sin^2 \gamma_b + x^2} \right] \tag{3.8}$$

Where, α is the empirical component of wind shear, H is the rotor hub elevation (m), γ is the blade azimuthal angle (°),γ_b is the azimuthal angle of each blade (°),a is the tower radius (m), x is the distance from the tower midline to the blade origin (m) and the wind turbine coefficient m is defined as:

$$m = \left[1 + \alpha(\alpha-1) R^2 / (8H^2) \right] \tag{3.9}$$

Table 3.1

Wind turbine parameters

Rated wind speed	11.4 m/s
WT rated output power	2 MW
WT rotor radius	40m
Air density	1.225 kg/m^3
Gear box ratio	87

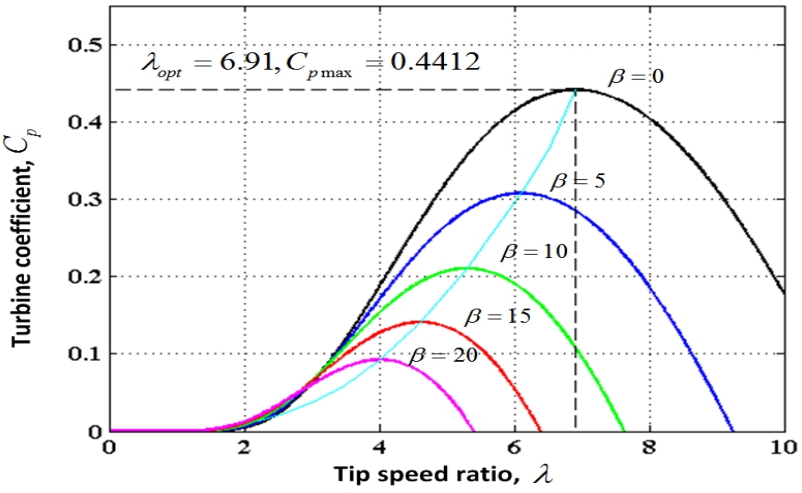

(a)

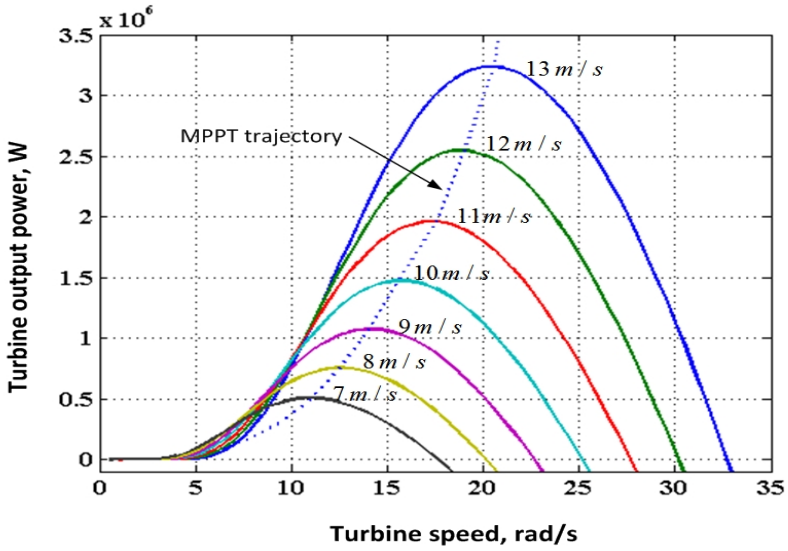

(b)

Figure 3.2 Typical WT characteristics: (a) C_p characteristics. (b) Power-speed characteristics.

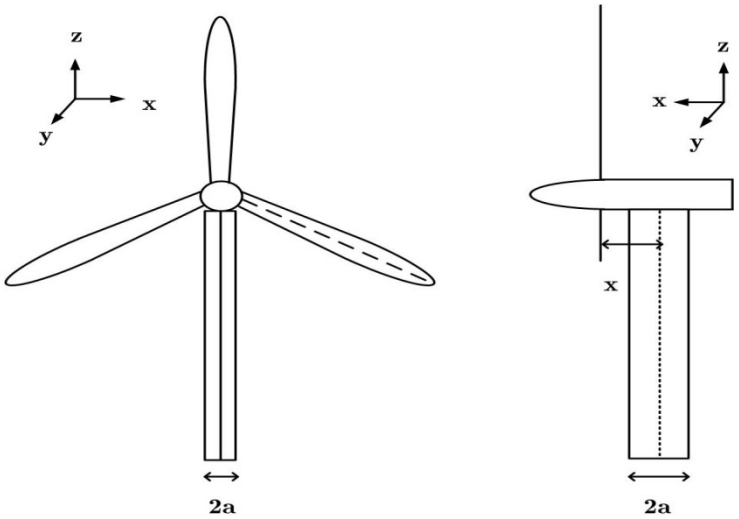

Figure 3.3 Dimensions used for tower shadow formula.

3.2.2 Mechanical Drive-train

In order to obtain accurate response of the WT's dynamic behavior during wind speed vagaries or during grid faults, the WT drive train system must be modeled at least as two-mass model which results in a more precise prediction of the influence on the host power system [6], [8]. Figure 3.4 demonstrates a schematic diagram for the used two-mass mechanical model which is connected by a flexible shaft with stiffness K_{sh} and damping coefficient D_{sh}. This flexible shaft is considered as a torsion spring connected between two masses. One mass depicts the WT inertia J_{wt} while the other mass represents the DFIG inertia J_{gen}. The high speed shaft is assumed stiff while the stiffness and damping aspects are modeled on the low-speed shaft. The gear-box is modeled with the exchange ratio 1:N_g.

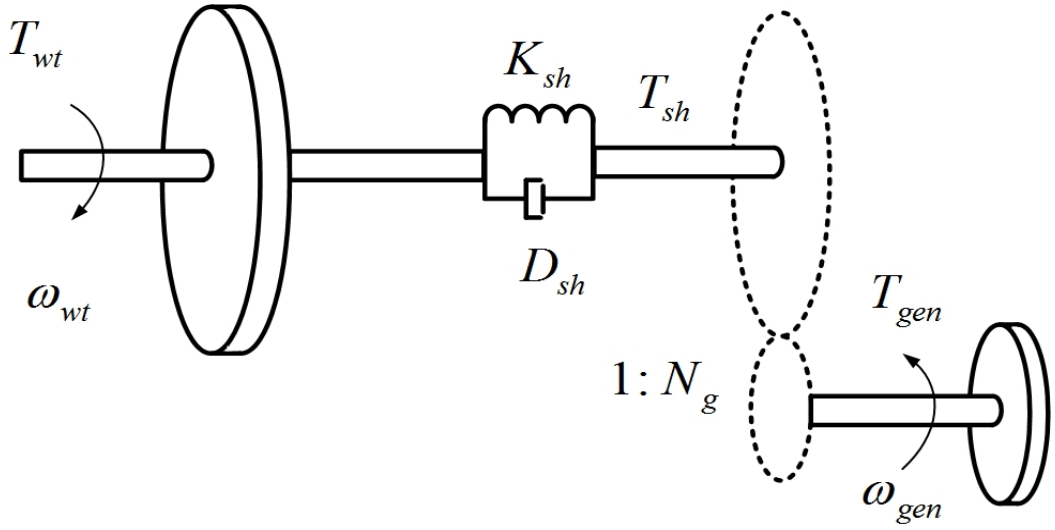

Figure 3.4 Mechanical drive-train two-mass model.

Referring all the terms to the high speed shaft, then the following transformations are obtained [8]:

$$J'_{wt} = J_{wt} / N_g \tag{3.10}$$

$$K'_{sh} = K_{sh} / N_g^2 \tag{3.11}$$

$$D'_{sh} = D_{sh} / N_g^2 \tag{3.12}$$

$$\omega'_{wt} = N_g \omega_{wt} \tag{3.13}$$

$$\theta'_{wt} = N_g \theta_{wt} \tag{3.14}$$

$$T'_{wt} = T / N_g \tag{3.15}$$

Hence, the WT mechanical drivetrain model can be expressed as:

$$T'_{wt} = J'_{wt} \frac{d\omega_{wt}}{dt} D'_{sh}\left(\omega'_{wt} - \omega_{gen}\right) + K_{sh}\left(\theta'_{wt} - \theta_{gen}\right) \tag{3.16}$$

$$-T_{gen} = J_{gen} \frac{d\omega_{gen}}{dt} + D'_{sh}\left(\omega_{gen} - \omega'_{wt}\right) + K_{sh}\left(\theta_{gen} - \theta'_{wt}\right) \tag{3.17}$$

$$\frac{d\theta'_{wt}}{dt} = \omega'_{wt} \tag{3.18}$$

$$\frac{d\theta_{gen}}{dt} = \omega_{gen} \tag{3.19}$$

$$-T'_{sh} = D'_{sh}\left(\omega'_{wt} - \omega_{gen}\right) + K_{sh}\left(\theta'_{wt} - \theta_{gen}\right) \tag{3.20}$$

Where, T_{wt} is the torque of the WT rotor; T_{sh} is the shaft toqure; T_{gen} is the wind generator torque; ω_{wt} is the rotor speed of the WT; ω_{gen} is the rotor speed of the wind generator; θ_{wt} is the WT angular position. θ_{gen} is the angular position of the generator.

The shaft stiffness is equivalent to the high and low speed shaft stiffness:

$$\frac{1}{K'_{sh}} = \frac{N_g^2}{K_{wt}} + \frac{1}{K_g} \tag{3.21}$$

Typically, to capture the maximum energy from the wind, the WT control is achieved by driving the wind generator to follow the optimum power-speed characteristic trajectory shown in Fig 3.5. Whenever the wind speed is higher than the cut-in speed and lower than a minimum speed, $V_{w-ci} \prec V_{ws} \prec V_{w-\min}$ in the zone AB, the reference generator rotor speed, ω_{r-ref} is set to a minimum value of $\omega_{r-\min} = 0.7\,\text{p.u}$ to ensure that the generator slip less than 0.3 [7]. Whereas, in the zone BC where the wind speed is higher than a minimum value and lower than the rated speed, $V_{w-\min} \prec V_{ws} \prec V_{w-nom}$, the DFIG is operated in a variable speed mode of operation so as to maximize the captured wind energy. Therefore, The DFIG reference rotor speed ω_{r-ref} is processed via a lookup table (calculated from Fig. 3.2) in order to maintain the optimal tip speed ratio λ_{opt}. If the wind speed is above the rated value, the reference rotor speed is set to the rated value and the BPA control is activated to limit the generator rotor over-speed and maintain the captured wind power equal to the nominal value.

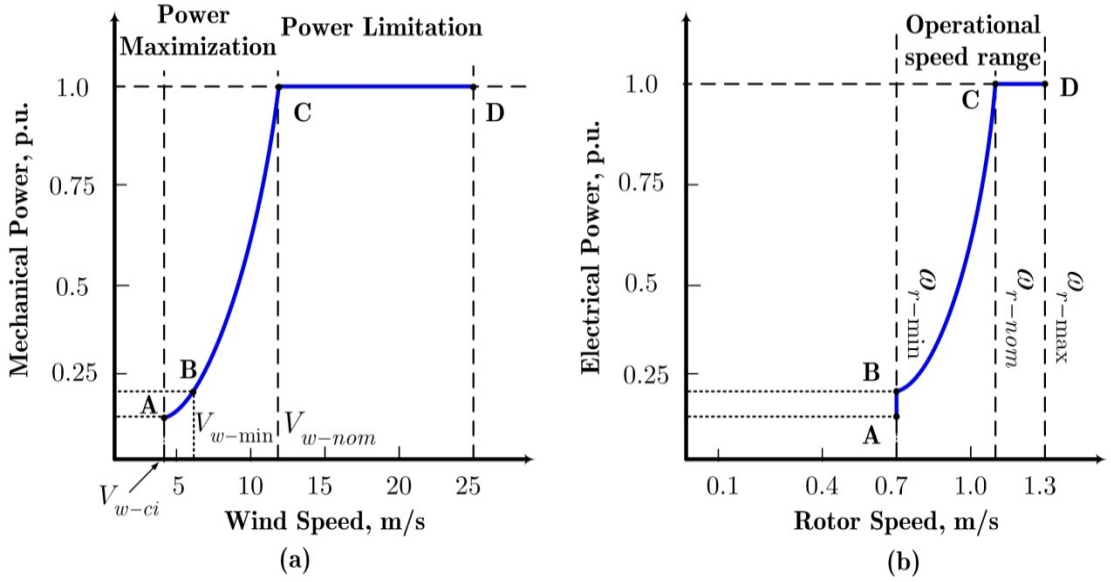

Figure 3.5 Typical characteristics of the DFIG WT: (a) Mechanical power versus wind speed. (b) Electrical output power versus rotor speed.

3.2.3 Blade Pitch Angle BPA Controller

The blade pitch angle BPA controller behaves as a rotational power limiter to prevent overrated power production when the wind speed exceeds the rated value. The BPA controller is inactive for wind speeds below the rated value. In this range of wind speeds, the extracted aerodynamic power is optimized. This can be achieved through regulating the tip speed ratio λ to achieve the maximum WT performance coefficient C_{pmax} during which the pitch angle is kept constant (normally zero).

On contrary, for wind speeds above the normal value, the pitch control is activated so as to limit the captured wind power to the rated value through regulating the reference rotor speed ω_{r-ref} to the rated speed ω_{r-nom}. In this case, the WT blades are pitched out of the wind speed direction. Being heavy, the WT blades rotation is facilitated either by electric or hydraulic servo drive. The pitch servo system is modeled as:

$$\frac{d\beta}{dt} = \frac{1}{T_{servo}}\left(\beta_{ref} - \beta\right) \qquad (3.22)$$

The servo drive mechanism model accounts for a time constant T_{Servo} and the limitation of the pitch angle (0 to 35 deg angle limit) with a gradient rate limit

(±10 deg/s) [8]. The rate-of-change limitation is crucial during system faults, as it implies how fast the aerodynamic power can be reduced in order to prevent the generator over-speed.

The BPA control scheme is illustrated in Fig. 3.6. The reference pitch angle β_{ref} is obtained as the summation of two PI regulators, namely, WT speed regulator and aerodynamic limiter. Whenever, the rotor speed and/or the output power overtake the rated value, the BPA controller is activated to maintain the rated operation.

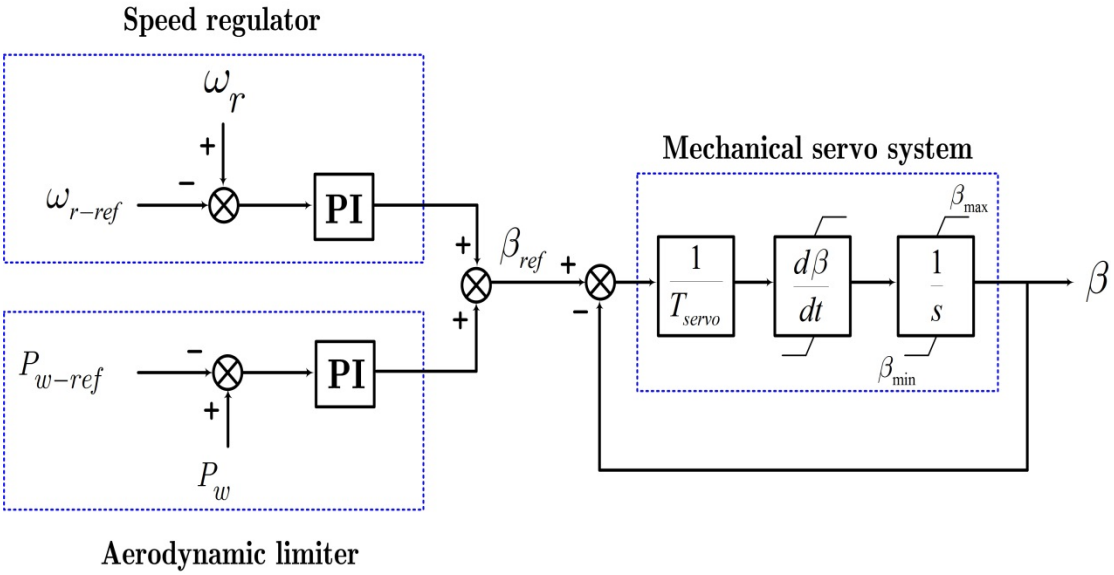

Figure 3.6 Schematic representation of the BPA control scheme.

3.2.4 DFIG Wind Generator

Figure 3.7 illustrates the DQ equivalent model of the DFIG. The DFIG RSC is controlled in a dq reference frame rotating with the synchronous speed with its d-axis aligned with the stator flux vector. The voltage equations of the DFIG generator stator and rotor circuits can be expressed using a rotating *dq* reference frame at synchronous speed as [8]:

$$u_{ds} = R_s i_{ds} - \omega_s \psi_{qs} + \frac{1}{\omega_b}\frac{d\psi_{ds}}{dt} \tag{3.23}$$

$$u_{qs} = R_s i_{qs} + \omega_s \psi_{ds} + \frac{1}{\omega_b}\frac{d\psi_{qs}}{dt} \tag{3.24}$$

$$u_{dr} = R_r i_{dr} - (\omega_s - \omega_r)\psi_{qr} + \frac{1}{\omega_b}\frac{d\psi_{dr}}{dt} \tag{3.25}$$

$$u_{qr} = R_r i_{qr} + (\omega_s - \omega_r)\psi_{dr} + \frac{1}{\omega_b}\frac{d\psi_{qr}}{dt} \tag{3.26}$$

Where, $u_{ds}, u_{qs}, u_{dr}, u_{qr}, i_{ds}, i_{qs}, i_{dr}, i_{qr}$ and $\psi_{ds}, \psi_{qs}, \psi_{dr}, \psi_{qr}$ are the *dq* stator and rotor voltages, currents and flux linkages. R_s, R_r are stator and rotor windings resistances, L_s, L_r, L_m are stator, rotor and mutual inductances respectively. $\omega_s, \omega_r, \omega_{sl}, \omega_b$ are stator, rotor, slip and base angular frequencies respectively.

Also, the DFIG electromagnetic torque T_{em} and stator active and reactive powers P_s, Q_s can be given as:

$$T_{em} = \frac{3}{2} p \frac{L_m}{L_s} \psi_s i_{qr} \tag{3.27}$$

$$P_s = -\frac{3}{2} u_s \frac{L_m}{L_s} i_{qr} \tag{3.28}$$

$$Q_s = \frac{3}{2}\frac{\psi_s}{L_s} u_s - \frac{3}{2} u_s \frac{L_m}{L_s} i_{dr} \tag{3.29}$$

Where, ψ_s, u_s are the stator flux and voltage magnitudes, *p* is the number of pole pairs. As implied from (3.28) and (3.29), stator active and reactive powers can be dictated via rotor dq currents, i_{qr}, i_{dr} respectively.

3.3 WTG Control Scheme

This section focuses on the basic DFIG WT control scheme and elaborates the proposed adaptive voltage control strategy for the mitigation of the POC voltage disturbances.

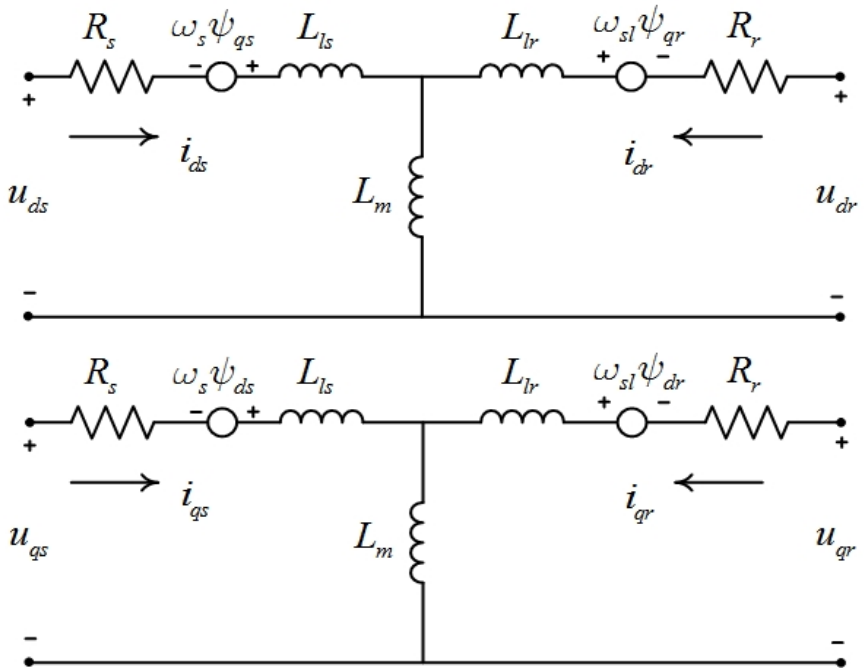

Figure 3.7 *Dq* DFIG equivalent circuits at a synchronously rotating reference frame.

3.3.1 DFIG Converters Controllers

Vector control techniques have been extensively studied for grid-connected DFIG WT systems. Two respective control schemes are employed for the control of the back-to-back converters as shown in Fig. 3.8. In order to achieve independent control of the exchanged active and reactive power between the GSC and the grid, the converter controller (Fig. 3.8-a) is operated in a synchronously rotating reference frame with the d-axis aligned with the grid voltage. The vector control of the GSC is dedicated to ensure a constant dc-link voltage V_{dc} irrespective of the transmitted power magnitude or direction and meanwhile provides sinusoidal currents [2]. In addition, controls the reactive power exchange Q_g between the converter and the grid side through adjusting $Q_{g\text{-}ref}$ to attain UPF or support the voltage during contingencies [9]. The objective of the rotor side converter RSC vector control is to provide the DFIG with a variable speed operation with decoupled control of stator side active and reactive powers. Likewise, to attain independent control of electromagnetic and rotor excitation current components, the DFIG is controlled in a stator flux oriented reference frame where its d-axis aligned with the stator flux vector. The RSC control scheme is depicted in Fig. 3.8-b. The reference stator active power $P_{s\text{-}ref}$ is normally

derived from the rotor speed controller. The DFIG reference rotor speed $\omega_{r\text{-}ref}$ is processed via a lookup table in order to ensure the optimal tip speed ratio λ_{opt}. Normally, grid-side and stator side reactive power set-points $Q_{g\text{-}ref}$,$Q_{s\text{-}ref}$ are fixed to zero to achieve UPF operation. However, in this study these reference values are dispatched through the proposed AVC scheme to continually regulate the POC voltage.

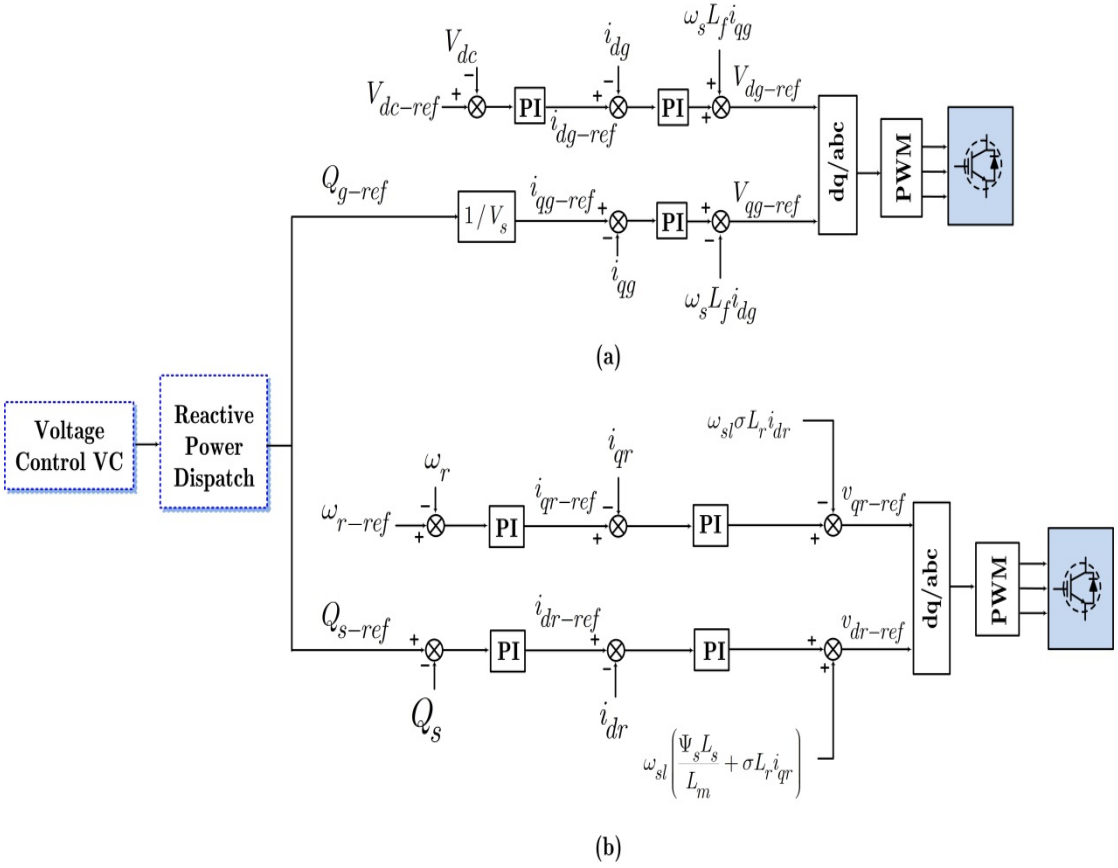

Figure 3.8 DFIG converters controllers: (a) GSC controller (b) RSC controller.

3.3.2 Adaptive Voltage Control AVC

In contrast to the operating point, variation of network parameters can adversely impact system dynamics [15] - [16]. Few papers address VC issue of WTs attached to weak networks with remarkably changing parameters. More specifically, Nickolas et.al. in [6] conducted an analytical eigenvalues stability study for a VSWT, with back-to-back full power converter attached to a weak network. Additionally, VC with modified fixed open-loop gain was suggested to improve the system stability under lower SCRs. Despite the modified control showed enhanced voltage response for lower SCR (10 to 4), system robustness to further network parameters

deteriorated. Besides, the impact of variable X/R ratio was not investigated.

This chapter presents a proposed adaptive voltage control AVC approach reliant on operating condition and network parameters. Although AVC is a pure control method which will not increase the system cost compared to conventional control techniques, however, its technical performance is superior. The latter can be attributed to the fact that AVC can adjust controller performance according to the grid strength and WT output power which assures keeping the POC voltage within allowable limits especially during very weak conditions. The proposed AVC scheme is demonstrated in Fig. 3.9. The reference reactive power demand $Q_{t\text{-}ref}$ is derived via the deviation from a reference voltage set-point $V_{poc\text{-}ref}$.

Basically, the priority of the reactive power compensation is devoted to the DFIG Q_s followed by the GSC contribution Q_g when Q_s attains the operational limit. Furthermore, The DFIG Q_s and GSC Q_g are dispatched according to $Q_{t\text{-}ref}$ and the DFIG capacity limit which will be discussed later. The system parameters are assumed to be measurable. The reactive power distribution of the whole DFIG system with the over-sized GSC under entire range of network parameters is explored here. Moreover, the significance of the proposed AVC under variable wind speed is also presented.

To increase the system stability and enhance the VC performance especially for very weak conditions, the open loop gain k_s will be constantly adjusted in order to optimize the VC. To ensure that the overall system performance is compromised for the typical range of network parameters, the rewarded AVC would mimic the latent behavior of the system.

The AVC open loop gain k_s would thus be scheduled according to the formula:

$$k_s = k_0\sqrt{P_t\left(X_{eq}/R_{eq} + R_{eq}/X_{eq}\right)} \qquad (p.u.) \tag{3.30}$$

Where k_0 is a design factor which can be selected to optimize the AVC. The significance of the selected adaptive gain k_s formula can be inferred from (2.4)-(2.5) where the VC can be reluctant to the change of the system variants, i.e., P_t, R_{eq}, X_{eq} (which significantly affect the performance of the VC) through adjusting the reference compensated reactive power Q_t in such a way to minimize the impacts of the terms $P_tR_{eq} + Q_tX_{eq}$, $P_tX_{eq} - Q_tR_{eq}$, for the entire range of network parameters so that the level of POC voltage variation is minimized, viz:

$$A \approx 0.5V_n^2 \text{ and } V_{poc} \approx V_n \tag{3.31}$$

In this sense, the reactive power set-point $Q_{t\text{-}ref}$ constantly responds according to these variations to smooth the POC voltage under all conceivable operating conditions. To further increase the system robustness against system parameters change, a differential gain k_d is adaptively designed as:

$$k_d = k\,k_s \tag{3.32}$$

Where k is a design factor. Additionally, the differential term includes filtering in order to suppress high-frequency noise extension [5].

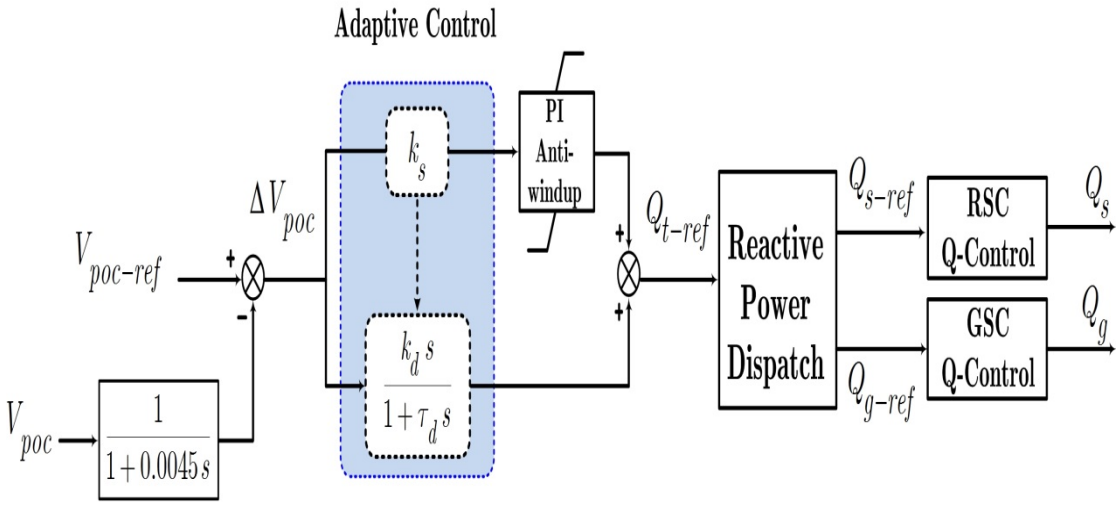

Figure 3.9 Proposed AVC strategy.

3.3.3 Reactive Power Dispatch

A proposed reactive power dispatch strategy to manage reactive power coordination between the DFIG Q_s and the GSC Q_g is illustrated in the flowchart shown in Fig. 3.10. Have the POC voltage deviates from the reference set-point, the VC correspondingly adapts the reactive power $Q_{t\text{-}ref}$ to regulate the voltage. This reactive power is compensated through the DFIG Q_s which is processed via the RSC Q-control as long as it lies within DFIG reactive power capacity, i.e., $Q_{sa\text{-}max} \leq Q_{t\text{-}ref} \leq Q_{sg\text{-}max}$. On the other hand, if the POC voltage overtakes the allowable margins –5% ~ +5% and meanwhile $Q_{t\text{-}ref}$ exceeds the DFIG Q_s limits identified in chapter 2, the excess reactive power is dictated by the GSC Q_g while the DFIG Q_s is accordingly set to the maximum absorption or injection capacity, $Q_{sa\text{-}max}$, $Q_{sg\text{-}max}$ respectively to benefit the DFIG reactive power and optimize the GSC size.

To verify the effectiveness of the adaptive control terms embedded in the AVC scheme, the system of Fig. 3.1 is examined at very weak grid condition, i.e., SCR of 1 and X/R of 0.5 with sporadically wind speed profile. A 10 m/s average wind speed with 0.1 turbulence intensity is used which is the highest given by WT manufacturer IEC flicker test [1]. The 3p oscillation model of [2] is also employed. As the WT rotational speed varies, the 3p oscillations frequency would correspondingly change. Fig. 3.10 shows the POC voltage response under three distinct control aspects, 'CVC' for conventional (PI) voltage control, 'AVC-WOD' for adaptive voltage control without differential term (k_s only) while 'AVC' signifies adaptive voltage control (k_s, k_d).

Compared to CVC, the AVC scheme with two adaptive parts effectively alleviates the POC voltage fluctuations particularly at higher wind speed conditions (higher WT output power). Also, for low to moderate wind speeds, the AVC satisfactorily suppresses 3p voltage oscillations. Furthermore, the adaptive differential term contributes to further damped performance.

3.4 Results and Discussions

The following section provides a set of case studies to investigate the detailed test system performance under stochastic wind speed. Moreover, the AVC effectiveness is also studied under different network parameters.

3.4.1 System Response under Stochastic Wind Speed

To assess the control system performance for the VSWT concept with DFIG, a set of case studies with stochastic wind speed with turbulence, wind shear and tower shadow effects are performed. Based on this approach, the control system parameters can be designed and optimized and also to evaluate the model under different operating conditions [10].

In the following, DFIG system performance is investigated under a stochastic wind speed with a mean value of 9 and 12 m/s. Figure 3.12 shows the DFIG WT output results for a fluctuating wind speed with a mean value of 9 m/s and turbulence intensity 10%. While the DFIG adapts to capture the maximum power out of the wind, the blade pitch angle is kept to zero. The DFIG rotor speed and the delivered active power are tracking the wind speed slow variations.

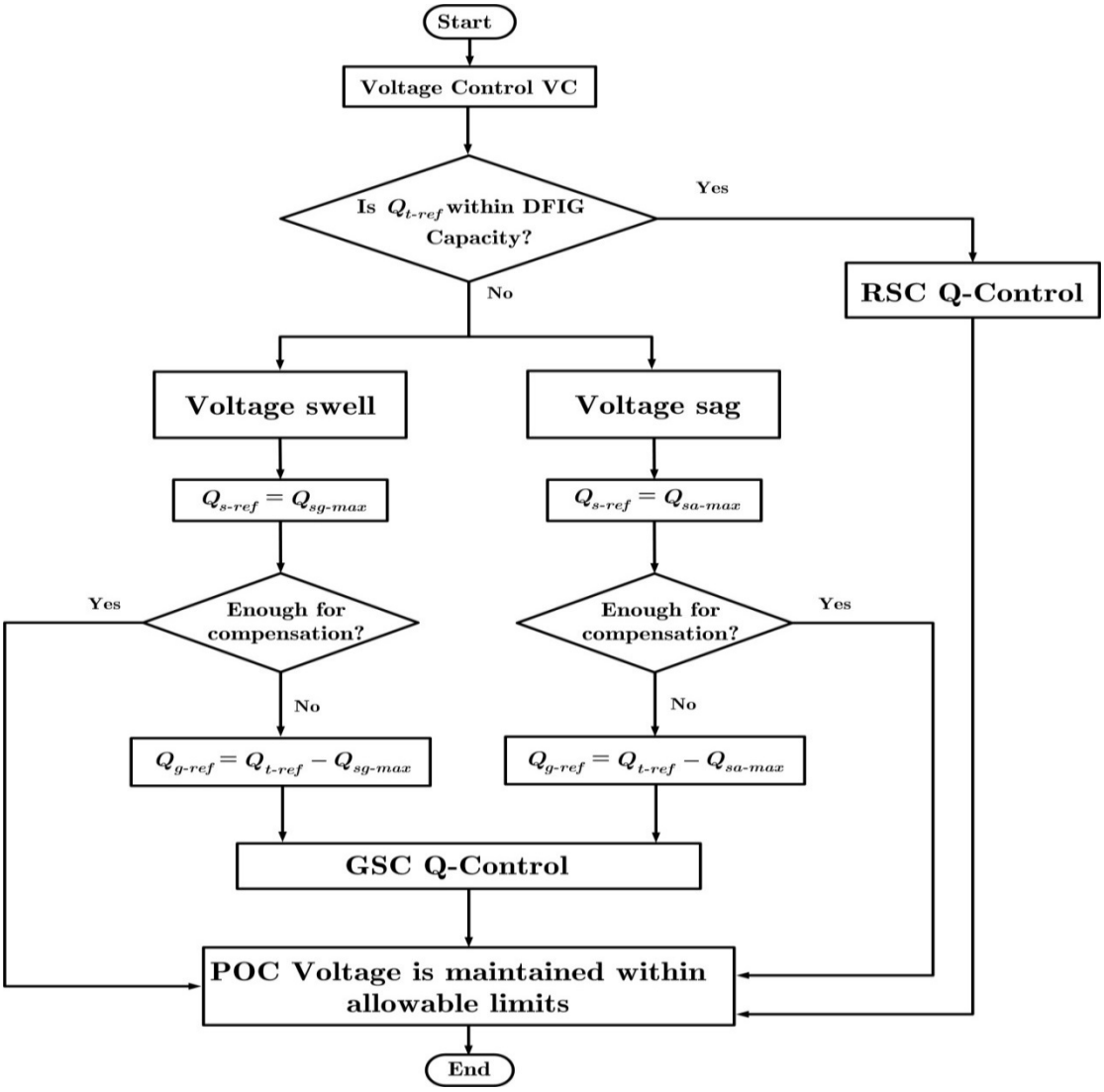

Figure 3.10 Flowchart for reactive power dispatch.

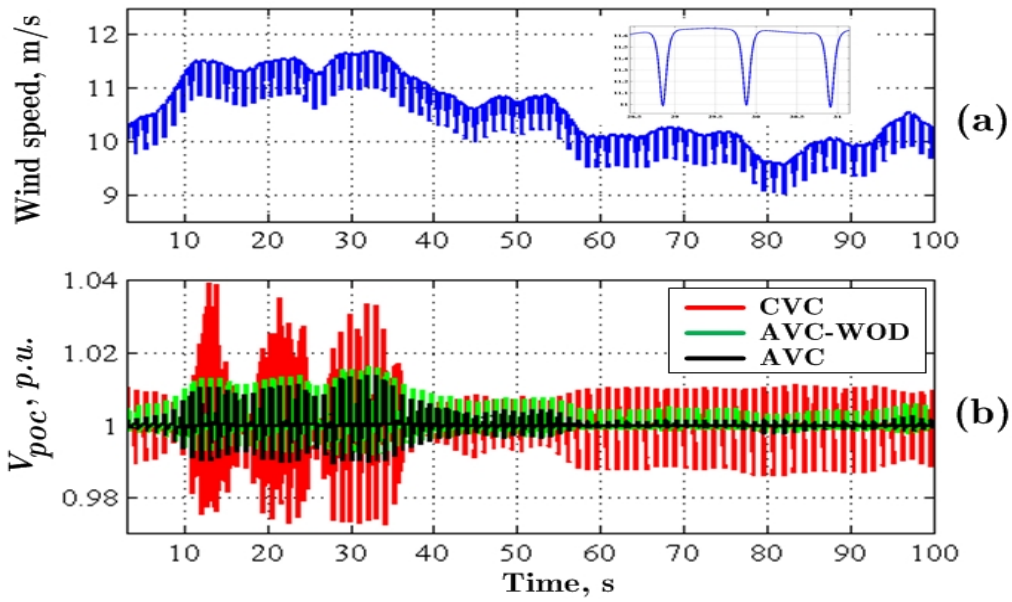

Figure 3.11 POC Voltage response: (a) Wind speed (b) POC Voltage.

Figure 3.13 depicts the DFIG WT response for a fluctuating wind speed with a mean value of 13 m/s and turbulence intensity 10%. When the wind speed exceeds its rated value, the pitch controller mechanism is activated (Fig. 3.13-b) and the output active power is limited to the rated value (Fig. 3.13-c). It can be seen from Fig. 3.13-d that small dynamic variations of the generator speed above the rated value is permitted in order to absorb the wind gusts and accordingly reduces the drive-train mechanical stress of the DFIG WT.

3.4.2 Verification of Analytical Study

In order to verify the analytical steady-state study of the simplified system presented in chapter 2 compared to the detailed simulation model, Fig 3.14 is presented. Equation (2.15) obtained from the analytical study is used to represent the POC voltage behavior for a long-term variable speed as that in Fig. 3.11 at rated WT output power and unity power factor scenario for grid SCR=1, X/R=0.5. Besides, the simulation model does not employ voltage control/reactive power compensation. As seen from Fig. 3.14, that the POC voltage analytical model conforms to that of the detailed model which verify the accuracy of the analytical study. Consequently, such analytical study can be readily applied to other WECS configurations after considering its active/reactive power capacity.

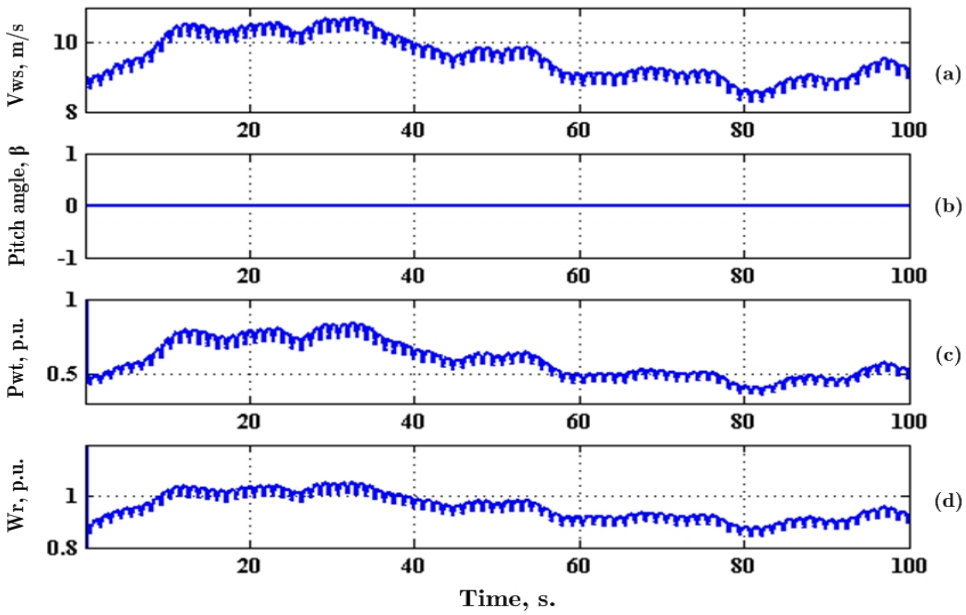

Figure 3.12 DFIG WT with a stochastic wind speed of 9 m/s mean value:
(a) Wind speed (b) Pitch angle (c) Active power (d) Rotor speed.

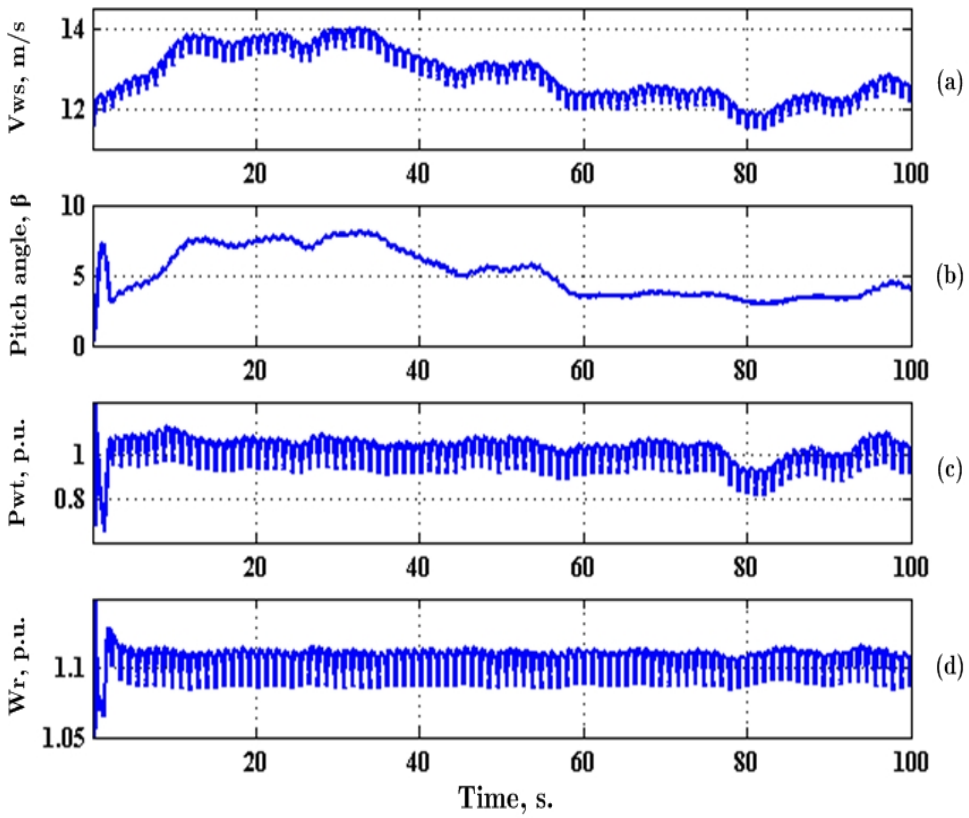

Figure 3.13 DFIG WT with a stochastic wind speed of 13 m/s mean value: (a) Wind speed (b) Pitch angle (c) Active power (d) Rotor speed.

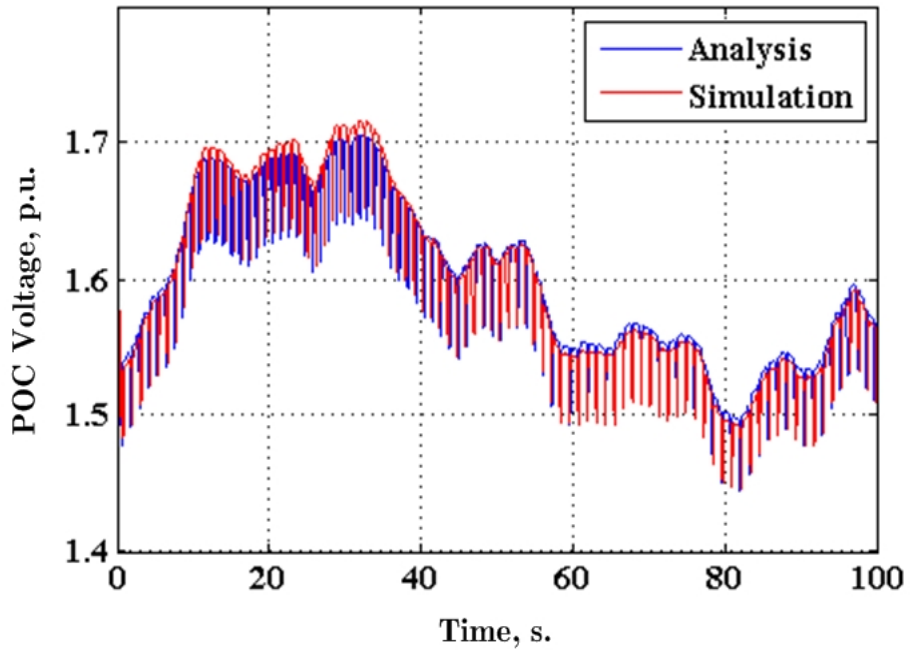

Figure 3.14 POC voltage response for SCR=1, X/R=0.5.

3.4.3 Effectiveness of AVC Strategy

To verify the significance and robustness of the proposed AVC, a detailed system model in MATLAB/SIMULINK software environment is implemented while the test system is examined at wide range of SCR and X/R variations. The hardware specifications of the computer used to conduct the study is Intel (R) Xeon (R) CPU E5-2650 v2@2.6 GHz with 64 GB installed memory. The 2 MW DFIG WT test system parameters are listed in Appendix C.

Figure 3.15 illustrates a long-term system response to a very weak grid condition which corresponds to SCR of 1 and X/R of 0.5. As it shows, POC voltage fluctuations are induced due to the high network impedance, wind speed variations and also 3p oscillations. Consequently, higher reactive power absorption Q_t is required in this case to compensate the voltage. Being over the DFIG Q_s capacity, Q_t can be fully compensated by virtue of an over-sized GSC which can absorb a maximum Q_g of 0.17 p.u. to regulate the voltage while the DFIG Q_s is attaining the maximum permissible absorption capacity $Q_{sa\text{-}max}$. Normally, GSC is rated at 25% of the DFIG rated power (0.5 MVA). Yet, 6% overrated GSC (0.53 MVA rating) is adequate in this case to drive the POC voltage within safe limits.

Being acting on minifying the impact of system variants change to counteract voltage variations, the AVC scheme causes minimal voltage oscillations with better damped performance compared to CVC as depicted in Fig. 3.15 particularly for high wind speed due to high WT output power which contributes to higher voltage fluctuations. The significant CVC oscillations are accordingly reflected on the system reactive power as depicted from Q_t, Q_s and Q_g waveforms.

Besides, the system is examined at another weak network condition with SCR of 2 and X/R of 0.7 and the relevant results are demonstrated in Fig. 3.16. As mentioned before in chapter 2, the demanded reactive power Q_t becomes more sensitive to the voltage deviation the higher the SCR. Therefore, Q_t =0.63 p.u. is essential to adjust the voltage which is beyond the DFIG Q_s capability. Hence, a GSC with Q_g = 0.26 p.u. (0.66 MVA rating) can absorb the deficit reactive power, as seen in Fig. 3.16. Moreover, the AVC provides higher voltage fluctuation mitigation capability which is also reflected on the DFIG Q_s signal as seen in the depicted figure.

Figure 3.17 shows the system response for SCR of 7 and X/R of 5. As the network features an inductive characteristic (higher X/R), less amount of reactive power can regulate the voltage which can be fully dictated by the DFIG Q_s.

Compared to the former case, the system requires less Q_t in case of SCR and X/R of 10 (relatively strong network) as depicted in Fig. 3.18. In this manner, DFIG releases Q_s =0.022 p.u. to ensure voltage constancy. Despite, the relatively strong network conditions (Figs. 3.17-18), the AVC preserves satisfactory performance and enhanced POC voltage profile.

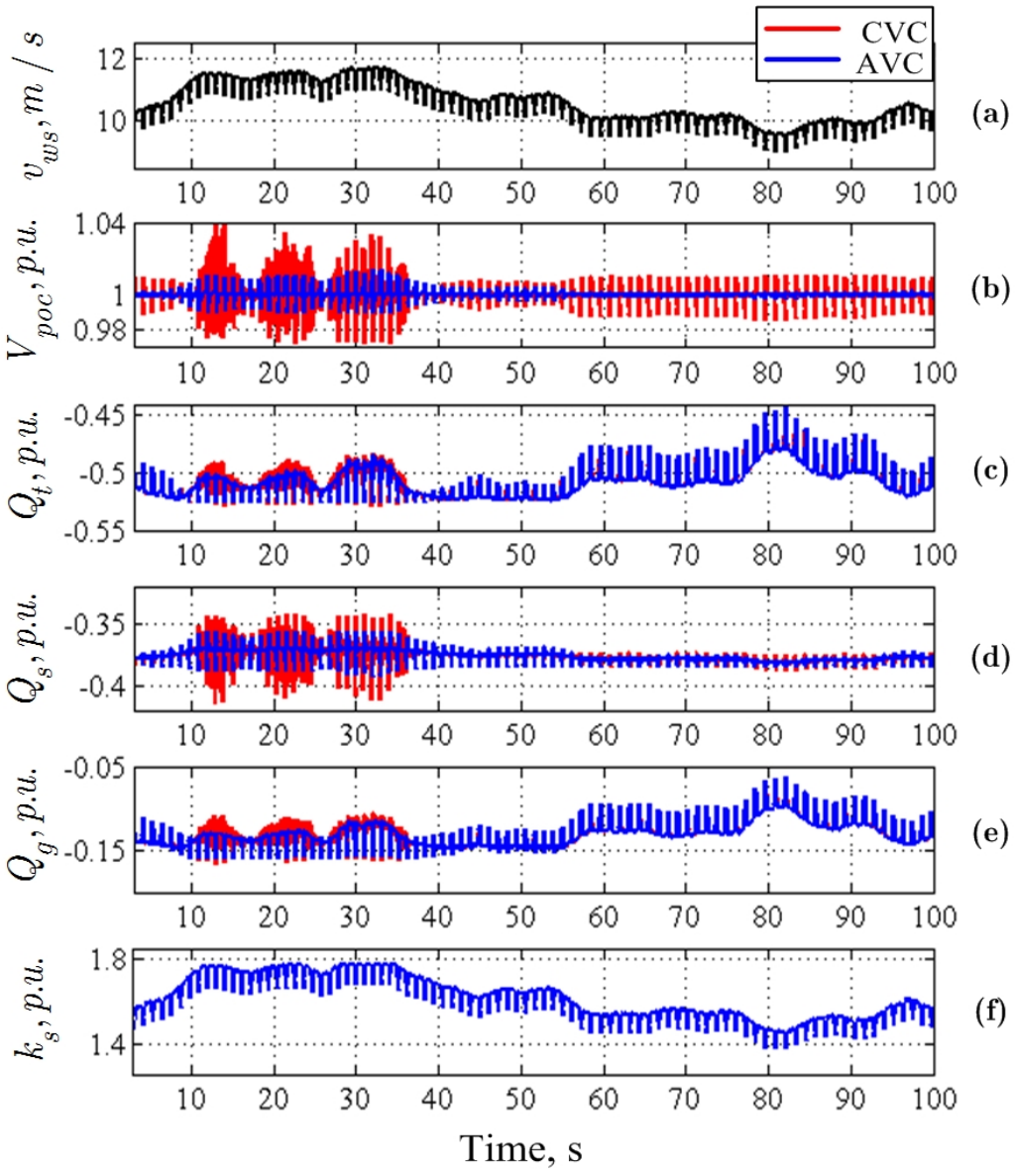

Figure 3.15 Long-term view of system response, SCR=1, X/R = 0.5:
(a) wind speed (b) POC voltage (c) total reactive power (d) stator side reactive power (e) GSC reactive power (f) AVC gain k_s.

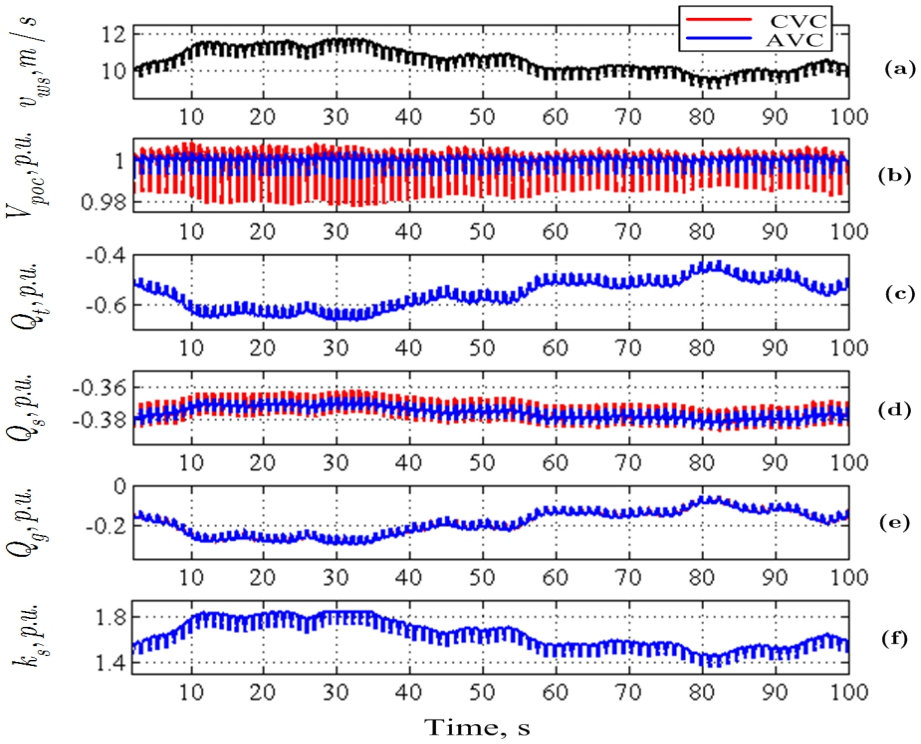

Figure 3.16 Long-term view of system response, SCR=2, X/R = 0.7: (a) wind speed (b) POC voltage (c) total reactive power (d) stator side reactive power (e) GSC reactive power (f) AVC gain k_s.

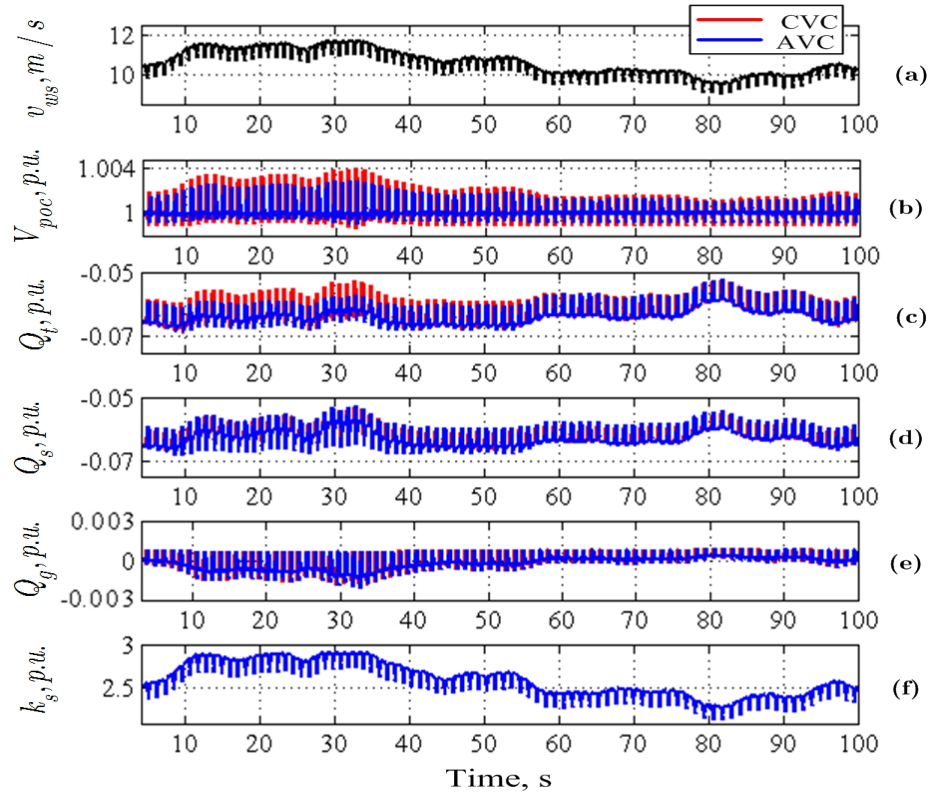

Figure 3.17 Long-term view of system response, SCR=7, X/R = 5: (a) wind speed (b) POC voltage (c) total reactive power (d) stator side reactive power (e) GSC reactive power (f) AVC gain k_s.

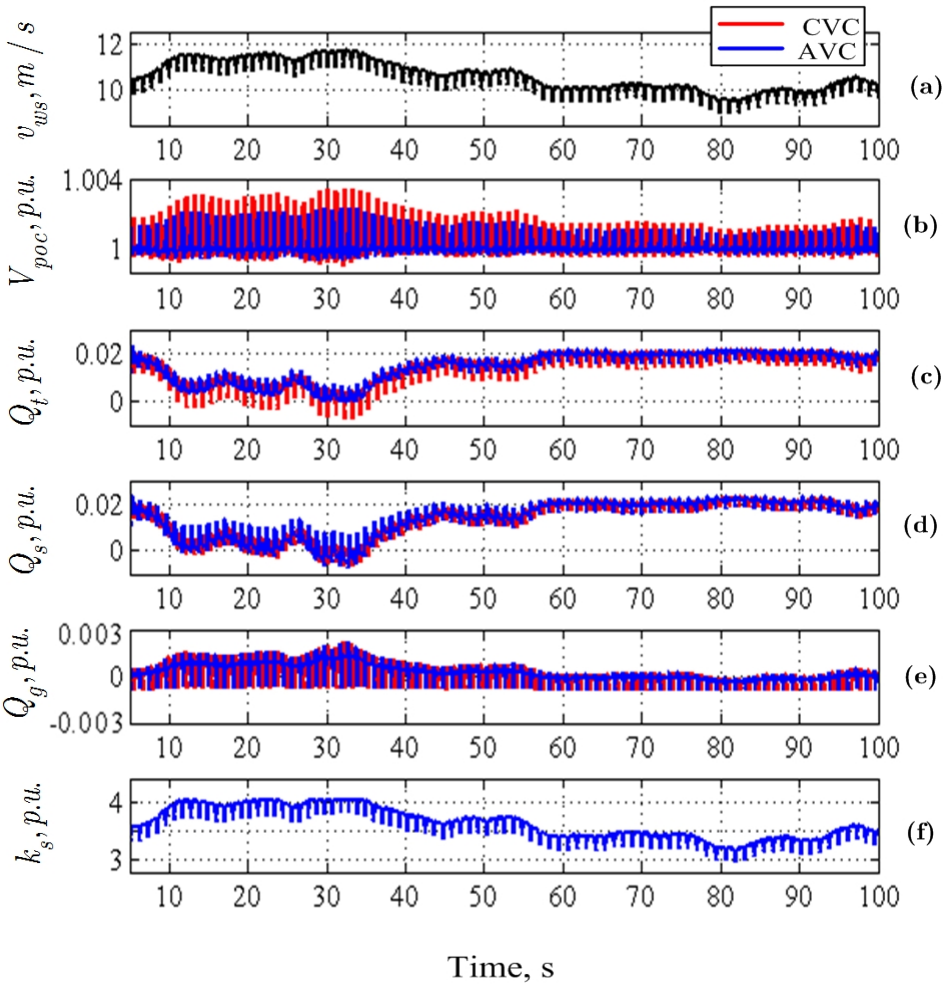

Figure 3.18 Long-term view of system response, SCR= X/R = 10:
(a) wind speed (b) POC voltage (c) total reactive power (d) stator side reactive power (e) GSC reactive power (f) AVC gain ks.

3.4.4 Safe Operation Zones

To further evaluate the effectiveness of the proposed AVC strategy, the safe operation zones are investigated under various conditions, as shown in Fig. 3.19. The safe operation zones are examined under variable wind speed profile as that in Fig. 3.11-a. Furthermore, the examination is carried out for the entire range of SCR and X/R variations. Note that the safe regions are shown only for X/R from 0.5 to 1.0 which denotes the worst conditions whilst, the study has been carried out for the X/R range from 0.5 to 10. In the shown figures, the white-colored regions refer to scenarios with safe operation i.e., the POC voltage is maintained within acceptable limits, ±5% while the grey-colored ones signify the voltage violation scenarios.

The obtained results are carried out by executing numerous simulations to the system of Fig 3.1 using the proposed AVC strategy. Besides, for the shown figure, the

adopted X/R ratio step change is 0.1. As it shows, at a given SCR, the operation regions incur insecure areas particularly at very low X/R ratio and higher output power. This is because the higher output power provokes larger voltage deviations which make the demanded reactive power more vulnerable to the voltage variations especially at very low X/R ratios.

It is worth mentioning that the GSC is additionally overrated to Q_g = 0.38 p.u. (0.86 MVA rating) to tackle the voltage swell for the entire range of SCR with the lowest X/R ratio of 0.5. Subsequently, the POC voltage profile associated with this investigation with the eventual GSC rating is demonstrated in Fig. 3.20.

According to the analytical study conducted in chapter 2, it has been deduced that at very lower SCR and X/R, DFIG requires a certain amount of reactive power to counteract the voltage deviation. This amount of reactive power increases with the SCR at a specific X/R ratio. However, a network with higher SCR is unlikely cause larger voltage perturbation.

From Fig 3.19, At SCR=1"high network impedance", a significant reactive power drawn by the WT ensures safe operation. However, the voltage exceeds the allowable margin for 2≤SCR≤4 as a result of the DFIG and GSC reactive power limitation with maximum voltage detected of 1.066 p.u. at SCR of 3 The corresponding maximum voltage values are tabulated in Table 3.2.

Hence, it can be concluded that for the range 2≤SCR≤4 (with unsafe zones), the grid is more sensitive to voltage deviation and thus requires higher amount of reactive power regulation. Additionally, the maximum sensitivity occurs at SCR=3 which causes maximum detected voltage as depicted in Fig 3.20. Furthermore, the voltage swell decreases again with higher SCR 'lower impedance'. Therefore, For SCR≥5 even with X/R = 0.5, safe operation is ensured.

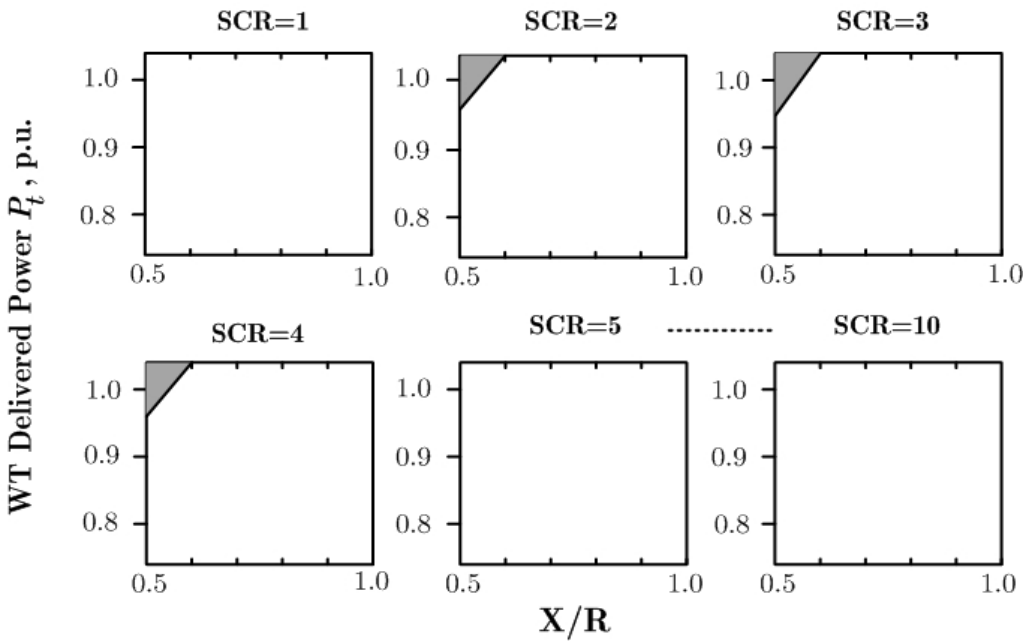

Figure 3.19 Safe operation zones for the entire range of network parameters.

Table 3.2

Maximum detected POC voltage

SCR	2	3	4	5
V_{max} *(p.u.)*	1.054	1.066	1.057	1.048

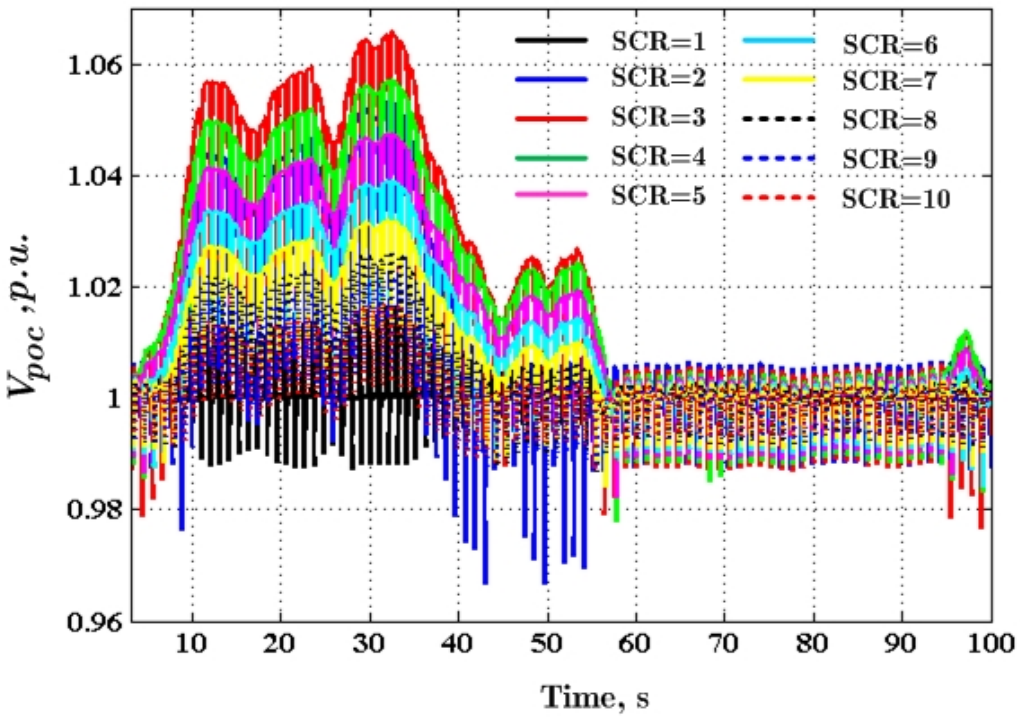

Figure 3.20 POC voltage response with the eventual GSC rating for X/R of 0.5.

3.4.5 Reactive Power Sharing

In order to demonstrate the actual reactive power demand to regulate the voltage for the entire range of network parameters and also the sharing among the DFIG Q_s and the GSC Q_g with the AVC scheme, Fig. 3.21 is presented. The figure depicts the maximum reactive power dictated by Q_s and/or Q_g to compensate the voltage in response to the reactive power dispatch under different network parameters and wind speed. The results conform to that in the analytical study (chapter 2), as larger reactive power is essential to compensate the voltage at very low X/R ratios which necessitates additional GSC Q_g contribution.

Except for some specific conditions such as very low X/R ratios (0.5 to 1), the DFIG can effectively regulate the voltage with the inherent reactive power. Accordingly, the GSC effectively manipulates the reactive power deficit at very low X/R ratios to maintain the voltage as can be seen from the figure.

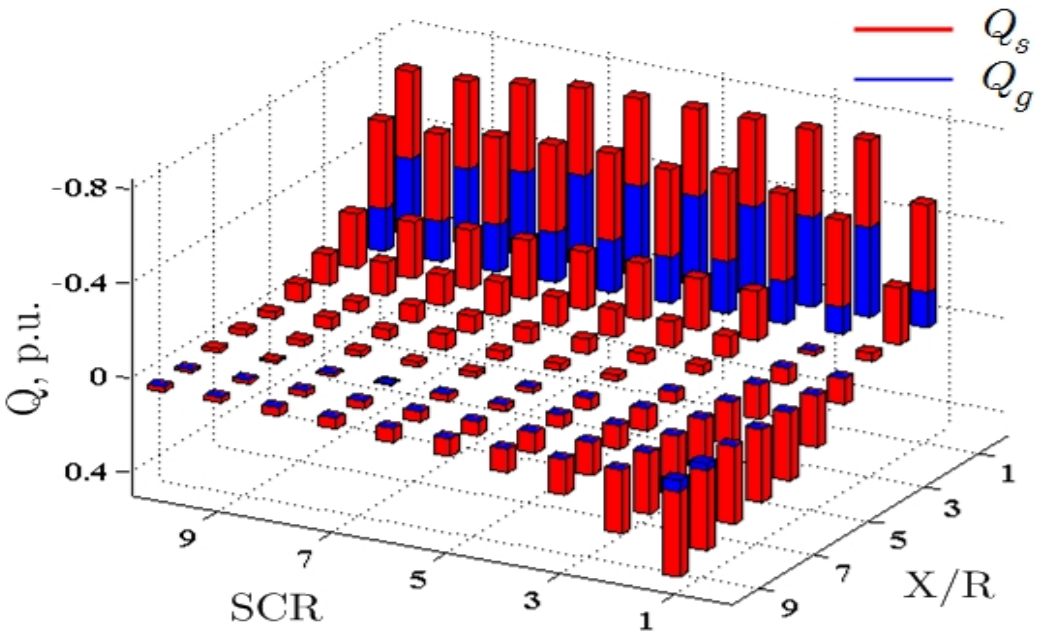

Figure 3.21 Reactive power contributions of the DFIG and GSC for the entire range of network parameters.

3.5 Summary

An AVC strategy for a DFIG variable-speed wind turbine connected to widely varying weak network parameters has been presented in this chapter. A proposed reactive power sharing strategy to manage the reactive power flow from/to the DFIG is also presented. Intensive simulation case studies have been carried out to verify the effectiveness of the proposed AVC scheme. The AVC strategy showed pronounced mitigation capability with better damped performance particularly at very weak grid condition.

Bibliography

[1] M. Ammar, and G. Joos, "Impact of distributed wind generators reactive power behavior on flicker severity," IEEE Trans. Energy Convers., vol. 28, no. 2, pp. 425–433, June. 2013.

[2] W. Hu, Z. Chen, Y. Wang, and Z. Wang, "Flicker mitigation by active power control of variable-speed wind turbines with full-scale back-to-back power converters," IEEE Trans. Energy Convers., vol. 24, no. 3, pp. 640–649, Sep. 2009.

[3] G. Mokryani, P. Siano, A. Piccolo and Z. Chen, "Improving fault ride-through capability of variable speed wind turbines in distribution networks", IEEE Sys. Journal., vol. 7, no. 4, pp. 713-722, Dec. 2013.

[4] Z. Zhao, H. Yan, J. Zuo, Y. Tian, and G. Zillante, "A critical review of factors affecting the wind power generation industry in China" Ren. Sus. Energy Rev., vol. 19, no. 7, pp. 499-508, Mar. 2013.

[5] X. Chen, et.al., "Increasing the flexibility of combined heat and power for wind power integration in china: modeling and implications" IEEE Trans. Power Syst. vol. 30, no. 4, pp. 1848–1857, July. 2015.

[6] N. P. W. Strachan, and D. Jovcic, "Stability of a variable-speed permanent magnet wind generator with weak AC grids", IEEE Trans. Power Del., vol. 25, no. 4, pp. 2779-2788, Oct. 2010.

[7] European Standard. EN 50160, voltage characteristics of electricity supplied by public electricity networks; 2011.

[8] Y. Zhang, Z. Chen, W. Hu, and Cheng, "Flicker mitigation by individual pitch control of variable speed wind turbines with DFIG," IEEE Trans. Energy Convers.,

vol. 29, no. 1, pp. 20–28, Mar. 2014.

[9] L. Yang, Z. Xu, J. Østergaard, Z. Y. Dong, and K. P. Wong, "Advanced control strategy of DFIG wind turbines for power system fault ride through", IEEE Trans. Power Syst., vol. 27, no. 2, pp. 713-722, Jul. 2012.

[10] G. Michalke , "Variable speed wind turbines modelling, control, and impact on power systems," PhD thesis, Darmstadt Technical University, Germany, 2008.

[11] M. E. Montilla-DJesus, D. Santos-Martin, S. Arnaltes, and E. D., Castronuovo, "Optimal operation of offshore wind farms with line-commutated HVDC link connection," IEEE Trans. Energy Convers., vol. 25, no. 2, pp. 504–513, June. 2010.

[12] S. Lo, and C. Wu, "Evaluating the performance of wind farms in China: An empirical review" Electrical Power and Energy Systems., vol. 69, no. 1, pp. 58 – 66, July. 2015.

[13] D. S. L. Dolan and P. W. Lehn, "Simulation model of wind turbine 3p torque oscillations due to wind shear and tower shadow," IEEE Trans. Energy Convers., vol. 21, no. 3, pp. 717–724, Sep. 2006.

[14] T. Ejdemo, and P. Söderholm, "Wind power, regional development and benefit-sharing: The case of northern Sweden" Ren. Sus. Energy Rev., vol. 47, no. 7, pp. 476-485, July. 2015.

[15] F. D. Kanellos, and N. D. Hatziargyriou, "The effect of variable-speed wind turbines on the operation of weak distribution networks," IEEE Trans. Energy Convers., vol. 17, no. 4, pp. 543–548, June. 2010.

[16] C. Han, et.al. , "STATCOM impact study on the integration of a large wind farm into a weak loop power system," IEEE Trans. Energy Convers., vol. 23, no. 1, pp. 226–133, Mar. 2008.

Chapter 4

Fault Ride-through FRT Response for DFIG WT Connected to a Stiff Network

This chapter presents a new decentralized control strategy for a Doubly-fed Induction generator wind turbine, DFIG WT connected to a stiff network considering the Danish grid code requirements. A nonlinear controller is adopted for the grid side converter, GSC, to ensure decoupled control of the DC link voltage and the reactive power, and counteract the DC link voltage run-away. Moreover, the GSC is dedicated to inject more reactive power during voltage dips to satisfy the grid code reactive power support obligation. A conventional PI controller is devoted to control the rotor side converter, RSC, with additional compensation terms to reduce the rotor over-speed, and limit the rotor and stator large transient currents. A diverse set of symmetrical and asymmetrical voltage excursions are investigated to evaluate the effectiveness of the proposed method using MATLAB/SIMULINK environment.

4.1 Introduction

According to the modern grid codes, newly installed wind turbines must provide higher fault ride-through (FRT) capability against various faults and meanwhile support the power system. Grid support during contingencies is inevitable otherwise tripping of large WPPs during system faults would result in significant loss of power supply which can seriously affect system stability and reliability.

Recently, variable-speed wind turbine based Doubly-fed Induction generator is the most commonly used wind turbine technology in large WPPs, e.g., the Danish offshore wind farm Horns Rev [2]. This is mainly due to the rotor circuit partial scale converters compared to the full scale converters concept (type D) which is considered as a main financial aspect. Such converters offer a potential control which can be exploited in FRT and grid support purposes. Despite the financial advantage, partial scale converters require careful protection against system faults which typically results in remarkable over currents and overvoltage as well [3]-[6].

Generally speaking, two main drawbacks are reported in the literature for the DFIG operation during faults which are the higher transient stator and rotor currents at the instant of a fault as well as DC link overvoltage due to the incapability of the grid side converter, GSC to transmit the rotor circuit power [3]-[8].

Traditionally, a crowbar is inserted in the rotor circuit and activated during faulty conditions to address the aforementioned shortcomings. However, once the crowbar is activated, the rotor side converter, RSC is disabled and its control is temporarily lost, meanwhile the machine behaves as an induction motor drawing higher reactive power [8]. Advanced control strategies for DFIG have proven to be the optimal solution to ride-through the DFIG drawbacks during faults [2]-[8]. In the literature, significant focus was given to FRT against symmetrical faults only while investigation of DFIG support capability against asymmetrical faults was not sufficient.

This chapter presents a new decentralized control strategy for the control of a DFIG WT connected to a stiff network to ride-through different disturbances as well as to fulfill the Danish grid code commitments as an example. A nonlinear feedback controller is proposed for the GSC to achieve independent control between the DC link voltage and the reactive power, suppress the DC voltage fluctuations and concurrently inject reactive power during contingencies to fulfil the reactive power support requirement. Additional proposed terms are incorporated with the conventional PI controller of the RSC, with the target of reducing the rotor and stator currents during faulty conditions and limiting the rotor over-speed as well.

4.2 DFIG Dynamic Response during Faults

Figure 4.1 demonstrates a schematic representation of a DFIG wind turbine connected to a stiff grid through 20 km double transmission line. The system comprises a 2 MW DFIG WT. The WT -represented with the rotor as a two mass model- is operated according to the well-known maximum power point tracking, MPPT to extract the maximum available power at each wind speed below the rated value and holds a constant power over the rated wind speed. The DFIG rotor speed is controlled via the pitch angle controller having a structure as earlier in chapter 3. The DFIG is connected to the ac system through two PWM back-to-back AC-DC-AC partial converters and a coupling transformer. The transmission line is attached to the main grid through a high voltage transformer.

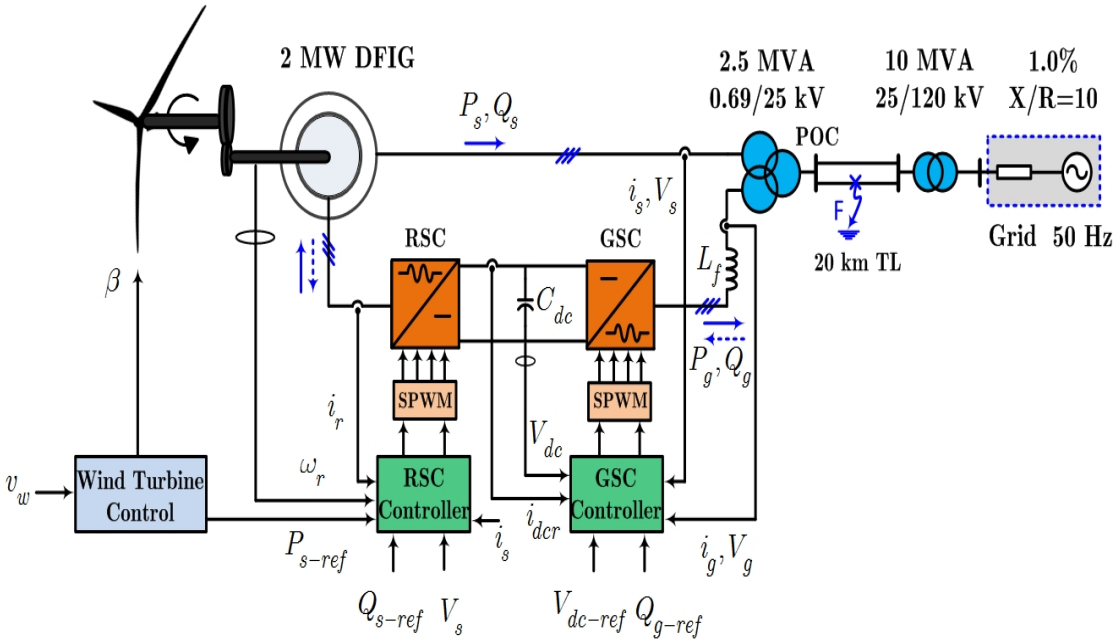

Figure 4.1 Schematic representation of the DFIG WT grid connected system.

4.2.1 Grid Side Converter GSC

Considering the grid side converter GSC connected to the ac grid as shown in Fig 4.1, the voltage at the GSC terminals can be expressed as:

$$v_{gabc} = R_f i_{abc} + L_f \frac{di_{abc}}{dt} + v_{cabc} \tag{4.1}$$

The model of the GSC in a dq reference frame whose d-axis is aligned with the grid voltage vector is described by the following set of differential equations:

$$\frac{di_{dg}}{dt} = -\frac{R_f}{L_f} i_{dg} + \omega_g i_{qg} + \frac{1}{L_f}\left(v_{dg} - v_{dc}\right) \tag{4.2}$$

$$\frac{di_{qg}}{dt} = -\frac{R_f}{L_f} i_{qg} - \omega_g i_{dg} + \frac{1}{L_f}\left(v_{qg} - v_{qc}\right) \tag{4.3}$$

Where, subscripts, v,i,ω, signify voltage, current, and angular speed. Subscripts, g,c refer to grid and converter sides. Indexes d,q stand for direct and quadrature axes of dq reference frame. R_f,L_f refer to resistance and inductance of the GSC interface reactor.

The active and reactive power exchange between the GSC and the grid can be formulated as:

$$P_g = \frac{3}{2}\left(v_{dg} i_{dg} + v_{qg} i_{qg}\right) \tag{4.4}$$

$$Q_g = \frac{3}{2}\left(v_{qg} i_{dg} - v_{dg} i_{qg}\right) \quad (4.5)$$

As the d-axis of the dq reference frame is aligned with the grid voltage, it follows that:

$$v_{dg} = V_g, v_{qg} = 0 \quad (4.6)$$

It follows that the exchanged active and reactive power are simplified to:

$$P_g = \frac{3}{2} v_{dg} i_{dg} \quad (4.7)$$

$$Q_g = -\frac{3}{2} v_{dg} i_{qg} \quad (4.8)$$

As seen from (4.7), (4.8), active and reactive powers can be independently controlled via acting on active and reactive power current components, i_{dg},i_{qg} respectively.

4.2.1.1 Conventional GSC Controller

The GSC controller is devoted to regulate the DC link voltage, V_{dc} and control the reactive power flow between the GSC and the grid Q_g. Under normal conditions, the GSC usually operates with a unity power factor by regulating Q_g to zero. The DC link voltage and reactive power are controlled via regulating the grid side converter current components i_{dg},i_{qg} respectively. The output of the control loops is the GSC reference voltage $v_{gabc-ref}$. The GSC conventional control strategy is illustrated in Fig. 4.2.

Subsequent to a fault, a large transient rotor current will flow and a surplus rotor power as well which need to be transmitted by the GSC. Nonetheless, due to the lack of sufficient ac voltage at the GSC terminals, the DC link voltage rises quickly [5]. Also, the more the GSC is incapable of transmitting the power to/from the grid, the higher the GSC current, which can be destructive to the converter switches. To overcome this shortcoming, a faster GSC control method with higher ability to decouple the GSC control variables should be employed, which is elaborated next.

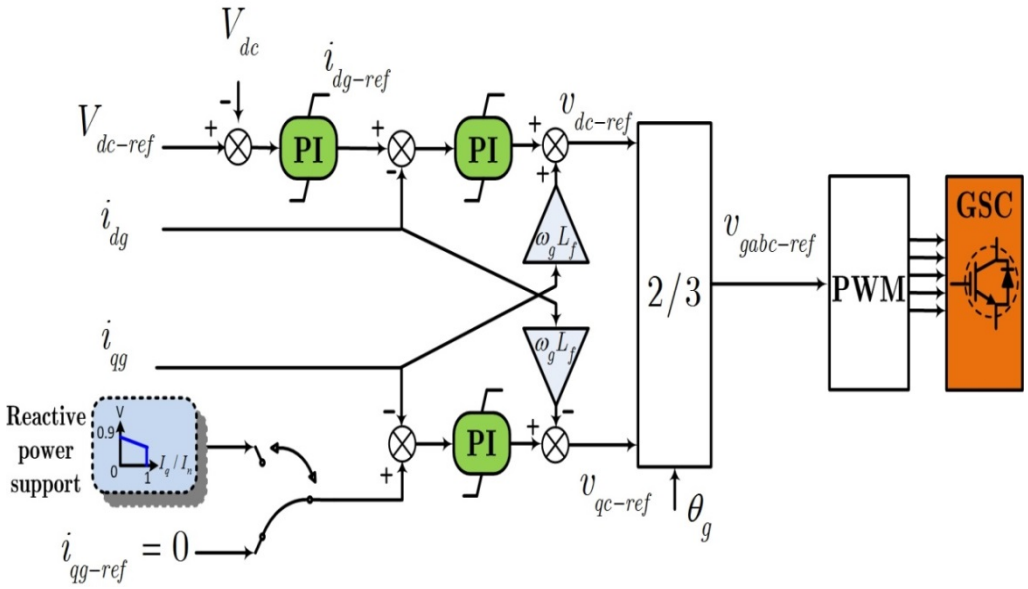

Figure 4.2 GSC conventional control strategy.

4.2.1.2 Proposed GSC Nonlinear Controller

The conventional PI controllers suffer poor and sluggish response especially during transients due to the coupling among its control loops [3]. This coupling makes the control loops of PI controllers highly interactive. Nonlinear feedback linearization controller has been introduced to improve the system transient performance. As noticed from (4.2), (4.3), a coupling between active and reactive current components equations exists although the model is translated into rotating reference frame. Accordingly, nonlinear state feedback type control scheme is introduced to provide decoupling and linearized relation between the system control variables which renders fast and improved performance especially during transients. The nonlinear feedback control is proposed to ensure better transient performance and decoupled control between the DC link voltage and the reactive power. Figure 4.3 shows a block diagram of the proposed nonlinear control strategy.

Similar to the conventional GSC controller, the output of the nonlinear control loops is the GSC reference voltage $v_{gabc-ref}$. Figure 4.3 illustrates the GSC proposed nonlinear control scheme. The input variables of the nonlinear controller are defined as:

$$y_1 = V_{dc}, y_2 = Q_g \tag{4.9}$$

The DC link dynamics can be described by:

$$\dot{y}_1 = \frac{1}{C_{dc}}\left(i_{dcg} - i_{dcr}\right) \tag{4.10}$$

Assuming lossless GSC,

$$P_{dc} = V_{dc} i_{dcg} = P_g - P_f \tag{4.11}$$

Where,

C_{dc},i_{dcg},i_{dcr} are the DC link capacitance and currents respectively (see Fig 4.3). P_{dc},P_f are the DC link transmitted power and the power loss through the interface reactor connecting the GSC to the grid respectively. To achieve linearization between the control algorithm inputs and outputs, "(4.9)", is to be differentiated till a direct relationship between them is obtained as:

$$\begin{bmatrix} \ddot{y}_1 \\ \dot{y}_2 \end{bmatrix} = \begin{bmatrix} A_1 & 0 \\ 0 & A_3 \end{bmatrix} \begin{bmatrix} v_{dc} \\ v_{qc} \end{bmatrix} + \begin{bmatrix} A_2 \\ A_4 \end{bmatrix} \tag{4.12}$$

Where,

$$A_1 = -\frac{3}{2L_f C_{dc} V_{dc}} v_{dg} + \frac{3R_f}{L_f C_{dc} V_{dc}} i_{dg} \tag{4.13}$$

$$A_2 = \frac{3R_f^2}{L_f C_{dc} V_{dc}} i_{dg}^2 - \frac{3R_f}{L_f C_{dc} V_{dc}} P_g + \frac{\omega_g}{C_{dc} V_{dc}} Q_g + \frac{3}{2L_f C_{dc} V_{dc}} v_{dg}^2 - \frac{3R_f \omega_g}{C_{dc} V_{dc}} i_{dg} i_{qg} + \frac{3}{2C_{dc} V_{dc}} v_{qg} \frac{di_{qg}}{dt} - \frac{3R_f}{C_{dc} V_{dc}} i_{qg} \frac{di_{qg}}{dt} - \frac{1}{C_{dc}} \frac{di_{dcr}}{dt} \tag{4.14}$$

$$A_3 = -\frac{3}{2L_f} v_{dg} \tag{4.15}$$

$$A_4 = \frac{3}{2L_f} v_{dg} v_{qg} - \omega_g P_g - \frac{R_f}{L_f} Q_g + \frac{3}{2} i_{qg} \frac{dv_{dg}}{dt} \tag{4.16}$$

To obtain linear decoupled relationship with good tracking performance even with parameter uncertainty, v_{dc-ref} , v_{qc-ref} are expressed as [9]:

$$v_{dc-ref} = \frac{1}{A_1}\left(k_1 e_1 + k_2 \int e_1 dt + k_3 \dot{e}_1 + \ddot{y}_1^* - A_2\right) \tag{4.17}$$

$$v_{qc-ref} = \frac{1}{A_3}\left(k_4 e_2 + k_5 \int e_2 dt + \dot{y}_2^* - A_4\right) \tag{4.18}$$

Where,

$$e_1 = y_1^* - y_1,\ e_2 = y_2^* - y_2 \tag{4.19}$$

Substituting, (4.17), (4.18) into (4.12), yields a decoupled system error model as:

$$\dddot{e}_1 + k_3\ddot{e}_1 + k_1\dot{e}_1 + k_2 e_1 = 0 \tag{4.20}$$

$$\ddot{e}_2 + k_4\dot{e}_2 + k_5 e_2 = 0 \tag{4.21}$$

Where, k_i (i=1,2,3,4,5) are design control gains which can be selected to optimize the controller performance.

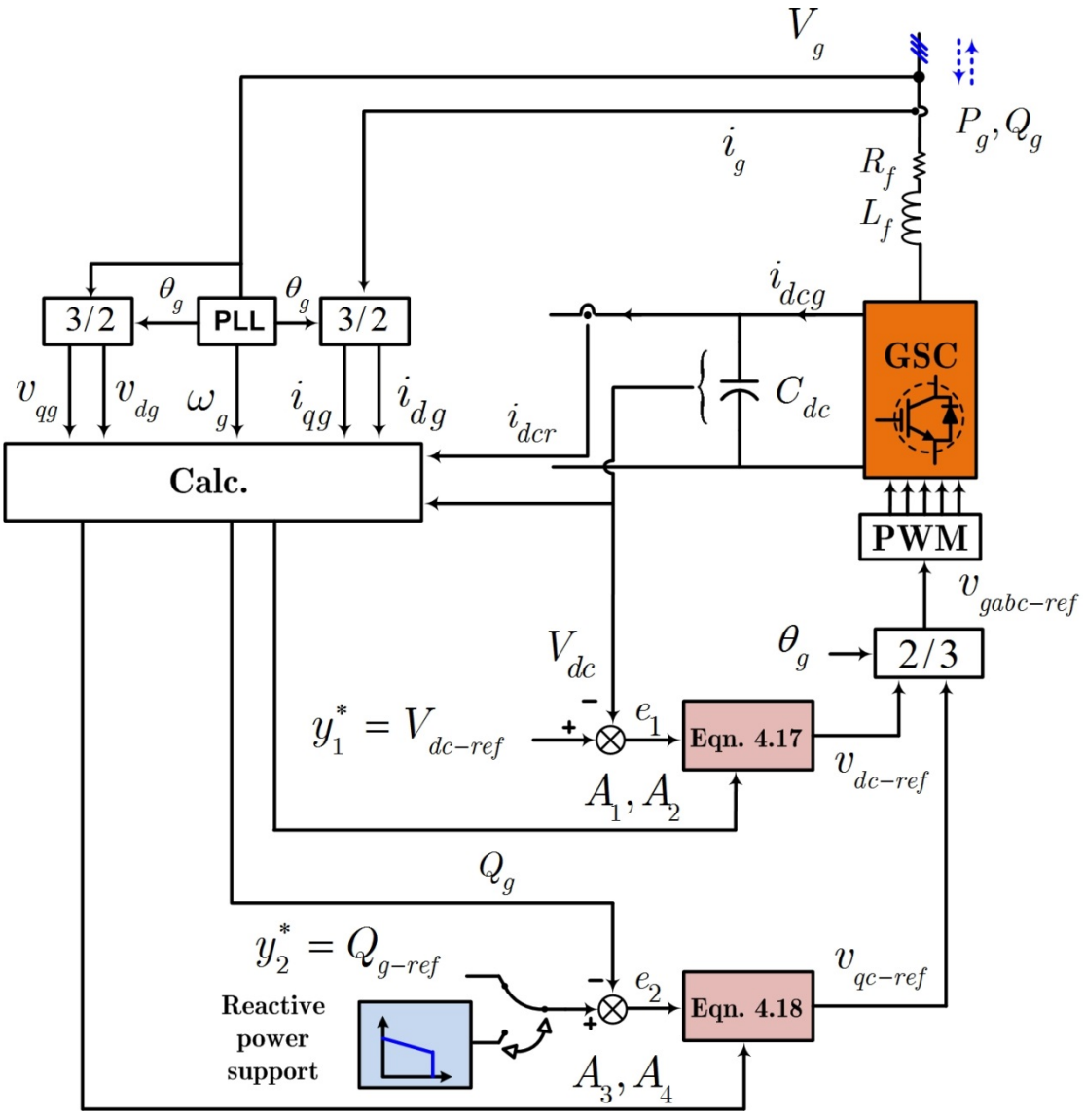

Figure 4.3 Proposed nonlinear control scheme for GSC

4.2.2 Rotor Side Converter RSC

The control structure of the RSC side is as shown in Fig. 4.3. The RSC control strategy is implemented in a synchronous reference frame with the d-axis oriented with the DFIG stator voltage [10]. The RSC is dedicated to ensure decoupled control of stator side active and reactive powers and also to provide the DFIG with a variable speed operation (±30% speed range). The stator active and reactive powers,P_s,Q_s are controlled via controlling the rotor side current components,i_{dr},i_{qr} respectively. The output of the control loops is the RSC input voltage, $v_{rabc-ref}$. During normal operation, the DFIG is controlled to achieve variable speed operation according to the MPPT while absorbing the required excitation Q_{sn-ref} from the reactive power control loop [10].

According to the Danish grid code, the supply of reactive power has the first priority in area B over the active power supply (see Fig. 1.9). However, a suitable margin of active power must be retained in proportion to the voltage dip magnitude [11]. Therefore, once a faulty condition is detected, the MPPT is deactivated and the active power is kept to a minimum value to help suppress rotor and stator currents as well as to limit rotor over-speed. Furthermore, the RSC controller can contribute to additional reactive power support with the remnant reactive current to satisfy the reactive power support criterion.

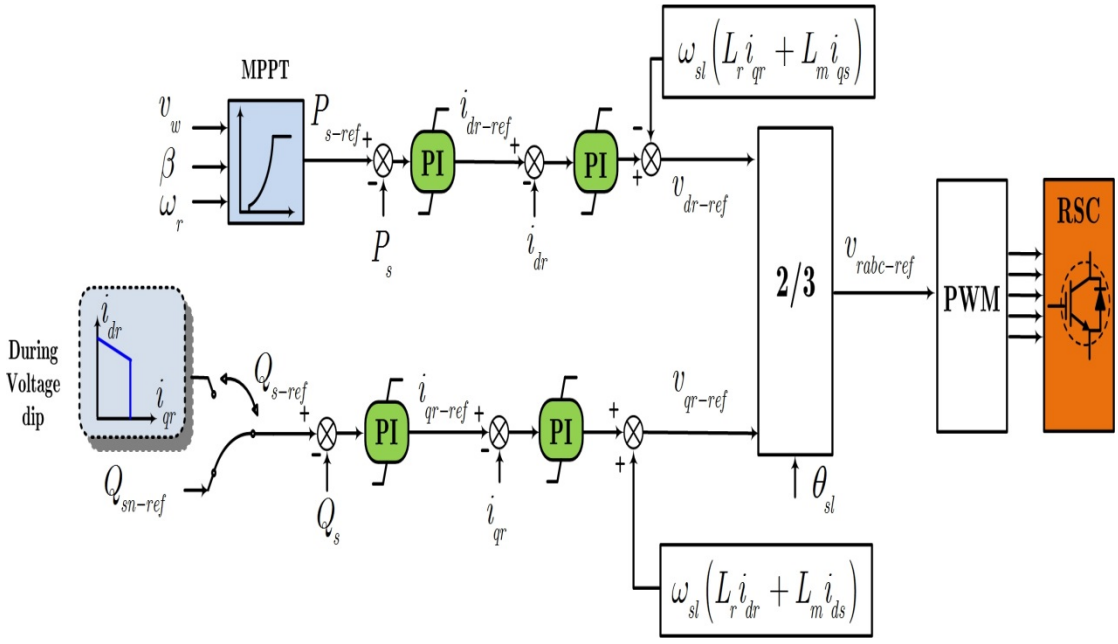

Figure 4.4 RSC control strategy.

4.3 Results and Discussions

To investigate the DFIG dynamic performance under different operating conditions, a set of case studies are performed for the system under study shown in Fig. 4.1. The system is simulated in the MATLAB/SIMULINK environment using SimPowerSystems toolbox and Simulink for system modeling and simulation. The system parameters are listed in Appendix C. The case studies are carried out at the nominal wind speed of the WT (11.4 m/s). Among the different simulation tests, certain safe limits (marked with dashed lines in the output results) are imposed on the system variables for protection purpose.

4.3.1 LVRT and Grid Code Compliance

The system response to a three-phase fault in the middle of one of the transmission lines (see Fig. 4.1) with duration of 0.5 s is illustrated in Fig. 4.5. The fault results in stator voltage dip close to 0.2 p.u (Fig. 4.5-a). At the instant of voltage dip, higher stator and rotor currents are noticed as in Fig. 4.5-b,c. Owing to the abrupt increase of the rotor current, the rotor power which is fed to the GSC through the DC link simultaneously increases, which causes higher DC voltage oscillations due to lower ac voltage at the GSC terminals.

Higher DC voltage fluctuation in case of the conventional controller is recorded in Fig. 4.5-e compared to that of the proposed controller. This can be attributed to the fast injection of reactive power (Fig. 4.5-g) which contributes to supporting the ac voltage and consequently transporting more power through the GSC, and eventually results in relieving the DC voltage fluctuations.

Since the voltage drop impedes transferring all the wind mechanical power, the mismatch between the electromagnetic and mechanical torques results in rotor over-speed [7], as in Fig. 4.5-d but remains within the allowed limit. The active power in Fig. 4.5-f is reduced at the fault instant to a minimum value to limit the rotor over-speed and the system currents.

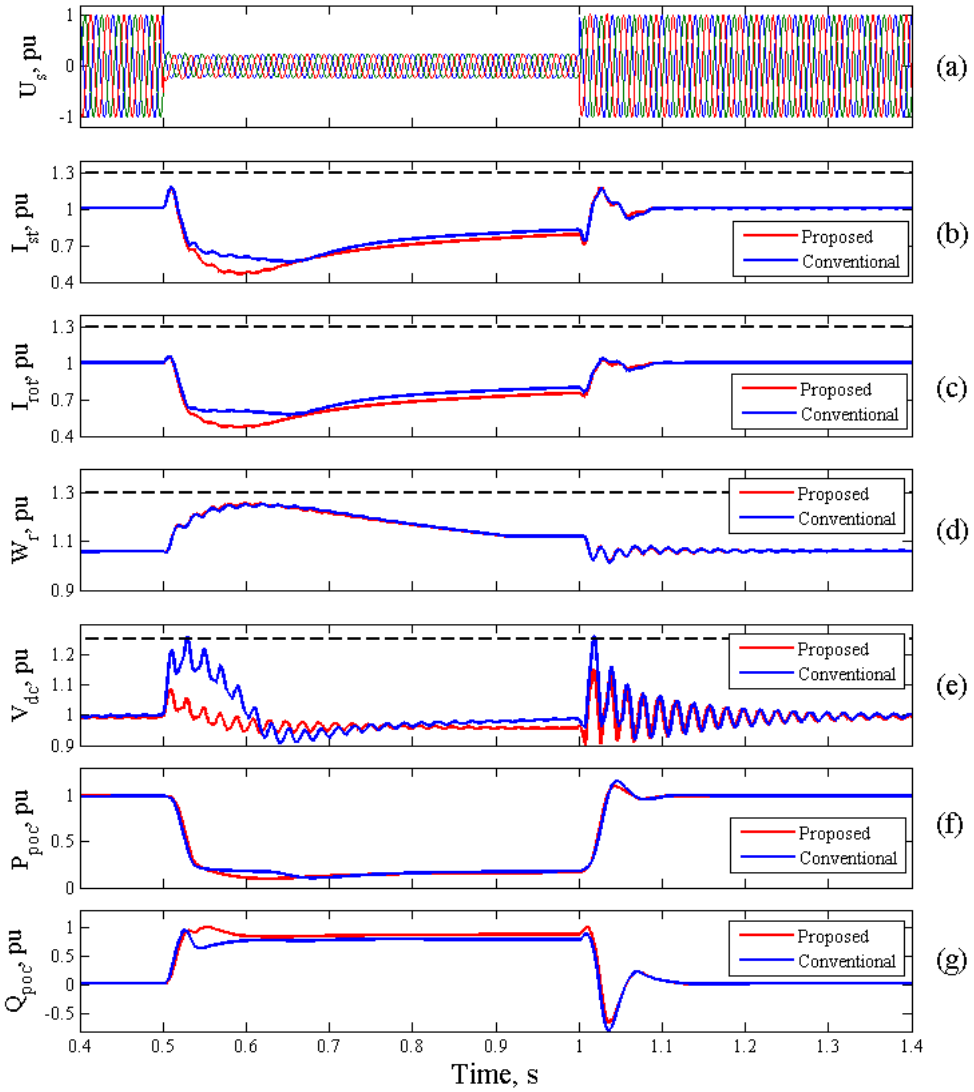

Figure 4.5 Response of the DFIG WT system to a three-phase fault: (a) DFIG stator voltage (b) Stator current (c) Rotor current (d) DFIG rotor speed (e) DC link voltage (f) Delivered active power (g) Delivered reactive power.

4.3.2 Asymmetrical Faults Response

Asymmetrical faults are recurring and lead to negative sequence currents of double frequencies which usually accompanied with higher oscillations that propagate in the DC link and may cause transient overvoltage [6]. The system responses to a single phase-to-ground and phase-to-phase faults are shown in Figs. 4.6,4.7 respectively. The faults occur at t = 0.5 s and cleared 150 ms later and cause 58% and 37% voltage dip respectively. It is obvious that double frequency component due to negative sequence currents is superimposed on the DC link voltage waveform as seen in Figs. 4.6-e, 4.7-e.

Comparing the results, it can be concluded that the phase-to-phase fault is severer as it causes higher voltage drop. Accordingly, higher DC link oscillations close to the limit are depicted in Fig. 4.7-e. |Besides, the proposed controller is superior to its counterpart in both cases as it encounters lower overshoots, shorter settling time with damped performance. The rotor speed, stator and rotor currents are maintained below the limit in both methods.

4.3.3 HVRT Response

To validate the HVRT requirement of the Danish grid code, a double-open circuit fault at the point of common connection POC for 200 ms is applied and the obtained results are shown in Fig. 4.8. The stator voltage magnitude (Fig. 4.8-b) fluctuates during the fault and even exceeds the Danish grid code limit (1.2 p.u.). At the fault onset, the delivered active power rises which in turn increases the power fed to the GSC and thus leads to higher DC voltage oscillations. The DC link voltage in case of conventional controller violates the limit. To counteract the voltage swell, the stator and rotor currents start to decrease to render the active power constant while the active power fluctuates around the nominal value. Compared with the conventional controller, the proposed controller has a higher capability to overcome the voltage swell and significant better damped transient performance.

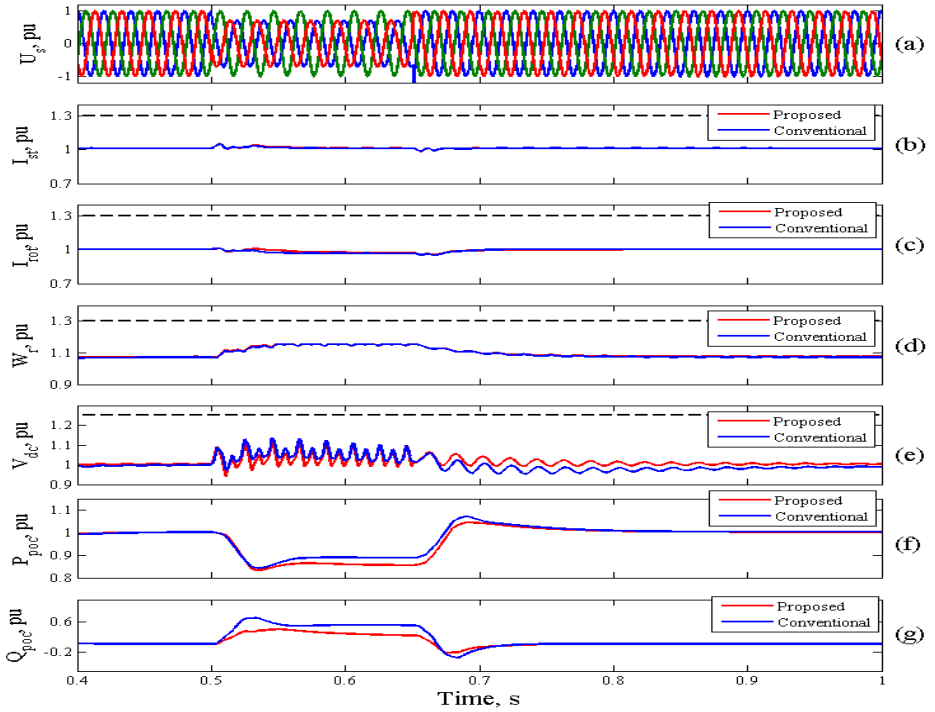

Figure 4.6 Response of the DFIG WT system to a single-phase to ground fault (a) DFIG stator voltage (b) Stator current (c) Rotor current (d) Rotor speed (e) DC link voltage (f) Delivered active power (g) Delivered reactive power.

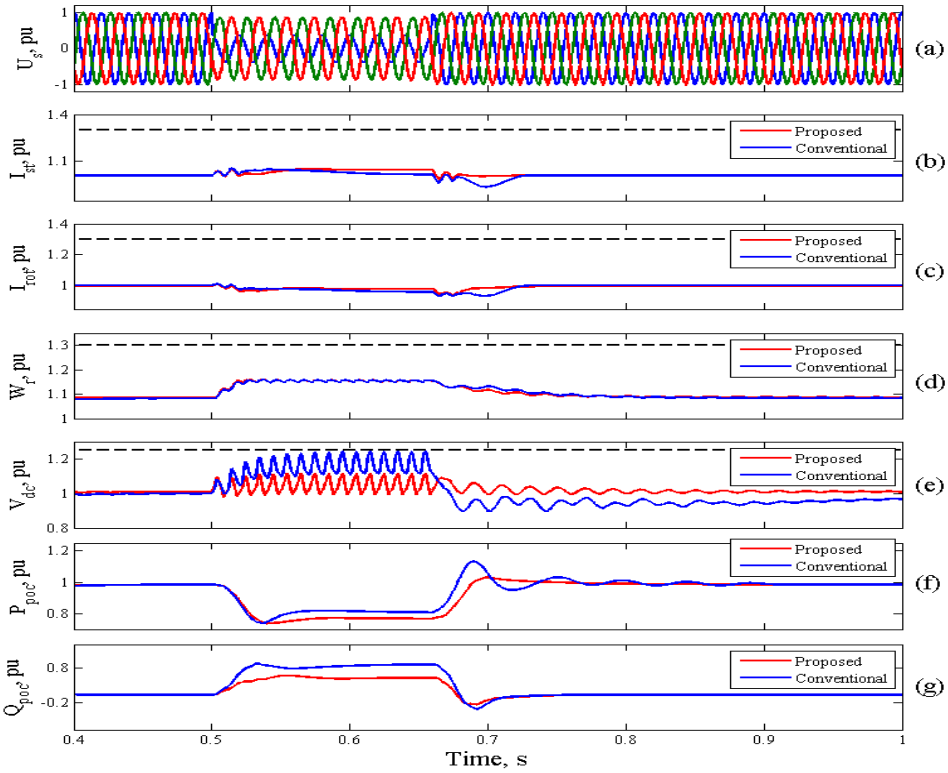

Figure 4.7 Response of the DFIG WT system to a phase-to-phase fault: (a) DFIG stator voltage (b) Stator current (c) Rotor current (d) DFIG rotor speed (e) DC link voltage (f) Delivered active power (g) Delivered reactive power.

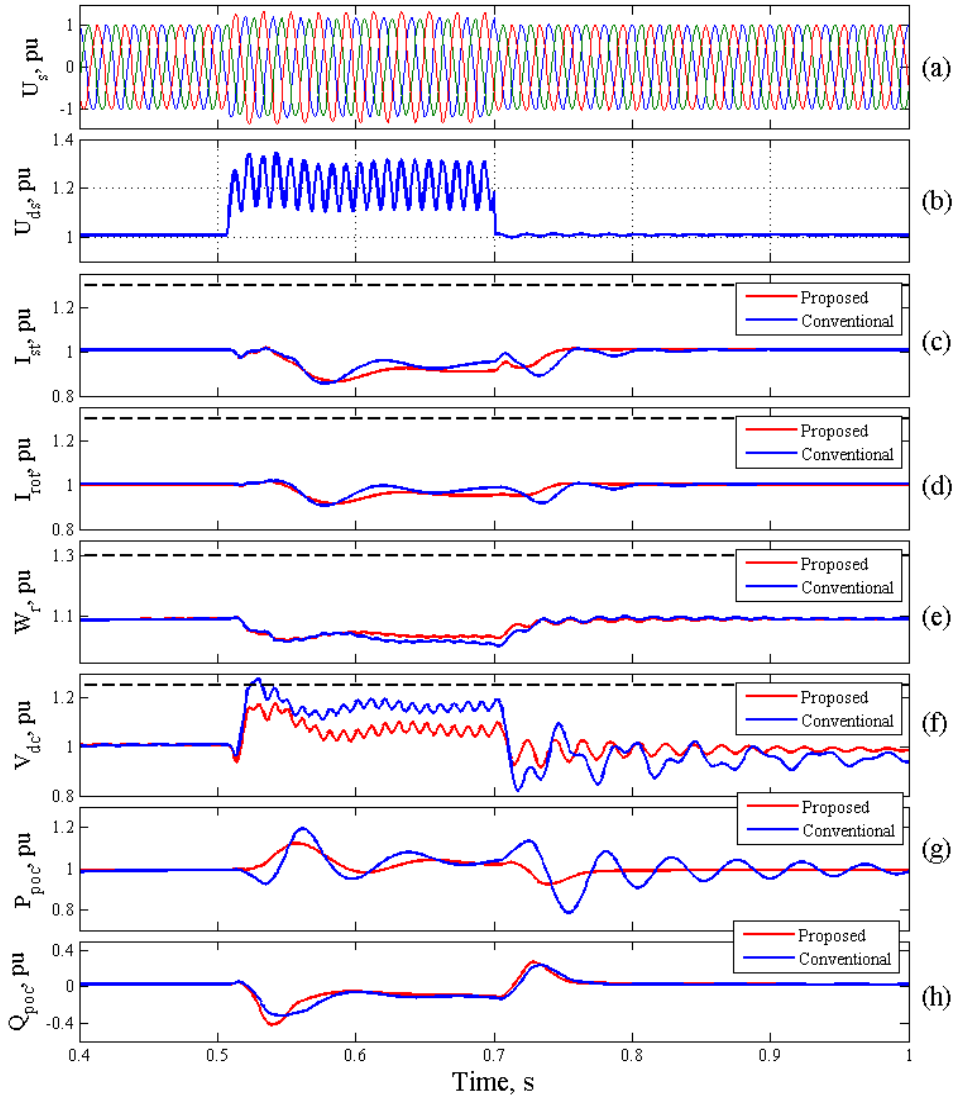

Figure 4.8 Response of the DFIG WT system to a double open circuit fault at the POC: (a) DFIG stator voltage (b) Stator voltage magnitude (c) Stator current (d) Rotor current (e) DFIG rotor speed (f) DC link voltage (g) Delivered active power (h) Delivered reactive power.

4.4 Summary

In this chapter, the dynamic behavior of a DFIG WT connected to a stiff network during system faults has been investigated. A nonlinear controller has been presented for the GSC to achieve high dynamic performance, decoupled control between the DC link voltage and reactive power and meanwhile injects reactive power during voltage dips to support the system voltage.

Additionally, the obtained output results reveal fast response with high dynamic performance for a wide range of operating conditions and assure the FRT

capability of the proposed control strategy in compliance with the Danish grid code without additional hardware circuits.

Bibliography

[1] M. Mohseni and S. M. Islam, "Review of international grid codes for wind power integration: diversity, technology and a case for global standard", *Ren. Sustain. Energy Rev.,* vol. 16, no. 6, pp. 3876-3890, Aug. 2012.

[2] G. Michalke, "Variable speed wind turbines modelling, control, and impact on power systems," PhD thesis, Darmstadt Technical University, Germany, 2008.

[3] M. Mohseni and S. M. Islam, "Transient Control of DFIG-Based Wind Power Plants in Compliance With the Australian Grid Code", IEEE Trans. Power Electron., vol. 27, no. 6, pp. 2813-2824, Jun. 2012.

[4] C. Wessels, F. Gebhardt, and F. W. Fuchs, "Fault ride-through of a DFIG wind turbine using a dynamic voltage restorer during symmetrical and asymmetrical grid faults", IEEE Trans. Power Electron., vol. 26, no. 3, pp. 807-815, Mar. 2011.

[5] T. Sun, Z. Chen, F. Blaabjerg, "Transient Stability of DFIG Wind Turbines at an External Short-Circuit Fault", Wind Energy, 2005, 8:345-360.

[6] X. Yan, G. Venkataramanan, P. S. Flannery, Y. Wang, Q. Dong, and B. Zhang, "Voltage-sag tolerance of DFIG wind turbine with a series grid side passive-impedance network", IEEE Trans. Energy Convers., vol. 25, no. 4, pp. 1048-1056, Dec. 2010.

[7] A. E. Leon, J. M. Mauricio, and J. A. Solsona, "Fault ride-through enhancement of DFIG-based wind generation considering unbalanced and distorted conditions", IEEE Trans. Energy Convers., vol. 27, no. 3, pp. 775-783, Sept. 2012.

[8] L. Yang, Z. Xu, J. Østergaard, Z. Y. Dong, and K. P. Wong, "Advanced control strategy of DFIG wind turbines for power system fault ride through", IEEE Trans. Power Syst., vol. 27, no. 2, pp. 713-722, Jul. 2012.

[9] S. Abulanwar, Zhe Chen and Birgitte Bak-Jensen, "Study of DFIG Wind Turbine Fault Ride-Through According to The Danish Grid Code" in Proc. IEEE Power & Energy Society General Meeting, Vancouver, Canada, 2013.

[10] R. Sarrias, L. M. Fernández, C. A. García, and F. Jurado, "Coordinate operation of power sources in a doubly-fed induction generator wind turbine/battery hybrid power system", Power sources., vol. 205, no. 1, pp. 354-336, May 2012.

[11] Energinet. Technical regulation 3.2.5 for wind power plants with a power output greater than 11 kW; September 2010. Available at: http://www.energinet.dk.

Chapter 5

Fault Ride-through FRT Response for DFIG WT Connected to a Weak Network

An enhanced coordinated low voltage ride-through, LVRT, control strategy for a Doubly-fed Induction generator (DFIG)-based wind energy conversion system, WECS, connected to a weak grid is presented in this chapter. The compliance with the grid code commitments is also considered. A proposed decoupled double synchronous reference frame (DDSRF) current controller is adopted for the design of grid side converter, GSC, controller to counteract current oscillations during asymmetrical faults and tackle the DC link voltage run-away. For a precise detection of the grid voltage position even under severe voltage dips/unbalanced conditions, A DDSRF-PLL is proposed and analyzed to extract clean synchronization signal in order to improve the overall system performance. Moreover, a fast decomposition based positive and negative sequence algorithm is utilized for rapid fault detection and to engage the LVRT protection scheme. Furthermore, additional compensation terms are incorporated with the traditional GSC and rotor side converter, RSC, controllers to effectively suppress rotor as well as stator currents and meanwhile regulate the rotor speed. A diverse set of voltage excursions are conducted to evaluate the effectiveness of the proposed control strategy using MATLAB/SIMULINK platform.

5.1 Introduction

Various technical challenges impede the successful integration of wind power into weak power systems. Due to the anticipated integration of more wind energy all over the world, it's expected that the short circuit capacity of power systems will decrease. The increasing integration of renewable energy sources RES into the power systems has resulted in the development of new grid codes devoted to ensure a proper performance under normal as well as abnormal grid conditions [1]. Safety, reliability and efficiency and are now becoming the targets of the control techniques developed by researchers and engineers for the related RES. More specifically, low voltage ride-

through LVRT capability of wind energy conversion systems WECS and the associated control of its power converters are one of the most challenging issues to be improved [2].

In the literature, most of the work about fault ride through FRT of WECS is related to symmetrical grid voltage sags. However, more than 90% of the grid faults lead to asymmetrical voltage excursions with positive and negative sequence components [3],[4]. Unbalanced system voltages can readily generate heating in the WECS generator windings resulting in sustained toque oscillations, and unwanted mechanical vibrations [5]. Additionally, the unbalanced grid voltages can give rise to uncontrolled oscillations in the delivered active and reactive power [6].

Though this effect can be mitigated via injecting reference unbalanced currents, this objective cannot be accurately implemented using the traditional synchronous reference frame SRF dq current controllers which render deficient performance during unbalanced utility conditions [2], [7].

According to some grid codes requirements, WPP has to provide voltage support capability even with zero voltage dip during a system fault [5]. However, the detection of the grid voltage vector position required for the relevant dq transformations and the control algorithms can be challenging in this case. SRF phase-locked loop PLL, are the most intensively used technique for detecting the magnitude and position of the positive-sequence grid voltage [8]. However, its performance during unbalanced utility conditions is poor even with reduced band width.

In this chapter, an improved coordinated fault ride-through FRT control strategy for a doubly fed induction generator DFIG based wind turbine, WT, connected to weak grid is presented. Two different techniques for grid synchronization against voltage excursions, i.e., a Dual Second Order Generalized Integrator – Frequency Locked Loop DSOGI-FLL and a decoupled double synchronous reference frame DDSRF based phase-locked loop, DDSRF-PLL are utilized to extract a robust grid voltage synchronization signal irrespective of the mains condition to enhance the overall system performance. Besides, a decoupled double synchronous reference frame DDSRF dq current controller is devoted for the grid side converter, GSC, controller to counteract current ripples and tackle the DC link voltage fluctuations. Also, a reactive power support scheme to manage the DFIG reactive power during contingencies and fulfil the grid codes obligations is presented.

Moreover, additional control terms are employed with the DFIG converters controllers to counteract rotor as well as stator currents and regulate the rotor speed.

5.2 Grid Synchronization

This section provides conventional as well as advanced synchronization detection techniques used for the orientation of the dq reference frames with the grid voltage so that system converter controllers can function properly during normal and abnormal grid conditions.

5.2.1 SRF-PLL Grid Synchronization

Among the different aspects for the control of the grid connected converters, is the exact synchronization with the utility voltage. Phase Locked Loop (PLL) based synchronous reference frame (SRF-PLL) is the most intensively used technique for detecting the magnitude and position of the positive-sequence grid voltage [8]. The basic structure of SRF-PLL is shown in Fig. 5.1.

The SRF-PLL translates the three phase system voltage from the abc reference frame into rotating dq reference frame using Park's transformation. The dq reference frame angular position θ_s is obtained through regulating the voltage q-component to zero [9]. This estimated phase angle is necessary for the dq transformations in order to implement the control algorithms, obtain active and reactive current components and generate the required voltages at the output terminals of the power converters. The d-component depicts the amplitude of the positive sequence component of the system voltage.

The system voltage dq components using Park's transformation are expressed as:

$$\begin{bmatrix} v_d \\ v_q \end{bmatrix} = [T_\theta] \begin{bmatrix} v_a \\ v_b \\ v_c \end{bmatrix}, [T_\theta] = \frac{2}{3} \begin{bmatrix} \cos(\theta_s) & \cos(\theta_s - 2\pi/3) & \cos(\theta_s + 2\pi/3) \\ -\sin(\theta_s) & -\sin(\theta_s - 2\pi/3) & -\sin(\theta_s + 2\pi/3) \end{bmatrix} \quad (5.1)$$

$$[T_\theta] = [T_{dq}] \cdot [T_{\alpha\beta}], [T_{dq}] = \begin{bmatrix} \cos(\theta_s) & \sin(\theta_s) \\ -\sin(\theta_s) & \cos(\theta_s) \end{bmatrix}, [T_{\alpha\beta}] = \frac{2}{3} \begin{bmatrix} 1 & -1/2 & -1/2 \\ 0 & \sqrt{3}/2 & -\sqrt{3}/2 \end{bmatrix} \quad (5.2)$$

Despite its good behavior under normal conditions, SRF-PLL provides poor dynamic response under unbalanced grid conditions even with reduced bandwidth [8] - [11].

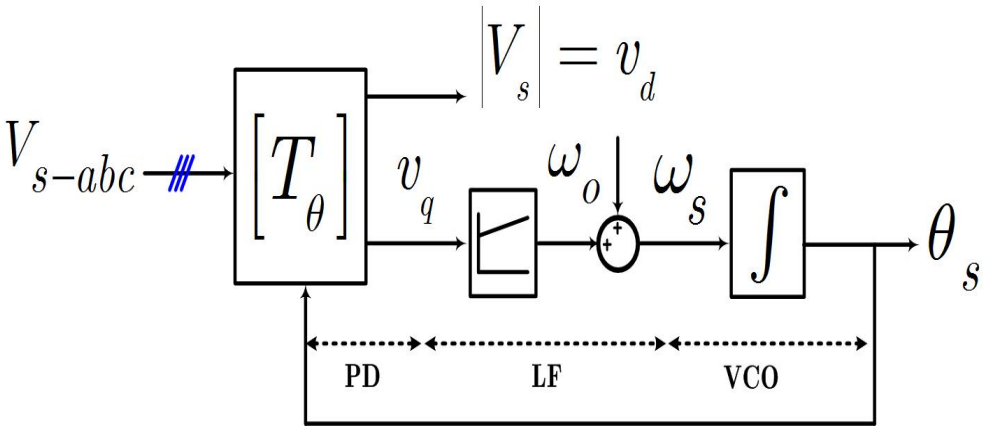

Figure 5.1 SRF-PLL structure.

5.2.2 DDSRF-PLL Grid Synchronization

Decoupled double synchronous reference frame (DDSRF) based PLL is an improved grid synchronization technique that uses two synchronous reference frames rotating with positive and negative synchronous speeds. The purpose of this technique is to decouple the effect of negative sequence component- which is typically existed during unbalanced system voltage- from the detected dq signals of that of the positive synchronous reference frame and vice versa in order to obtain a clean and accurate grid synchronization angle even under severe balanced/unbalanced conditions [8], [10]. The accurate grid voltage angle and detected dq signals will improve the performance of the control scheme of the WECS and also enable fulfilling the grid code requirements during different contingencies.

Figure 5.2 shows the decomposition of the grid voltage during unbalanced condition using double synchronous reference frame DSRF, with positive and negative rotating reference frames (dq^+, dq^-) rotating with the synchronous speed ($\pm\omega'$) with angular positions ($\pm\theta'$) respectively.

Assuming that the angular position of the positive reference frame matches that of the positive sequence voltage vector, $\theta' = \omega t$, hence, the unbalanced voltage vector components using DSRF are expressed as:

$$v_{dq}^{+} = \begin{bmatrix} v_d^{+} \\ v_q^{+} \end{bmatrix} = \left[T_{dq}^{+}\right] \cdot \left[v_{\alpha\beta}\right] = V^{+} + V^{-} \begin{bmatrix} \cos(-2\omega t) \\ \sin(-2\omega t) \end{bmatrix} \tag{5.3}$$

$$v_{dq}^{-} = \begin{bmatrix} v_d^{-} \\ v_q^{-} \end{bmatrix} = \left[T_{dq}^{-}\right] \cdot \left[v_{\alpha\beta}\right] = V^{-} + V^{+} \begin{bmatrix} \cos(2\omega t) \\ \sin(2\omega t) \end{bmatrix} \tag{5.4}$$

Where,

$$\left[T_{dq}^{+}\right] = \left[T_{dq}^{-}\right]^{T} = \begin{bmatrix} \cos(\theta') & \sin(\theta') \\ -\sin(\theta') & \cos(\theta') \end{bmatrix} \tag{5.5}$$

From (5.3), (5.4), it's evident that, a coupling between positive and negative sequence components with double frequency oscillation 2ω exists as a consequence of the rotation of the voltage vectors in opposite directions. In order to cancel out this double frequency oscillation and render accurate response of the voltage components, decoupling terms are employed within the DSRF-PLL.

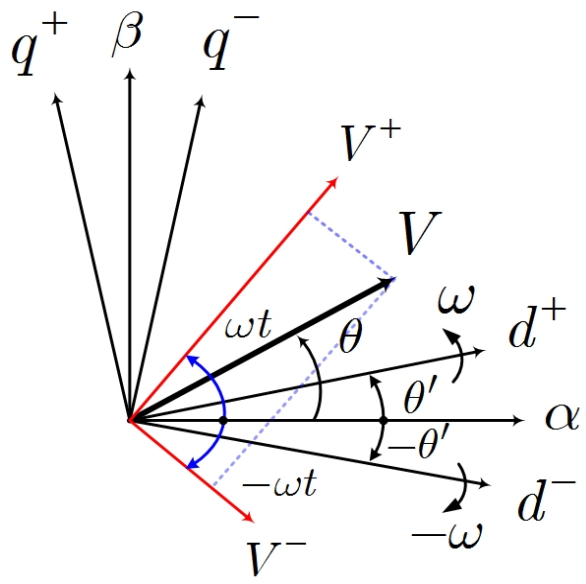

Figure 5.2 DDSRF respective reference frames phasor diagram.

5.2.2.1 Decoupling Terms of the DSRF

Augmenting a decoupling cell allows for cancellation of the reciprocal 2ω coupling effect of positive and negative sequence between both reference frames. Thereby, precise grid synchronization is possible even under unbalance utility conditions. Figure 5.3 shows a block diagram of the DDSRF-PLL. The estimated output *dq* voltage components of the DDSRF-PLL can be formulated as [8]:

$$\bar{V}^{*}_{dq^{+}} = \begin{bmatrix} \bar{V}^{*}_{d^{+}} \\ \bar{V}^{*}_{q^{+}} \end{bmatrix} = [LPF]\left(V_{dq^{+}} - \left[T^{+2}_{dq}\right]\bar{V}^{*}_{dq^{-}}\right) \tag{5.6}$$

$$\bar{V}^{*}_{dq^{-}} = \begin{bmatrix} \bar{V}^{*}_{d^{-}} \\ \bar{V}^{*}_{q^{-}} \end{bmatrix} = [LPF]\left(V_{dq^{-}} - \left[T^{-2}_{dq}\right]\bar{V}^{*}_{dq^{+}}\right) \tag{5.7}$$

Where,

$$LPF(s) = \frac{\omega_f}{\omega_f + s} \tag{5.8}$$

$$\left[T^{+2}_{dq}\right] = \left[T^{-2}_{dq}\right]^{T} = \begin{bmatrix} \cos(2\omega_s t) & \sin(2\omega_s t) \\ -\sin(2\omega_s t) & \cos(2\omega_s t) \end{bmatrix} \tag{5.9}$$

As shown in Fig 5.3, a cross-feedback decoupling cell is augmented to estimate the average value of the positive and negative sequence components of the grid voltage in both reference frames which is $\bar{V}^{*}_{d+}, \bar{V}^{*}_{q+}, \bar{V}^{*}_{d-}, \bar{V}^{*}_{q-}$. The low pass filter, LPF, cut-off frequency, ω_f can be properly set to retain a better damping performance with fast response ($\omega_f = \omega_s / \sqrt{2}$) rad/s. It is worth mentioning that, as the PLL filter is located outside the control loop, the DDSRF-PLL bandwidth is not affected.

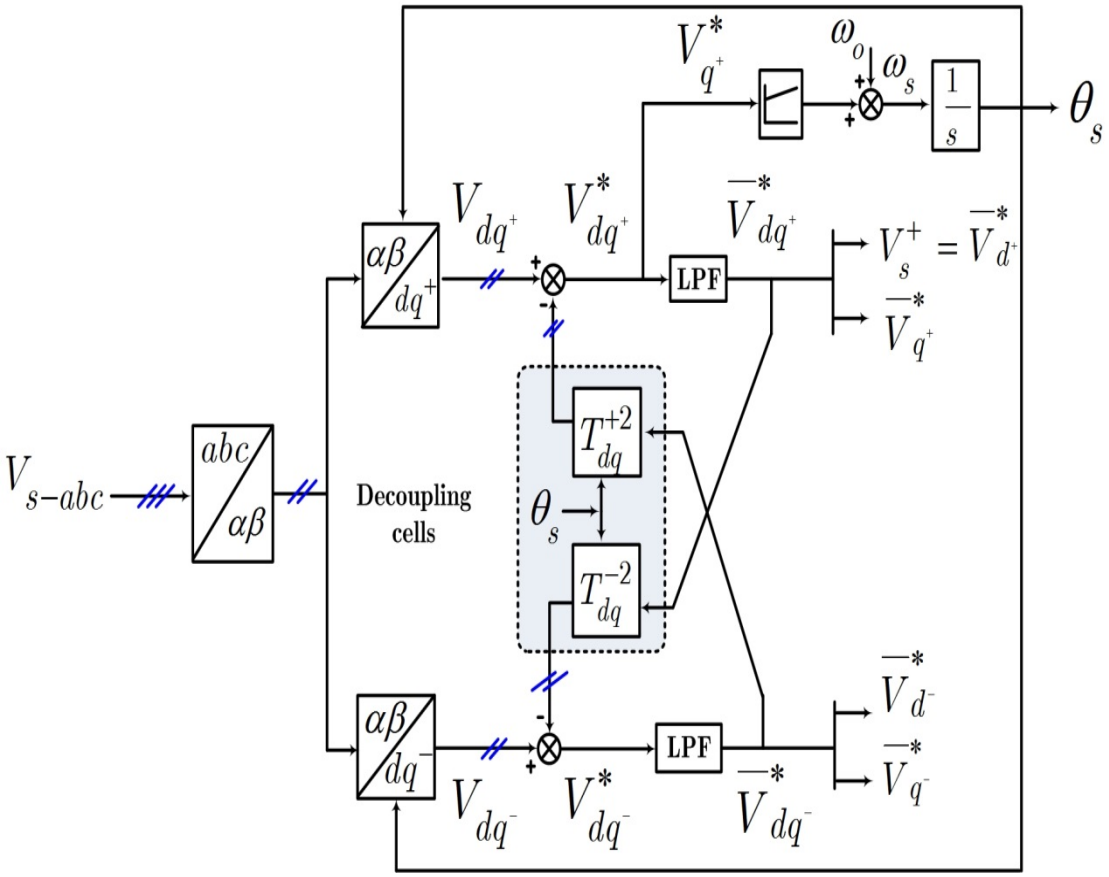

Figure 5.3 DDSRF-PLL basic structure.

5.2.3 DFOGI-FLL Grid Synchronization

Dual Second Order Generalized Integrator (DSOGI) based Frequency Locked Loop (DSOGI-FLL) is an insensitive frequency-adaptive synchronization mechanism which benefits the instantaneous symmetrical component analysis considering adaptive filters [9]. Being frequency-based, DSOGI-FLL can efficiently ride through grid perturbations, provides a clean synchronization signal and attenuates grid voltage high-frequency components [12].

The symmetrical components analysis method can be applied in the time domain reference frame using Lyon transformation [9]. According to this criterion, a grid voltage vector V_s consisting of three unbalanced sinusoidal components can be divided into its instantaneous positive, negative and zero-sequence components, through applying the following transformations:

$$V_{s-abc}^{+}=\left[T^{+}\right]V_{s-abc};\begin{bmatrix}V_{sa}^{+}\\V_{sb}^{+}\\V_{sc}^{+}\end{bmatrix}=\frac{1}{3}\begin{bmatrix}1 & a & a^{2}\\a^{2} & 1 & a\\a & a^{2} & 1\end{bmatrix}\begin{bmatrix}V_{sa}\\V_{sb}\\V_{sc}\end{bmatrix} \tag{5.10}$$

$$V_{s-abc}^{-}=\left[T^{-}\right]V_{s-abc};\begin{bmatrix}V_{sa}^{-}\\V_{sb}^{-}\\V_{sc}^{-}\end{bmatrix}=\frac{1}{3}\begin{bmatrix}1 & a^{2} & a\\a & 1 & a^{2}\\a^{2} & a & 1\end{bmatrix}\begin{bmatrix}V_{sa}\\V_{sb}\\V_{sc}\end{bmatrix} \tag{5.11}$$

$$V_{s-abc}^{0}=\left[T^{0}\right]V_{s-abc};\begin{bmatrix}V_{sa}^{0}\\V_{sb}^{0}\\V_{sc}^{0}\end{bmatrix}=\frac{1}{3}\begin{bmatrix}1 & 1 & 1\\1 & 1 & 1\\1 & 1 & 1\end{bmatrix}\begin{bmatrix}V_{sa}\\V_{sb}\\V_{sc}\end{bmatrix} \tag{5.12}$$

Where, a is an operator represents a 120° time shift.

The sequence components of the grid voltage can be also expressed using its αβ components as:

$$V_{\alpha\beta}^{+}=\left[T_{\alpha\beta}\right]V_{s-abc}^{+} \tag{5.13}$$

$$V_{\alpha\beta}^{-}=\left[T_{\alpha\beta}\right]V_{s-abc}^{-} \tag{5.14}$$

Substituting (5.10), (5.11) into (5.13), (5.14) yields:

$$V_{\alpha\beta}^{+}=\left[T_{\alpha\beta}\right]\left[T^{+}\right]V_{s-abc} \tag{5.15}$$

$$V_{\alpha\beta}^{-}=\left[T_{\alpha\beta}\right]\left[T^{-}\right]V_{s-abc} \tag{5.16}$$

Equations (5.15), (5.16) can be also expressed by its inverse transformation as:

$$V_{\alpha\beta}^{+}=\left[T_{\alpha\beta}\right]\left[T^{+}\right]\left[T_{\alpha\beta}\right]^{-1}V_{\alpha\beta} \tag{5.17}$$

$$V_{\alpha\beta}^{-}=\left[T_{\alpha\beta}\right]\left[T^{-}\right]\left[T_{\alpha\beta}\right]^{-1}V_{\alpha\beta} \tag{5.18}$$

Hence, the following expressions can be obtained:

$$V_{\alpha\beta}^{+}=\left[T_{\alpha\beta}^{+}\right]V_{\alpha\beta};\left[T_{\alpha\beta}^{+}\right]=\frac{1}{2}\begin{bmatrix}1 & -q\\q & 1\end{bmatrix} \tag{5.19}$$

$$V_{\alpha\beta}^{-}=\left[T_{\alpha\beta}^{-}\right]V_{\alpha\beta};\left[T_{\alpha\beta}^{-}\right]=\frac{1}{2}\begin{bmatrix}1 & q\\-q & 1\end{bmatrix} \tag{5.20}$$

Where, $q=e^{-j\pi/2}$

5.2.3.1 Structure of DSOGI

One of the techniques of implementing DSOGI is quadrature signal generator (QSG) which is adopted here [9]. Figure 5.4 depicts the general structure of the DSOGI-FLL. The operator q in (5.19) and (5.20) is implemented using a second-order adaptive filter based on a SOGI (SOGI-QSG), which is used in the literature as an effective approach for obtaining two in-quadrature output signals from a given sinusoidal input signal. Additionally, the SOGI-QSG filtering feature can attenuate distorting high-order harmonics effect from the input to the output. Figure 5.5 illustrates a schematic representation of the DSOGI. Typically, two SOGI-QSGs are dedicated to generate the direct and in-quadrature signals for the input voltage αβ components, i.e. $V'_\alpha, V'_\beta, qV'_\alpha, qV'_\beta$ respectively. These signals are given as input to a positive negative sequence calculation PNSC block which calculates the respective αβ reference frame sequence components based on (5.19) and (5.20).

5.2.3.2 FLL Technique of the DSOGI

DSOGI requires a frequency locked loop (FLL) to become frequency adaptive which is depicted in Fig 5.6. in this FLL, the two frequency error signals of the αβ QSGs are combined in order to compute the average error signal as:

$$\varepsilon_{av} = \frac{1}{2}\left(\varepsilon_v(\alpha) qV'_\alpha + \varepsilon_v(\beta) qV'_\beta\right) \tag{5.21}$$

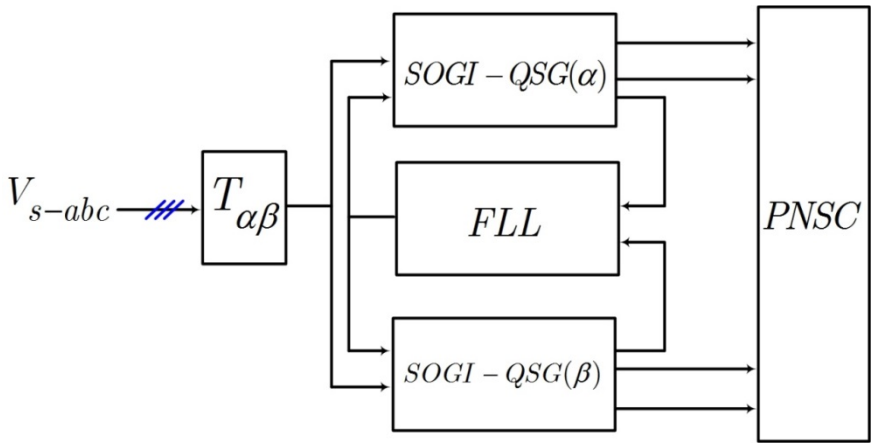

Figure 5.4 General structure of the DSOGI-FLL.

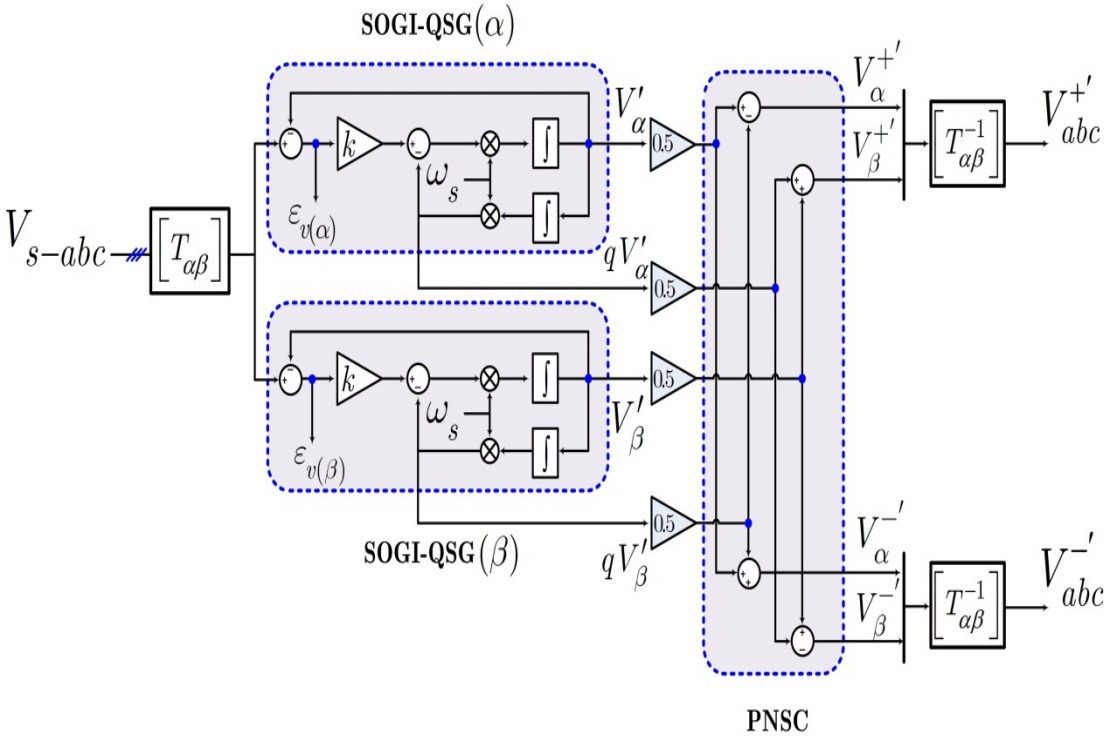

Figure 5.5 Detailed schematic representation of DSOGI.

The gain of the FLL is then normalized using the square of the amplitude of the positive and negative sequence voltage components which yields a first order exponential linearized response. Accordingly, DSOGI-FLL not only allows a decoupled estimation of the input three-phase voltage symmetrical components on the *αβ* reference frame, but also the value of the grid frequency.

It worth mentioning that DDSRF and DSOGI are two equivalent techniques, which perform the same function through sequence separation but on two different reference frames. However, the performance of the DSOGI relies on the frequency detected by the FLL, whereas the DDSRF performance depends on the phase angle detected by the PLL. Hence, in practice the dynamic response of the DSOGI-FLL and the DDSRF-PLL based systems will not be the same due to the differences between the PLL and FLL [9]. Moreover, Performance dynamic comparison between SRF-PLL, DDSRF-PLL and DSOGI-FLL will be presented through the presented case studies.

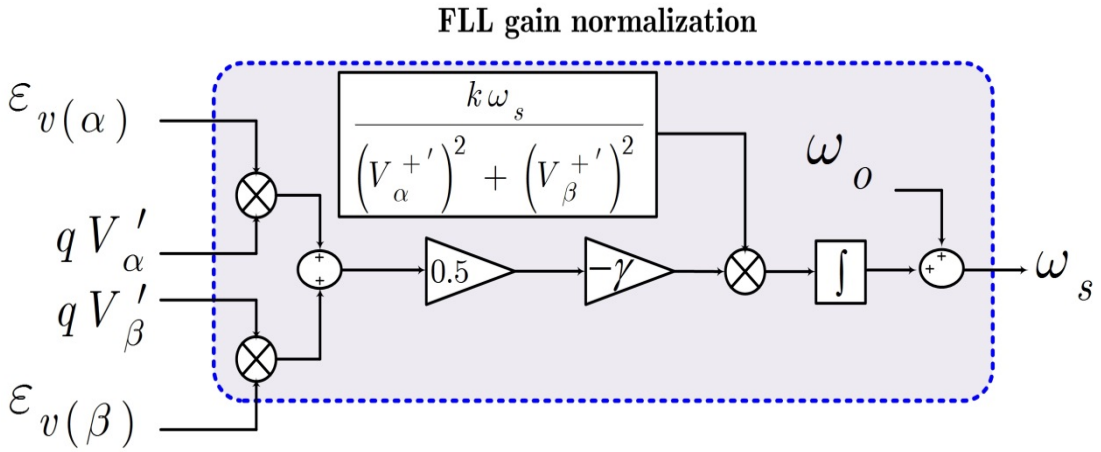

Figure 5.6 Schematic diagram of the FLL.

5.3 Fault Detection Algorithm

Fast fault detection is a key point for rapid triggering of the FRT control strategy and thus effectively suppresses the large transient currents. A fault detection algorithm, based positive and negative sequence component decomposition is adopted here [13]. In a broader context, the detection method is capable of decomposing the sequence components using the sample data at two points on the three-phase waveform [14]. Hence, the decomposition process can be executed after one sampling period. The stator voltage positive sequence component, V_s^+, is used as an indicator for a fault. Whenever, $V_s^+ \prec 0.9\ p.u.$, a fault is detected and thereby, the proposed FRT control strategy is activated to tackle the fault.

For a three-phase system voltage, a space complex vector representation can be used as:

$$\hat{V}_s(t) = V_\alpha(t) + jV_\beta(t) \tag{5.22}$$

Where,

$$V_\alpha(t) = \frac{2}{3}\left[V_a(t) - \frac{1}{2}V_b(t) - \frac{1}{2}V_c(t)\right] \tag{5.23}$$

$$V_\beta(t) = \frac{1}{\sqrt{3}}\left[V_b(t) - V_c(t)\right] \tag{5.24}$$

This voltage can be also expressed using its sequence components as:

$$\hat{V}_s(t) = V^+(t)e^{j(\omega_s t+\theta_p)} + V^-(t)e^{-j(\omega_s t+\theta_n)} \tag{5.25}$$

$V^+, V^-, \theta_p, \theta_n$ are the system voltage positive and negative sequence components and its phase angles respectively. ω_s is the fundamental frequency. By time delaying (5.25) with r/ω, the following expression is obtained:

$$\hat{V}_s(t-r/\omega) = V^+(t-r/\omega)e^{j(\omega_s t+\theta_p)}e^{-jr} + V^-(t-r/\omega)e^{-j(\omega_s t+\theta_n)}e^{jr} \tag{5.26}$$

Assuming that the delay r is very small, (5.26) can be simplified to:

$$\hat{V}_s(t-r/\omega) \approx V^+(t)e^{j(\omega_s t+\theta_p)}e^{-jr} + V^-(t)e^{-j(\omega_s t+\theta_n)}e^{jr} \tag{5.27}$$

From (5.25), (5.27), the following expressions can be obtained:

$$\hat{V}_s(t-r/\omega) - \hat{V}_s(t)e^{jr} = -2j\sin r V^+(t)e^{j(\omega_s t+\theta_p)} \tag{5.28}$$

$$V^+(t)e^{j(\omega_s t+\theta_p)} = \frac{j}{2\sin r}\left[\hat{V}_s(t-r/\omega) - \hat{V}_s(t)e^{jr}\right] \tag{5.29}$$

Equation (5.29) represents a decomposition of the positive sequence component from the voltage signal. Using (5.22), (5.29) can be formulated with its αβ components as:

$$\begin{aligned} V^+(t)e^{j(\omega_s t+\theta_p)} &= \frac{1}{2\sin r}\left[V_\beta(t)\cos r + V_\alpha(t)\sin r - V_\beta(t-r/\omega)\right] \\ &+ \frac{j}{2\sin r}\left[V_\alpha(t-r/\omega) - V_\alpha(t)\cos r + V_\beta(t)\sin r\right] \end{aligned} \tag{5.30}$$

Hence, from (5.30) the αβ sequence components can be derived:

$$V_\alpha^+(t) = \frac{1}{2}V_\alpha(t) - \frac{1}{2\sin r}\left[V_\beta(t-r/\omega) - V_\beta(t)\cos r\right] \tag{5.31}$$

$$V_\alpha^+(t) = \frac{1}{2}V_\beta(t) + \frac{1}{2\sin r}\left[V_\alpha(t-r/\omega) - V_\alpha(t)\cos r\right] \tag{5.32}$$

Figure 5.7 illustrates a block diagram for the sequence decomposition method. As implied from (5.31), (5.32), the smaller the delay r/w, the faster the algorithm response and hence the fault detection as well. However, the system can be easily susceptible to noise if r/w is extremely small. Therefore, the selection of the delay r/w should compromise between the rewarded fast response and reducing the noise.

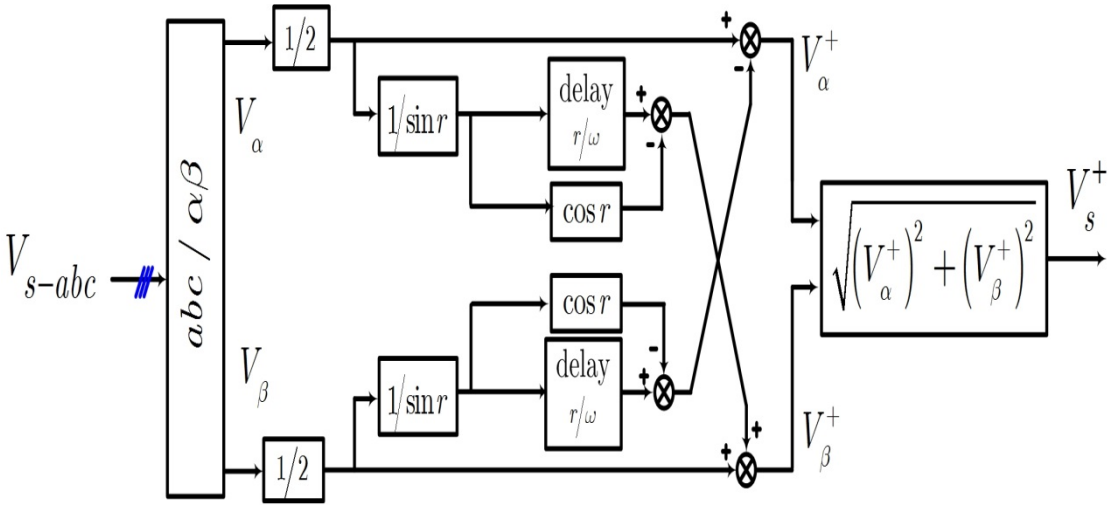

Figure 5.7 Fault detection schematic diagram.

5.4 DFIG FRT Control Strategy

This section provides the conventional and proposed FRT control scheme for the DFIG converters, i.e., the grid-side converter GSC and rotor side converter RSC considering the grid codes requirements.

5.4.1 Reactive Power Support

A cascaded reactive power control scheme shown in Fig. 5.8 is devoted to manage the reactive power sharing via DFIG stator as well GSC sides is adopted here [14]. The priority for the reactive power aid is given to the DFIG stator side -which is processed via the RSC control- followed by the GSC side whenever the stator side attains the limit - due to severe faults - which is pre-defined through the DFIG capability limit. The reactive power support is initiated once the rms stator voltage, V_s slips more than 0.1 p.u out of the reference value; $V_{s\text{-}ref}$. Typical limiters are incorporated to ensure that the released reactive power does not overtake the respective capability limits of stator and GSC each. Such management scheme is efficient as the GSC reactive power support starts subsequent to the stator side injection which allows for active power transmission at the fault onset and thus mitigating the unwanted transient DC voltage fluctuations [15].

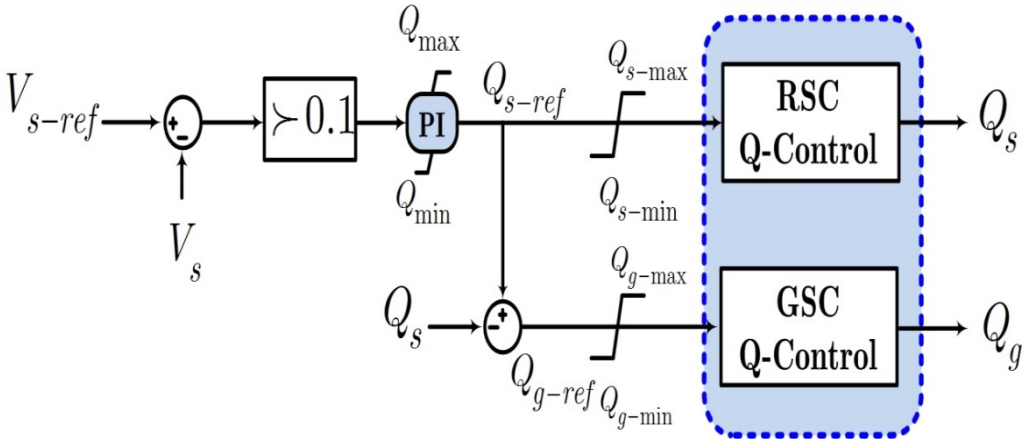

Figure 5.8 Reactive power control scheme.

5.4.2 Grid Side Converter Controller

The GSC controller is applied in a reference frame whose d-axis is oriented with the stator voltage, $v_{qs} = 0$. The dc link voltage, V_{dc} and the reactive power exchanged between the grid and the GSC sides, Q_g can be controlled through acting on the dq GSC voltage components. The dq voltage equations of the GSC connected to the grid can be expressed as:

$$v_{dg} = v_{ds} + \omega_s L_f i_{qg} - L_f \frac{di_{dg}}{dt} - R_f i_{dg} \tag{5.33}$$

$$v_{qg} = -\omega_s L_f i_{dg} - L_f \frac{di_{qg}}{dt} - R_f i_{qg} \tag{5.34}$$

Where, subscripts v, i, ω, stand for voltage, current, and angular speed. Subscripts, s,g signify stator and grid sides. Indexes d,q stand for direct and quadrature axes of dq reference frame. R_f ,L_f refer to GSC interface reactor resistance and inductance.

The active and reactive power flow between the GSC and the grid can be written as:

$$P_g = \frac{3}{2} v_{ds} i_{dg} \tag{5.35}$$

$$Q_g = -\frac{3}{2} v_{ds} i_{qg} \tag{5.36}$$

The DC link dynamics is given by:

$$\frac{1}{2}C_{dc}\frac{dV_{dc}^2}{dt} = P_r - P_g \tag{5.37}$$

In normal conditions, the GSC typically operates with a unity power factor, Q_g=0. Figure 5.9 illustrates The GSC traditional control scheme. To mitigate the dc voltage fluctuations during interruptions, a proposed term (P_g/V_{dc}) is activated and added to the dc link voltage control loop to reflect the transitory variation of the GSC power. The latter can be attributed to the power imbalance between the RSC and GSC resulting from the surplus rotor power followed by the transient voltage dip which adversely impacts the dc voltage transient response [14].

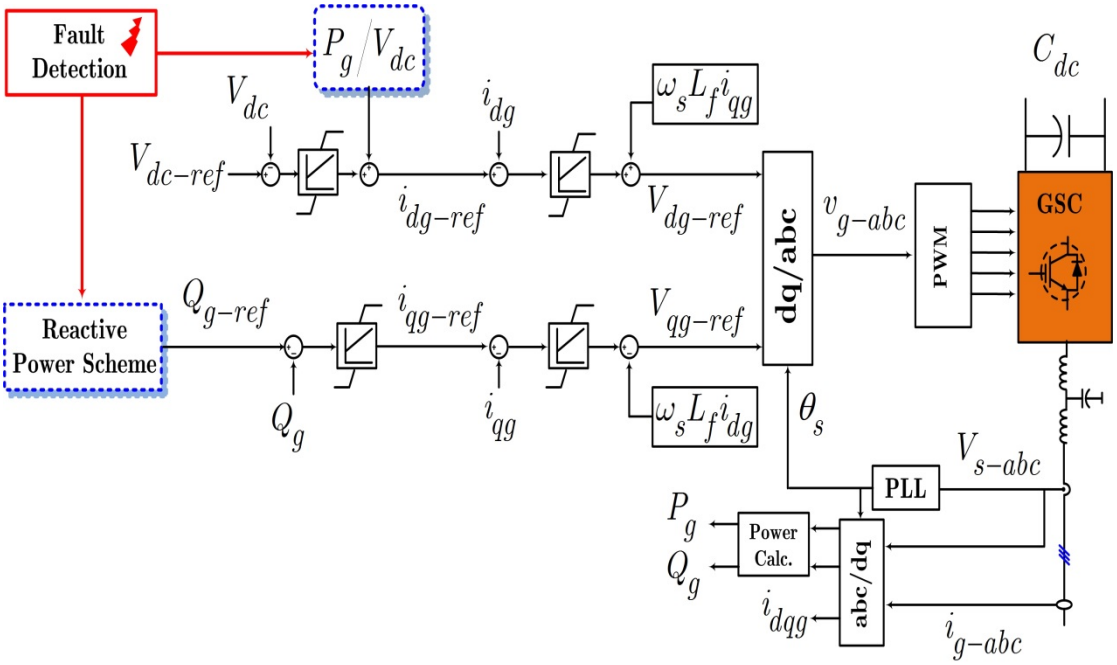

Figure 5.9 GSC conventional control scheme.

5.4.3 Proposed GSC Controller

Voltage sags can give rise to unbalanced grid voltages which may result in sustained oscillations in the delivered active and reactive power. Whilst it is generally accepted that traditional SRF dq current controllers are extensively used and implemented in different applications. Nevertheless, the performance of such controllers during unbalanced conditions is deficient [16]. Double synchronous reference frame DSRF for controlling positive and negative sequences using PI compensators seems to be better solution for unbalanced utilities. In DSRF current

controllers, two dq synchronous controllers (positive and negative) synchronized with their respective angular position θ_s^+, θ_s^- are utilized.

For an unbalanced grid voltage $v_{g-\alpha\beta}$:

$$v_{g-\alpha\beta} = v_{g-\alpha\beta}^+ + v_{g-\alpha\beta}^- = V_g^+ \begin{bmatrix} \cos\left(\omega_s t + \phi^+\right) \\ \sin\left(\omega_s t + \phi^+\right) \end{bmatrix} + V_g^- \begin{bmatrix} \cos\left(-\omega_s t + \phi^-\right) \\ \sin\left(-\omega_s t + \phi^-\right) \end{bmatrix} \tag{5.38}$$

Where,

$$\theta_s^+ = \omega_s t + \phi^+ ; \theta_s^- = -\omega_s t + \phi^- \tag{5.39}$$

Similarly, current vector can be described as:

$$i_{g-\alpha\beta} = i_{g-\alpha\beta}^+ + i_{g-\alpha\beta}^- = I_g^+ \begin{bmatrix} \cos\left(\omega_s t + \delta^+\right) \\ \sin\left(\omega_s t + \delta^+\right) \end{bmatrix} + I_g^- \begin{bmatrix} \cos\left(-\omega_s t + \delta^-\right) \\ \sin\left(-\omega_s t + \delta^-\right) \end{bmatrix} \tag{5.40}$$

Figure 5.10 depicts the positive and negative sequence components of the grid voltage and currents with the respective DSRF. The positive and negative dq current components can be expressed as:

$$i_{dq}^+ = e^{-j\theta_s^+} \cdot i_{\alpha\beta} = \underbrace{\begin{bmatrix} i_{dg}^+ \\ i_{qg}^+ \end{bmatrix}}_{dc\,term} + \underbrace{\begin{bmatrix} i_{dg}^- \cos\left(\theta_s^+ - \theta_s^-\right) + i_{qg}^- \sin\left(\theta_s^+ - \theta_s^-\right) \\ -i_{dg}^- \sin\left(\theta_s^+ - \theta_s^-\right) + i_{qg}^- \sin\left(\theta_s^+ - \theta_s^-\right) \end{bmatrix}}_{ac\,term} \tag{5.41}$$

$$i_{dq}^- = e^{-j\theta_s^-} \cdot i_{\alpha\beta} = \underbrace{\begin{bmatrix} i_{dg}^- \\ i_{qg}^- \end{bmatrix}}_{dc\,term} + \underbrace{\begin{bmatrix} i_{dg}^+ \cos\left(\theta_s^- - \theta_s^+\right) + i_{qg}^+ \sin\left(\theta_s^- - \theta_s^+\right) \\ -i_{dg}^+ \sin\left(\theta_s^- - \theta_s^+\right) + i_{qg}^+ \cos\left(\theta_s^- - \theta_s^+\right) \end{bmatrix}}_{ac\,term} \tag{5.42}$$

Where,

$$\begin{aligned} i_{dg}^+ &= I_g^+ \cos\left(\delta^+ - \phi^+\right) \\ i_{qg}^+ &= I_g^+ \sin\left(\delta^+ - \phi^+\right) \\ i_{dg}^- &= I_g^- \cos\left(\delta^- - \phi^-\right) \\ i_{qg}^- &= I_g^- \sin\left(\delta^- - \phi^-\right) \end{aligned} \tag{5.43}$$

From expressions (5.41), (5.42), it can be noted that a cross-coupling with double frequency $2\omega_s$ exists between both axes in the DSRF reference frames. This cross-coupling results in an overlapping ac term with $2\omega_s$ on the dq signals on both frames. Due to the limited PI controllers bandwidth, the steady-state error caused by

the $2\omega_s$ oscillations can't be cancelled out completely which degrades the controller performance [9].

An DSRF dq current controller incorporated with decoupling cells to eliminate the mutual $2\omega_s$ cross-coupled oscillations arising from positive and negative sequence currents is adopted and dedicated for the control of the GSC which known as DDSRF dq current controller [16]. Moreover, to make sure that the DDSRF dq controller is working properly, information about the current tracking error is fed so that if a current error exists, this dc error is subtracted from the reference value to retain the exact value of the current magnitude in the respective SRF.

Similar to the decoupling cells approach used for DDSRF-PLL, the resultant DDSRF dq current controller can be expressed as:

$$i'^{+}_{dqg} = i^{+}_{dqg} + \underbrace{e^{-j(\theta_s^{+}-\theta_s^{-})}\cdot i^{-}_{dqg}}_{\text{AC Term}} - \underbrace{e^{-j(\theta_s^{+}-\theta_s^{-})}\cdot\left(i^{-}_{dqg-ref} - \overline{\Delta i^{-}_{dqg}}\right.}_{\text{Decoupling cell}} \tag{5.44}$$

$$i'^{-}_{dqg} = i^{-}_{dqg} + \underbrace{e^{-j(\theta_s^{-}-\theta_s^{+})}\cdot i^{+}_{dqg}}_{\text{AC Term}} - \underbrace{e^{-j(\theta_s^{-}-\theta_s^{+})}\cdot\left(i^{+}_{dqg-ref} - \overline{\Delta i^{+}_{dqg}}\right.}_{\text{Decoupling cell}} \tag{5.45}$$

The LPF cut-off frequency ω_f which is used for obtaining the mean value of the current error is selected as $\omega_f = \omega_s / \sqrt{2}$) rad/s. the DDSRF controller block diagram which abridges (5.44), (5.45) is shown in Fig. 5.11. The outer controller of the DDSRF current controller is the same as that in [4].

5.4.4 Conventional RSC Controller

During normal operation, the DFIG stator active and reactive power decoupled control can be realized through vector control technique with a reference frame aligned with the stator voltage vector. The RSC control structure is as shown in Fig. 5.12. The RSC control strategy is implemented in a synchronous reference frame with the *d-axis* oriented with the DFIG stator voltage. The RSC is dedicated to attain

decoupled control of stator side active and reactive powers and also provides the DFIG with a variable speed operation. The *d-axis* control loop regulates the stator active power, P_s, via regulating the reference rotor active power current component current $i_{dr\text{-}ref}$, which is generated by the outer control loop that provides variable speed operation according to the WT MPPT. The *q-axis* corresponds to the stator reactive power control which is controlled through the reference rotor reactive power current component, $i_{qr\text{-}ref}$.

The output of the control loops is the RSC input voltage, $v_{rabc-ref}$. Once the stator voltage dips, the DFIG delivered output power decreases as well. Meanwhile, the reference input power should be restrained to regain power balance; otherwise, power imbalance will give rise to higher rotor current and rotor over-speed.

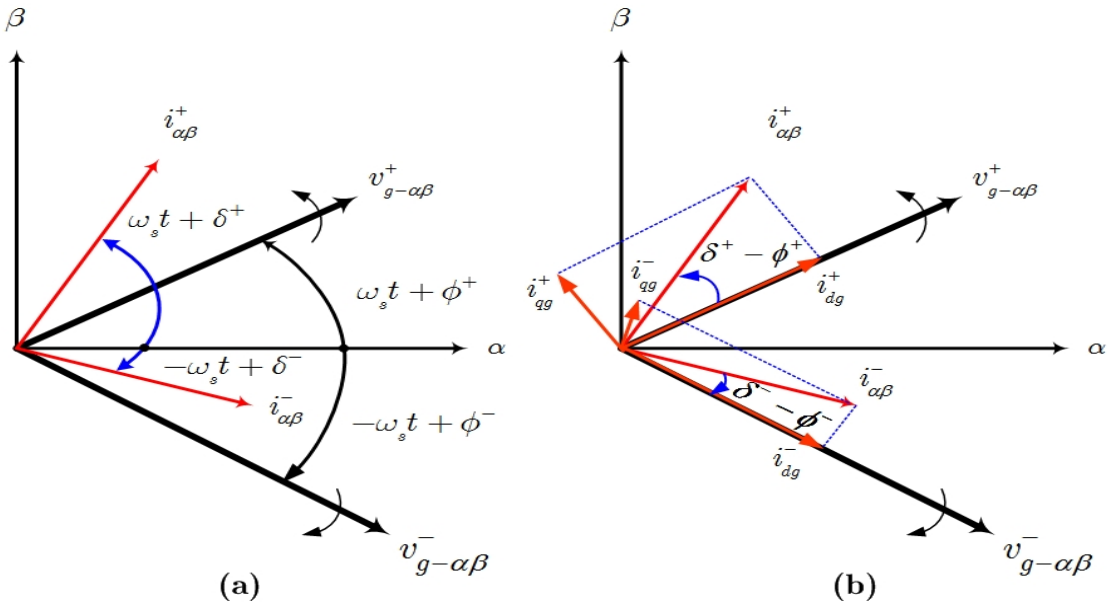

Figure 5.10 (a) Grid voltage positive/negative sequence components and injected (b) *dq* components of the positive/negative sequence current vector.

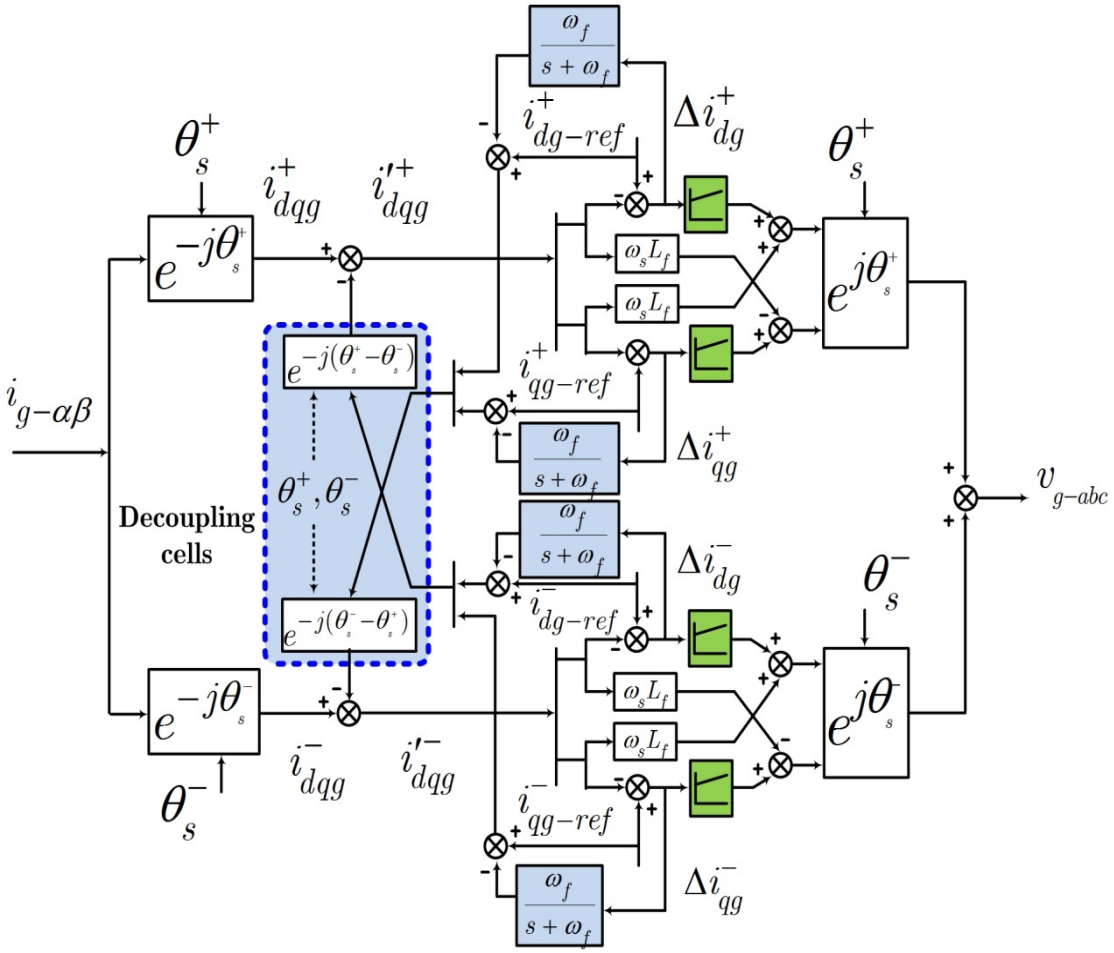

Figure 5.11 GSC DDSRF dq current controller.

Under normal operation, the DFIG output power can be defined as:

$$P_t = k_{opt}\,\omega_{r-ref}^3 \tag{5.46}$$

Where,

$$k_{opt} = \frac{0.5\rho A_b r_b^3 C_{p-\max}}{N_g^3 \lambda_{opt}^3} \tag{5.47}$$

To suppress the rotor as well as stator currents during contingencies, whenever, a faulty condition is detected, the MPPT is deactivated and the reference active power is given by:

$$P_{s-ref} = k_r k_{opt} \left(V_s / V_{so}\right)^2 \omega_{r-ref}^3 \tag{5.48}$$

Where, k_r is a reduction factor. V_{s0}, V_s signify the stator voltage pre and during the fault respectively. Equation (5.48) implies that the rotor active power current component will be reduced during the fault but pursuing less active power production

which is recommended by the British and Danish grid codes [1], [17]. With the aid of the reactive power support scheme, the RSC concurrently injects reactive current support with the remnant rotor current to fulfill the grid code commitment and restore the ac voltage.

5.4.5 Proposed RSC Controller

For further improvement of the RSC transient response, proportional integral resonance PIR current regulators are employed in the RSC controller as shown in Fig. 5.13 [18]. The parallel resonant blocks are tuned at $\omega_s, 2\omega_s$. ω_c is the cut-off frequency and k_{ir} is the proportional gain at the resonant frequency. Hence, the RSC dq voltage components are set as:

$$v_{dr} = PIR\left(i_{dr-ref} - i_{dr}\right) - \omega_{sl}\left(L_r i_{qr} + L_m i_{qs}\right) \quad (5.49)$$

$$v_{qr} = PIR\left(i_{qr-ref} - i_{qr}\right) + \omega_{sl}\left(L_r i_{dr} + L_m i_{ds}\right) \quad (5.50)$$

Where, i_{dr}, i_{qr} are the rotor active and reactive current components respectively. i_{ds}, i_{qs} are the stator side active and reactive current components. ω_{sl} is the slip frequency. L_r, L_m refer to rotor and magnetizing inductances.

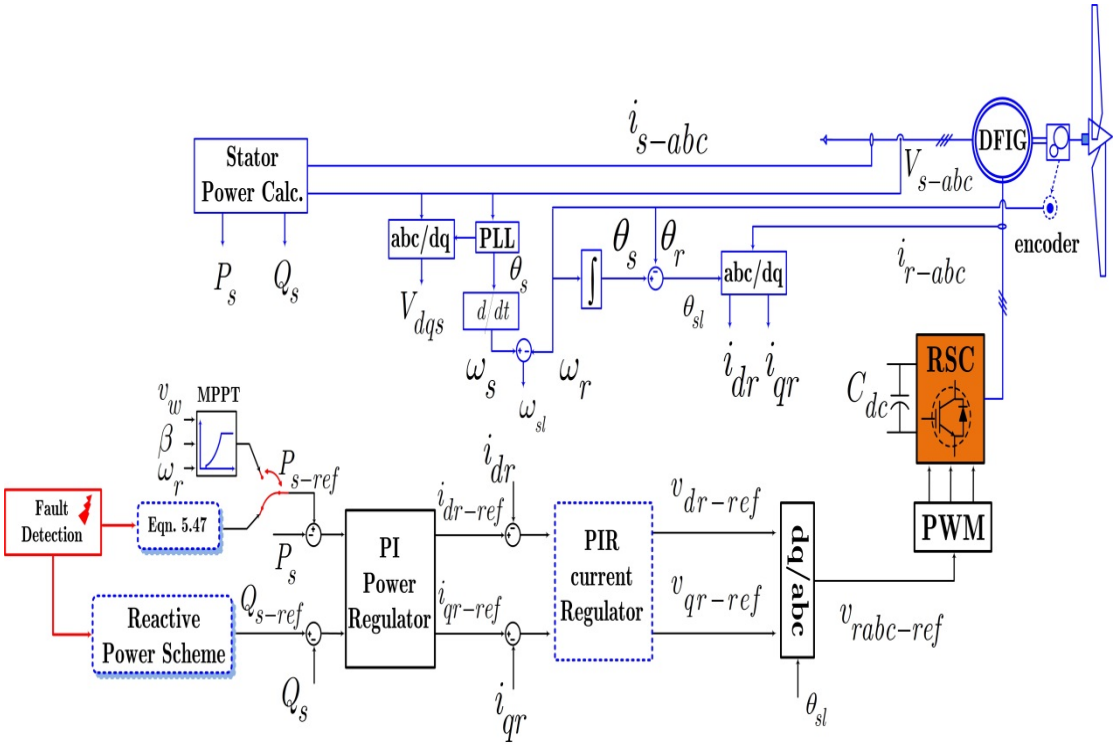

Figure 5.12 DFIG RSC control strategy.

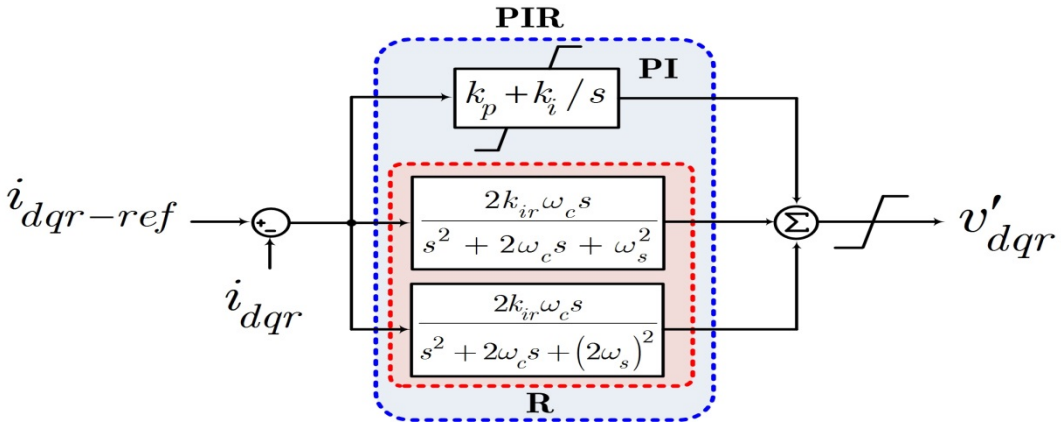

Figure 5.13 RSC PIR inner current controller.

5.5 Results and Discussions

This section provides a set of simulation test cases to verify the DFIG dynamic response using different control schemes and PLL structures under different fault scenarios. Conventional control method refers to the basic GSC and RSC controllers and the SRF-PLL. Whereas, control method 1 refers to the GSC DDSRF current controller and the DDSRF-PLL and control method 2 denotes the GSC controller using DDSRF current controller, proposed RSC controller and DSOGI-FLL. Moreover, the system compliance to the grid codes requirements during faulty conditions is also examined.

Figure 5.14 depicts the test system used for the simulation where a 2 MW DFIG WT is connected to a weak grid of SCR=3 and X/R=10. The system is simulated in the MATLAB/SIMULINK platform. As the wind speed is not expected to encounter significant change during a fault, the simulations are carried out at the nominal wind speed of the WT (11.4 m/s).

For the safety of system operation, the maximum allowed limit for the DC voltage is 1.25 p.u. Stator and rotor protection thresholds are set to 1.5 p.u. However, the RSC can sustain 2 p.u overcurrent for a very short time [16]. Moreover, the pitch controller will be activated during voltage dips to regulate the rotor speed.

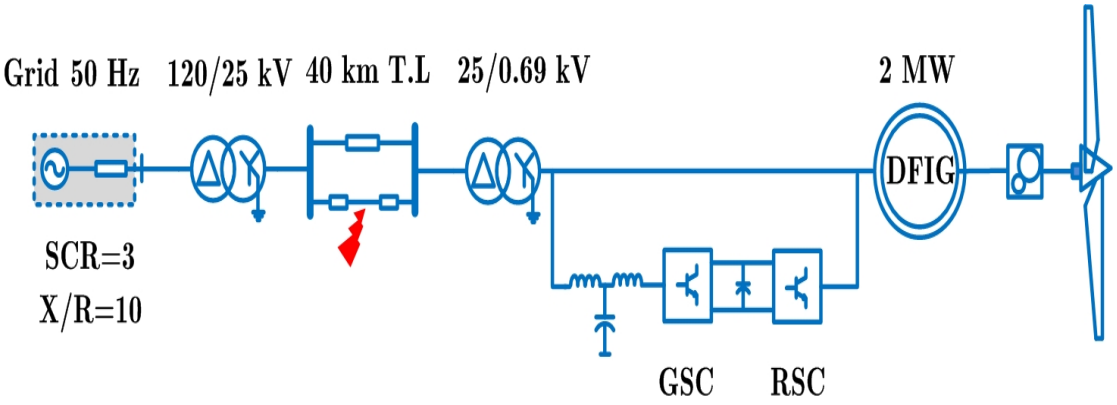

Figure 5.15 Single line diagram of the test system.

5.5.1 LVRT Operational Scenario

The system response to a symmetrical three-phase fault ($X_f/R_f = 5$) in the transmission system (see Fig. 5.14) with duration of 0.5 s is depicted in Fig. 5.16 using the different control aspects. During the fault, the stator voltage (Fig. 9.a) falls down to 95% which corresponds to a severe fault, while the FRT protection is triggered via the fault detection algorithm for protection purpose. At t=1.2s, the fault is cleared and later the normal operation is retrieved. At the onset of voltage dip, higher stator and rotor transient currents are noticed for the different controllers. Owing to the transient increase of the rotor current, the rotor power transmitted through the DC link simultaneously increases, which causes higher DC voltage oscillations due to lower ac voltage at the GSC terminals.

Compared to the proposed control strategies, the DC voltage for the conventional scheme encounters higher spike (1.32 p.u) and even exceeds the safe margins as recorded in Fig. 10.l6-A whereas, in case of the proposed strategies 1,2, the DC voltage is effectively regulated in the allowed range with faster response and lower settling time.

Moreover, it can be seen from the results that the activation of the FRT scheme in the RSC controller plays a significant role in regulating the power balance mismatch by reducing the DFIG input power in response to the output power reduction due to the fault and thus limiting stator as well as rotor currents by the control methods. Also, due to triggering the pitch control, the rotor over-speed is limited subsequent to the fault moment.

According to the grid codes, reactive current support should be resumed with the voltage dip remnant value below 0.9 p.u. Figure 5.15 also depicts the WT reactive power current component released in response to the voltage dip via stator and GSC sides. Obviously, it can be seen that the reactive current in case of the proposed methods attain its maximum value steadily during the fault period while for the conventional method, fluctuates and loses the successful reactive current support. This can be attributed to the loss of the exact vector control orientation as a consequence to the severe voltage dip with 95% drop due to the fluctuation caused by the lower weak grid SCR.

On the other hand, Fig 5.16 evidences that the DDSRF-PLL and DSOGI-FLL are capable of extracting a clean and unaffected synchronization signal with more damped transient performance at the fault moments which in turn enhances the overall system performance under such sever fault and also fulfil the grid code requirement.

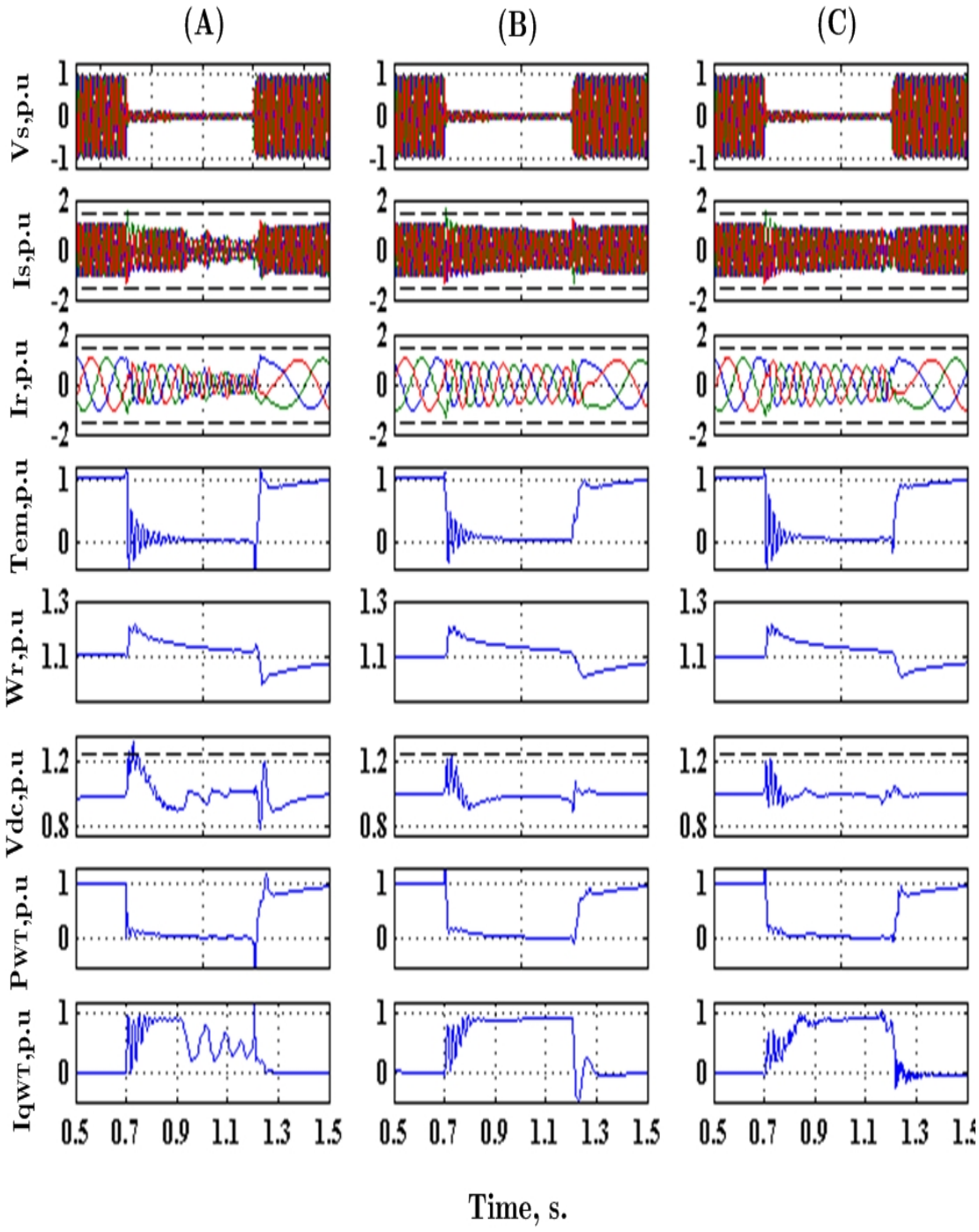

Figure 5.15 Response of the DFIG WT system to a symmetrical three-phase fault with $X_f/R_f = 5$: (A) Conventional control strategy. (B) Control strategy 1 (C) Control strategy 2.

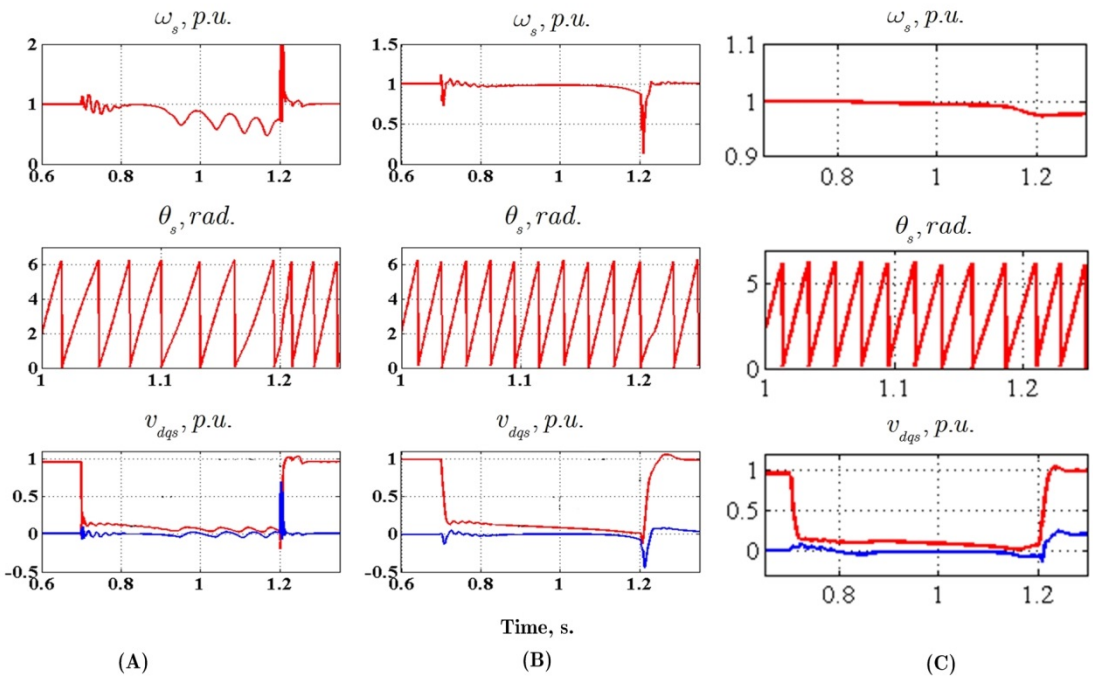

Figure 5.16 Tracking response of the system PLL for a symmetrical 3ph-fault: (A) SRF-PLL. (B) DDSRF-PLL. (C) DSOGI-FLL.

5.5.2 Asymmetrical Faults Scenario

Asymmetrical faults are widely recurring and accompanied with negative sequence currents which can result in sustained DC voltage and electromagnetic torque oscillation. In a broader context, the latter can adversely impact the WT coupling shaft while the former can damage the WT converters which eventually might trip the DFIG WT during such faults [3]. The system responses to a phase-to-ground fault in phase A with 90% voltage dip and a phase-to-phase fault with 50% voltage dip are shown in Figs. 5.17-18 respectively. The faults occur at t= 0.7 s and cleared 150 ms later as implied by grid codes [18].

Pre-fault, the dominant rotor current frequency is $|s|\omega_s/2\pi = 5$ Hz while during the fault, $|2 - s|\omega_s/2\pi = 105$ Hz. With the sequence currents controlled via the GSC DDSRF current controller, the DC voltage oscillation is mitigated (using proposed control methods 1,2) compared to that of the conventional method. It can be noticed from the results that the stator and rotor currents are effectively restrained below 2 p.u. Moreover, the stator active power and injected reactive current during both faults are oscillated dramatically due to the limited control capability of the RSC

[19]- [20]. Nonetheless, the oscillation is less in case of the proposed control strategy 1,2 with better post-fault recovery performance. This is due to the identical control efforts done by the proposed GSC controller for the sequence currents [6] and concurrently the robust performance of the DDSRF-PLL and DSOGI-FLL which extract an unaffected signal irrespective of the unbalanced grid voltage as seen in Figs. 5.19-20. Furthermore, the distorted stator voltage phase angle and its respective dq voltage components detected by the SRF-PLL impacts the commonly used vector control orientation scheme and adversely affect the control objectives.

Comparing the results, it can be concluded that the phase-to-phase fault is severer as it causes lower ac voltage and larger currents. Accordingly, higher DC link overshoots of 1.4 p.u are depicted in Fig. 5.18 which is quite far from the allowable limit under conventional control method. Furthermore, it was found that the rotor speed was increased slightly (5.5%) due to the activation of the pitch controller in response to the voltage dip. Besides, as the grid frequency is a more stable variable compared to the grid voltage phase-angle, DSOGI-FLL retains a robust and smoother response than the DDSRF-PLL during system transient faults.

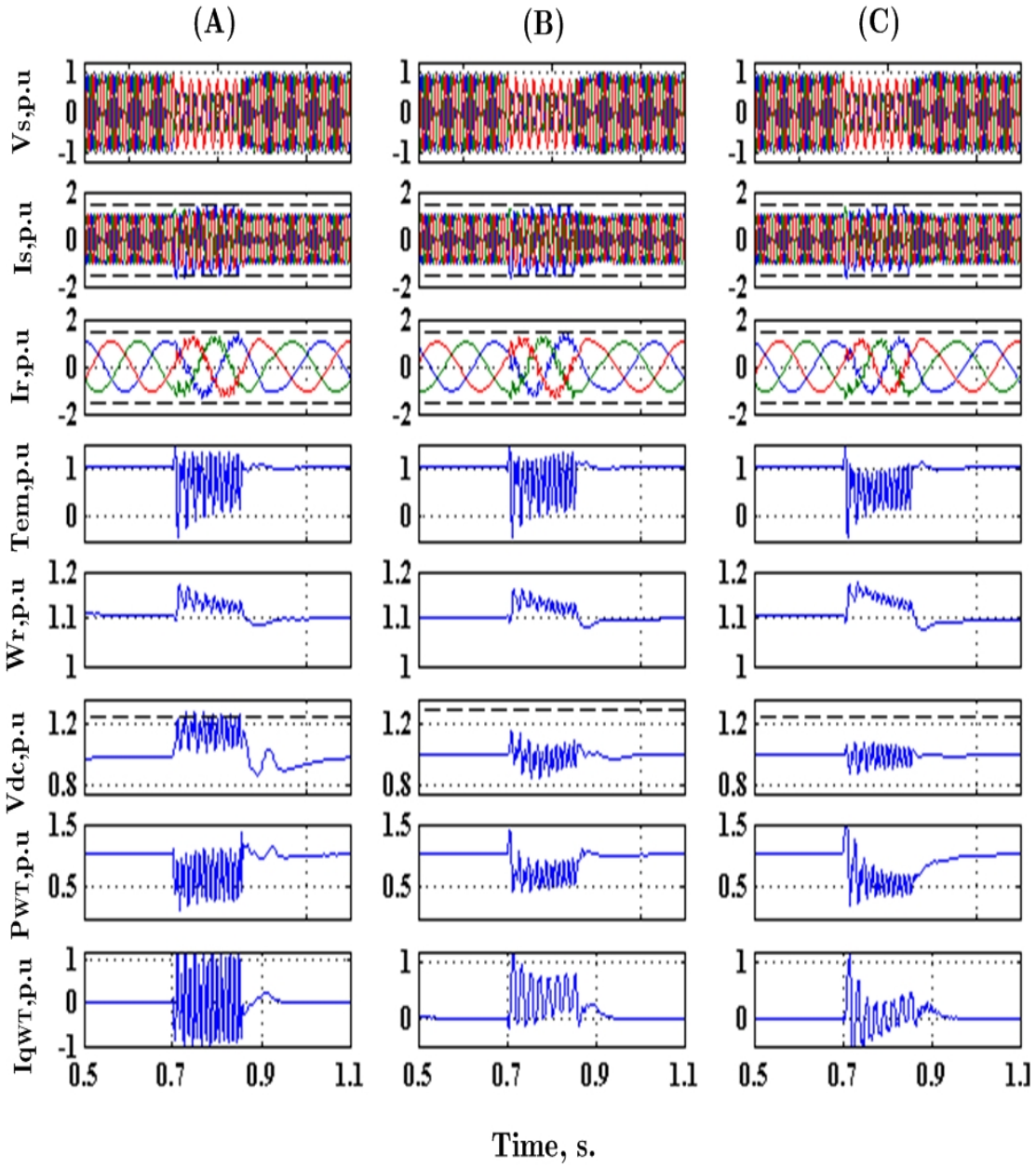

Figure 5.17 Response of the DFIG WT system to a single-phase to ground fault with $X_f/R_f = 5$ (A) Conventional control strategy. (B) Control strategy 1 (C) Control strategy 2.

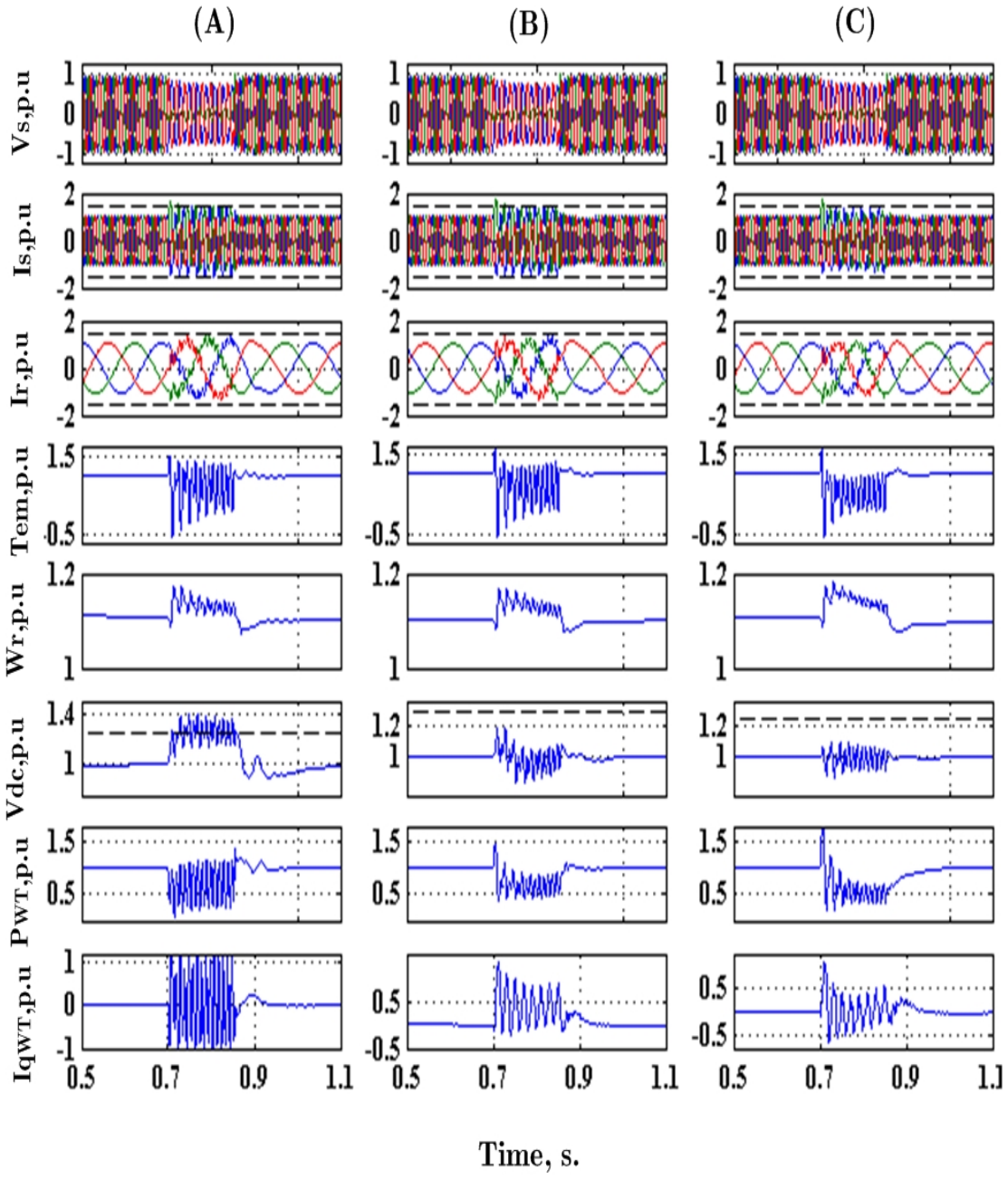

Figure 5.18 Figure 5.18 Response of the DFIG WT system to a phase-to-phase fault with X_f/R_f= 5 (A) Conventional control strategy. (B) Control strategy 1 (C) Control strategy 2.

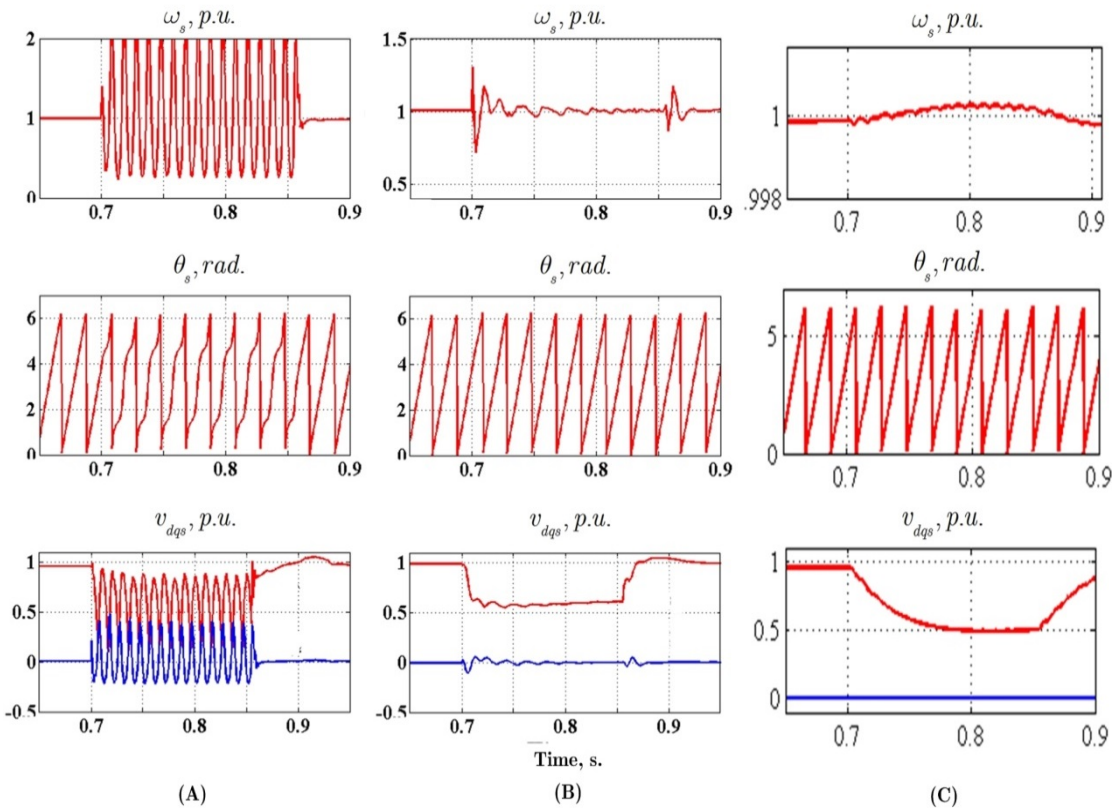

Figure 5.19 Tracking response of the system PLL for a single phase-to-ground fault.

(A) SRF-PLL. (B) DDSRF-PLL. (C) DSOGI-FLL.

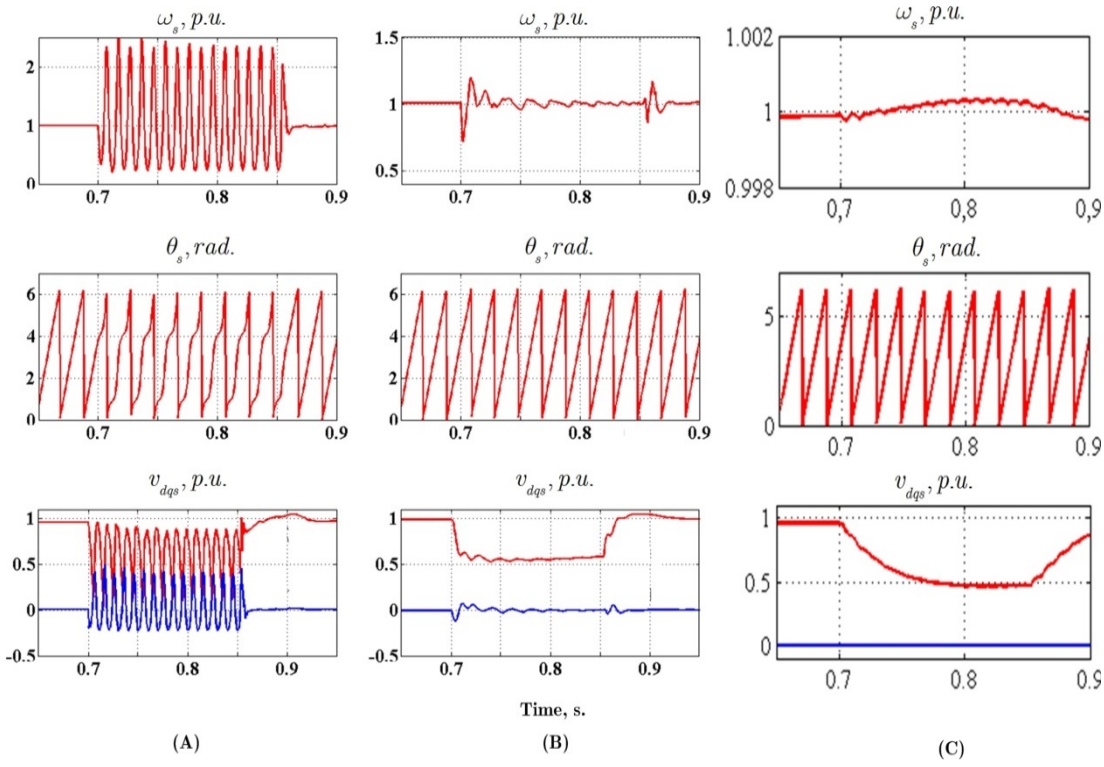

Figure 5.20 Tracking response of the system PLL for a phase-to-phase fault.

(A) SRF-PLL. (B) DDSRF-PLL. (C) DSOGI-FLL.

5.6 Summary

This chapter has studied the conventional and advanced control and synchronization techniques for WPPs connected to weak networks for the purpose improving the overall performance and fulfilling the modern grid codes commitments. A DDSRF current controller for GSC has been presented to achieve high dynamic performance, counteract current oscillations and regulate the DC link voltage during disturbances.

A DDSRF-PLL and DSOGI-FLL to extract a clean, robust synchronization phase angle irrespective of the grid voltage waveform have been also presented to enhance the overall system performance under severe voltage dips.

Additional terms have been augmented with the RSC and GSC controllers to suppress the stator and rotor currents and limit the rotor over-speed during faults. Besides, a fast decomposition algorithm for rapid fault detection has been discussed. Diverse simulations have been conducted to assess the impact of the FRT proposed strategy on the DFIG WT connected to a weak grid. The obtained results assure the capability of the DFIG WT connected to a weak grid of SCR of 3 to comply with the grid codes requirements using the proposed control strategies.

Bibliography

[1] M. Mohseni and S. M. Islam, “Review of international grid codes for wind power integration: diversity, technology and a case for global standard”, *Ren. Sustain. Energy Rev.,* vol. 16, no. 6, pp. 3876-3890, Aug. 2012.

[2] M. Reyes, et al., “Enhanced decoupled double synchronous reference frame current controller for unbalanced grid-voltage conditions”, IEEE Trans. Power Electron., vol. 27, no. 9, pp. 3934-3943, Sep. 2012.

[3] H. Geng, C. Liu and G. Yang, “LVRT capability of DFIG-based WECS under asymmetrical grid fault condition”, IEEE Trans. Ind. Electron., vol. 60, no. 6, pp. 2495-2509, Jun. 2013.

[4] N. Jelani and M. Molinas, “Mitigation of asymmetrical grid faults in induction generator-based wind turbines using constant power load”, Energies, vol. 6. pp. 1700-1717, Mar. 2013.

[5] S. Abulanwar, Zhe Chen and Florin Iov, "Enhanced LVRT Control Strategy for DFIG Based WECS in Weak Grid", in Proc. The International Conference on Renewable Energy Research and Applications, ICRERA 2013, Madrid, Spain, 2013.

[6] S. Xiao, G. Yang, H. Zhou and H. Geng, "An LVRT control strategy based on flux linkage tracking for DFIG-based WECS", IEEE Trans. Ind. Electron., vol. 60, no. 7, pp. 2820-2832, July. 2013.

[7] J. Yao, et al., "Enhanced control of a DFIG-based wind-power generation system with series grid-side converter under unbalanced grid voltage conditions", IEEE Trans. Power Electron., vol. 28, no. 7, pp. 3167-3181, July. 2013.

[8] P. Rodríguez et al., "Decoupled double synchronous reference frame PLL for power converters control", IEEE Trans. Power Electron., vol. 22, no. 2, pp. 584-592, Mar. 2007.

[9] R. Teodorescu, M. Liserre, and P. Rodríguez., "Grid converters for photovoltaic and wind power systems", Wiley IEEE Press, 2011.

[10] Chen, Z., Wei, M. "A voltage quality detection method", The Third International Conference on Electric Utility Deregulation and Restructuring and Power Technologies (DRPT 2008), 6-9 April 2008, Nanjing, China.

[11] Wei, M., Chen, Z., "A fast PLL method for power electronic systems connected to distorted grids", the 33st Annual Conference of the IEEE Industrial Electronics Society, IECON 2007, pp 1702-1707.

[12] P. Rodríguez et. al., "Advanced grid synchronization system for power converters under unbalanced and distorted operating conditions", in Proc IEEE Industrial Electronics, IECON, Paris, France, 2006 , pp. 5173-5178.

[13] Y. Liang, "A new time domain positive and negative sequence component decomposition algorithm," in Proc. Power Eng. Soc. Gen. Meeting, Toronto, ON, Canada, 2003, vol. 3, pp. 1638-1643.

[14] D. Xie, et al., "A comprehensive LVRT control strategy for DFIG wind turbines with enhanced reactive power support", IEEE Trans. Power Sys., vol. 28, no. 3, pp. 3302-3310, Aug. 2013.

[15] S. Abulanwar, Zhe Chen and Florin Iov, "Improved FRT Control Scheme for DFIG Wind Turbine Connected to a Weak Grid", in Proc. IEEE PES Asia-Pacific Power and Energy Engineering Conference 2013 (IEEE PES APPEEC 2013), Hong Kong, 2013.

[16] M. Reyes, et al., "Enhanced decoupled double synchronous reference frame current controller for unbalanced grid-voltage conditions", IEEE Trans. Power Electron., vol. 27, no. 9, pp. 3934-3943, Sep. 2012.

[17] Energinet. Technical regulation 3.2.5 for wind power plants with a power output greater than 11 kW; September 2010. Available at: http://www.energinet.dk.

[18] J. Liang, D. F. Howard, J. A. Restrepo and R. G. Harley, "Feed-forward transient compensation control for DFIG wind turbines during both balanced and unbalanced grid disturbances", IEEE Ind. Apps., vol. 49, no.

[19] X. Yan, G. Venkataramanan, P. S. Flannery, Y. Wang, Q. Dong, and B. Zhang, "Voltage-sag tolerance of DFIG wind turbine with a series grid side passive-impedance network", IEEE Trans. Energy Convers., vol. 25, no. 4, pp. 1048-1056, Dec. 2010.

[20] R. Sarrias, L. M. Fernández, C. A. García, and F. Jurado, "Coordinate operation of power sources in a doubly-fed induction generator wind turbine/battery hybrid power system", Power sources., vol. 205, no. 1, pp. 354-336, May 2012.

Chapter 6

Conclusions and Future Work

6.1 Conclusions

Recently, wind energy attracted the attention of many researchers as well as politicians owing to its steady gross in the global market. The development of wind power not only represents onshore power plants but also offshore wind farms with a capacity hundreds of MW. With a remarkable penetration level in many countries, the integration of wind power into power systems would seriously impact the stability and operation scenario and therefore brings different technical issues. Such challenges are more prominent and effective in case of weak power systems that have lower system strength.

Besides, with the increase of wind power penetration level worldwide, the transmission system operators issued the so called Grid Codes which impose a set of regulations on wind power plants WPPs in order to maintain the system stability and reliability during normal and abnormal conditions. Therefore, WPPs are requested to provide ancillary services as conventional generators in order to maintain the system voltage. Such commitment will represent another challenge when considering wind power plants connected to weak ac grid which already suffers voltage perturbations.

Consequently, this dissertation is dedicated to address some of the technical issues that impede the efficient integration of wind power into weak power systems with very low system strength. The study also investigates the fault ride-trough response of wind power generators that are connected to stiff and weak networks considering the grid codes regulations. To identify the technical challenges that confront integration of wind power into weak power systems, a simplified model that depicts a grid-connected DFIG WT has been studied under a wide range of grid short circuit capacity ratio SCR and also X/R ratio. Accordingly, the voltage and active/reactive power constraints of this typical configuration have been identified. It has been found that, a grid with $1 \leq SCR \leq 4$ and/or $X/R \leq 1$ is susceptible to dramatic voltage perturbations as a consequence to high system impedance which accordingly

represents a serious limitation for delivering the available wind power. Therefore, reactive power support is crucial to maintain the system voltage within permissible limits.

A detailed model representing a typical configuration of a grid-connected DFIG WT has been also studied to examine the system performance under a wide range of system strength, and verify the analytical study. A mega-watt level DFIG which is widely implemented in the wind energy market has been considered because it employs partial converters and thus its control especially during abnormal conditions will be more challenging. To provide a unified mitigation facility of the point of connection POC voltage perturbations during different system strengths, an adaptive voltage control AVC strategy based system strength and operating point has been proposed.

In a broader context, the AVC aims at maximizing the wind power penetration into weak networks. Moreover, a proposed reactive power dispatch algorithm to manage the reactive power flow from/to the wind generator WG is presented. Throughout different case studies performed, it has been deduced that the AVC provides a higher mitigation capability compared to traditional voltage controllers. Additionally, owing to the limited reactive power capacity of the DFIG, overrating the grid side converter represents a cost-effective solution to maintain the POC voltage within allowable limits at very low SCRs. It was found that a GSC with 0.38 p.u. rating (compared to 0.25 p.u. normal rating) is sufficient to keep the system voltage within normal limits for the entire range of the studied network parameters. The overall system stability using safe operation zones was examined using numerous simulations for $1 \leq SCR \leq 10$ and $0.5 \leq X/R \leq 10$ in the studied system with the AVC and the overrated GSC.

It was concluded that, at a given system strength ($2 \leq SCR \leq 4$ and $X/R \leq 0.5$), the operation regions incur insecure areas at higher WT output power. This is because the higher output power provokes larger voltage deviations which make the demanded reactive power more vulnerable to the voltage variations especially at very low X/R ratios. However, the voltage swell decreases again with higher SCR ‘lower impedance’ as the network with higher SCR is unlikely cause larger voltage perturbations. Therefore, For $SCR \geq 5$ even with $X/R = 0.5$, safe operation is ensured. Furthermore, except for $0.5 \leq X/R \leq 1$, the DFIG can effectively regulate the voltage

with the latent reactive power. Accordingly, the GSC effectively manipulates the reactive power deficit at very low X/R ratios to maintain the voltage.

Typically, two main deficiencies are reported in the literature for the DFIG which are the higher transient stator and rotor currents at the instant of abrupt voltage dip as well as DC link overvoltage due to the imbalance between the rotor power and the delivered GSC power during a fault. The DFIG transient response due to symmetrical and asymmetrical faults has been investigated for both stiff and weak networks. For a DFIG WT connected to a stiff network, a nonlinear controller has been presented for the GSC to achieve high dynamic performance, decoupled control between the DC link voltage and reactive power and meanwhile injects reactive power during voltage dips to support the system voltage. Due to the steady voltage of a stiff network, the obtained output results evidences that using a proper DFIG control during transients can overcome its former shortcomings. The GSC nonlinear control results reveal fast response, high dynamic performance and assure the FRT capability of the proposed control strategy in compliance with the Danish grid code without additional hardware circuits.

Asymmetrical faults are widely recurring and accompanied with negative sequence currents which can result in electromagnetic torque oscillation that can adversely impact the WT drive-train. Also, due to the voltage perturbations caused by SCR and/or X/R variations, voltage is difficult to control in case of weak networks. For these reasons, Decoupled double synchronous reference frame phase locked loop DDSRF-PLL and dual second order generalized integrator based frequency locked loop DSOGI-FLL synchronization techniques have been implemented for accurate and clean grid voltage position detection irrespective of the mains conditions. A decoupled double synchronous reference frame (DDSRF) current controller is adopted for the design of grid side converter, GSC, controller to counteract negative sequence double frequency current oscillations raised by unbalanced voltages and tackle the DC link voltage run-away.

A set of case studies carried out during balanced as well as unbalanced faults show that the synchronization techniques are capable of extracting a clean voltage position signal and dq components which accordingly improves the controller performance and maintain the WT grid connected to the mains to fulfill the grid codes

requirement. Additionally, the DDSRF GSC current controller keeps the DC voltage within the permissible limits especially during unbalanced faults compared to traditional controllers.

6.2 Future Work

Based on the achievement and findings of this dissertation work, several future research points are suggested in the area of wind power integration as follows.

- The power fluctuations caused by wind speed 3p oscillations needs further mitigation for improvement of the POC voltage especially during very low SCR and X/R ratios.

- Advanced control techniques for controlling the positive and negative sequence components at the RSC can be considered for further improvement of the system performance during asymmetrical faults.

- The DFIG FRT response needs to be investigated for a wide range of SCR and X/R variations of a weak grid in order to come up with a unified FRT control strategy suitable for both stiff and very weak networks.

- The application of energy storage ES is an effective mean to improve the system voltage performance during normal and abnormal conditions. The different ES types could be studied using proposed control methods to overcome voltage variations.

- The proposed AVC significance could be expanded to a wind farm WF level connected to a weak network to investigate the POC voltage performance with the different wind turbines. Also, the reactive power dispatch strategy could be modified due to the reactive power contribution of the whole WF.

Appendix A

The DFIG Capacity Mathematical Equation

$$\left(P_s\right)^2+\left(Q_s+3\frac{V_{poc}^2}{X_s}\right)^2=\left(3\frac{X_m}{X_s}V_{poc}I_r\right)^2 \qquad (A.1)$$

Assuming

$$A=\frac{1}{X_s},B=\left(\frac{X_m}{X_s}I_r\right)^2 \qquad (A.2)$$

Rearranging (A.1), yields:

$$Q_s^2+Q_s\left(2AV_{poc}^2\right)+A^2V_{poc}^4-BV_{poc}^2+P_s^2=0 \qquad (A.3)$$

For the general quadratic equation:

$$ax^2+bx+c=0 \qquad (A.4)$$

The roots of (A.4) can be obtained using the formula:

$$x=\frac{-b\pm\sqrt{b^2-4ac}}{2a} \qquad (A.5)$$

It follows that the roots of (A.1) are:

$$Q_s=\frac{-2AV_{poc}^2\pm\sqrt{4A^2V_{poc}^2-4A^2V_{poc}^2+4BV_{poc}^2-4P_t^2}}{2} \qquad (A.6)$$

From (A.6), it follows that, the maximum generation and absorption capacity can be expressed as:

$$Q_{sg-\max}=\sqrt{BV_{poc}^2-P_t^2}-AV_{poc}^2=\sqrt{\left(\left(X_m/X_s\right)V_{poc}I_r\right)^2-P_t^2}-V_{poc}^2/X_s \qquad (A.7)$$

$$Q_{sa-\max}=-AV_{poc}^2=-V_{poc}^2/X_s \qquad (A.8)$$

Appendix B

Derivation of POC Voltage Equation

Rearranging (2.2), yields

$$V_{poc}V_{poc}^{*} = V_{n}V_{poc}^{*} + \left(P_{t} - jQ_{t}\right)\left(R_{eq} + jX_{eq}\right) \qquad (B.1)$$

As V_{poc} can be defined as

$$V_{poc} = \left|V_{poc}\right| e^{j\varphi} = V_{poc}\left(\cos\varphi + j\sin\varphi\right) \qquad (B.2)$$

Combining (B.1), (B.2), yields:

$$\left|V_{poc}^{2}\right| = V_{n}\left|V_{poc}\right|\cos\varphi + \left(P_{t}R_{eq} + Q_{t}X_{eq}\right) + j\left(P_{t}X_{eq} - Q_{t}R_{eq} - V_{n}\left|V_{poc}\right|\sin\varphi\right) \qquad (B.3)$$

As the LHS of (B.3) is real, it follows that the RHS is also real, then

$$\sin\varphi = \frac{P_{t}X_{eq} - Q_{t}R_{eq}}{V_{n}\left|V_{poc}\right|} \qquad (B.4)$$

Using the trigonometric identity

$$\sin\varphi = \sqrt{\cos^{2}\varphi - 1} \qquad (B.5)$$

Combining (B.4), (B.5) gives:

$$\cos\varphi = \sqrt{\frac{\left(V_{n}\left|V_{poc}\right|\right)^{2} - \left(P_{t}X_{eq} - Q_{t}R_{eq}\right)^{2}}{V_{n}\left|V_{poc}\right|}} \qquad (B.6)$$

From (B.3), (B.6), yields

$$\left|V_{poc}^{2}\right| = P_{t}R_{eq} + Q_{t}X_{eq} + \sqrt{\left(V_{n}\left|V_{poc}\right|\right)^{2} - \left(P_{t}X_{eq} - Q_{t}R_{eq}\right)^{2}} \qquad (B.7)$$

Rearranging and squaring of (B.7), gives

$$\left(\left|V_{poc}^{2}\right| - \left(P_{t}R_{eq} + Q_{t}X_{eq}\right)\right)^{2} = \left(V_{n}\left|V_{poc}\right|\right)^{2} - \left(P_{t}X_{eq} - Q_{t}R_{eq}\right)^{2} \qquad (B.8)$$

$$V_{poc}^{4} - V_{poc}^{2}\left(V_{n}^{2} + 2\left[P_{t}R_{eq} + Q_{t}X_{eq}\right] + \left(R_{eq}^{2} + X_{eq}^{2}\right)\left(P_{t}^{2} + Q_{t}^{2}\right)\right) = 0 \qquad (B.9)$$

For the general quadratic equation

$$ax^2 + bx + c = 0 \qquad (B.10)$$

The roots of Eqn. (B.10) can be obtained using the formula

$$x = \frac{-b \pm \sqrt{b^2 - 4ac}}{2a} \qquad (B.11)$$

It follows that the roots of (B.9) are

$$V_{poc}^2 = \frac{V_n^2 + P_t R_{eq} + Q_t X_{eq} \pm \sqrt{\left[V_n^2 + 2\left(P_t R_{eq} + Q_t X_{eq}\right)\right]^2 - 4\left(P_t^2 + Q_t^2\right)\left(R_{eq}^2 + X_{eq}^2\right)}}{2} \qquad (B.12)$$

After solving (B.12), the POC voltage can be expressed as:

$$V_{poc} = \sqrt{0.5\, V_n^2 + A} \qquad (B.13)$$

Where,

$$A = P_t R_{eq} + Q_t X_{eq} + \sqrt{0.25\, V_n^4 + \left(P_t R_{eq} + Q_t X_{eq}\right) V_n^2 - \left(P_t X_{eq} - Q_t R_{eq}\right)^2} \qquad (B.14)$$

The positive sign only of (B.13) is accepted so that at zero power, the equations is valid, i.e.,

$$V_{poc} = V_n \qquad (B.15)$$

Appendix C

Parameters of the DFIG Variable-Speed Wind Turbine

Parameter	Value
Rated power	2 MW
Rated Voltage	0.69 kV
Rated frequency	50 Hz
Stator Resistance	0.00488 p.u.
Stator leakage inductance	0.1656 p.u.
Rotor resistance	0.00549 p.u.
Rotor leakage inductance	0.1763 p.u.
Magnetizing inductance	3.9257 p.u.
Number of pole pairs	2
Lumped inertia constant	4.5 s
Gear box ratio	87
Rated DC link voltage	1200 V
DC link capacitor	16000 μF
Rotor hub elevation	80 m
WT rotor radius	40 m
Wind shear empirical component (α)	0.3
Tower radius (a)	2 m
Distance from the blade origin to the tower midline (x)	5 m
Turbulence Intensity	10%
Transformer rated Power	2.5 MVA
Primary winding rated voltage	11 kV
Secondary winding rated voltage	0.69 kV
Short circuit impedance	0.0033+j0.039 p.u.

List of Publications

[1] **S. Abulanwar**, W. Hu, Z. Chen and F. Iov "Adaptive voltage control strategy for variable-speed wind turbine connected to a weak network*", IET Renewable Power Generation,* vol. 10, no. 2, pp. 238-249, 2016.

[2] **S. Abulanwar**, W. Hu, F. Iov and Z. Chen, "Characterization and assessment of voltage and power constraints of DFIG WT connected to a weak network," in Proc. *IEEE PES General Meeting*, Washington, US, 2014, pp. 1-5.

[3] **S. Abulanwar**, Zhe Chen and Birgitte Bak-Jensen, "Study of DFIG wind turbine fault ride-through according to the Danish grid code" in Proc. *IEEE Power & Energy Society General Meeting*, Vancouver, Canada, 2013, pp. 1-5.

[4] **S. Abulanwar**, Zhe Chen and Florin Iov, "Enhanced LVRT control strategy for DFIG based WECS in weak grid", in Proc. *The International Conference on Renewable Energy Research and Applications, ICRERA, Madrid, Spain, 2013, pp. 476 – 481.*

[5] **S. Abulanwar**, Zhe Chen and Florin Iov, "Improved FRT control scheme for DFIG wind turbine connected to a weak grid", in Proc. *IEEE PES Asia-Pacific Power and Energy Engineering Conference (IEEE PES APPEEC), Hong Kong, 2013, pp. 1-6.*

AALBORG UNIVERSITY
DENMARK

Supervisor statement

As the supervisor for the below mentioned PhD student I hereby declare that the PhD programme described below fulfills the requirements for the PhD degree laid down in the Ministerial Order.

Ph.D.-student: Elsayed Mohamed Mohamed Abulanwar

Title of thesis: ***Integration of Wind Power into Weak Power Systems***

The other activities related with his PhD study are given as follows:

Course activities:

Joint Courses	**Time and Location**	**ECTS**
Preparation of research plan for PhD's	Spring 2012, AAU	1.0
An introduction to qualitative research approaches in technology, science and education	Fall 2012, AAU	3.0
Design and analysis of experiments	Fall 2012, AAU	3.0
Bayesian statistics, simulation and software	Spring 2013, AAU	4.0
AC Micro Grids	Fall 2012, AAU	2.0

Project-related courses:		
Wind power generators	Fall 2012, AAU	3.0
Dispersed Generation of Electricity	Fall 2012, AAU	3.0
Modelling, control and simulation of power converters	Spring 2012, AAU	2.0
Introduction to Wind Power	Spring 2012, AAU	4.0
Power System Stability and Control	Spring 2012, AAU	4.0

Conference Participation		
IEEE PESGM 2013	July 2013	1.5
IEEE PESGM 2014	July 2014	1.5
Total		**32 ECTS**

The above-mentioned courses have all been evaluated.

Communication of scientific knowledge:

Writing/presentation of papers:

During the PhD study, Elsayed Abulanwar has published 4 conference papers. He also presented a poster paper at the Danish wind industry annual event, 2014. He also has one journal paper published by IET Renewable Power Generation, 2016.

Presentations:

Elsayed Abulanwar has attended and has made presentations in the conferences listed in the following table.

Conference	Time and Location
Asia Pacific Power and Energy Engineering Conference (APPEEC), 2013	8-11 December, 2013, Hong Kong, China
IEEE PES General Meeting Conference 2014	27-31 July, 2014, Washington D.C. USA
IEEE PES General Meeting Conference 2013	21-25 July, 2013, Vancouver, Canada
IEEE ICRERA 2013 Conference 2013	20-23 Oct., 201, Madrid, Spain
Danish Wind Industry Annual Event, 2014	26-27 March, 2014, Herning, Denmark

External stay:

From 4st August to 26th September 2014, Elsayed Abulanwar had an external study at the Institution of Electrical Engineering, Chinese Academy of Science, IEE-CAS, Beijing, China. He has done a part of his research work with collaboration of researchers in that institute.

EL-Sayed Abulanwar

2016-02-29

Date

Zhe Chen, Professor, Ph.D.

Co-author statement in connection with submission of PhD thesis

With reference to Ministerial Order no. 1039 of August 27 2013 regarding the PhD Degree § 12, article 4, statements from each author about the PhD student's part in the shared work must be included in case the thesis is based on already published or submitted papers.

Paper title: Study of DFIG Wind Turbine Fault Ride-Through According to The Danish Grid Code

Publication outlet:
Proc. IEEE Power and Energy Society General Meeting Conference, Vancouver, Canada, July 21-25, 2013.

List of authors:
Elsayed Abulanwar, Zhe Chen and Birgitte Bak-Jensen

PhD student:
Elsayed Abulanwar

Scientific contribution of the PhD student (all participating PhD students) to the paper:

The paper was written by Elsayed Abulanwar (85%) with some inputs from Zhe Chen and Birgitte Bak-Jensen (15%).
Elsayed Abulanwar (PhD student) contributed to defining the overall problem and proposed the core scientific idea to solve it. The PhD student wrote the entire draft version of the paper and revised it according to the co-authors comments. The PhD student derived the key methodology and the student implemented the simulations.
Zhe Chen and Birgitte Bak-Jensen provided comments and suggestions regarding the contents of the paper and simulation results.

Signature, PhD student

EL-Sayed Abulanwar

Elsayed Abulanwar

Signatures, co-authors

Zhe Chen

Birgitte Bak-Jensen

Co-author statement in connection with submission of PhD thesis

With reference to Ministerial Order no. 1039 of August 27 2013 regarding the PhD Degree § 12, article 4, statements from each author about the PhD student's part in the shared work must be included in case the thesis is based on already published or submitted papers.

Paper title: Characterization and assessment of voltage and power constraints of DFIG WT connected to a weak network

Publication outlet:
Proc. IEEE Power and Energy Society General Meeting Conference, Washington, D.C, USA, July 27-31, 2014.

List of authors:
Elsayed Abulanwar, Weihao Hu, Florin Iov and Zhe Chen

PhD student:
Elsayed Abulanwar

Scientific contribution of the PhD student (all participating PhD students) to the paper:
The paper was written by Elsayed Abulanwar (85%) with some inputs from Weihao Hu, Florin Iov and Zhe Chen (15%).
Elsayed Abulanwar (PhD student) contributed to defining the overall problem and proposed the core scientific idea to solve it. The PhD student wrote the entire draft version of the paper and revised it according to the co-authors comments. The PhD student derived the key methodology and the student implemented the simulations.
Weihao Hu, Florin Iov and Zhe Chen provided comments and suggestions regarding the contents of the paper and simulation results.

Signature, PhD student

EL-Sayed Abulanwar

Elsayed Abulanwar

Signatures, co-authors

Weihao Hu

Florin Iov

Zhe Chen

Co-author statement in connection with submission of PhD thesis

With reference to Ministerial Order no. 1039 of August 27 2013 regarding the PhD Degree § 12, article 4, statements from each author about the PhD student's part in the shared work must be included in case the thesis is based on already published or submitted papers.

Paper title: Improved FRT Control Scheme for DFIG Wind Turbine Connected to a Weak Grid

Publication outlet:
Proc. IEEE PES Asia-Pacific Power and Energy Engineering Conference, APPEEC, Hong Kong, Dec. 8-11, 2013.

List of authors:
Elsayed Abulanwar, Zhe Chen and Florin Iov

PhD student:
Elsayed Abulanwar

Scientific contribution of the PhD student (all participating PhD students) to the paper:
The paper was written by Elsayed Abulanwar (85%) with some inputs from Zhe Chen and Florin Iov (15%).
Elsayed Abulanwar (PhD student) contributed to defining the overall problem and proposed the core scientific idea to solve it. The PhD student wrote the entire draft version of the paper and revised it according to the co-authors comments. The PhD student derived the key methodology and the student implemented the simulations. The student identified relevant performance metrics and interpreted the simulation results.
Zhe Chen and Florin Iov provided comments and suggestions regarding the contents of the paper and simulation results. They assisted in careful reviewing of the paper and proposed further refinements to the paper draft made by the student.

Signature, PhD student

EL-Sayed Abulanwar

Elsayed Abulanwar

Signatures, co-authors

Zhe Chen

Florin Iov

Co-author statement in connection with submission of PhD thesis

With reference to Ministerial Order no. 1039 of August 27 2013 regarding the PhD Degree § 12, article 4, statements from each author about the PhD student's part in the shared work must be included in case the thesis is based on already published or submitted papers.

Paper title: Adaptive Voltage Control Strategy for Variable-Speed Wind Turbine Connected to a weak network

Publication outlet:
IET Renewable Power Generation, vol. 10, no. 2, pp. 238-249, 2016.

List of authors:
Elsayed Abulanwar, Weihao Hu, Zhe Chen and Florin Iov

PhD student:
Elsayed Abulanwar

Scientific contribution of the PhD student (all participating PhD students) to the paper:
The paper was written by Elsayed Abulanwar (85%) with some inputs from Weihao Hu, Zhe Chen and Florin Iov (15%).
Elsayed Abulanwar (PhD student) contributed to defining the overall problem and proposed the core scientific idea to solve it. The PhD student wrote the entire draft version of the paper and revised it according to the co-authors comments. The PhD student derived the key methodology and the student implemented the simulations. The student identified relevant performance metrics and interpreted the simulation results.
Weihao Hu, Zhe Chen and Florin Iov provided comments and suggestions regarding the contents of the paper and simulation results. They assisted in careful reviewing of the paper and proposed further refinements to the paper draft made by the student.

Signature, PhD student

EL-Sayed Abulanwar

Elsayed Abulanwar

Signatures, co-authors

Weihao Hu

Zhe Chen

Florin Iov

Co-author statement in connection with submission of PhD thesis

With reference to Ministerial Order no. 1039 of August 27 2013 regarding the PhD Degree § 12, article 4, statements from each author about the PhD student's part in the shared work must be included in case the thesis is based on already published or submitted papers.

Paper title: Enhanced LVRT Control Strategy for DFIG Based WECS in Weak Grid

Publication outlet:
Proc. The International Conference on Renewable Energy Research and Applications, ICRERA, Madrid, Spain, Oct. 20-23, 2013.

List of authors:
Elsayed Abulanwar, Zhe Chen and Florin Iov

PhD student:
Elsayed Abulanwar

Scientific contribution of the PhD student (all participating PhD students) to the paper:
The paper was written by Elsayed Abulanwar (85%) with some inputs from Zhe Chen and Florin Iov (15%).
Elsayed Abulanwar (PhD student) contributed to defining the overall problem and proposed the core scientific idea to solve it. The PhD student wrote the entire draft version of the paper and revised it according to the co-authors comments. The PhD student derived the key methodology and the student implemented the simulations. The student identified relevant performance metrics and interpreted the simulation results.
Zhe Chen and Florin Iov provided comments and suggestions regarding the contents of the paper and simulation results. They assisted in careful reviewing of the paper and proposed further refinements to the paper draft made by the student.

Signature, PhD student

EL-Sayed Abulanwar

Elsayed Abulanwar

Signatures, co-authors

Zhe Chen

Florin Iov

AALBORG UNIVERSITET

The Faculty of Medicine and Faculty of Engineering and Science
Niels Jernes Vej 10
9220 Aalborg East

Declaration of Compliance with Good Scientific Practice for the PhD Thesis

By signing this declaration, I confirm that the PhD thesis submitted by me was done, to the best of my belief, in accordance with good scientific practice (according to the faculty guidelines and practice in the area), and that I am aware of and agree that a finding of serious violations of good scientific practice will be handled according to the faculty guidelines and will preclude a positive assessment of the thesis and/or possibly result in the revocation of the degree awarded to me.

PLEASE USE CAPITAL LETTERS TO FILL IN THIS FORM

Full name:	ELSAYED MOHAMED MOHAMED ABULANWAR
Title of the PhD thesis:	WIND POWER INTEGRATION INTO WEAK POWR SYSTEMS

13th April, 2016, El-Sayed Abulanwar

Date and signature

Study of DFIG Wind Turbine Fault Ride-Through According to The Danish Grid Code

S. Abulanwar,[1,2] *Graduate Student Member, IEEE,* Zhe Chen[1,2] *Senior Member, IEEE,* Birgitte Bak-Jensen[1,2] *Member, IEEE*
[1]Energy Technology Dept., Aalborg University, [2]Sino-Danish Centre for Education and Research
Pontoppidanstraede 101, Aalborg East, Denmark
ema@et.aau.dk

***Abstract*—This paper presents a new decentralized control strategy to enable a Doubly-fed Induction generator wind turbine, DFIG WT, to fulfill the Danish grid code requirements during different perturbations. A nonlinear controller is adopted for the grid side converter, GSC, to ensure decoupled control of the DC link voltage and the reactive power, and counteract the DC link voltage run-away. Moreover, the GSC is dedicated to inject more reactive power during voltage dips to satisfy the grid code reactive power support obligation. A conventional PI controller is devoted to control the rotor side converter, RSC, with additional compensation terms to reduce the rotor over-speed, and limit the rotor and stator large transient currents. A diverse set of symmetrical and asymmetrical voltage excursions are investigated to evaluate the effectiveness of the proposed method using MATLAB/SIMULINK environment. The obtained results assure the capability of the proposed control strategy to satisfy the Danish grid code requirements.**

***Index Terms*-- Asymmetrical faults, Danish grid code, DFIG, nonlinear control.**

I. INTRODUCTION

With the steady increase of decentralized wind power plants WPP, the transmission system operators, TSO in many countries have stipulated some regulations to the integration of wind power plants, WPP which are known as grid codes [1]. Using partial scale converters, Doubly-fed Induction generator wind turbine, DFIG WT, still dominate the global market as it acquires more than 50% of the current installed wind power [2], [3].

Generally speaking, two main drawbacks are reported in the literature for the DFIG which are the higher transient stator and rotor currents at the instant of a fault as well as DC link overvoltage due to the incapability of the grid side converter, GSC to transmit the rotor circuit power [2]-[5]. Traditionally, a crowbar is inserted in the rotor circuit and activated during faulty conditions to address the aforementioned shortcomings. However, once the crowbar is activated, the rotor side converter, RSC is disabled and its control is temporarily lost, meanwhile the machine behaves as an induction motor drawing higher reactive power [4]. Advanced control strategies for DFIG have proven to be the optimal solution to ride-through the DFIG drawbacks during faults [2],[4],[5]. To enhance the Low Voltage Ride-Through, LVRT of DFIG, [3] proposed a hybrid fault tolerant current controller to the DFIG RSC and GSC. A standard PI controller is used for normal conditions whereas a vector-based hysteresis current controller is utilized to overcome LVRT and High Voltage Ride-Through, HVRT conditions. However, more asymmetrical fault cases are not investigated.

In [4], a compensation term is added to the conventional controller of the GSC to overcome the DC link overvoltage during voltage dips. In addition, the RSC control method increases the rotor speed during faults to transform the additional power into kinetic energy and limit current oscillations. Nevertheless, if the rotor speed is above the rated value (higher wind speed), the pitch controller will be activated, hence, the proposed control method will not be highly effective.

This paper presents a new decentralized control strategy for the control of DFIG WT to ride-through different disturbances as well as to fulfill the Danish grid code commitments.

A nonlinear feedback controller is proposed for the GSC to achieve independent control between the DC link voltage and the reactive power, suppress the DC voltage fluctuations and concurrently inject reactive power during contingencies to fulfill the reactive power support requirement. Additional proposed terms are incorporated with the conventional PI controller of the RSC, with the target of reducing the rotor and stator currents during faulty conditions and limiting the rotor over-speed as well.

II. DANISH GRID CODE REVIEW

Being one of the countries that has significant wind power share, the transmission system operators (Energinet.dk) in Denmark has introduced the Danish grid code which is a set of requirements that wind power plant, WPP has to satisfy in order to remain connected to the power system [6]. Fig. 1-a shows the LVRT requirement imposed by the Danish grid code on the WTs connected to the transmission system [1],[6]. As seen, it implies three operational modes; (1) The WPP must remain connected to the power system in area A for voltage higher than 0.9 p.u. (2) The WPP should not only remain connected to the power system in area B but also provides reactive power support to the grid as demanded in Fig. 1-b to help stabilize the voltage with full reactive current injection in the area B'. (3) The disconnection of the WPP is allowed in area C. On the other hand, the Danish grid code has stipulated another requirement for high voltage

978-1-4799-1303-9/13/$31.00 ©2013 IEEE

operation known as high-voltage ride-through, HVRT as depicted in Fig. 1-c. Such operating condition may arise due to disconnecting large load or a grid fault [1].

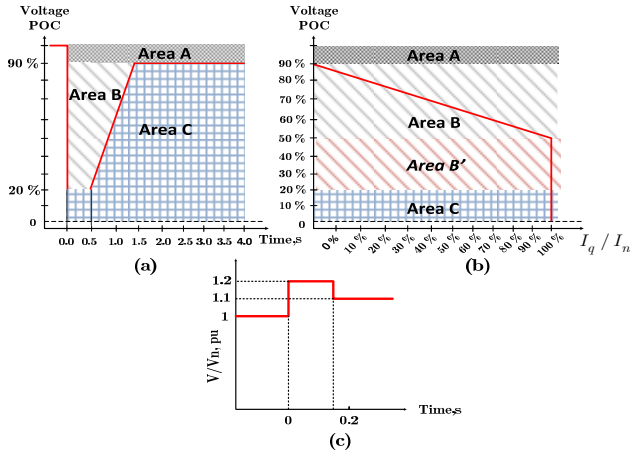

Fig. 1 Danish grid code requirements, (a) LVRT, (b) Reactive power support criterion, (c) HVRT [16]

III. DFIG WT System Modeling

Fig. 2 demonstrates a schematic diagram of a DFIG wind turbine connected to the main grid through 20 km double transmission line. The system comprises a 2 MW DFIG WT. The WT-represented with the rotor as a lumped mass model- is operated according to the well-known maximum power point tracking, MPPT to extract the maximum available power at each wind speed below the rated value and holds a constant power over the rated wind speed [5]. The DFIG rotor speed is controlled via the pitch angle controller having a structure as in [4]. The DFIG is connected to the ac system through two two-level PWM back-to-back voltage-source converters, VSC namely, RSC and GSC and a coupling transformer. The transmission line is attached to the main grid through a high voltage transformer.

IV. DFIG Fault Ride-Through FRT Control Strategy

A. RSC Control Strategy

The control structure of the RSC side is as shown in Fig. 3. The RSC control strategy is implemented in a synchronous reference frame with the d-axis oriented with the DFIG stator voltage [7]. The RSC is dedicated to ensure decoupled control of stator side active and reactive powers and also to provide the DFIG with a variable speed operation ($\pm 30\%$ speed range). The stator active and reactive powers, P_s, Q_s are controlled via controlling the rotor side current components, i_{dr}, i_{qr} respectively. The output of the control loops is the RSC input voltage, U^*_{rabc}. During normal operation, the DFIG is controlled to achieve variable speed operation according to the MPPT while absorbing the required excitation $\left(Q^*_{sn}\right)$ from the reactive power control loop [7]. According to the Danish grid code, the supply of reactive power has the first priority in area B over the active power supply. However, a suitable margin of active power must be retained in proportion to the voltage dip magnitude [1], [6]. Therefore, once a faulty condition is detected, the MPPT is deactivated and the active power is kept to a minimum value to help suppress rotor and stator currents as well as to limit rotor over-speed. Furthermore, the RSC controller can contribute to additional reactive power support with the remnant reactive current to satisfy the reactive power support criterion (see Fig. 1-b, Fig. 3).

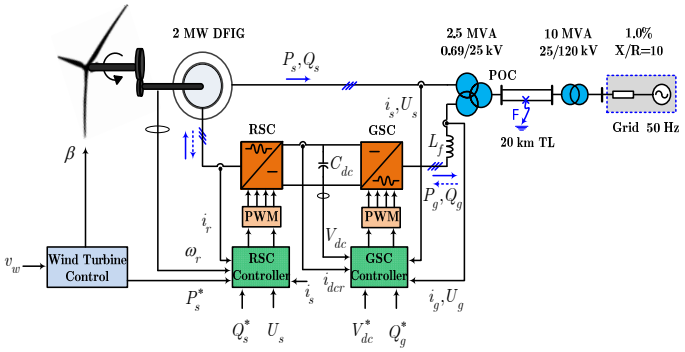

Fig. 2 Schematic diagram of the DFIG wind turbine grid connected system

B. GSC Control Strategy

The model of the GSC in a dq reference frame whose d-axis is aligned with the voltage vector $\overline{U}_g$ is described by the following set of differential equations:

$$di_{dg}/dt = -\left(R_f/L_f\right)i_{dg} + \omega_g i_{qg} + \left(U_{dg} - U_{dc}\right)/L_f \quad (1)$$

$$di_{qg}/dt = -\left(R_f/L_f\right)i_{qg} - \omega_g i_{qg} + \left(U_{qg} - U_{qc}\right)/L_f \quad (2)$$

Where, subscripts, U,i,ω, signify voltage, current, and angular speed. Subscripts, g,c refer to grid and converter sides. Indexes d,q stand for direct and quadrature axes of dq reference frame. R_f, L_f refer to resistance and inductance of the GSC interface reactor.

The active and reactive power exchange between the GSC and the grid can be formulated as:

$$P_g = 1.5\left(U_{dg} i_{dg} + U_{qg} i_{qg}\right) \quad (3)$$

$$Q_g = 1.5\left(U_{qg} i_{dg} - U_{dg} i_{qg}\right) \quad (4)$$

The GSC controller is devoted to regulate the DC link voltage, V_{dc} and control the reactive power flow between the GSC and the grid. Under normal conditions, the GSC usually operates with a unity power factor by regulating Q_g to zero. The DC link voltage and reactive power are controlled via regulating the grid side converter current components i_{dg}, i_{qg} respectively. The output of the control loops is the GSC reference voltage U^*_{gabc}. The GSC conventional control strategy is illustrated in Fig. 4. Subsequent to the fault, a large transient rotor current will flow and a surplus

rotor power as well which need to be transmitted by the GSC. Nonetheless, due to the lack of sufficient ac voltage at the GSC terminals, the DC link voltage rises quickly [8]. Also, the more the GSC is incapable of transmitting the power to/from the grid, the higher the GSC current, which can be destructive to the converter switches. To overcome this shortcoming, a faster GSC control method with higher ability to decouple the GSC control variables should be employed, which is elaborated next.

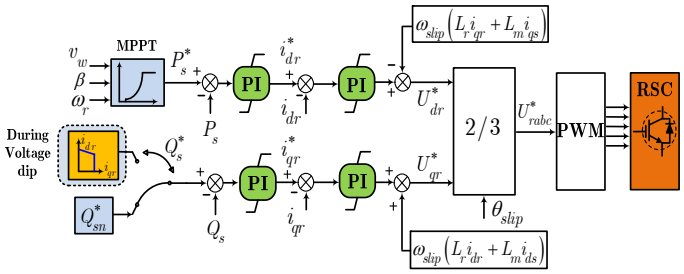

Fig. 3 RSC control scheme

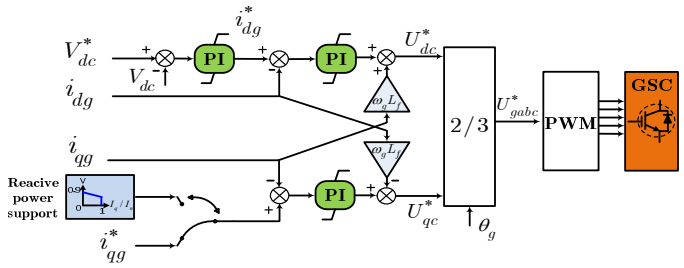

Fig. 4 Conventional GSC control scheme

C. GSC Proposed Nonlinear Controller

The conventional PI controllers suffer poor and sluggish response specially during transients due to the coupling among its control loops [2]. The nonlinear feedback control is proposed to ensure better transient performance and decoupled control between the DC link voltage and the reactive power. Fig. 5 shows a block diagram of the proposed nonlinear control strategy. Similar to the conventional GSC controller, the output of the control loops is the GSC reference voltage, U^*_{gabc}. The input variables of the nonlinear controller are defined as:

$$y_1 = V_{dc}, y_2 = Q_g \tag{5.a}$$

The DC link dynamics can be described by:

$$\dot{y}_1 = 1/C_{dc}\left(i_{dcg} - i_{dcr}\right) \tag{5.b}$$

For lossless GSC,

$$P_{DC} = V_{dc} i_{dcg} = P_g - P_f \tag{6}$$

Where, P_{DC}, P_f are the DC link transmitted power and the power loss through the interface reactor connecting the GSC to the grid respectively. C_{dc}, i_{dcg}, i_{dcr} are the DC link capacitance and currents respectively. To achieve linearization between the control algorithm inputs and outputs, "(5)", is to be differentiated till a direct relationship between them is obtained as:

$$\begin{bmatrix} \ddot{y}_1 \\ \ddot{y}_2 \end{bmatrix} = \begin{bmatrix} C_1 & 0 \\ 0 & C_3 \end{bmatrix} \begin{bmatrix} U_{dc} \\ U_{qc} \end{bmatrix} + \begin{bmatrix} C_2 \\ C_4 \end{bmatrix} \tag{7}$$

Where,

$$C_1 = -\left(1.5 / L_f C_{dc} V_{dc}\right) U_{dg} + \left(3R_f / L_f C_{dc} V_{dc}\right) i_{dg}$$

$$C_3 = -\left(1.5 / L_f\right) U_{dg}$$

$$C_2 = \left(3R_f^2 / L_f C_{dc} V_{dc}\right) i_{dg}^2 - \left(3R_f / L_f C_{dc} V_{dc}\right) P_g + \left(\omega_g / C_{dc} V_{dc}\right) Q_g + \left(1.5 / L_f C_{dc} V_{dc}\right) U_{dg}^2 - \left(3R_f \omega_g / C_{dc} V_{dc}\right) i_{dg} i_{qg} + \left(1.5 / C_{dc} V_{dc}\right) U_{qg} di_{qg} / dt - \left(3R_f / C_{dc} V_{dc}\right) i_{qg} di_{qg} / dt - \left(1 / C_{dc}\right) di_{dcr} / dt$$

$$C_4 = \left(1.5 / L_f\right) U_{dg} U_{qg} - \omega_g P_g - \left(R_f / L_f\right) Q_g + 1.5 i_{qg} dU_{dg} / dt$$

To obtain linear decoupled relationship with good tracking performance even with parameter uncertainty, U^*_{dc}, U^*_{qc} are expressed as [9]:

$$U^*_{dc} = 1 / C_1 \left(k_1 e_1 + k_2 \int e_1 dt + k_3 \dot{e}_1 + \ddot{y}^*_1 - C_2\right) \tag{8.a}$$

$$U^*_{qc} = 1 / C_3 \left(k_4 e_2 + k_5 \int e_2 dt + \dot{y}^*_2 - C_4\right) \tag{8.b}$$

Where, $e_1 = y^*_1 - y_1$, $e_2 = y^*_2 - y_2$

Substituting, (8) into (7), yields a decoupled system error model as:

$$\dddot{e}_1 + k_3 \ddot{e}_1 + k_1 \dot{e}_1 + k_2 e_1 = 0$$

$$\ddot{e}_2 + k_4 \dot{e}_2 + k_5 e_2 = 0$$

Where, $k_1, \ldots, k_5$ are control gains.

V. Simulation Results

To investigate the dynamic performance of the proposed control strategy under different operating conditions according to the Danish grid code, an intensive set of simulation case studies are performed for the system under study shown in Fig. 2. The system is simulated in the MATLAB/SIMULINK environment using SimPowerSystems toolbox and Simulink for system modeling and simulation. The system parameters are listed in the appendix. The simulations are carried out at the nominal wind speed of the WT (11m/s). Among the different simulation tests, certain safe limits (marked with dashed lines in the output results) are imposed on the system variables for protection purpose.

The maximum allowed limit for the DC voltage is 1.25 p.u., and 1.3 p.u., for the stator, RSC and GSC currents while 1.3 p.u., for the rotor speed.

A. LVRT and Grid Code Compliance

The system response to a three-phase fault in the middle of one of the transmission lines (see Fig. 2) with duration of 0.5 s is illustrated in Fig. 6. The fault results in stator voltage dip close to

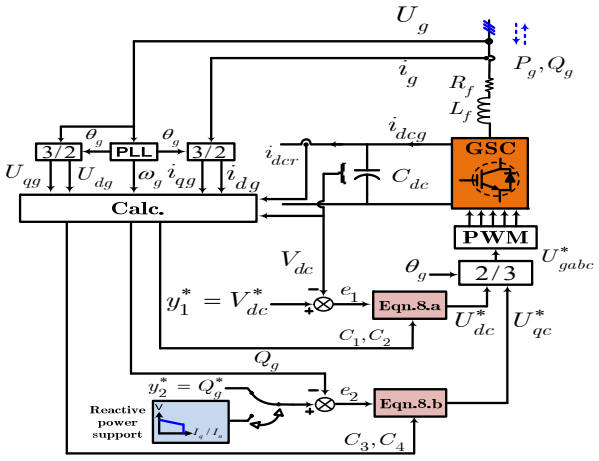

Fig. 5 GSC Nonlinear control scheme

0.2 p.u (Fig. 6-a). At the instant of voltage dip, higher stator and rotor currents are noticed as in Fig. 6-b,c. Owing to the abrupt increase of the rotor current, the rotor power which is fed to the GSC through the DC link simultaneously increases, which causes higher DC voltage oscillations due to lower ac voltage at the GSC terminals.

Higher DC voltage fluctuation in case of the conventional controller is recorded in Fig. 6-e compared with that of the proposed controller. This can be attributed to the fast injection of reactive power (Fig. 6-g) which contributes to supporting the ac voltage and consequently transporting more power through the GSC, and eventually results in relieving the DC voltage fluctuations.

Since the voltage drop impedes transferring all the wind mechanical power, the mismatch between the electromagnetic and mechanical torques results in rotor over-speed [5], as in Fig. 6-d but remains within the allowed limit. The active power in Fig. 6-f is reduced at the fault instant to a minimum value to limit the rotor over-speed and the system currents.

B. Asymmetrical Faults Response

Asymmetrical faults are recurring faults and lead to negative sequence currents of double frequencies which usually accompanied with higher oscillations that propagate in the DC link and may cause transient overvoltage beyond the limit [10], [11]. The system responses to a single-phase to ground fault and a phase-to-phase fault are shown in Figs. 7,8 respectively. The faults occur at t= 0.5 s and cleared 150 ms later [6] and cause 58% and 37% voltage dip respectively. It is obvious that double frequency component due to negative sequence currents is superimposed on the DC link voltage waveform as seen in Figs. 7,8-e. Comparing the results, it can be concluded that the phase-to-phase fault is severer as it causes higher voltage drop. Accordingly, higher DC link oscillations close to the limit are depicted in Fig. 8-e. The proposed controller is superior to its counterpart in both cases as it encounters lower overshoots, shorter settling time with damped performance as seen in Fig. 8-e,f. The rotor speed, stator and rotor currents are maintained below the limit for both methods.

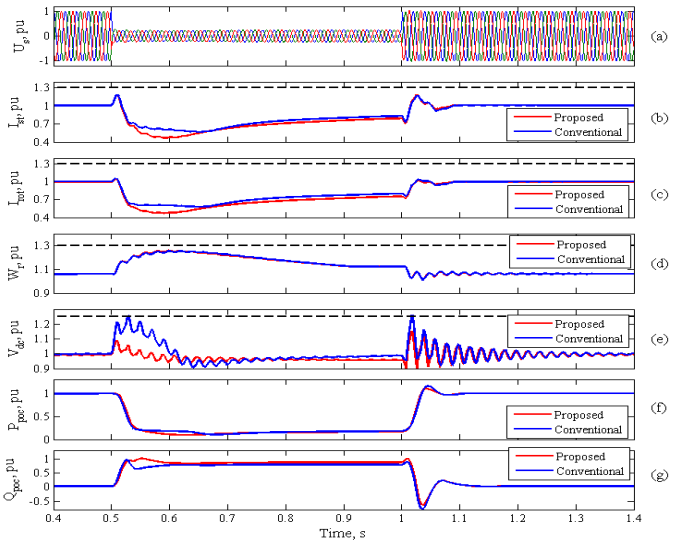

Fig. 6 Response of the DFIG WT system to a three-phase fault (a) DFIG stator voltage (b) Stator current (c) Rotor current (d) DFIG rotor speed (e) DC link voltage (f) Delivered active power (g) Delivered reactive power.

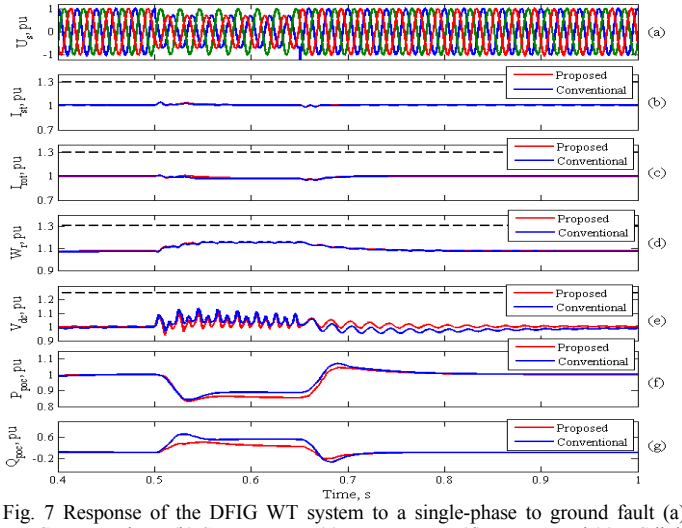

Fig. 7 Response of the DFIG WT system to a single-phase to ground fault (a) DFIG stator voltage (b) Stator current (c) Rotor current (d) Rotor speed (e) DC link voltage (f) Delivered active power (g) Delivered reactive power.

C. HVRT Response

To validate the HVRT requirement of the Danish grid code (Fig. 1-c), a double-open circuit fault at the point of common connection POC for 200 ms is applied and the obtained results are shown in Fig. 9. The stator voltage magnitude (Fig. 9-b) fluctuates during the fault and even exceeds the Danish grid code limit (1.2 p.u.). At the fault onset, the delivered active power rises which in turn increases the power fed to the GSC and thus

leads to higher DC voltage oscillations. The DC link voltage in case of conventional controller violates the limit as in Fig. 9-f. To counteract the voltage swell, the stator and rotor currents start to decrease to render the active power constant while the active power fluctuates around the nominal value. Compared with the conventional controller, the proposed controller has a higher capability to overcome the voltage swell and significant better transient performance.

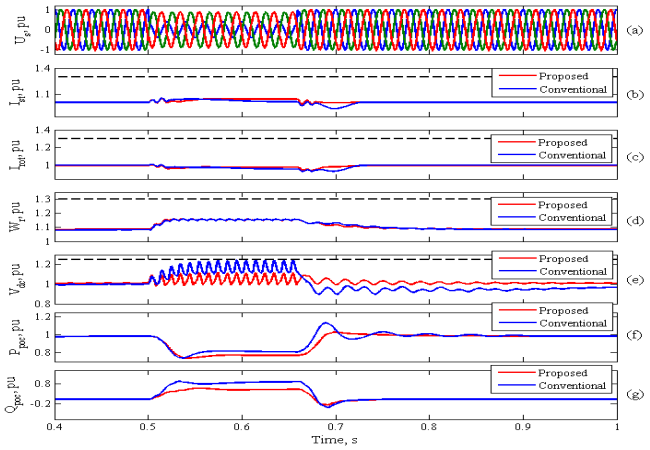

Fig. 8 Response of the DFIG WT system to a phase-to-phase fault (a) DFIG stator voltage (b) Stator current (c) Rotor current (d) DFIG rotor speed (e) DC link voltage (f) Delivered active power (g) Delivered reactive power.

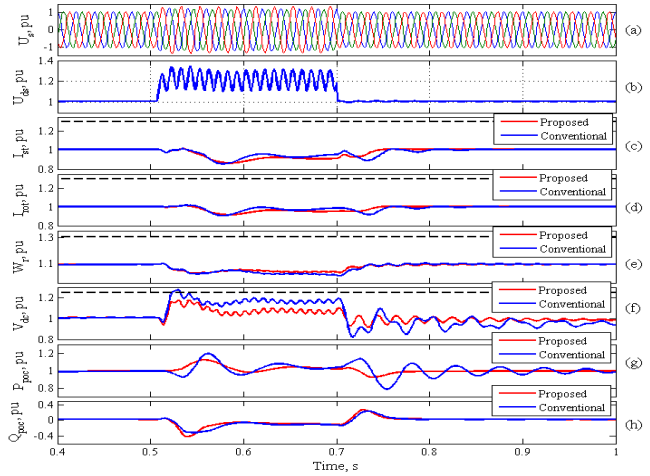

Fig. 9 Response of the DFIG WT system to a double open circuit fault at the POC. (a) DFIG stator voltage (b) Stator voltage magnitude (c) Stator current (d) Rotor current (e) DFIG rotor speed (f) DC link voltage (g) Delivered active power (h) Delivered reactive power.

VI. Conclusion

A Nonlinear controller has been presented for the GSC to achieve high dynamic performance, decoupled control between the DC link voltage and reactive power and meanwhile injects more reactive power during voltage dips to support the system voltage. Additional terms have been augmented with The RSC controller to suppress the stator and rotor currents and limit the over-speed of the rotor during faults. Besides, the RSC is dedicated to release additional reactive power to fulfill the grid code reactive power support requirement. Intensive simulation case studies have been carried out to assess the impact of the proposed control strategy on the FRT of DFIG WT.

The obtained output results reveal fast response with high dynamic performance for a wide range of operating conditions and assure the FRT capability of the proposed control strategy in compliance with the Danish grid code without additional hardware circuits.

Appendix

DFIG rated power, 2 MW; Number of pole pairs, 2; Stator resistance, 0.00488 p.u.; Stator leakage inductance, 0.1656 p.u.; Rotor resistance, 0.00549 p.u.; Rotor leakage inductance, 0.1763 p.u.; Mutual inductance, 3.9257 p.u.; Lumped inertia constant, 3 s; Rated rotor speed, 1.1 p.u.; Interface reactor resistance, 0.0063 p.u.; Interface reactor inductance, 1.98 p.u.; Rated DC link voltage, 1200 V; DC link capacitor, 16000 μF; Transmission line impedance, 0.11+j0.32 Ω/km.

References

[1] M. Mohseni and S. M. Islam, "Review of international grid codes for wind power integration: diversity, technology and a case for global standard", *Ren. Sustain. Energy Rev.,* vol. 16, no. 6, pp. 3876-3890, Aug. 2012.

[2] M. Mohseni and S. M. Islam, "Transient Control of DFIG-Based Wind Power Plants in Compliance With the Australian Grid Code", *IEEE Trans. Power Electron.,* vol. 27, no. 6, pp. 2813-2824, Jun. 2012.

[3] C. Wessels, F. Gebhardt, and F. W. Fuchs, "Fault ride-through of a DFIG wind turbine using a dynamic voltage restorer during symmetrical and asymmetrical grid faults", *IEEE Trans. Power Electron.,* vol. 26, no. 3, pp. 807-815, Mar. 2011.

[4] L. Yang, Z. Xu, J. Østergaard, Z. Y. Dong, and K. P. Wong, "Advanced control *strategy* of DFIG wind turbines for power system fault ride through", *IEEE Trans. Power Syst.,* vol. 27, no. 2, pp. 713-722, Jul. 2012.

[5] A. E. Leon, J. M. Mauricio, and J. A. Solsona, "Fault ride-through enhancement of DFIG-based wind generation considering unbalanced and distorted conditions", *IEEE Trans. Energy Convers.,* vol. 27, no. 3, pp. 775-783, Sept. 2012.

[6] Energinet. Technical regulation 3.2.5 for wind power plants with a power output greater than 11 kW; September 2010. Available at: http://www.energinet.dk.

[7] R. Sarrias, L. M. Fernández, C. A. García, and F. Jurado, "Coordinate operation of power sources in a doubly-fed induction generator wind turbine/battery hybrid power system", *Power sources.,* vol. 205, no. 1, pp. 354-336, May 2012.

[8] T. Sun, Z. Chen, F. Blaabjerg, "Transient Stability of DFIG Wind Turbines at an External Short-Circuit Fault", Wind Energy, 2005, 8:345-360.

[9] M. Rashed, S. M. A. El-Anwar, F. M. H. Youssef, "Nonlinear control scheme for VSC-HVDC transmission systems", *12th Int. Middle East Conf., MEPCON, 2008, pp. 486-491.*

[10] X. Yan, G. Venkataramanan, P. S. Flannery, Y. Wang, Q. Dong, and B. Zhang, "Voltage-sag tolerance of DFIG wind turbine with a series grid side passive-impedance network", *IEEE Trans. Energy Convers.,* vol. 25, no. 4, pp. 1048-1056, Dec. 2010.

[11] N. Aparicio, , Z. Chen, H. Beltran, E. Belenguer, , "Performance of Doubly-Fed Wind Power Generators During Voltage Dips", *International Workshop on Next Generation Regional Energy System Development, IWRES07, (invited paper), Seoul, Korea, January 2007*

Enhanced LVRT Control Strategy for DFIG-Based WECS in Weak Grid

S. Abulanwar [1,2]
[1]Energy Technology Department
[2]Sino-Danish Centre for Education and Research
Aalborg University
Aalborg, Denmark
ema@et.aau.dk

Zhe Chen[1,2]
[1]Energy Technology Department
[2]Sino-Danish Centre for Education and Research
Aalborg University
Aalborg, Denmark
zch@et.aau.dk

F. Iov [1]
[1]Energy Technology Department
Aalborg University
Aalborg, Denmark
fi@et.aau.dk

***Abstract*—An enhanced coordinated low voltage ride-through, LVRT, control strategy for a Doubly-fed Induction generator (DFIG)-based wind energy conversion system, WECS, connected to a weak grid is presented in this paper. The compliance with the grid code commitments is also considered. A proposed decoupled double synchronous reference frame (DDSRF) current controller is adopted for the design of grid side converter, GSC, controller to counteract current oscillations during asymmetrical faults and tackle the DC link voltage run-away. For a precise detection of the grid voltage position even under severe voltage dips/unbalanced conditions, A DDSRF-PLL is proposed and analyzed to extract clean synchronization signal in order to improve the overall system performance. Moreover, a fast decomposition based positive and negative sequence algorithm is utilized for rapid fault detection and to engage the LVRT protection scheme. Furthermore, additional compensation terms are incorporated with the traditional GSC and rotor side converter, RSC, controllers to effectively suppress rotor as well as stator currents and meanwhile regulate the rotor speed. A diverse set of voltage excursions are conducted to evaluate the effectiveness of the proposed control strategy using MATLAB/SIMULINK platform.**

Keywords-component; DFIG, LVRT, weak grid, DDSRF, PLL, grid code.

I. INTRODUCTION

Many countries are experiencing a rapid growth of wind energy, imposing significant stresses on transmission networks. A significant part of the expected wind energy will be via offshore wind farms which is usually located at a long distance from the main grid. Consequently, it is expected that the short circuit power of power systems will decrease which results in operation of wind power in weak grids [1]. Integration of wind power into weak grids can pose serious impacts regarding voltage fluctuation, post-fault power variation and finite transmission capacity to accommodate more wind power [2]. Adverse impacts on voltage, frequency and system stability emerged in China owing to the steady increase of wind power penetration into weak networks [3]. Due to the progressive increase of decentralized wind power plants, WPPs, the transmission system operators, TSO, in many countries have stipulated stringent regulations to the integration WPP which are known as grid codes [4]. Fig. 1.a depicts the German, Scottish and Irish grid code low voltage ride-through, LVRT, commitment which implies that the wind turbines, WTs, must remain connected if the terminal voltage within the shaded area [5]. As seen in Fig. 1.a, E.ON LVRT is onerous as it requests fault ride-through, FRT, capability for different faults accompanied with zero voltage dips for 150 ms duration. Irish grid code requires FRT against faults with remnant voltage of 0.15 p.u for more than 500 ms. According to the grid codes, WTs not only have to withstand grid excursions but also provide ancillary service regarding reactive power support as traditional generators to recover the ac voltage. Fig.1.b illustrates the Spanish and German reactive power support obligation. Typically, no reactive power support is demanded for voltage dips with remnant voltage of 0.9 p.u. Nevertheless, maximum reactive current support is required for voltage dips below 0.5 p.u. Among different topologies of wind energy conversion systems, WECS, Doubly-fed Induction generator wind turbine, DFIG WT, is intensively used due to certain features as variable speed operation and independent control of active and reactive power via using partial scale converters rated at 25-30% of rated power [5]. However, due to the direct connection of its stator to the grid, DFIG is sensitive to the grid disturbances and thus prone to different serious defects [6].

Typically, two main deficiencies are reported in the literature for the DFIG which are the higher transient stator and rotor currents at the instant of abrupt voltage dip as well as DC link overvoltage due to the inability of the grid side converter, GSC to transmit the surplus rotor circuit power [5],[6]. Traditionally, a crowbar is attached to the rotor circuit and activated during fault periods to address the aforementioned shortcomings. Nonetheless, once the crowbar is engaged, the rotor side converter, RSC is out of control, meanwhile the machine behaves as conventional induction generator absorbing higher reactive power [7]. With the aid of advanced control schemes during faults, DFIG LVRT can be successfully accomplished [3]-[8].

An analytical stability study of a 2 MW permanent magnet WT connected to ac grid of widely varying strength is presented

978-1-4799-1464-7/13/$31.00 ©2013 IEEE

by Nicholas *et al.* [1]. It has been concluded that operation of wind power in weak grids for SCRs below 4 is unsatisfactory unless if an advanced ac voltage controller is adopted. The impact of gain factor of the injected reactive current to support the ac voltage following sudden symmetrical voltage dips in weak grids was investigated by T. Neumann *et al.* [8]. It was found that, for weak grids having SCR of 4, WT can provide reactive power support through fast voltage control without any additional devices. However, for SCRs between 2 and 3, additional compensation devices are required to compensate the voltage level.

This paper presents an enhanced coordinated LVRT control strategy for DFIG WT operating in weak grid having SCR of 3 under symmetrical as well as asymmetrical faults. Besides, the proposed control scheme fulfills the grid codes obligations.

A decoupled double synchronous reference frame, DDSRF, current controller is adopted for the GSC controller to counteract the 2ω current oscillations during unbalanced operating conditions to regulate the DC link voltage during such cases. In addition, in order to cleanly extract the fundamental frequency positive-sequence component of grid voltage under various faults, a DDSRF based phase-locked loop, DDSRF-PLL is utilized. Additional proposed terms are incorporated with the conventional PI compensators of the GSC and RSC, to avoid the rotor and stator currents swell during voltage interruptions and limiting the rotor over-speed as well.

II. DFIG WT System Description

Fig. 2 demonstrates a schematic diagram of a DFIG WT connected to the grid. The system comprises a 2 MW DFIG WT, drive train and partial converters. The DFIG stator side is directly connected to the grid while the rotor side is connected via two two-level back-to-back PWM converters. The WT drive train is represented with the well-known two mass model. The overall DFIG WT control system is composed of two level control schemes, namely, wind turbine controller and DFIG converters controller. The former controls the WT mechanical output power via controlling the pitch angle and provides the reference rotor speed ω_{r-ref} corresponding to the maximum power point tracking, MPPT. The latter, is dedicated to control the DFIG converters, for regulating WT output active and reactive power using vector control theory.

III. Grid Synchronisation

A. Conventional SRF-PLL

The precise detection of the magnitude and phase angle of positive-sequence grid voltage is a crucial aspect for reliable operation of a grid-connected power electronic converter. A phase-locked loop, PLL, is a synchronization technique used to synchronize its output signal in phase and frequency with an input signal. The most widely used PLL within the area of power electronics and power systems, for positive-sequence detection is the three-phase, PLL based synchronous reference frame, SRF-PLL of which structure is depicted in Fig.3 [9]. A reliable PLL should render a clean phase angle irrespective of the grid voltage waveform. Under ideal utility conditions, SRF-PLL yields quick

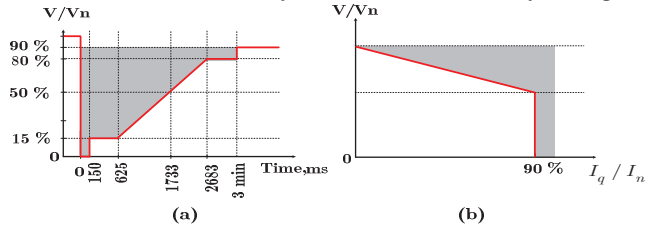

Figure 1. Typical WT Grid code requirements, (a) LVRT, (b) Reactive power support

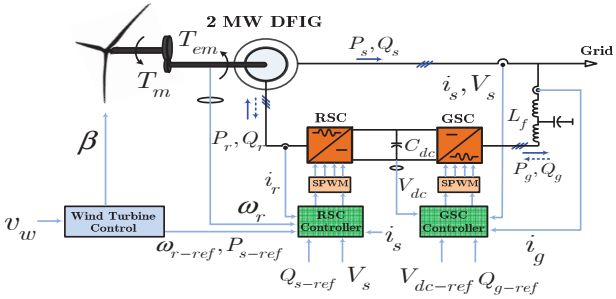

Figure 2. Schematic diagram of the DFIG wind turbine grid connected system

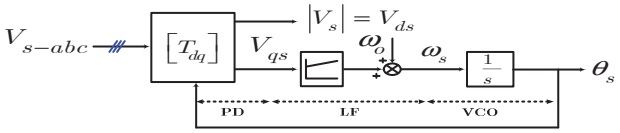

Figure 3. SRF-PLL basic structure

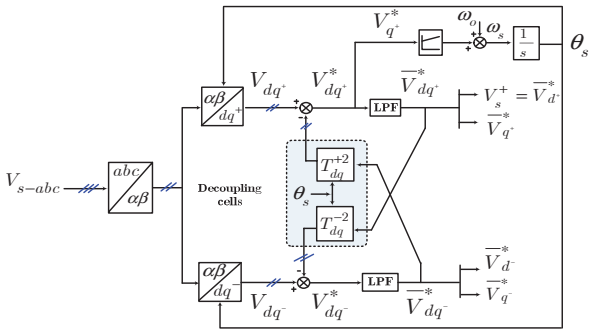

Figure 4. DDSRF-PLL basic structure

and accurate detection of grid voltage position. Whilst, under distorted/unbalanced grid voltage, SRF-PLL suffers poor dynamic performance even with reduced bandwidth [9]. Since grid codes require stringent regulations even with zero voltage dips, a high efficient PLL capable of extracting clean phase angle even with highly distorted or zero grid voltage is vital for achieving the grid code requirements.

B. DDSRF-PLL Structure

An enhanced SRF-PLL using double synchronous reference frames, DSRF, rotating with positive and negative synchronous

speeds is known as DSRF-PLL [9]. Augmenting a decoupling cell allows for cancellation of the reciprocal 2ω coupling effect of positive and negative sequence between both reference frames. Thereby, precise grid synchronization is possible even under unbalance utility conditions. Fig. 4 shows a block diagram of the DDSRF-PLL. The estimated output *dq* voltage components of the DDSRF-PLL can be formulated as [9]:

$$\bar{V}^{*}_{dq^{+}} = \begin{bmatrix} \bar{V}^{*}_{d^{+}} \\ \bar{V}^{*}_{q^{+}} \end{bmatrix} = \left[LPF \right] \left(V_{dq^{+}} - \left[T^{+2}_{dq} \right] \bar{V}^{*}_{dq^{-}} \right) \quad (1)$$

$$\bar{V}^{*}_{dq^{-}} = \begin{bmatrix} \bar{V}^{*}_{d^{-}} \\ \bar{V}^{*}_{q^{-}} \end{bmatrix} = \left[LPF \right] \left(V_{dq^{-}} - \left[T^{-2}_{dq} \right] \bar{V}^{*}_{dq^{+}} \right) \quad (2)$$

Where,

$$LPF(s) = \frac{\omega_f}{\omega_f + s} \quad (3)$$

$$\left[T^{+2}_{dq} \right] = \left[T^{+2}_{dq} \right]^{T} = \begin{bmatrix} \cos(2\omega_s t) & \sin(2\omega_s t) \\ -\sin(2\omega_s t) & \cos(2\omega_s t) \end{bmatrix} \quad (4)$$

The low pass filter, LPF, cut-off frequency, ω_f can be properly set to retain a better damping performance with fast response ($\omega_f = \omega_s/\sqrt{2}$) rad/s.

It is worth mentioning that, as the PLL filter is located outside the control loop, the DDSRF-PLL bandwidth is not affected.

IV. DFIG LVRT Control Strategy

A. Fault Detection Algorithm

Fast fault detection is a key point for rapid triggering of the FRT control strategy and effectively suppress the large transient currents. A fault detection algorithm, FDA, based positive and negative sequence component decomposition is adopted here [7]. In a broader context, the detection method is capable of decomposing the sequence components using the sample data at two points on the three-phase waveform [7]. Hence, the decomposition process can be executed after one sampling period. The stator voltage positive sequence component, V_s^+, is used as an indicator for a fault. Whenever, $V_s^+ < 0.9\ p.u.$, a fault is detected and thereby, the proposed FRT control strategy is activated to tackle the fault.

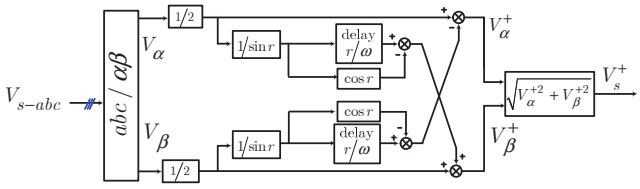

Figure 5. Fault Detection Schematic Diagram

B. GSC Controller

The model of the GSC in a *dq* reference frame whose *d-axis* is aligned with the stator voltage vector $\bar{V}_s$ can be described by the following set of differential equations:

$$di_{dg}/dt = -\left(R_f/L_f\right) i_{dg} + \omega_s i_{qg} + \left(V_{ds} - V_{dg}\right)/L_f \quad (5)$$

$$di_{qg}/dt = -\left(R_f/L_f\right) i_{qg} - \omega_s i_{qg} + \left(V_{qs} - V_{qg}\right)/L_f \quad (6)$$

Where, subscripts, *V,i,ω*, signify voltage, current, and angular speed. Subscripts, *s,g* refer to stator and grid sides. Indexes *d,q* stand for direct and quadrature axes of *dq* reference frame. R_f ,L_f refer to resistance and inductance of the GSC interface reactor.

The active and reactive power exchange between the GSC and the grid can be formulated as:

$$P_g = 1.5\left(V_{ds} i_{dg} + V_{qs} i_{qg}\right) \quad (7)$$

$$Q_g = 1.5\left(V_{qs} i_{dg} - V_{ds} i_{qg}\right) \quad (8)$$

The DC link dynamics can be written as:

$$\frac{1}{2} C_{dc} \frac{dV_{dc}^2}{dt} = P_r - P_g \quad (9)$$

The GSC controller is dedicated to regulate the DC link voltage, V_{dc} and control the reactive power flow between the GSC and the grid. During ideal conditions, the GSC usually operates with a unity power factor by regulating Q_g to zero. The DC link voltage and reactive power are controlled via regulating the grid side converter active and reactive current components i_{dg},i_{qg} respectively. The GSC control loops output is the reference GSC input voltage, V^*_{gabc}. Fig. 4 shows The GSC conventional control strategy. Subsequent to a fault, a large transient rotor current will flow and a surplus rotor power as well which need to be transmitted by the GSC. Owing to the transient unbalanced power flow between RSC and GSC, the DC link voltage rises quickly [5]. Accordingly, a proposed term $\left(P_g/V_{dc}\right)$ is augmented with the DC link voltage outer control loop during contingencies to reflect the momentary fluctuation of the GSC power and hence, enhancing the DC link voltage transient response. Besides, the GSC is dedicated to contribute to the reactive current support during voltage interruptions to satisfy the grid code requirement regarding reactive power support.

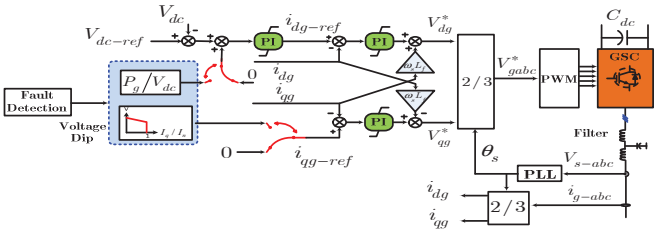

Figure 6. Conventional GSC control scheme

C. Proposed GSC Controller

Voltage sags can give rise to unbalanced grid voltages which may result in sustained oscillations in the delivered active and reactive power. Whilst it is generally accepted that traditional SRF *dq* current controllers are extensively used and implemented in different applications. Nevertheless, the performance of such controllers during unbalanced conditions is deficient [10]. DSRF for controlling positive and negative sequences using PI compensators seems to be better solution for unbalanced utilities.

An DSRF *dq* current controller incorporated with decoupling cells to eliminate the mutual 2ω cross-coupled oscillations arising from positive and negative sequence currents is adopted and dedicated for the control of the GSC which known as DDSRF *dq* current controller [10].

Similar to the decoupling cells approach used for DDSRF-PLL, the resultant DDSRF *dq* current controller can be expressed as:

$$i'^{+}_{g-dq} = i^{+}_{g-dq} + \underbrace{e^{-j(\theta^{-}_{s}-\theta^{+}_{s})}\cdot i^{-}_{g-dq}}_{\text{AC Term}} - \underbrace{e^{-j(\theta^{+}_{s}-\theta^{-}_{s})}\cdot\left(i^{-}_{dqg-ref} - \overline{\Delta i^{-}_{dqg}}\right)}_{\text{Decoupling cell}} \quad (10)$$

$$i'^{-}_{g-dq} = i^{-}_{g-dq} + \underbrace{e^{-j(\theta^{-}_{s}-\theta^{+}_{s})}\cdot i^{+}_{g-dq}}_{\text{AC Term}} - \underbrace{e^{-j(\theta^{-}_{s}-\theta^{+}_{s})}\cdot\left(i^{+}_{dqg-ref} - \overline{\Delta i^{+}_{dqg}}\right)}_{\text{Decoupling cell}}$$

The LPF cut-off frequency ω_f is selected as $(\omega_f = \omega_s/\sqrt{2})$ rad/s. the DDSRF controller block diagram which abridges (10) is shown in Fig.7. The outer controller of the DDSRF current controller is the same as that in [11].

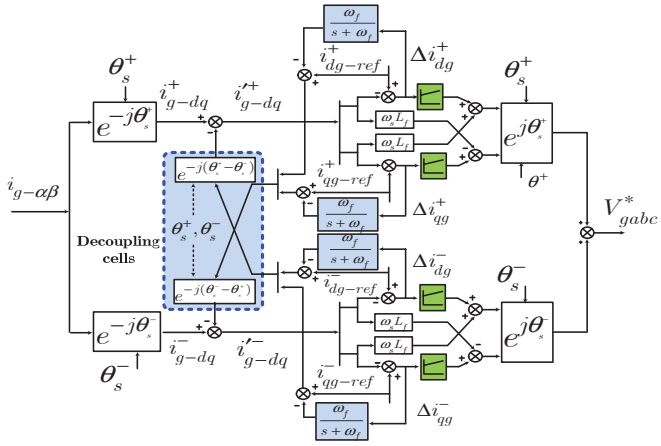

Figure 7. GSC DDSRF dq current controller

D. RSC Controller

In normal operation, the DFIG stator active and reactive power decoupled control can be realized through vector control technique with a reference frame aligned with the stator voltage vector. The RSC control structure is as shown in Fig. 8. The RSC control strategy is implemented in a synchronous reference frame with the *d-axis* oriented with the DFIG stator voltage. The RSC is dedicated to attain decoupled control of stator side active and reactive powers and also provides the DFIG with a variable speed operation. The *d-axis* control loop regulates the stator active power, P_s, via regulating the reference rotor active power current component, $i_{dr\text{-}ref}$, which is generated by the outer control loop that provides variable speed operation according to the WT MPPT. The *q-axis* corresponds to the stator reactive power control which is controlled through the reference rotor reactive power current component, $i_{qr\text{-}ref}$. The output of the control loops is the RSC input voltage, V^{*}_{rabc}. Once the stator voltage dips, the DFIG delivered output power decreases as well. Meanwhile, the reference input power should be restrained to regain power balance, otherwise, power imbalance will give rise to higher rotor current and rotor over-speed. Under normal operation, the DFIG output power can be defined as:

$$P_t = k_{opt}\,\omega^{3}_{r-ref} \quad (11)$$

Where,

$$k_{opt} = \frac{0.5\rho A_b r_b^{3} C_{p-\max}}{N_g^{3}\lambda_{opt}^{3}} \quad (12)$$

To suppress the rotor as well as stator currents during contingencies, whenever, a faulty condition is detected, the MPPT is deactivated and the reference active power is given by [12]:

$$P_{s-ref} = k_p k_{opt}\left(V_s/V_{so}\right)^{2}\omega^{3}_{r-ref} \quad (13)$$

Where, k_p is a reduction factor. V_{s0}, V_s signify the stator voltage pre and during the fault respectively. Equation "13" implies that the rotor active power current component will be reduced during the fault but pursuing less active power production which is recommended by the British and Danish grid codes [5], [12]. Furthermore, the RSC controller concurrently releases reactive current support with the remnant rotor current to satisfy the grid code reactive power support commitment.

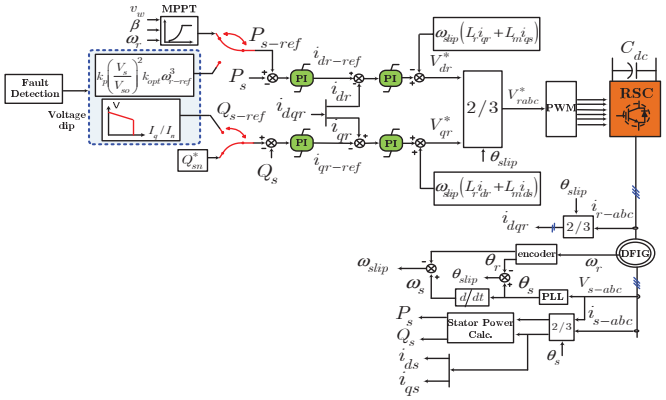

Figure 8. RSC control scheme

V. Simulation Verifications

To clarify the effectiveness of the proposed control strategy under diverse excursions, a set of simulations are conducted for a 2 MW DFIG WT system shown in Fig. 9. The system is simulated in the MATLAB/SIMULINK platform. The simulations are carried out at the nominal wind speed of the WT (11.4m/s).

For the safety of system operation, the maximum allowed limit for the DC voltage is 1.25 p.u. Stator and rotor protection thresholds are set to 1.5 p.u. However, the RSC can sustain 2 p.u overcurrent for a very short time [8]. Moreover, the pitch controller will be activated during voltage dips to regulate the rotor speed. To hold a fair comparison, the fault detection algorithm and the FRT additional terms for RSC and GSC will be added to the conventional control strategy within the simulations.

A. *LVRT Operational Scenario*

The system response to a symmetrical 3ϕ fault ($X_f/R_f = 5$) in the transmission system (see Fig. 9) with duration of 0.5 s is depicted in Fig. 10. During the fault, the stator voltage (Fig. 10.a) falls down to 95% which corresponds to a severe fault, while the FRT protection is triggered via the FDA for protection purpose. At t=1.2s, the fault is cleared and later the normal operation is retrieved. At the onset of voltage dip, higher stator and rotor transient currents are noticed in Fig. 10.c-f. Owing to the abrupt increase of the rotor current, the rotor power fed to the GSC through the DC link simultaneously increases, which causes higher DC voltage oscillations due to lower ac voltage at the GSC terminals.

Compared with the proposed control strategy, the DC voltage for the conventional scheme encounters higher spike (1.32 p.u) and even exceeds the safe margins as recorded in Fig.10.l whereas, in case of the proposed strategy, the DC voltage is effectively regulated in the allowed range with faster response and lower settling time, see Fig.10.k.

Moreover, it can be seen from the results (Fig.10.m,n) that the activation of the FRT scheme in the RSC controller plays a significant role in regulating the power balance mismatch by reducing the DFIG input power in response to the output power reduction due to the fault and thus limiting stator as well as rotor currents (Fig.10.c-f) by both control methods.

The rotor over-speed is also limited subsequent to triggering the pitch control, see Fig 10.i,j. According to the grid code (Fig.1.b), reactive current support should be resumed with the voltage dip remnant value below 0.9 p.u. Fig.10.o,p demonstrates the WT reactive power current component released in response to the voltage dip via stator and GSC sides. Obviously, it can be seen that the reactive current in case of the proposed method attain its maximum value steadily during the fault while for the conventional method, fluctuates and loses the successful reactive current support. This can be attributed to the loss of the exact vector control orientation as a consequence to the severe voltage dip with 95% drop due to the fluctuation caused by the lower weak grid SCR as noticed in Fig.11.b,d. On the other hand, Fig.11.a,c evidences that The DDSRF-PLL extracts a clean and unaffected synchronization signal which in turn enhances the overall system performance under such sever fault and also fulfill the grid code requirement.

B. *Asymmetrical Faults Response*

Asymmetrical faults are widely recurring and accompanied with negative sequence currents which can result in sustained DC voltage and electromagnetic torque oscillations. In a broader context, the latter can adversely impact the WT coupling shaft while the former can damage the WT converters which eventually might trip the DFIG WT during such faults [6]. The system responses to a $\phi - g$ fault in phase A with 90% voltage dip and a 2ϕ fault with 50% voltage dip are shown in Figs. 12,13 respectively. The faults occur at t= 0.7 s and cleared 150 ms later. Pre-fault, the dominant rotor current frequency is $|s|\omega_s/2\pi = 5\,Hz$ while during the fault, $|2-s|\omega_s/2\pi = 105\,Hz$. With the sequence currents controlled via the GSC proposed method, the DC voltage oscillation is mitigated (Figs.12,13.k) compared with that of the conventional method (Figs.12,13.l). It can be noticed from the results that the stator and rotor currents are effectively restrained below 2 p.u. It is worth mentioning that, the stator active power and injected reactive current (Fig.12,13.m-p) during both faults are oscillated dramatically due to the limited control capability of the RSC [6]. Nonetheless, the oscillation is less in case of the proposed control strategy with better post-fault recovery performance (Figs.12,13.m-p). This is due to the identical control efforts done by the proposed GSC controller for the sequence currents [6] and concurrently the robust performance of the DDSRF-PLL which extracts an unaffected signal irrespective of the unbalanced grid voltage as seen in Fig.11.i,o. Moreover, the distorted stator voltage phase angle (Fig.11.j,p) and its respective *dq* voltage components (Fig.11.l,r) detected by the SRF-PLL impacts the commonly used vector control orientation scheme and adversely affects the control objectives.

Comparing the results, it can be concluded that the 2ϕ fault is severer as it causes lower voltage and larger currents. Accordingly, higher DC link overshoots of 1.4 p.u are depicted in Fig. 13.l which is quite far from the limit under conventional GSC control method. Furthermore, it was found that the rotor speed was increased slightly (5.5%) due to the activation of the pitch controller in response to the voltage dip.

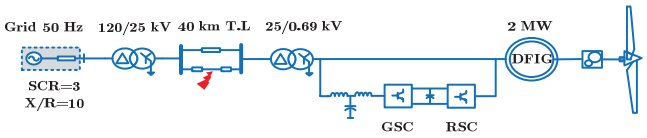

Figure 9. Single line diagram of the studied system

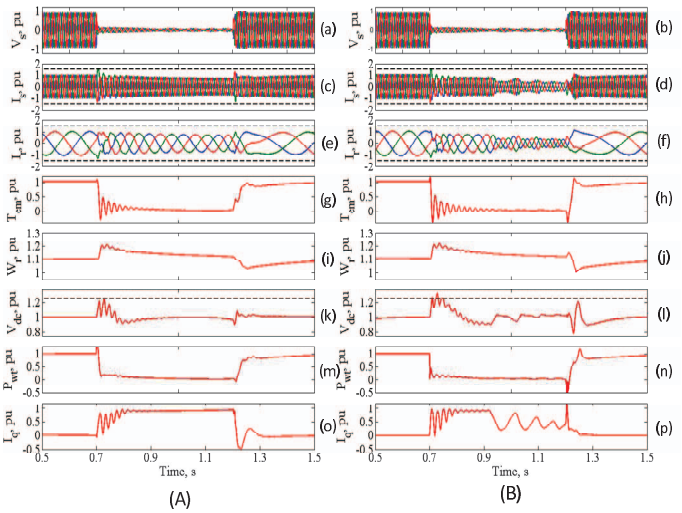

Figure 10. Response of the DFIG WT system to a symmetrical 3ϕ fault with $X_f/R_f = 5$ (A) proposed control strategy (B) Conventional control strategy.

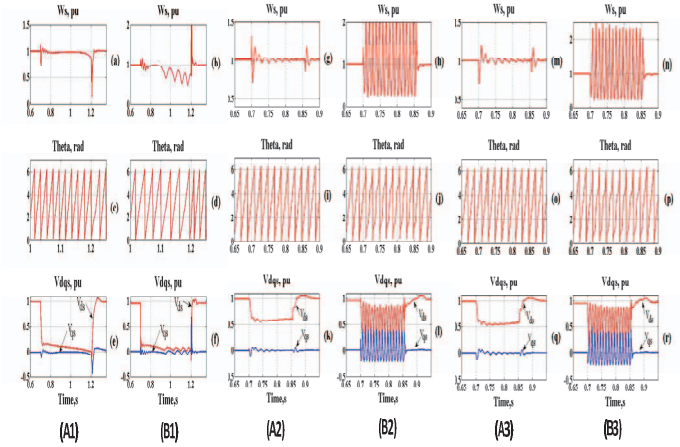

Figure 11. Tracking response of the PLL for $3\phi, \phi - g$ *and* 2ϕ faults respectively. (A1-A3) DDSRF-PLL. (B1-B3) SRF-PLL

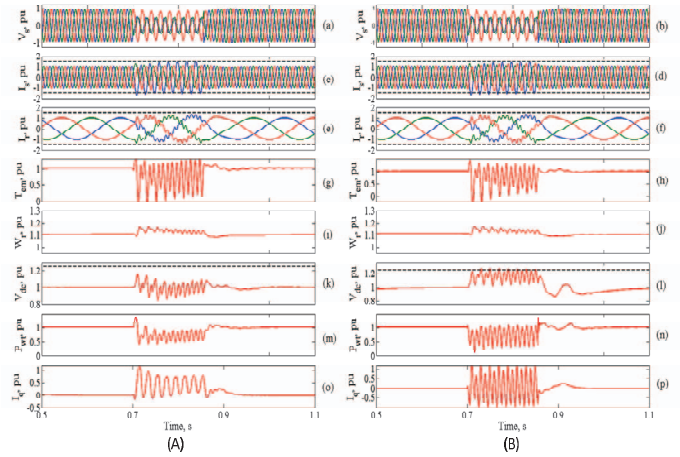

Figure 12. Response of the DFIG WT system to asymmetrical $\phi - g$ fault with $X_f/R_f = 5$ (A) proposed control strategy (B) Conventional control strategy.

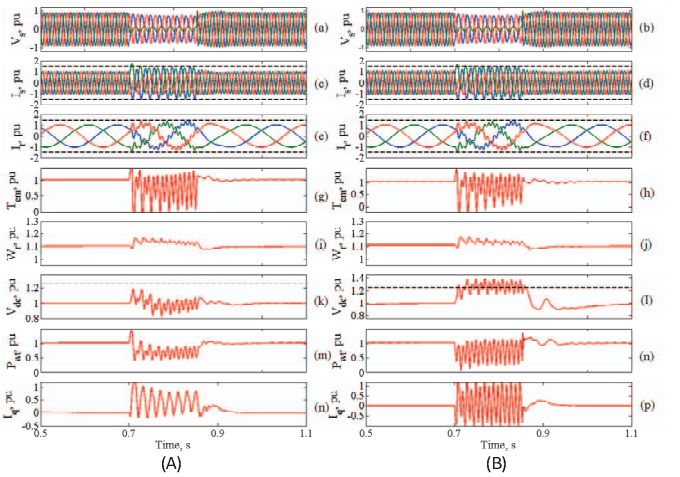

Figure 13. Response of the DFIG WT system to asymmetrical 2ϕ fault with $X_f/R_f = 5$ (A) proposed control strategy (B) Conventional control strategy.

VI. CONCLUSION

A DDSRF current controller for GSC has been presented to achieve high dynamic performance, counteract current oscillations and regulate the DC link voltage during disturbances.

A DDSRF-PLL to extract a clean, unaffected synchronization signal irrespective of the grid voltage waveform has been also presented to enhance the overall system performance under severe voltage dips.

Additional terms have been augmented with The RSC and GSC controllers to suppress the stator and rotor currents and limit the rotor over-speed during faults and fulfill the grid code requirements. Besides, a fast decomposition algorithm for rapid fault detection has been discussed. Diverse simulations have been conducted to assess the impact of the LVRT proposed strategy on the DFIG WT connected to a weak grid.

The obtained results assure the capability of the DFIG WT connected to a weak grid of SCR of 3 to comply with the grid codes requirements using the proposed control strategy.

REFERENCES

[1] T. Neumann, C. Feltes and I. Erlich "Response of DFG-based wind farms operating on weak grids to voltage sags", *Power and Energy Society General Meeting Conf*., pp. 1-6, July. 2011.

[2] N. Strachan and D. Jovcic "Stability of a variable-speed permanent magnet wind generator with weak AC grids", *IEEE Trans. Power Del*., vol. 25, no. 4, pp. 2779-2788, Oct. 2010.

[3] X. Zhao., et al., "Constraints on the effective utilization of wind power in China: An illustration from the northeast China grid," *Ren. Sus. Energy Rev*., vol. 16, no. 7, pp. 4508-4514, Sep. 2012.

[4] M. Mohseni and S. M. Islam, "Review of international grid codes for wind power integration: diversity, technology and a case for global standard", *Ren. Sustain. Energy Rev.,* vol. 16, no. 6, pp. 3876-3890, Aug. 2012.

[5] D. Xie, et al., "A Comprehensive LVRT Control Strategy for DFIG Wind Turbines With Enhanced Reactive Power Support", *IEEE Trans. Power Sys*., In press.

[6] H. Geng, C. Liu and G. Yang, "LVRT capability of DFIG-based WECS under asymmetrical grid fault condition", *IEEE Trans. Ind. Electron.,* vol. 60, no. 6, pp. 2495-2509, Jun. 2013.

[7] J. Yao, et al., "Enhanced control of a DFIG-based wind-power generation system with series grid-side converter under unbalanced grid voltage conditions", *IEEE Trans. Power Electron.,* vol. 28, no. 7, pp. 3167-3181, July. 2013.

[8] S. Xiao, G. Yang, H. Zhou and H. Geng, "An LVRT control strategy based on flux linkage tracking for DFIG-based WECS", *IEEE Trans. Ind. Electron.,* vol. 60, no. 7, pp. 2820-2832, July. 2013.

[9] P. Rodríguez et al., "Decoupled double synchronous reference frame PLL for power converters control", *IEEE Trans. Power Electron*., vol. 22, no. 2, pp. 584-592, Mar. 2007.

[10] M. Reyes, et al., "Enhanced decoupled double synchronous reference frame current controller for unbalanced grid-voltage conditions", *IEEE Trans. Power Electron*., vol. 27, no. 9, pp. 3934-3943, Sep. 2012.

[11] N. Jelani and M. Molinas, "Mitigation of asymmetrical grid faults in induction generator-based wind turbines using constant power load", *Energies,* vol. 6. pp. 1700-1717, Mar. 2013.

[12] Energinet. Technical regulation 3.2.5 for wind power plants with a power output greater than 11 kW; September 2010. Available at: http://www.energinet.dk.

Improved FRT Control Scheme for DFIG Wind Turbine Connected to a Weak Grid

S. Abulanwar [1,2], *Graduate Student Member, IEEE,* Zhe Chen[1,2], *Senior Member, IEEE,* F. Iov[1], *Senior Member, IEEE*
[1]Energy Technology Dept., Aalborg University, [2]Sino-Danish Centre for Education and Research
Pontoppidanstraede 101, Aalborg East, Denmark
ema@et.aau.dk

***Abstract*— This paper presents an improved coordinated fault ride-through (FRT) control strategy for a doubly fed induction generator (DFIG) based wind turbine, (WT), in a weak grid. A technique for grid synchronization against voltage excursions, i.e., a Dual Second Order Generalized Integrator – Frequency Locked Loop (DSOGI-FLL) is utilized to extract a robust grid voltage synchronization signal irrespective of the mains condition to enhance the overall system performance. Besides, a decoupled double synchronous reference frame (DDSRF) dq current controller is devoted for the grid side converter, (GSC), controller to counteract current ripples and tackle the DC link voltage fluctuations. Also, a reactive power support scheme to manage the DFIG reactive power during contingencies and fulfill the grid codes obligations is presented. Moreover, additional control terms are employed with the DFIG converters controllers to counteract rotor as well as stator currents and regulate the rotor speed. Simulation results which assure the effectiveness of the proposed control scheme is presented.**

Index Terms*— DFIG, DSOGI-FLL, FRT, grid code, weak grid.

I. INTRODUCTION

Wind energy conversion systems (WECS) are typically located in remote zones and connected to the grid via long feeders with lower short circuit ratios (SCRs). In the areas which geographically rich in wind energy, the transmission of huge amount of wind power to the power grid is restricted due to the transmission network weak structure [1]. In a weak grid, a change in active and/or reactive power can pose considerable voltage variation which can be a limiting factor for the integration of more wind power [2]. Besides, the impact of WT output power on the voltage quality can be another limiting factor which necessitates the incorporation of enhanced control systems to address such defects [2], [3].

Owing to the steady growth of decentralized wind power plants, (WPPs) many countries have imposed stringent regulations to the (WPPs) integration which known as grid codes [3]-[5]. Fig. 1.a shows the low voltage ride-through (LVRT) regulation for the German, Scottish and Irish grid code in which the wind turbines (WTs) must stay connected when the terminal voltage lies in or above the shaded area [3]. As illustrated in Fig. 1.a, E.ON LVRT demands fault ride-through (FRT) for voltage levels down to zero with 150 ms duration. Moreover, WTs should release reactive power support as traditional generators to boost and recover the ac voltage. Fig.1.b depicts the German and Spanish reactive power support requirement. Basically, reactive current support is substantial for voltage dips with remnant voltage less than 0.9 p.u., while full reactive current support is necessary for severe voltage dips with remnant voltage lower than 0.5 p.u [3], [4]. DFIG WTs, are extensively preferred due to variable speed operation using partial scale converters rated at 25-30% that allows for independent control of active and reactive power [4]. Nevertheless, DFIG is sensitive to the grid faults and thus prone to various serious issues due to the direct connection of its stator to the grid [2]-[4].

Subsequent to a fault, the rotor side and grid side converters, RSC, GSC respectively are prone to overcurrents and overvoltage unless an additional protection is incorporated. Usually, a crowbar circuit is inserted in the rotor side and activated upon fault detection to mitigate the above-mentioned shortcomings. However, triggering the crowbar results in blocking the RSC, meanwhile the machine absorbs higher reactive power as a conventional induction generator [3]. Using advanced control strategies, DFIG LVRT can be dramatically achieved [2]-[5].

In [5], a stability study for a permanent magnet WT connected to a weak grid is presented. It was shown that the operation of WTs in weak grids with SCRs below 4 is viable by means of advanced ac voltage controllers. The influence of the injected reactive current control to support the ac voltage due to symmetrical faults in a weak grid is investigated in [6]. It has been concluded that, DFIG WT can readily provide reactive power support via fast voltage control for weak grids with SCR of 4. Despite this, further compensation circuits are necessary to support the terminal voltage for SCRs between 2 and 3.

This paper provides an improved coordinated FRT control scheme for DFIG WT connected to a weak grid of SCR of 3 under different contingencies to fulfill the grid code requirements.

Typically, classical synchronous reference frame (SRF) dq current controllers render deficient performance during unbalanced utility conditions. To overcome such shortcoming, a decoupled double synchronous reference frame, (DDSRF) current controller is dedicated to control the GSC to tackle the double-frequency current oscillations and regulate the dc link voltage during disturbances. A reactive power support control scheme is presented to effectively satisfy the grid codes reactive

978-1-4799-2522-3/13/$31.00 ©2013 IEEE

power boost obligation. Besides, a Dual Second Order Generalized Integrator – Frequency Locked Loop (DSOGI-FLL) is utilized so as to furnish a robust grid voltage synchronization signal against various perturbations.

For better regulation of the transient rotor currents, proportional integral plus resonant, PIR controllers are employed in the RSC controller. Additional proposed blocks are integrated with the DFIG converters controllers, to mitigate the rotor and stator overcurrents during voltage interruptions.

II. DFIG WT Capability Limits

The capability limits of a 2 MW DFIG considering stator and rotor currents heating constraints due to Joule's losses, maximum and minimum active and reactive power is shown in Fig.2 [1]. Identifying the control abilities of the DFIG aims at optimally design the DFIG control system in order to improve the system operation. More details about such capability limits can be found in [2].

III. Grid Synchronization

A. SRF-PLL Synchronization

Among the different aspects for the control of the grid-connected converters, is the exact synchronization with the utility voltage. Phase Locked Loop, PLL based synchronous reference frame, SRF-PLL is the most intensively used technique for detecting the magnitude and position of the positive-sequence grid voltage.

The basic structure of SRF-PLL is shown in Fig.3. Despite its good behaviour under normal conditions, SRF-PLL provides poor dynamic response under unbalanced grid conditions even with reduced bandwidth [7].

B. DSOGI-FLL Synchronization

Fulfilling the grid codes requirements and keeping the WT connected during contingencies entails the usage of alternative synchronization technique. Dual Second Order Generalized Integrator, DSOGI based Frequency Locked Loop, DSOGI-FLL is an insensitive frequency-adaptive synchronization mechanism which benefits the instantaneous symmetrical component analysis considering adaptive filters [7]. Being frequency-based, DSOGI-FLL can efficiently ride-through the grid perturbations, provides a clean synchronization signal and attenuates grid voltage high-frequency components [8]. Fig. 4 illustrates the DSOGI-FLL structure. Further details about DSOGI-FLL can be obtained from [7], [8]. Performance comparison between SRF-PLL and DSOGI-FLL will be presented through the simulation.

IV. Proposed DFIG FRT Control Scheme

This section provides an insight into the coordinated DFIG FRT control strategy used to improve the system performance and meanwhile satisfy the grid codes requirements.

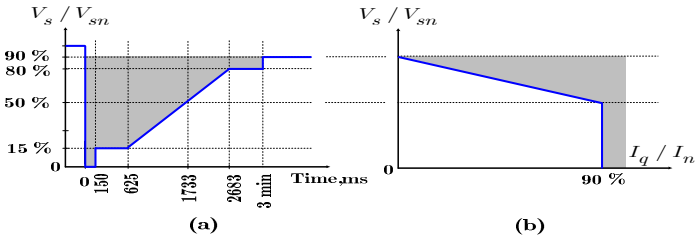

Figure 1. Typical WT Grid code requirements, (a) LVRT (b) Reactive power support

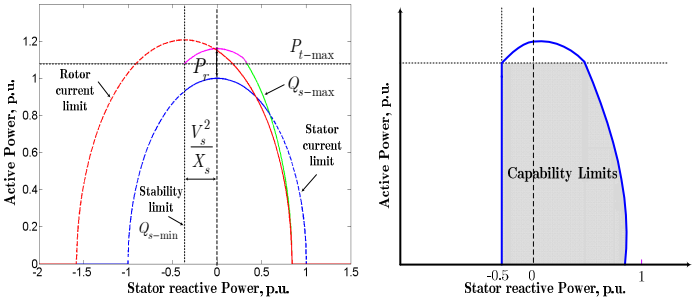

Figure 2. DFIG capability limits (a) Capability limits (b) Final capability area

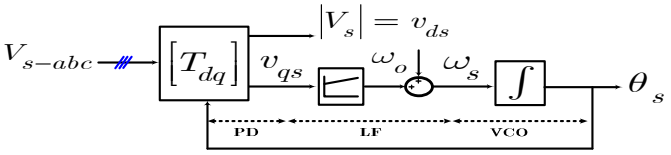

Figure 3. SRF-PLL basic structure

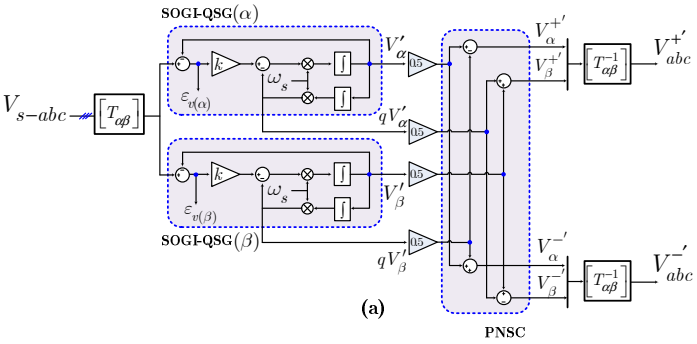

Figure 4. DSOGI-FLL basic structure

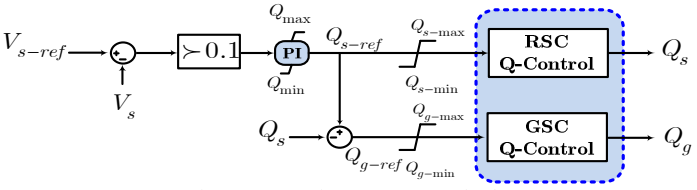

Figure 5. Reactive power control scheme

A. Reactive Power Support Control Scheme

A cascaded reactive power control scheme (see Fig.5) devoted to manage the reactive power sharing via DFIG stator as well GSC sides is adopted here [3]. The priority for the reactive power aid is given to the DFIG stator side -which processed via the RSC control- followed by the GSC side whenever the stator side attains the limit - due to severe faults - which pre-defined through the DFIG capability limit mentioned in section II. The reactive power support is initiated once the rms stator voltage, V_s slips more than 0.1 p.u (see Fig.1) out of the reference value, V_{s-ref}. Typical limiters are incorporated to ensure that the released reactive power does not overtake the respective capability limits of stator and GSC each. Such management scheme is efficient as the GSC reactive power support starts subsequent to the stator side injection which allows for active power transmission at the fault onset and thus mitigating the unwanted transient DC voltage fluctuations.

B. RSC Control Scheme

The stator side active and reactive powers, P_s, Q_s can be regulated via acting on the respective rotor dq voltage components. The RSC applied control scheme is demonstrated in Fig.6. The RSC controller is implemented in a reference frame of which *d-axis* is aligned with the stator voltage vector.

For further improvement of the RSC transient response, PIR current regulators are employed in the RSC controller as shown in Fig. 7 [9]. The parallel resonant blocks are tuned at $\omega_s, 2\omega_s$. ω_c is the cut-off frequency and k_{ir} is the proportional gain at the resonant frequency. Hence, the RSC dq voltage components are set as:

$$v_{dr} = PIR\left(i_{dr-ref} - i_{dr}\right) - \omega_{slip}\left(L_r i_{qr} + L_m i_{qs}\right) \quad (1.a)$$

$$v_{qr} = PIR\left(i_{qr-ref} - i_{qr}\right) + \omega_{slip}\left(L_r i_{dr} + L_m i_{ds}\right) \quad (1.b)$$

Where, i_{dr}, i_{qr} are the rotor active and reactive current components respectively. i_{ds}, i_{qs} are the stator side active and reactive current components. ω_{slip} is the slip frequency. L_r, L_m refer to rotor and magnetizing inductances.

The stator active and reactive powers, P_s, Q_s can be regulated via the RSC currents, i_{dr}, i_{qr} and subsequently rotor dq voltage components, v_{dr}, v_{qr}.

Whenever the stator voltage dips, the DFIG output power decreases as well. Accordingly, to tackle the transient rotor as well as stator currents and maintain the power balance, the MPPT is deactivated and the reference active power is set as [10]:

$$P_{s-ref} = k_p k_{opt}\left(V_s / V_{so}\right)^2 \omega_{r-ref}^3 \quad (2)$$

$$k_{opt} = 0.5\rho A_b r_b^3 C_{p-\max} / N_g^3 \lambda_{opt}^3 \quad (3)$$

Where, k_p is a gain factor. V_{s0}, V_s refer to the stator voltage before and during the fault respectively and ω_{r-ref} is the reference rotor speed. With "2", tiny active power supply is sustained during severe faults as recommended by the British and Danish grid codes [3], [10]. With the aid of the reactive power support scheme, the RSC concurrently injects reactive current support with the remnant rotor current to fulfill the grid code commitment and restore the ac voltage.

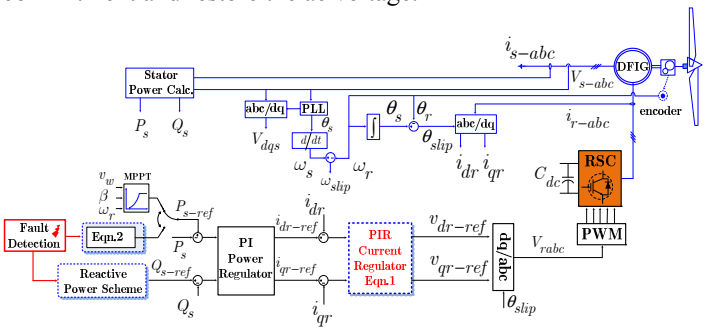

Figure 6. RSC control scheme

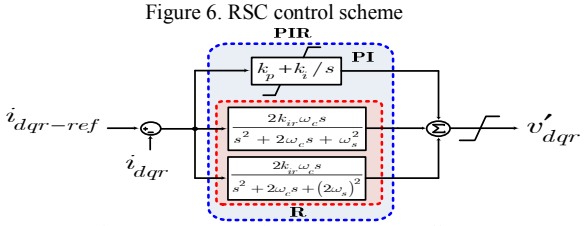

Figure 7. RSC PIR inner current controller

C. Conventional GSC Control Scheme

Likewise, the GSC controller is applied in a reference frame whose d-axis is oriented with the stator voltage$(v_{qs} = 0)$. The dc link voltage, V_{dc} and the reactive power exchanged between the grid and the GSC sides,Q_g can be controlled through acting on the dq GSC voltage components which can be expressed as:

$$v_{dg} = v_{ds} + \omega_s L_f i_{qg} - L_f\, di_{dg}/dt - R_f i_{dg} \quad (4)$$

$$v_{qg} = -\omega_s L_f i_{dg} - L_f\, di_{qg}/dt - R_f i_{qg} \quad (5)$$

Where, subscripts, v,i,ω, stand for voltage, current, and angular speed. Subscripts, s,g signify stator and grid sides. Indexes d,q stand for direct and quadrature axes of dq reference frame. R_f ,L_f refer to GSC interface reactor resistance and inductance.

The active and reactive power flow between the GSC and the grid can be written as:

$$P_g = 1.5 v_{ds} i_{dg} \quad (6)$$

$$Q_g = -1.5 v_{ds} i_{qg} \quad (7)$$

The DC link dynamics is given by:

$$\frac{1}{2} C_{dc} \frac{dV_{dc}^2}{dt} = P_r - P_g \quad (8)$$

In normal conditions, the GSC typically operates with a unity power factor, $Q_g = 0$. Fig. 8 illustrates The GSC traditional control scheme. To mitigate the dc voltage fluctuations during interruptions, a proposed term (P_g/V_{dc}) is activated and added to

the dc link voltage control loop to reflect the transitory variation of the GSC power. The latter can be attributed to the power imbalance between the RSC and GSC resulting from the surplus rotor power followed by the transient voltage dip which adversely impacts the dc voltage transient response [3].

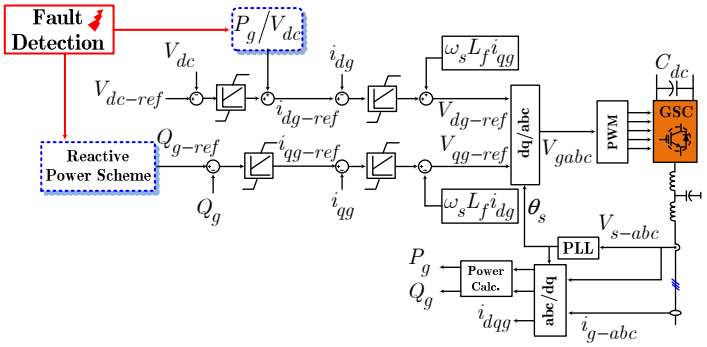

Figure 8. Conventional GSC control scheme

D. *Proposed GSC Controller*

Undoubtedly, LVRT and the associated DFIG WT converters control is a key point to satisfy the grid code requirements. Unbalanced grid voltages emerging from asymmetrical voltage dips can certainly cause sustained oscillations in the DFIG generated active and reactive power. Though this demerit can be overcome via injecting appropriate unbalanced currents by negative sequence controllers, the conventional SRF *dq* current controllers cannot accurately accomplish such objective due to sluggish dynamic performance [11].

Using DDSRF based PI regulators for controlling positive and negative sequences has been intensively implemented and thus can meet the target under such unbalanced grid conditions. Fig.9 shows the DDSRF respective positive and negative reference frames (dq^+, dq^-) rotating with the synchronous speed ($\pm\omega_s$) with angular positions ($\pm\theta'$) respectively. In this regard, decoupling cells to eliminate the reciprocal double-frequency cross-coupled ripples affecting both SRFs are added to enhance the controller performance during unbalanced conditions [10].

Thereby, the resultant DDSRF *dq* current controller can be expressed as [11]:

$$i'^{+}_{g-dq} = i^{+}_{g-dq} + \underbrace{e^{-j(\theta^{+}_{s}-\theta^{-}_{s})}\cdot i^{-}_{g-dq}}_{\text{AC Term}} - \underbrace{e^{-j(\theta^{+}_{s}-\theta^{-}_{s})}\cdot\left(i^{-}_{dqg-ref} - \overline{\Delta i^{-}_{dqg}}\right)}_{\text{Decoupling Term}} \quad (9)$$

$$i'^{-}_{g-dq} = i^{-}_{g-dq} + \underbrace{e^{-j(\theta^{-}_{s}-\theta^{+}_{s})}\cdot i^{+}_{g-dq}}_{\text{AC Term}} - \underbrace{e^{-j(\theta^{-}_{s}-\theta^{+}_{s})}\cdot\left(i^{+}_{dqg-ref} - \overline{\Delta i^{+}_{dqg}}\right)}_{\text{Decoupling Term}} \quad (10)$$

The cut-off frequency of the LPF, ω_f is selected as ($\omega_f = \omega_s/\sqrt{2}$) rad/s. A schematic diagram that abridges (9-10) for the GSC DDSRF dq current controller is shown in Fig.10. The outer controller of the DDSRF current controller is the same as that in [12].

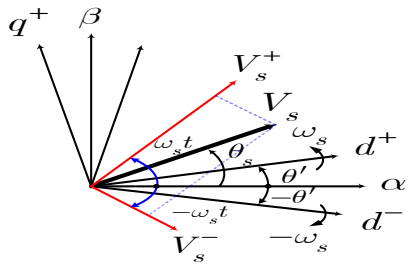

Figure 9. DDSRF respective reference frames phasor diagram

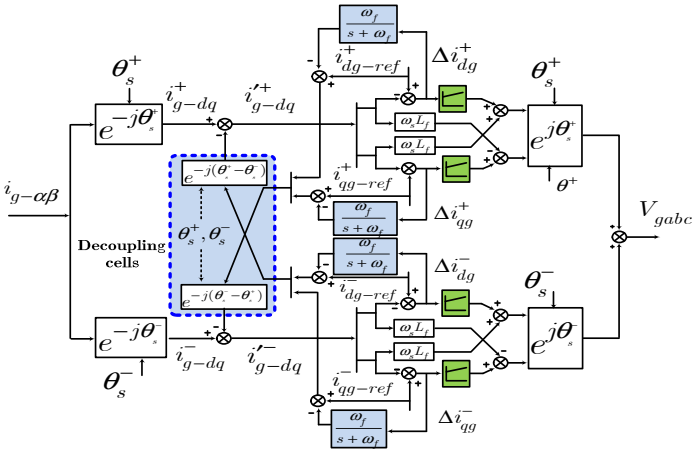

Figure 10. GSC DDSRF dq current controller

V. Simulation Verifications

A 2 MW, 0.69kV DFIG WT system used for the simulation is shown in Fig.11. The system is modeled and simulated in MATLAB/SIMULINK environment to evaluate the effectiveness of the proposed control strategy under various excursions. The simulations tests are performed at the nominal WT wind speed (11.4m/s). Whenever, a voltage dip is detected, the FRT protection strategy is enabled to safeguard the DFIG WT and the associated converters. Throughout the simulations, the maximum allowed dc voltage is set as 1.25 p.u. Stator and rotor currents protection maxima are set to 1.5 p.u. Nonetheless, the DFIG system converters, i.e., RSC and GSC can sustain 2 p.u overcurrent for a transitory time [4]. Furthermore, the pitch controller will be triggered in case of severe voltage dips to handle the rotor speed.

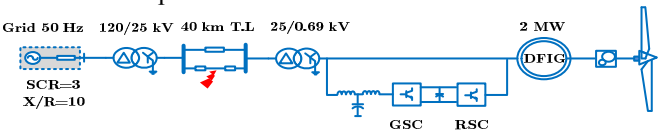

Figure 11. Schematic diagram of the system under study

A. *Symmetrical Fault Response*

Initially, the DFIG WT is supplying the rated output power while the delivered reactive power is set to zero ($Q_s, Q_g = 0$). The corresponding DFIG rotor speed is $\omega_r = 1.1$ p.u. At t=0.7s, the system is subjected to a severe symmetrical 3ϕ fault ($X_f/R_f = 5$) in the transmission line (see Fig. 11). The fault lasts

for 500 ms and cleared at 1.2s while normal operation is retrieved later as depicted in Fig. 12. The stator voltage (Fig. 12.a) drops to 95% during the fault, meanwhile the FRT protection is activated via a fault detection algorithm as that in [4]. Subsequent to the voltage dip, higher stator and rotor transient currents are noticed in Fig. 12.c-f. As a consequence to the transient rotor current growth, the GSC absorbed power -via the RSC side- rises instantaneously, which results in higher dc voltage fluctuations. However, the proposed control strategy is superior to its counterpart in maintaining the dc link voltage within the allowed limits as seen in Figs.12.k,l.

Besides, the adopted RSC fault ride-through, FRT, strategy in in both control schemes (see Figs.12.m,n) proved to regulate the power imbalance via curtailing the DFIG input power based on "2" in response to the reduction of the DFIG active power caused by the voltage dip and accordingly restricting stator as well as rotor overcurrents (Fig.12.c-f). Moreover, the pitch controller is engaged during the fault so as to regulate the rotor speed as seen in Figs. 12.i,j which still below the threshold limit (1.3 p.u.).

As reactive current aid should be released as a consequence to the stator voltage dip as stipulated by the grid codes (see Fig.1.b), the aforementioned reactive power scheme (see Fig.5) is activated to achieve this target in response to the stator voltage dip. The reactive current support led by the WT is shown in Figs.12.o,p. Though adopting the same reactive power scheme, it can be obviously noted from Fig.12.o that the proposed control method holds steadily the maximum reactive current support during the fault whereas, the conventional control method experiences unsuccessful reactive current support as depicted in Fig.12.p. The latter can be assigned to the loss of the accurate PLL synchronization and vector control orientation, VCO, caused by the severe symmetrical fault with 95% dip besides the voltage fluctuation led by the grid lower SCR. Fig.13.a,b show the synchronization signal detected by the DSOGI-FLL and SRF-PLL respectively. Compared with the SRF-PLL detected signal, the DSOGI-FLL extracts unaffected equidistant synchronization signal which correspondingly improves the overall system performance and satisfies the grid code obligations.

B. Asymmetrical Faults Response

Being accompanied with negative sequence currents, asymmetrical faults lead to dc voltage and electromagnetic torque ripples which influence the system converters and the coupling shaft of the WT and might eventually trip the DFIG WT [13]. Under the same pre-fault conditions assumed in the preceding test, the system response to asymmetrical faults is also examined. Figs. 14,15 show the system response to 150 ms, 90% voltage dip $\phi - g$ fault and 50% voltage dip 2ϕ fault respectively. Thanks to the control of the sequence currents via the GSC DDSRF current controller, the dc voltage ripples is well mitigated (Figs.14,15.k) compared with that of the conventional method (Figs.14,15.l) which exceeded the pre-defined limit with 1.32 p.u., voltage overshoot. Also, the transient stator and rotor currents are efficiently regulated below 2 p.u. Moreover, the DFIG delivered active power and injected reactive current (Figs.14,15.n,p) during both faults significantly fluctuate due to the limited RSC control capability [13]. On the other hand, lower oscillations are depicted in Figs.14,15.m,o by means of the proposed control strategy with better response. The superior performance of the proposed controller (Fig.14,15-A) over the conventional one, (Fig.14,15-B) is due to the comparative GSC DDSRF control effort exerted to regulate the sequence currents [13] and concurrently the excellent performance of the DSOGI-FLL of rendering a robust and clean synchronization signal compared with that of the conventional SRF-PLL regardless of the unbalanced mains as seen in Fig.13.c-f.

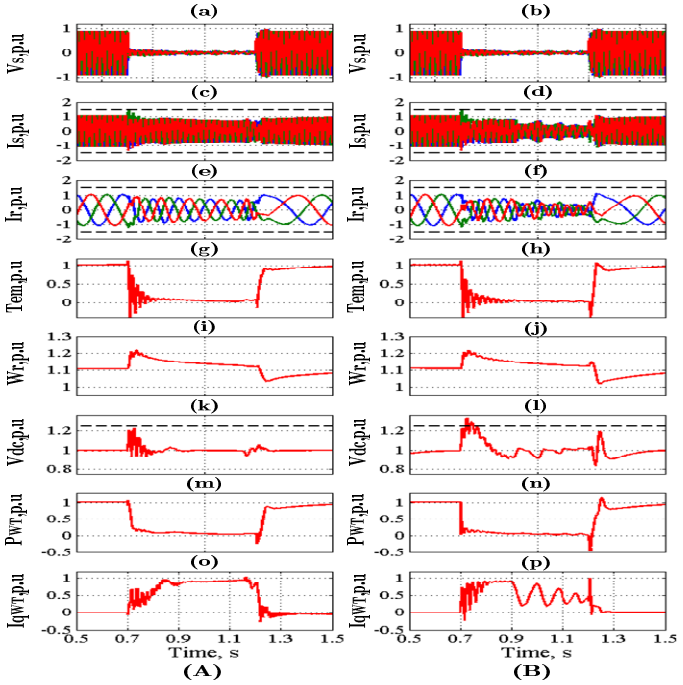

Figure 12. Simulated transient response of the studied system to a symmetrical 3ϕ fault ($X_f/R_f = 5$) (A) proposed control scheme (B) Conventional control scheme.

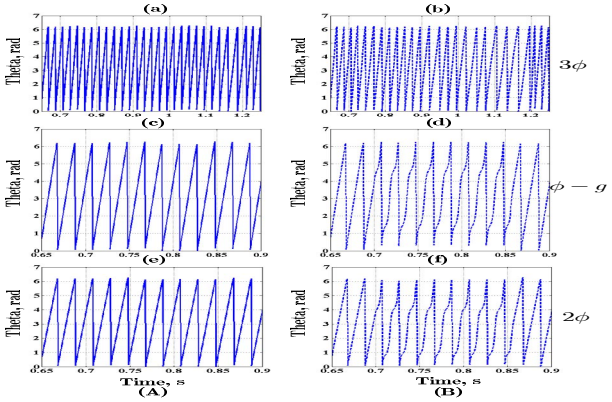

Figure 13. Tracking response of the PLL for $3\phi, \phi - g$ *and* 2ϕ faults respectively. (A) DSOGI-FLL. (B) SRF-PLL

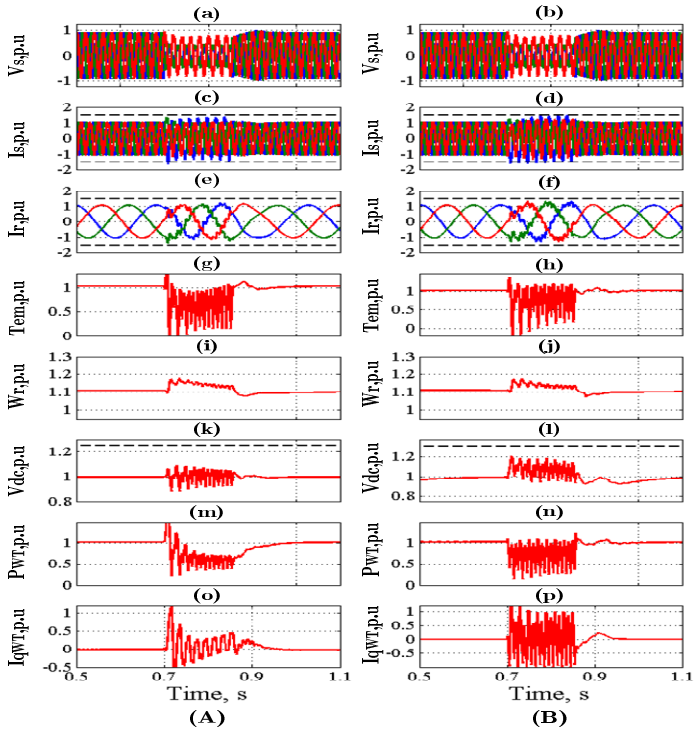

Figure 14. Simulated transient response of the studied system to single $\phi - g$ fault ($X_f/R_f = 5$) (A) proposed control scheme (B) Conventional control scheme.

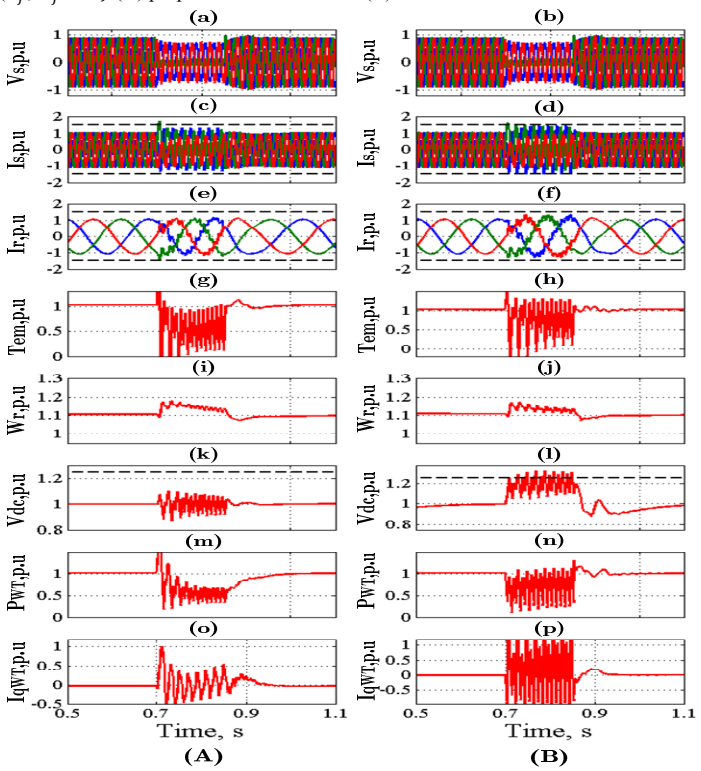

Figure 15. Simulated transient response of the studied system to 2ϕ fault ($X_f/R_f = 5$) (A) proposed control scheme (B) Conventional control scheme.

VI. Conclusions

A proposed coordinated control strategy has been presented to enable a DFIG WT to operate in a weak grid under different contingencies. A DDSRF dq current controller is devoted to control the GSC to mitigate the dc link voltage fluctuations and tackle current ripples.

A DSOGI-FLL is dedicated not only to render robust and clean synchronization signal detection irrespective of the utility condition, but also improve the overall system performance under severe disturbances.

A reactive power control scheme is used to manage reactive power injection during faults to satisfy the grid code obligation. Besides, extra terms are employed with RSC and GSC controllers to suppress the transient stator and rotor currents and regulate the rotor speed. The obtained results revealed the superiority of the proposed strategy that effectively enabled the DFIG WT to satisfy the grid code commitments in a weak grid.

References

[1] X. Zhao., et.al., "Constraints on the effective utilization of wind power in China: An illustration from the northeast China grid" *Ren. Sus. Energy Rev*., vol. 16,no. 7, pp. 4508-4514, Sep. 2012

[2] G. Mokryani, P. Siano, A. Piccolo and Z. Chen, "Improving fault ride-through capability of variable speed wind turbines in distribution networks", *IEEE Sys. Journal*., In Press.

[3] D. Xie, et al., "A comprehensive LVRT control strategy for DFIG wind turbines with enhanced reactive power support", *IEEE Trans. Power Sys*., vol. 28, no. 3, pp. 3302-3310, Aug. 2013.

[4] S. Xiao, G. Yang, H. Zhou and H. Geng, "An LVRT control strategy based on flux linkage tracking for DFIG-based WECS", *IEEE Trans. Ind. Electron.,* vol. 60, no. 7, pp. 2820-2832, July. 2013.

[5] N. Strachan and D. Jovcic "Stability of a variable-speed permanent magnet wind generator with weak AC grids", *IEEE Trans. Power Del*., vol. 25, no. 4, pp. 2779-2788, Oct. 2010.

[6] T. Neumann, C. Feltes and I. Erlich, "Response of DFG-based wind farms operating on weak grids to voltage sags", *in Proc, IEEE PES General Meeting Conf*., pp. 1-6, July. 2011.

[7] R. Teodorescu, M. Liserre and P. Rodriguez, "Grid converters for photovoltaic and wind power systems", Wiley IEEE Press, 2011.

[8] P. Rodríguez, A. Luna, M. Ciobotaru, R. Teodorescu, and F. Blaabjerg, "Advanced grid synchronization system for power converters under unbalanced and distorted operating conditions", *in Proc., IEEE Ind. Elec. Conf.,* IECON, 2006, pp. 5173 - 5178.

[9] J. Liang, D. F. Howard, J. A. Restrepo and R. G. Harley, "Feed-forward transient compensation control for DFIG wind turbines during both balanced and unbalanced grid disturbances", *IEEE Ind. Apps*., vol. 49, no. 3, pp. 1452-1463, May/Jun. 2013.

[10] Energinet. Technical regulation 3.2.5 for wind power plants with a power output greater than 11 kW; September 2010. Available at: http://www.energinet.dk.

[11] M. Reyes, et al., "Enhanced decoupled double synchronous reference frame current controller for unbalanced grid-voltage conditions", *IEEE Trans. Power Electron.,* vol. 27, no. 9, pp. 3934-3943, Sep. 2012.

[12] N. Jelani and M. Molinas, "Mitigation of asymmetrical grid faults in induction generator-based wind turbines using constant power load", *Energies,* vol. 6. pp. 1700-1717, Mar. 2013.

[13] H. Geng, C. Liu and G. Yang, "LVRT capability of DFIG-based WECS under asymmetrical grid fault condition", *IEEE Trans. Ind. Electron.,* vol. 60, no. 6, pp. 2495-2509, Jun. 2013.

Characterization and assessment of voltage and power constraints of DFIG WT connected to a weak network

S. Abulanwar, [1,2], *Weihao Hu,* [1,2], *Florin Iov,* [1] , Zhe Chen, [1,2]
[1]Energy Technology Department
[2]Sino-Danish Centre for Education and Research
Aalborg University
Aalborg, Denmark
ema@et.aau.dk, whu@et.aau.dk, fi@et.aau.dk, zch@et.aau.dk

***Abstract*—This article thoroughly investigates the challenges and constraints raised by the integration of a Doubly-fed Induction generator wind turbine, DFIG WT, into an ac network of extensively varying parameters and very weak conditions. The objective is to mitigate the voltage variations at the point of common coupling, PCC, and maximize the wind power penetration into weak networks. As a basis of investigation, a simplified system model is utilized and the respective PCC voltage, active and reactive power stability issues are identified. Besides, a steady-state study for DFIG WT connected to a weak grid is presented and qualitative conclusions about the system inherent interactions and typical restraints are presented and discussed. The impact of the wind power feed-in and the reactive power flow on the PCC voltage is assessed under widely varying system parameters. Results verification is performed via MATLAB/SIMULINK platform to assure the obtained steady-state study conclusions.**

***Index Terms*— DFIG WT, PCC voltage, weak networks, wind power penetration.**

I. INTRODUCTION

Owing to the energy deficiency and environmental concerns arising from fossil fuels, fostering the renewable energy resources became imperative. The adopted pro-active policies posed by several countries led to large-scale exploitation and evolution of the wind energy to be the fastest mounting renewable energy technology around the world [1]. Wind farms, WFs, are geographically suited in areas with rich wind resources which is typically distant from the main grid [2]. The infrastructure of such remote areas is rather weak which poses serious constraints on the effective utilization of the available wind energy [3]. The short circuit ratio, SCR, as well as the feeder X/R exemplify a main index for the grid characterization [2]. With weak grid (higher impedance of the network feeders), wind energy conversion systems, WECS, at the point of common coupling, PCC, cause significant voltage fluctuations as well as power stability issues. Virtually, a weak grid is susceptible to considerable voltage deviation as a consequence to a change in either active and/or reactive power within the grid thus worsening the voltage quality and entailing reactive power compensation [3-5]. Hence, the wind power integration can be dramatically limited according to the network structure. Despite the rapid growth of the wind energy market in China in the recent years, almost 10 % of the generated wind power is curtailed due to the finite network capacity to accommodate the captured wind power [4]. The latter can be attributed to the weak network structure which is located at a distance from the load centers. Furthermore, the efficient integration of wind power was impaired due to further impacts on voltage, frequency and system stability [1,4].

With the steady increase of the wind power penetration into the distribution networks, the fault ride-through, FRT, of the wind turbines, WTs, will be more challenging particularly in weak networks due to the reactive power regulation and voltage control issues. Moreover, the grid codes, GCs, regulations stipulated by the transmission system operators, TSOs, in different countries will demand more precise control systems and/or network reinforcement to overcome the voltage fluctuations and maximize the wind power generation [6]. As the doubly-fed induction generator wind turbine, DFIG WT, is the prominent topology among the different WECS, the aforementioned concerns can be even more exacerbating. This is because of the limited capacity of the partial scale converters of this topology.

This paper is dedicated to investigate the diverse technical challenges experienced by integrating a DFIG WT into a weak grid of widely changing parameters. First of all, a simplified model is utilized to develop the assessment criterion to evaluate the impact of the active and reactive power feed-in on the PCC voltage under different conditions. The active and reactive power limitations according to the capability limits of the DFIG WT is also considered. Moreover, the impact of the PCC voltage deviation on the in-feed active and reactive power and also on the power factor of the system is presented. Finally, simulations investigations to verify the obtained results at different network strength are carried out.

II. SYSTEM DESCRIPTION AND MODELING

Fig.1 illustrates the structure of the grid-connected DFIG WT system. This simplified system is devoted to provide an insight

978-1-4799-6415-4/14/$31.00 ©2014 IEEE

into the different impacts posed by integrating a DFIG WT to a weak network, i.e., voltage-quality and active and reactive power constraints. The system comprises a 2 MW DFIG WT connected at the PCC to the host "stiff" power system with constant voltage, V_g via a long feeder with high impedance, $Z_{T.L}$. The PCC bus voltage, V_{pcc} can vary depending on the SCR and X/R seen at this bus. The SCR is defined as the ratio between the short circuit power seen at the PCC bus to the maximum apparent power of the wind generator. In the literature, inconsistency about a conclusive definition for a weak grid exists. However, a grid with SCR below 10 is considered as a weak grid [6]. In addition, another key indicator that denotes the grid impedance angle or the ratio between the grid reactance to its resistance is the X/R. For a certain SCR, the PCC voltage can encounter increment or decrement based on the X/R value [2]. To develop the analytical model that represents the system dynamics, the DFIG active and reactive power capability limits are first identified.

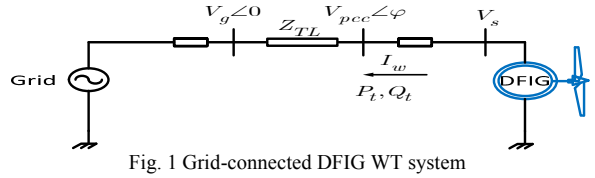

Fig. 1 Grid-connected DFIG WT system

A. DFIG WT Capability Limit

The capability limits of a 2 MW DFIG considering stator and rotor currents heating constraints due to Joule's losses, maximum and minimum active and reactive power is shown in Fig. 2 [3].

The total active power limit is given by:

$$P_{t-\max} = \left(1-s\right)P_s \tag{1}$$

The DFIG maximum and minimum reactive power limits can be given as:

$$Q_{t-\max} = \sqrt{\left(\left(X_m/X_s\right)V_s I_r\right)^2 - P_t^2} - V_s^2/X_s \tag{2}$$

$$Q_{t-\min} = -V_s^2/X_s \tag{3}$$

Where, symbols, V,P,Q,I, signify voltage, active power, reactive power and current respectively. Subscripts, t,s,r,w,m refer to total, stator, rotor, wind and magnetizing respectively. R,X,s refer to resistance, reactance and slip respectively.

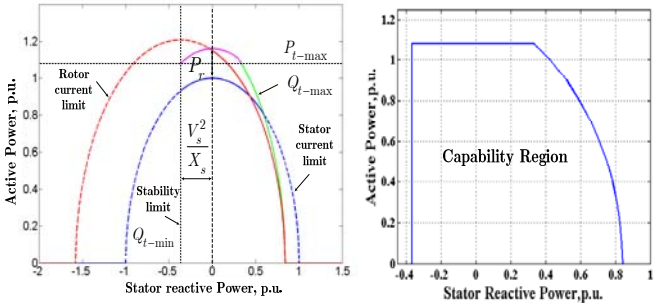

Fig. 2 DFIG WT Capability limit

B. Analytical Model

Considering the system shown in Fig.1, an analytical expression for the voltage, V_{pcc} can be obtained. The PCC voltage, V_{pcc} can be expressed as:

$$V_{pcc} = V_g + I_w \cdot Z_{T.L} = V_g + I_w \cdot \left(R + jX\right) \tag{4}$$

The WT total apparent power, S_t, can be defined as:

$$S_t = V_{pcc} I_w^* \tag{5}$$

Where, $\bar{V}_{pcc} = V_{pcc} e^{j\varphi}$ (6)

Where, φ is the PCC voltage phase angle.

Combining (4)-(6), yields:

$$V_{pcc}^4 - V_{pcc}^2\left(2\left(RP_t + XQ_t\right) + V_g^2\right) + \left(R^2 + X^2\right)\left(P_t^2 + Q_t^2\right) = 0 \tag{7}$$

Equation (7), describes the PCC voltage in terms of of the WT delivered active and reactive power and the feeder resistance and reactance which is dictated by the SCR and X/R ratios [2].

III. Voltage/Power Constraints

In the following section, the conceivable impacts of the DFIG generated power on the PCC voltage profile under a wide range of SCR and X/R and also at different power factor scenarios are discussed.

A. Impact of System Parameters

Fig. 3 demonstrates the PCC steady-state voltage profile in response to the SCR and X/R variations carried out at the rated DFIG generated power. The results are performed at different power factor scenarios to assess the influence of the reactive power flow on the PCC voltage. Clearly, it can be seen that the PCC voltage varies dramatically with the system strength. Based on the SCR and X/R, the voltage can encounter higher or lower voltage deviations. At very lower SCRs "very weak grid", i.e., below 3, the PCC voltage can readily cause higher deviations. In addition, according to the X/R value, the deviations can decline/exceed the nominal voltage.

The grid emulates an ohmic behavior at lower X/R ratio, particularly below 1, as larger voltage drop is caused by higher resistance and thereby the PCC voltage rises. While in case of higher X/R ratios, the inductive nature is the dominant and the voltage decreases. Also, it can be noticed that for leading power factor operating scenario, the PCC voltage causes higher increment at lower system strength as the wind generator injects reactive power rather than consuming to regulate the PCC voltage [2].

B. Impact of In-Feed Wind Power

Owing to the intermittent nature of wind speed, the WT produces unsteady active power which affects the PCC bus voltage connected to a weak network. Figs .4,5 depict the PCC voltage response versus active power variation under different SCR and X/R operating points.

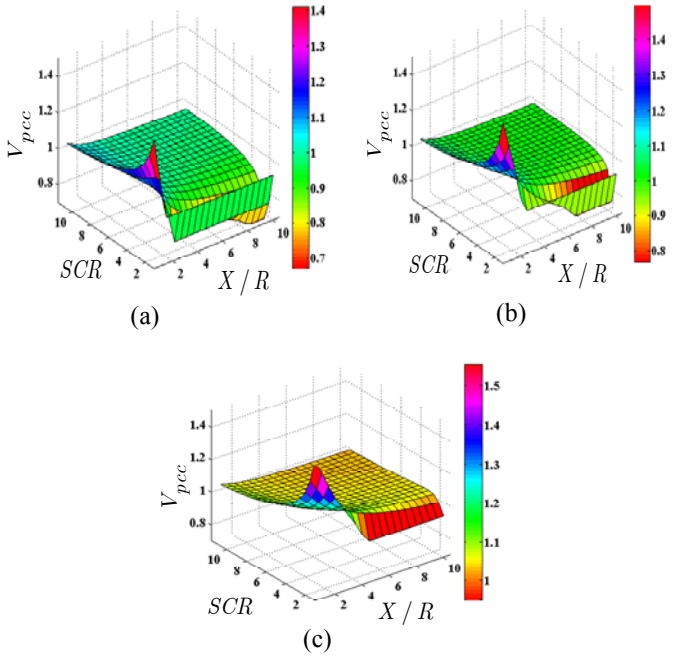

Fig. 3 PCC voltage response (a) 0.95 lagging PF (b) Unity PF (c) 0.95 leading PF

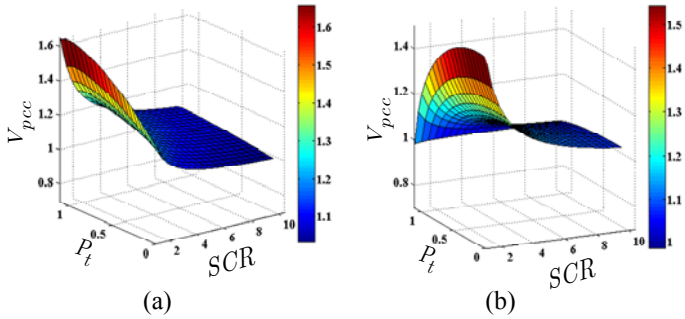

Fig. 4 PCC voltage behavior against in-feed wind power (a) X/R= 0.5 (b) X/R=10

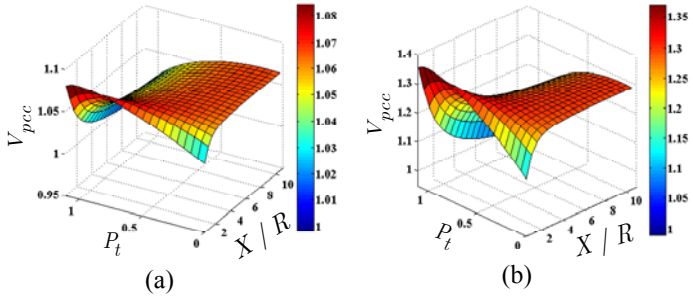

Fig. 5 PCC voltage behavior against in-feed wind power (a) SCR= 10 (b) SCR=2

As seen in Figs. 4.a,b, the PCC voltage rises with the active power growth at lower X/R, while the scenario is reversed at higher one. Such results can be explained with the help of Fig. 2 besides the following expressions.

The DFIG stator active and reactive powers can be given by:

$$P_t = 1.5 V_d I_{dw} \quad (8)$$

$$Q_t = -1.5 V_d I_{qw} \quad (9)$$

Where, V_d, I_{dw}, I_{qw} are the d-component stator voltage, d and q-axes WT current components respectively.

The feeder voltage deviation magnitude formula:

$$\Delta V_{pcc} = I_w \left(R + jX\right) = \left(RI_{wd} - XI_{wq}\right) + j\left(XI_{wd} + RI_{wq}\right) \quad (10)$$

As shown in Fig. 4.a, at minimum real power delivery, the voltage deviation is minimal due to the low reactance while increases with the increase of the real power supply. On contrary, the PCC voltage decreases with the growth of the wind power due to the high reactance (Fig. 4.b). On the other hand, the PCC voltage is slightly influenced by the wind power injection even with reduced X/R values in case of a strong network with higher SCR as illustrated in Fig. 5.a. Furthermore, the PCC voltage can readily overtakes the safe margins for a weak grid "low SCR" as described by Fig. 5.b especially at high wind speed conditions.

C. Active and Reactive Power Constrains

To evaluate the active and reactive power constraints imposed on the wind generator as a consequence to the weak grid SCR and X/R variations, (7) is solved for the reactive power and the result is shown in Fig. 6. The condition is to maintain a constant PCC voltage.

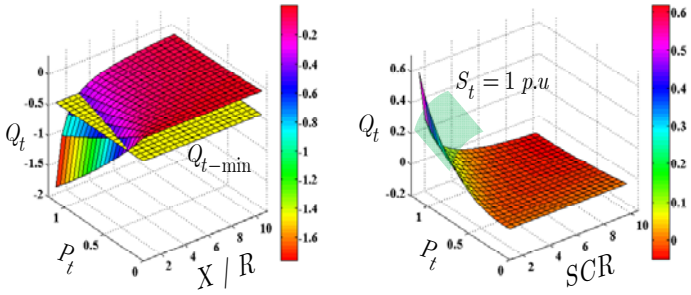

Fig. 6 DFIG PQ limitation due to SCR and X/R variation (a) SCR=10 (b) X/R=10

In Fig. 6.a, with a resistive grid (low X/R), V_{pcc} rises and thereby higher reactive power consumption is vital to maintain the voltage [5]. Nevertheless, due to stability consideration, the DFIG has reactive power consumption limitation. Consequently, operation beyond this boundary is unfeasible. Otherwise, for inductive grid (high X/R), Fig. 6.b, at higher SCR values, the DFIG can attain any active power to the grid with little reactive power consumption. Nonetheless, the lower the SCR, the reactive power support is larger due to the higher inductive part which tends to lower the PCC voltage. Hence, without exogenous reactive power compensation, the curtailment of the harvested wind power is imperative - due to the total capability limit of the DFIG WT - to allow for safe operation. The latter will significantly increase the wind energy loss [1,4] and adversely affect the grid codes commitments as discussed later.

D. Grid Codes Compliance

In addition to complying with the general GC requirements, wind power plants, WPPs, must be controlled in such a way that the operating point lies somewhere in the hatched area of Fig. 7 to retain a specific range of power factor operation [7]. Assuming that the DFIG WT in Fig. 1 is attached to the host grid via a pure inductive feeder with lower SCR=2, hence, the delivered active and reactive power at the PCC bus can be written as:

$$P_t^2 + \left(Q_t + V_g^2 / X\right)^2 = \left(V_{pcc} V_g / X\right)^2 \quad (11)$$

The PQ capability of the DFIG WT can be calculated in this case from (11). Fig. 7 shows the PQ capability regions for different PCC voltage example values which correspond to the allowable voltage margin along with the respective Energinet and E.ON grid codes requirements [7].

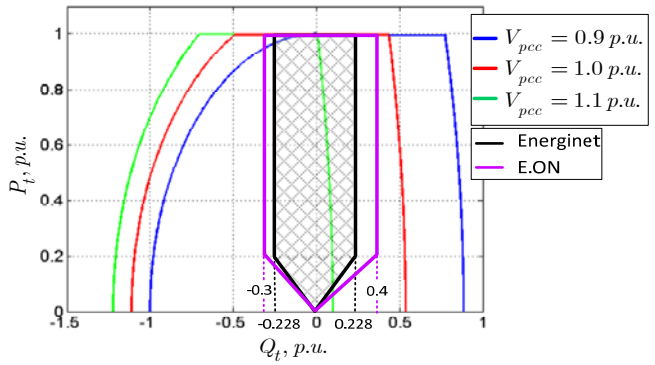

Fig.7 Grid codes compliance under PCC voltage deviation

Obviously, from Fig. 7 it can be seen that subsequent to the PCC voltage deviation, the DFIG WT is no longer capable of fulfilling the grid code requirements - set by either Energinet or E.ON - regarding reactive power/power factor regulation particularly when delivering the rated real power.

E. Reactive Power/Power factor Regulation

To counteract the PCC voltage significant perturbations and allow for higher wind power integration into weak networks and concurrently fulfill the grid code requirements regarding power factor operation, the reactive power regulation is inevitable [2,5]. The amount of reactive power consumption/generation to tackle the voltage swell/dip which depends upon the network strength can be calculated from (7) as:

$$Q_t = \left(\frac{1}{R^2 + X^2}\right)\left(V_{pcc}^2 X - \sqrt{V_{pcc}^2\left(V_g^2 + 2RP_t\right)\left(R^2 + X^2\right) - P_t^2\left(R^2 + X^2\right)^2 - V_{pcc}^4 R^2}\right) \quad (12)$$

Using (12), the reactive power consumption/generation as well as the corresponding power factor associated with ±10% PCC voltage variation at different network SCR and X/R are demonstrated in Fig. 8. Generally speaking, the amount of reactive power depends on PCC voltage variation, SCR and X/R operating range as seen in Fig. 8. Moreover, the associated power factor can be significantly affected due to the higher reactive power supplied/consumed (Fig. 8.b2-d2). As mentioned before, the PCC voltage cannot be regulated through higher consumption of reactive power via the DFIG WT due to the minimum reactive power capability limitation. Therefore, fostering the system with extra FACTS/Energy storage can be an effective alternative [6,8].

Furthermore, the higher the SCR, the larger the demanded absorbed/injected reactive power to maintain constant PCC voltage specially at lower X/R values (see Fig. 8.c1,d1). However, such issue might be insignificant as a grid with high SCR is unlikely to cause higher PCC voltage variation [2]. Also, it is worth noting that the slope of the Q_d surface is getting steeper the higher the SCR as obvious from Fig. 8.

Fig. 9 demonstrates the behavior of the Q_d slope against the voltage deviation for different network parameters, which clearly shows that the higher the SCR, the rapid the rate of change of the reactive power. This can also be deduced from (12) due to the lower impedance at high SCRs.

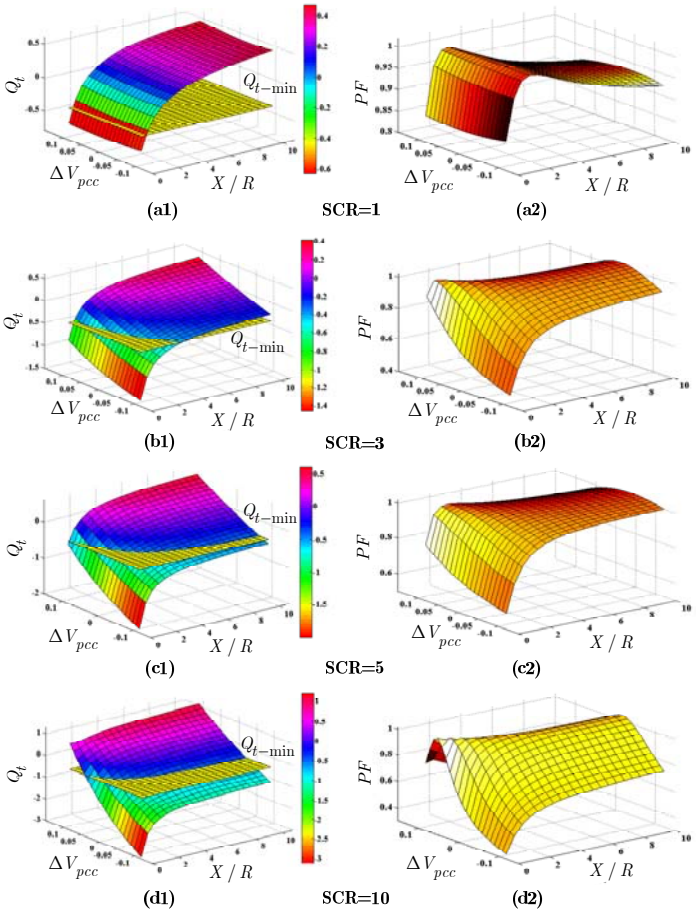

Fig.8 Reactive power/power factor regulation under PCC voltage deviation

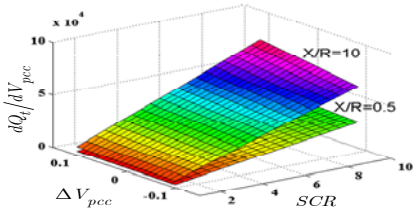

Fig.9 Rate of change of Q_d under different network parameters

IV. Simulation Verification

A set of simulation test cases is carried out to verify the aforementioned steady-state study. The system shown in Fig. 1 is used to conduct the test cases. A 2 MW DFIG WT is connected to a strong network with constant voltage, V_g, 690 V, via a long feeder which mimics a weak network. The control of the DFIG WT is out of the scope of this paper. However, modeling and control of the DFIG WT is the same as in [2]. The investigations will be performed at different network strength, i.e., different SCRs and X/Rs. Besides, a power factor control will be employed in the DFIG control system during the simulation to assess the impact of the reactive power flow through the system under weak conditions. The considered power factor operating points are 0.975 lag, unity and 0.975 lead respectively. Throughout the simulations, the system is subjected to a realistic wind speed profile to evaluate the PCC voltage response and the obtained results are depicted in Fig. 10. From the results, it can be deduced that the PCC voltage is significantly influenced by the real power feed-in especially at worst weak conditions (Fig. 10.A) where the PCC voltage exceeds the safe boundaries. Also, the reactive power flow (power factor) can contribute to further impact on the PCC voltage according to the system strength. Despite, the wind power curtailment can contribute to enhancing the PCC voltage, it represents a cost-ineffective action that results in huge wind power loss and misuse of the wind energy resources. Moreover, the results emphasize that additional compensation techniques are to be embedded to mitigate the PCC voltage fluctuations and facilitate higher wind power penetration into such weak networks.

V. Conclusion

A steady-state study for a DFIG WT attached to a weak ac network under different network strength has been presented. The various technical aspects and constraints imposed on the PCC voltage, real and reactive power have been assessed and discussed. The reactive power consumption/generation demanded to regulate the PCC voltage under different operating conditions has been investigated. A simulation study is conducted to verify the obtained steady-state results. Furthermore, the simulations results assure the analytical study and emphasize the requirement for extra compensation reinforcements to foster more wind power penetration, effective usage of wind energy resources and attain satisfactorily PCC voltage profile for different network conditions.

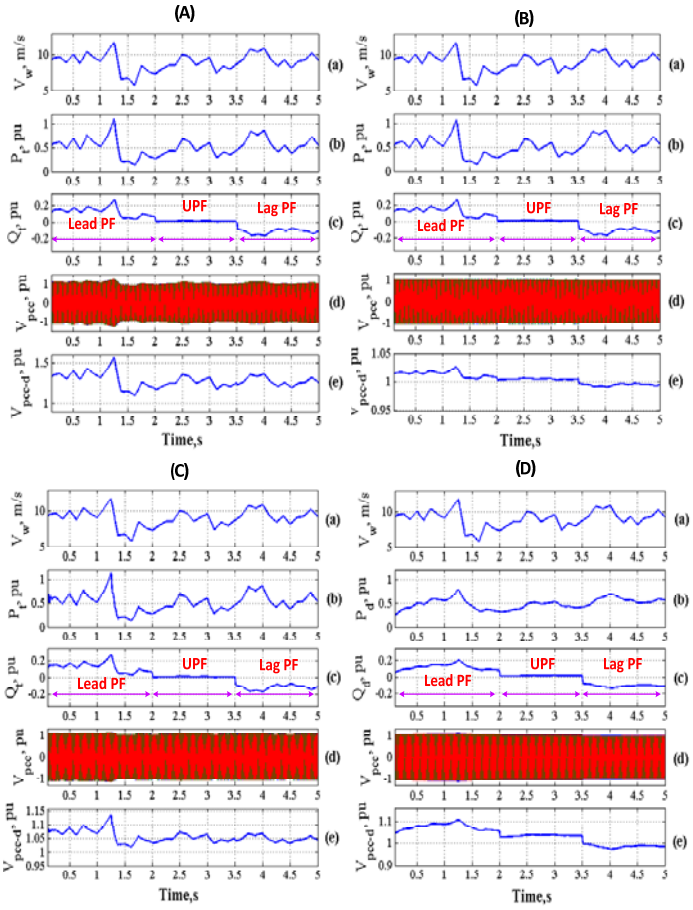

Fig. 10 System response to different network strength (A) SCR=1, X/R=0.5 (B) SCR=10, X/R=10 (C) SCR=5, X/R=1 (D) SCR=2, X/R=4

References

[1] Z. Zhao, et.al., "A critical review of factors affecting the wind power generation industry in China" *Ren. Sus. Energy Rev*., vol. 19, no. 7, pp. 499-508, Mar. 2013.

[2] J. O. Tande, G. Di Marzio, and K. Uhlen, "System requirements for wind power plants," SINTEF Energy Res., 2007. [Online]. Available: http://www.sintef.no/upload/ENERGI/pdf/Vind/TR%20A6586.pdf

[3] G. Mokryani, P. Siano, A. Piccolo and Z. Chen, "Improving fault ride-through capability of variable speed wind turbines in distribution networks", *IEEE Sys. Journal*., vol. 7, no. 4, pp. 713-722, Dec. 2013.

[4] X. Zhao., et.al., "Constraints on the effective utilization of wind power in China: An illustration from the northeast China grid" *Ren. Sus. Energy Rev*., vol. 16,no. 7, pp. 4508-4514, Sep. 2012

[5] W. Hu, Z. Chen, Y. Wang, and Z. Wang, "Flicker mitigation by active power control of variable-speed wind turbines with full-scale back-to-back power converters", *IEEE Trans. Energy Conv*.,vol. 24, no. 3,pp. 640-649, Sep. 2009

[6] N. Strachan and D. Jovcic "Stability of a variable-speed permanent magnet wind generator with weak AC grids", *IEEE Trans. Power Del*., vol. 25, no. 4, pp. 2779-2788, Oct. 2010.

[7] Energinet. Technical regulation 3.2.5 for wind power plants with a power output greater than 11 kW; September 2010. Available at: http://www.energinet.dk.

[8] C. Han, et.al., "STATCOM impact study on the integration of a large wind farm into a weak loop power system", *IEEE Trans. Energy Conv*., vol. 23, no. 1, pp. 226-233, Mar. 2008.

IET Renewable Power Generation

Research Article

IET Journals
The Institution of Engineering and Technology

Adaptive voltage control strategy for variable-speed wind turbine connected to a weak network

ISSN 1752-1416
Received on 23rd May 2015
Revised on 31st July 2015
Accepted on 28th August 2015
doi: 10.1049/iet-rpg.2015.0239
www.ietdl.org

Sayed Abulanwar[1,2], Weihao Hu[1,2] ✉, Zhe Chen[1,2], Florin Iov[1]

[1]*Department of Energy Technology, Aalborg University, Aalborg, DK 9220 Denmark*
[2]*Sino-Danish Centre for Education and research (SDC), Beijing, China*
✉ *E-mail: whu@et.aau.dk*

Abstract: Significant voltage fluctuations and power quality issues pose considerable constraints on the efficient integration of remotely located wind turbines into weak networks. Besides, 3p oscillations arising from the wind shear and tower shadow effects induce further voltage perturbations during continuous operation. This study investigates and analyses the repercussions raised by integrating a doubly-fed induction generator wind turbine into an ac network of different parameters and very weak conditions. An adaptive voltage control (AVC) strategy is proposed to retain voltage constancy and smoothness at the point of connection (POC) in order to maximise the wind power penetration into such networks. Intensive simulation case studies under different network topology and wind speed ranges reveal the effectiveness of the AVC scheme to effectively suppress the POC voltage variations particularly at very weak grid conditions during normal operation.

1 Introduction

With 282.5 GW installed capacity in 2012 compared with 94 GW in 2007, wind energy is potentially one of the fastest emerging renewable energy technology worldwide [1]. Motivated by the desire to reduce fossil fuel emissions, policy makers implement incentives for increasing investment in wind energy worldwide [2]. By the end of 2013, China possessed 91.4 GW cumulative capacity fostering its rank in the global wind market [1]. Wind farms (WFs) are geographically constructed in remotely located areas with favourable wind speed conditions [3, 4]. The structure of such locations is rather weak with lower fault level due to long feeders' (high impedance) connections. Moreover, significant voltage fluctuations and power quality/stability challenges pose substantial constraints on the efficient integration of wind power into weak networks. On the other hand, even relatively strong networks might also encounter markedly grid impedance change owing to load variations and/or lines tripping [5]. Typically, a weak network is liable to remarkable voltage deviation as a result of active and/or reactive power changes, worsening the point of connection (POC) voltage quality. Furthermore, wind power vagaries due to wind speed variations and 3p oscillations resulting from tower shadow and wind shear effects exacerbate voltage perturbations and power quality as well [6, 7]. Consequently, weak network connections impose dramatic wind power limitations in terms of grid structure and wind turbine (WT) output power [4–7]. In addition, voltage fluctuations provoke flicker emissions which represent a serious drawback impacting power quality and restrict the captured wind power [6–9]. Several serious concerns regarding voltage, frequency and system stability manifested recently due to connecting wind power plants (WPPs) to weak networks which irritated the proliferation of wind power. Despite the steady growth, onerous challenges impede wind power development in China. Owing to long distances between territories with high-density of wind power and load centres, curtailment rate reached about 15–25% in Northern China during 2012 [10]. The latter resulted in $1.6 billion nationwide economic loss in the same year. Additionally, voltage violations to some of the transmission networks have been detected in different regions due to the steady growth of wind power penetration [4].

Denmark looks forward to ~50% wind power penetration by 2020 which exemplifies additional burdens on transmission as well as distribution networks [11]. A significant portion of the Danish energy consumption is speculated via offshore WFs in the long term. Thereby, operation of wind power into weak networks is seen as an expected operating scenario in the near future in Denmark.

Traditionally, variable-speed WTs (VSWTs) are operated under fixed power factor control mode as stipulated by enforced grid codes. However, such operational mode shows pronounced limitation in case of weak grid scenario [8]. Fixed reactive power and voltage control (VC) are the two favourable operational modes in the literature for the control of VSWTs [3, 5–8]. Apart from entailing active/reactive power dispatch [8], reactive power control mode becomes insignificant when adopted for very weak networks. Virtually, VC is the increasingly desirable weaker grid to alleviate the POC voltage/power quality issues [5]. Besides, with the prominent wind power penetration development, ancillary services such as VC provided by VSWTs become exigent [12]. Furthermore, VC allows for maximum reactive power compensation (RPC) during utility contingencies.

This paper is first dedicated to provide an insight into the diverse technical issues raised by integration of megawatt-level variable speed doubly-fed induction generator (DFIG) into a weak network in light of network characteristics, operational limits and wind speed variations. Other authors have investigated weak networks in terms of short-circuit capacity ratio (SCR, the ratio between the POC short circuit power to the maximum apparent power of the wind generator) but with fixed feeder X/R ratio (the ratio between the grid reactance to its resistance, viz., stands for the grid impedance angle) [5]. Besides, the design of the relevant VC relies on fixed adaptive gains to improve the POC voltage performance. The novelty of this paper lies in a proposed adaptive VC (AVC) scheme reliant on network parameters to continually mitigate POC voltage variations for very weak networks with widely varying SCR as well as X/R ratios under different operating conditions. A reactive power dispatch strategy to manage the reactive power flow from/to the wind generator (WG) is proposed. Additionally, the paper not only quantifies the system reactive power associated with the network parameters change but also the reactive power sharing inside the WG and identifies the proper grid side converter (GSC) rating to tackle the voltage perturbations at the conceivable

system strengths and operating point. Furthermore, the overall system stability is investigated using AVC via identifying the safe operating regions for a wide range of system parameters. In a broader context, the proposed AVC aims at facilitating wind power penetration into weak power systems. The RPC is realised primarily via the DFIG inherent stator reactive power as well as an over-sized GSC which manipulates the reactive power deficit to address voltage disturbances. Moreover, a reactive power dispatch strategy to manage the reactive power coordination between the DFIG and the GSC is also presented.

2 System description and modelling

Fig. 1*a* illustrates a schematic representation of the DFIG WT test system model. The model comprises a VSWT, drive train, gear box, DFIG and two back-to-back AC–DC–AC partial converters, namely, GSC and generator-side (rotor side) converter (RSC). The WT is connected at the POC to the host network by means of an interface transformer and transmission line. A typical two-level control scheme is devoted to control the DFIG WT system. A WT control is utilised to regulate WT mechanical output power through appropriately adjusting both the pitch angle and the rotor speed according to the maximum power point tracking (MPPT) tracking. The blade pitch angle BPA controller model used in this paper is the same as that in [13].

2.1 DFIG wind generator

The voltage equations of the DFIG generator stator and rotor circuits can be expressed using a rotating *dq* reference frame at synchronous speed as [13]

$$u_{ds} = R_s i_{ds} - \omega_s \psi_{qs} + \frac{1}{\omega_b}\frac{d\psi_{ds}}{dt} \tag{1}$$

$$u_{qs} = R_s i_{qs} + \omega_s \psi_{ds} + \frac{1}{\omega_b}\frac{d\psi_{qs}}{dt} \tag{2}$$

$$u_{dr} = R_r i_{dr} - (\omega_s - \omega_r)\psi_{qr} + \frac{1}{\omega_b}\frac{d\psi_{dr}}{dt} \tag{3}$$

$$u_{qr} = R_r i_{qr} + (\omega_s - \omega_r)\psi_{dr} + \frac{1}{\omega_b}\frac{d\psi_{qr}}{dt} \tag{4}$$

where u_{ds}, u_{qs}, u_{dr}, u_{qr}, i_{ds}, i_{qs}, i_{dr}, i_{qr} and ψ_{ds}, ψ_{qs}, ψ_{dr}, ψ_{qr} are the *dq* stator and rotor voltages, currents and flux linkages. R_s, R_r are stator and rotor winding resistances, L_s, L_r, L_m are stator, rotor and mutual inductances, respectively. ω_s, ω_r, ω_b are stator, rotor and base angular frequencies, respectively. The RSC is controlled in a synchronously rotating *dq* reference frame with the *d*-axis oriented along the stator flux position. Hence, the DFIG electromagnetic torque T_{em} and stator

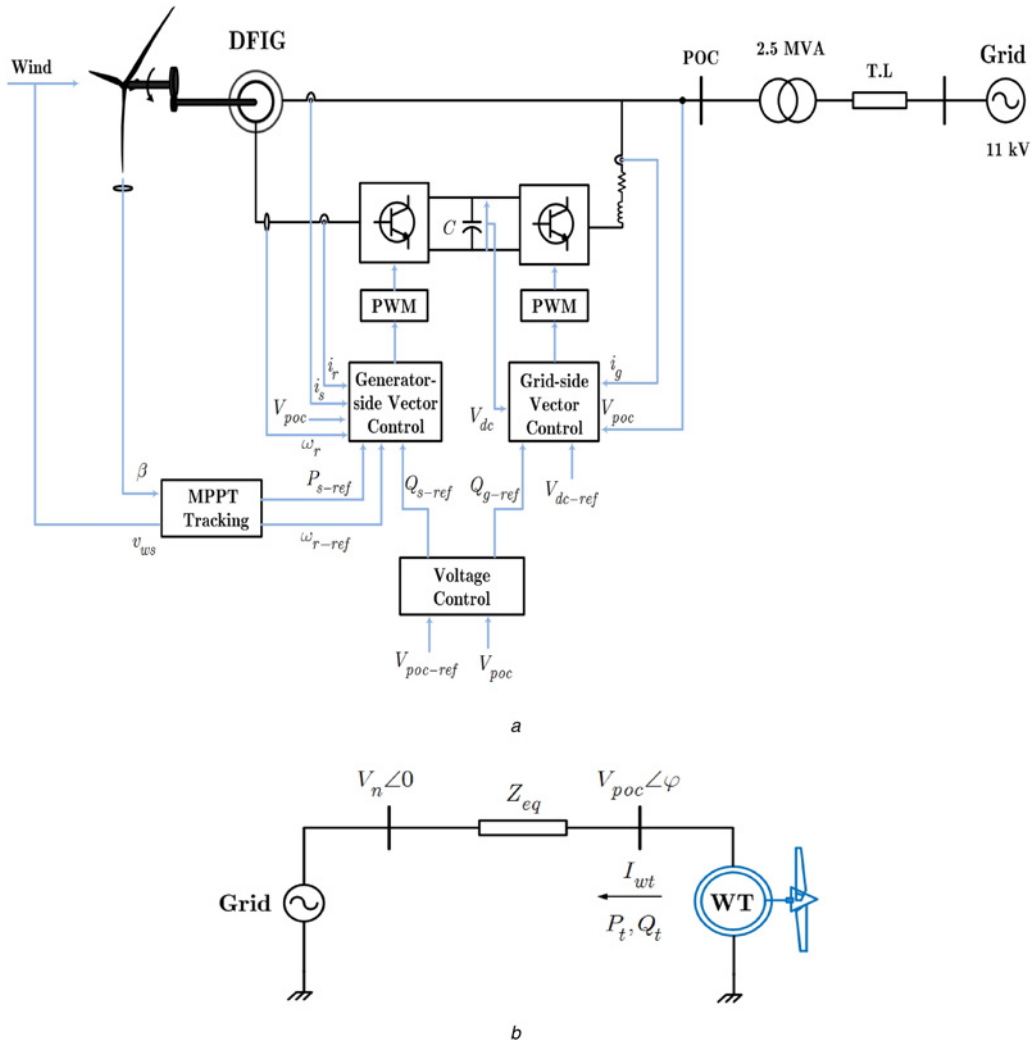

Fig. 1 *Schematic representation of the DFIG WT test system model*

a Block diagram of a grid-connected DFIG WT test system
b Grid-connected DFIG WT equivalent system

active and reactive powers P_s, Q_s can be given as [7]

$$T_{em} = \frac{3}{2} p \frac{L_m}{L_s} \psi_s i_{qr} \tag{5}$$

$$P_s = -\frac{3}{2} u_s \frac{L_m}{L_s} i_{qr} \tag{6}$$

$$Q_s = \frac{3}{2} \frac{\psi_s}{L_s} u_s - \frac{3}{2} u_s \frac{L_m}{L_s} i_{dr} \tag{7}$$

where ψ_s, u_s are the stator flux and voltage magnitudes, p is the number of pole pairs. As implied from (6) and (7), stator active and reactive powers can be dictated via rotor currents, i_{qr}, i_{dr}, respectively.

2.2 DFIG operation limits

Identification of the WT active/reactive power operational limits is vital for realisation of the rewarded RPC. During steady state, the capability limits of the DFIG can be obtained considering stator and rotor currents which respond to stator as well as rotor heating constraints due to Joule's losses [14]. The capacity limit encompasses DFIG maximum active and reactive restrains. The DFIG delivered active power capacity is given by

$$P_t = (1 - s) P_s \tag{8}$$

The stator maximum reactive power (generation and absorption) limits are

$$Q_{sg\text{-}max} = \sqrt{\left(\left(\frac{X_m}{X_s}\right) V_{poc} i_r\right)^2 - P_s^2} - \frac{V_{poc}^2}{X_s} \tag{9}$$

$$Q_{sa\text{-}max} = -V_{poc}^2 / X_s \tag{10}$$

where s is the rotor slip, i_r is the rotor current and X_m, X_s are the magnetising and stator reactance, respectively. Further details about such operational limits can be found in [14].

2.3 WT aerodynamic model

As the aim of this paper is to investigate the interaction between the WG and the host power system, a simplified aerodynamic model can therefore be sufficient to reflect the behaviour of the WT [6]. The DFIG WT aerodynamic torque can be expressed by the following formula

$$T_w = \frac{1}{2} \rho \pi R^3 v_{ws}^2 \frac{C_p(\beta, \lambda)}{\lambda} \tag{11}$$

where T_w is the WT extracted aerodynamic torque in N m, ρ is the air density in kg/m^3, R is the WT rotor radius in m, v_{ws} is the equivalent wind speed in m/s, β is the rotor pitch angle (deg), $\lambda = \omega_r R / v_{ws}$ is the tip speed ratio, ω_r is the WT rotor speed in rad/s and C_p is the rotor aerodynamic efficiency.

The 3p torque speed oscillations developed in [6], is applied here where the equivalent wind speed v_{ws} is expressed as

$$v_{ws} = v_H + v_{eq\text{-}WS} + v_{eq\text{-}TS} \tag{12}$$

$$v_{eq\text{-}WS} = v_H \left[\frac{(\alpha)(\alpha - 1)}{8} (R/H)^2 + \frac{(\alpha)(\alpha - 1)(\alpha - 2)}{60} (R/H)^3 \cos 3\beta\right] \tag{13}$$

$$v_{eq-TS} = \frac{m v_H}{3R^2} \sum_{b=1}^{3} \left[\frac{a^2}{\sin^2 \beta_b} \ln\left(\frac{R^2 \sin^2 \beta_b}{x^2} + 1\right) - \frac{2a^2 R^2}{R^2 \sin^2 \beta_b + x^2}\right] \tag{14}$$

where v_H, $v_{eq\text{-}WS}$ and $v_{eq\text{-}TS}$ are the hub-height, the wind shear and the tower shadow wind speed components (m/s), respectively. α is the empirical component of wind shear, H is the rotor hub elevation (m), β is the blade azimuthal angle (deg), β_b is the azimuthal angle of each blade (deg), α is the tower radius (m), x is the distance from the tower midline to the blade origin (m) and $m = [1 + \alpha(\alpha - 1) R^2/(8H^2)]$, is a WT coefficient.

2.4 Equivalent system model

Nowadays, WPPs are enforced to spontaneously manage reactive power to render a stable grid voltage and maintain grid connection in order to satisfy the onerous grid code commitments [12, 15]. Nevertheless, connecting an intermittent and stochastic WG to a weak power system with widely varying parameters aggravates the RPC. Voltage perturbations at the POC are directly related to different aspects, among which is the typology of the WT with the respective generator and embedded supervisory system [16]. Wind speed turbulences and profile also represents an important factor. Moreover, network characteristics, that is, SCR and feeders X/R ratio is a major aspect.

In this regard, an analytical study is conducted to assess the impacts of connecting a WT to a weak network under a range of different parameters and evaluate the associated voltage/power quality issues. Fig. 1*b* demonstrates an equivalent model of a grid-connected DFIG WT attached to a weak bus at the POC. The host utility denotes a stiff network with constant voltage, V_n. The equivalent impedance of the connection line and the coupling transformer is denoted by Z_{eq}. Large WPPs are usually connected to highly inductive transmission networks with X/R ratios between 1.4 and 11.4, whereas it can be around 0.5 in case of small WTs attached to distribution networks [8, 17]. Typically, SCR of 10 is perceived as a boundary below which the attached network is weak [5].

For the below analysis, reactive power at the POC is handled by the DFIG stator side only. Assuming that the WT produces line current I_{wt}, an expression for the POC voltage magnitude can be described by the following equation

$$V_{poc} = V_n + I_{wt}\left(R_{eq} + jX_{eq}\right) \tag{15}$$

$$V_{poc} = V_n + \frac{P_t - jQ_t}{V_{poc}^*}\left(R_{eq} + jX_{eq}\right) \tag{16}$$

$$V_{poc}^4 - \left(2V_{poc}^2\left(P_t R_{eq} + Q_t X_{eq} + V_n^2\right) - \left(R_{eq}^2 + X_{eq}^2\right)\left(P_t^2 + Q_t^2\right)\right) = 0 \tag{17}$$

Solving (16), yields

$$V_{poc} = \sqrt{0.5V_n^2 + A} \tag{18}$$

where

$$A = P_t R_{eq} + Q_t X_{eq} + \sqrt{0.25V_n^4 + \left(P_t R_{eq} + Q_t X_{eq}\right)V_n^2 - \left(P_t X_{eq} - Q_t R_{eq}\right)^2} \tag{19}$$

The relation between the POC voltage, WT total delivered active and reactive powers, P_t, Q_t as well as equivalent impedance parameters, R_{eq}, X_{eq} which directly influence SCR and X/R ratio is described by (17)–(19). It is worth to mentioning that some studies suppose that the POC voltage magnitude is mostly determined by the real term

IET Renew. Power Gener., 2016, Vol. 10, Iss. 2, pp. 238–249

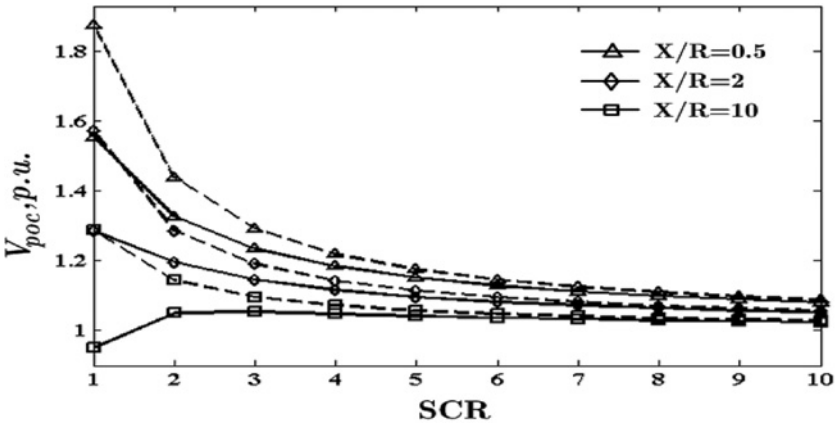

Fig. 2 *Actual (solid) and approximate (dashed) POC voltage versus SCR*

contribution of (16) which yields [8]

$$V_{\text{poc}} = V_{\text{n}} + \frac{P_{\text{t}}R_{\text{eq}} + Q_{\text{t}}X_{\text{eq}}}{V^{*}_{\text{poc}}} \tag{20}$$

Fig. 2 compares actual and approximate POC voltage profile obtained using (18), (20) corresponding to the rated WT output power and 0.975 leading power factor. Clearly, it can be seen that (20) can be fair only for stiff distribution networks characterised by SCR > 10. Nevertheless, for weak networks of lower SCRs, (18) is essential to accurately represent system behaviour. Thereafter, (18) is used to characterise the POC voltage.

3 Assessment of voltage and power constraints

This section investigates the diverse impacts posed by connecting a DFIG WT to a weak network. An emphasis is put on voltage quality, active and reactive power constraints under a wide range of SCR and X/R ratio variations.

3.1 Voltage constraints

The European Standard EN 50160 has been issued to limit the voltage variations and maintain voltage quality by imposing statistical limits in such a way that a time limited deviation exceeding them is allowable [18].

The POC voltage behaviour in response to SCR and X/R ratio variations is depicted in Fig. 3*a*. The WT is presumed to deliver the rated output power. In addition, different power factor (PF) scenarios are investigated to evaluate the impact of reactive power exchange on the POC voltage. The considered PF operating scenarios are 0.975 leading, 0.975 lagging and unity power factor (UPF) as recommended by the Danish grid code for WPPs with output power >1.5 MW [19]. As implied by Fig. 3*a*, the POC voltage evokes dramatic perturbations as a consequence to the system parameters change. At a certain SCR, the POC voltage can overtake the nominal value or even decrease according to the X/R ratio or alternatively, the network impedance angle. Moreover, it is worth noting that for $1 \le \text{SCR} \le 4$ and $\text{X/R} \le 2$, higher voltage spikes unfolded which indicates very weak network. In particular, weak grids suffer significant parameters change with the SCR and/or X/R ratio variations. The lower the SCR, the higher the network impedance and the voltage deviation too. Besides, the grid features a resistive characteristic in the lower X/R ratio, specially below 2 as indicated above which can readily induce considerable voltage fluctuations as illustrated in Fig. 3*a*.

Additionally, the recorded POC voltage spikes vary according to reactive power flow or the power factor operating scenario. The leading PF scenario resulted in the maximum voltage increment as the WT releases reactive power rather than absorbing to regulate the voltage. Owing to the intermittence of wind speed, the variability of WT output power provokes POC voltage deviations [16].

Fig. 3*b* shows the POC voltage behaviour in response to the WT delivered output power and SCR change at different feeder X/R ratios calculated using (18). The WT output reactive power Q_t corresponds to 0.975 leading PF. With higher SCR and X/R ratio 'stiff network', the POC voltage is slightly influenced by the active power growth. Compared with X/R of 10, the voltage rises quickly at X/R of 0.5 particularly at very lower SCRs and thereby exceeds the acceptable limits, which is chosen as % $-5\% \sim +5\%$ in this paper. The result emphasises on the impact of the feeder X/R ratio and the associated effect on the voltage-quality even at relatively higher SCRs.

3.2 Active/reactive power constrains

To quantify the reactive power required to retain rated POC voltage for the entire range of delivered active power and network parameters, (17) is solved for Q_{t} which results in

$$Q_{\text{t}} = \frac{1}{R^2_{\text{eq}} + X^2_{\text{eq}}}\left(V^2_{\text{poc}}X_{\text{eq}} - \sqrt{B}\right) \tag{21}$$

where

$$B = V^2_{\text{poc}}\left(V^2_{\text{n}} + 2P_{\text{t}}R_{\text{eq}}\right)\left(R^2_{\text{eq}} + X^2_{\text{eq}}\right) - P^2_{\text{t}}\left(R^2_{\text{eq}} + X^2_{\text{eq}}\right)^2 - V^4_{\text{poc}}R^2_{\text{eq}} \tag{22}$$

Fig. 3*c* demonstrates the desired reactive power targeted at obtaining zero voltage deviation at the POC bus. It can be obviously seen that due to the DFIG capacity/stability limitations (discussed in Section 2), infeasible operation in the entire active power range is depicted in Fig. 3*c* either for consumption or injection aspects especially at very low SCR and X/R ratio. Although wind power curtailment can sustain system normal operation, significant power loss is consequent. In an attempt to address the aforementioned shortcomings and allow for higher wind power expansion, exogenous reactive power reinforcement is imperative.

3.3 Reactive power regulation

RPC is a key factor to maintain the voltage quality of weak grid-connected DFIG WT systems [20]. Nonetheless, the effectiveness of RPC varies according to the network

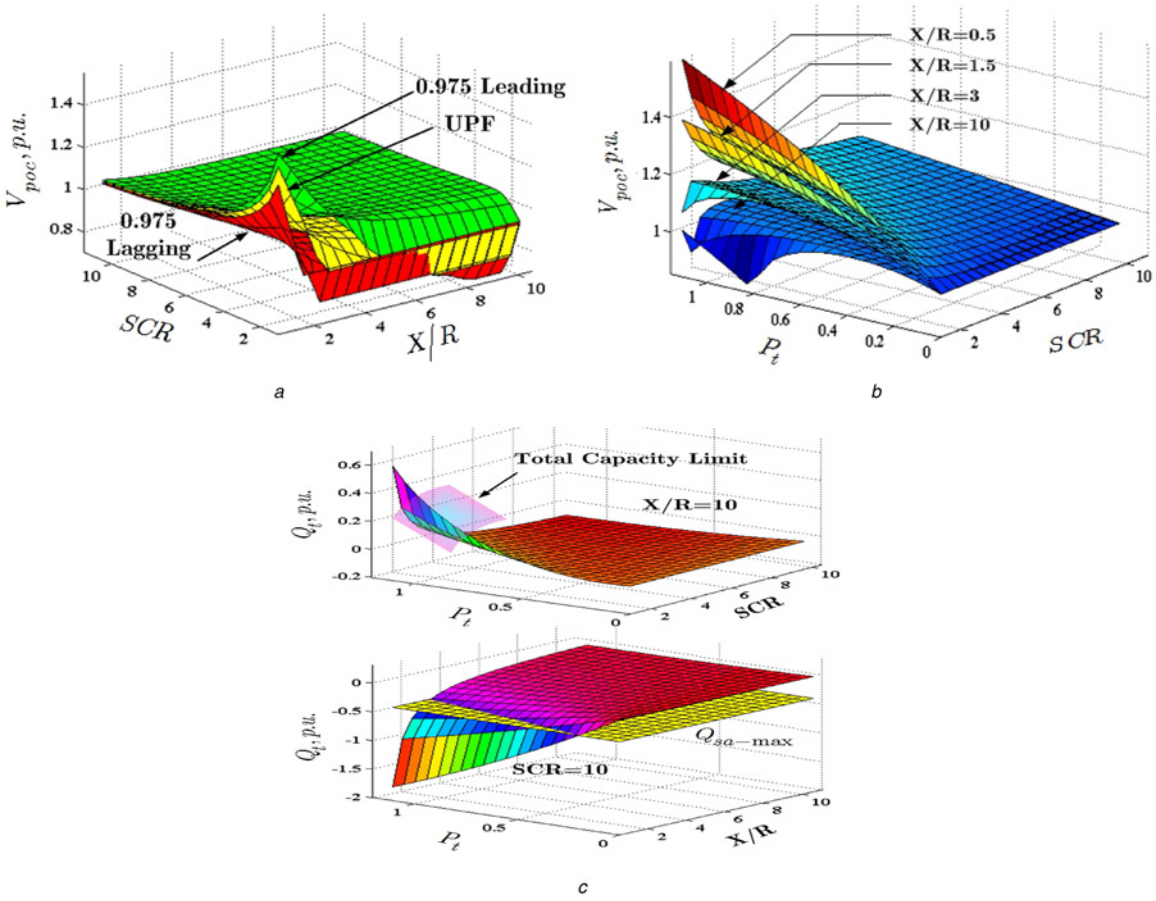

Fig. 3 *POC voltage behaviour in response to SCR and X/R ratio variations*

a POC voltage against grid parameters and power factor
b POC voltage response against in-feed wind power and grid parameters
c DFIG active/reactive power limitation due to SCR and X/R variation

characteristics. Equation (21) can be used to explore the in-feed reactive power desired for maintaining POC voltage deviation within the permissible levels $\Delta V_{\text{poc}} = \pm 5\%$, under various system strengths. The relevant results for the demanded reactive power are depicted in Figs. 4*a–f*. Generally speaking, reactive power dramatically varies with the magnitude of voltage deviation, SCR and X/R ranges. Moreover, the reactive power consumed/supplied via DFIG can be a cost-effective option to handle the POC voltage deviation at certain SCR and X/R ranges. Yet, at very low SCR and X/R ratios, the DFIG cannot be solely utilised to regulate the POC voltage due to the imposed reactive power operational limits. Furthermore, higher reactive power demand is requested to attain voltage constancy the higher the SCR. This is because Q_t is more sensitive to the voltage deviation at the higher SCR value which can be also recognised from (21).

Fig. 4*g* shows the sensitivity of Q_t to the voltage deviation versus ±5% POC voltage variation at different network parameters. The Q_t surface area is getting steeper, the higher the SCR with higher demand and the lower the X/R ratio 'resistive network'. Therewith, it is worth to mentioning that a network with higher SCR improbably evoke such significant voltage deviations [21]. Therefore, minimal reactive power can readily adjust the POC voltage at higher SCRs.

To sum up, significant voltage fluctuations are induced owing to weak networks with lower SCR and/or X/R ratio that WTs are connected to which impose remarkable limitation on effective integration of WT generated output power. Besides, wind speed variations worsen voltage fluctuations which entails accurate VC to constantly regulate voltage waveform to address the aforementioned shortcomings which is presented in the next section.

4 Proposed adaptive voltage control strategy

This section focuses on the basic DFIG WT control scheme and elaborates the proposed AVC strategy for the mitigation of the POC voltage disturbances.

4.1 DFIG vector control

Vector control techniques have been extensively studied for grid-connected DFIG WT systems. Two respective control schemes are employed for the control of the back-to-back converters as shown in Fig. 5. In order to achieve independent control of the exchanged active and reactive power between the GSC and the grid, the converter controller (Fig. 5*a*) is operated in a synchronously rotating reference frame with the *d*-axis aligned with the grid voltage. The vector control of the GSC is dedicated to ensure a constant dc-link voltage irrespective of the transmitted power magnitude or direction and meanwhile provides sinusoidal currents [6]. In addition, controls the reactive power exchange Q_g between the converter and the grid side through adjusting $Q_{\text{g-ref}}$ to attain UPF or support the voltage during contingencies [13]. The objective of the RSC vector control is to provide the DFIG with a variable speed operation with decoupled control of stator side active and reactive powers. Likewise, to attain independent control of electromagnetic and rotor excitation current components, the DFIG is controlled in a stator flux oriented reference frame where its *d*-axis is aligned with the stator flux vector. The RSC control scheme is depicted in Fig. 5*b*. The reference stator active power $P_{\text{s-ref}}$ is normally derived from the rotor speed controller. The DFIG reference rotor speed $\omega_{\text{r-ref}}$ is processed via a lookup table in

IET Renew. Power Gener., 2016, Vol. 10, Iss. 2, pp. 238–249

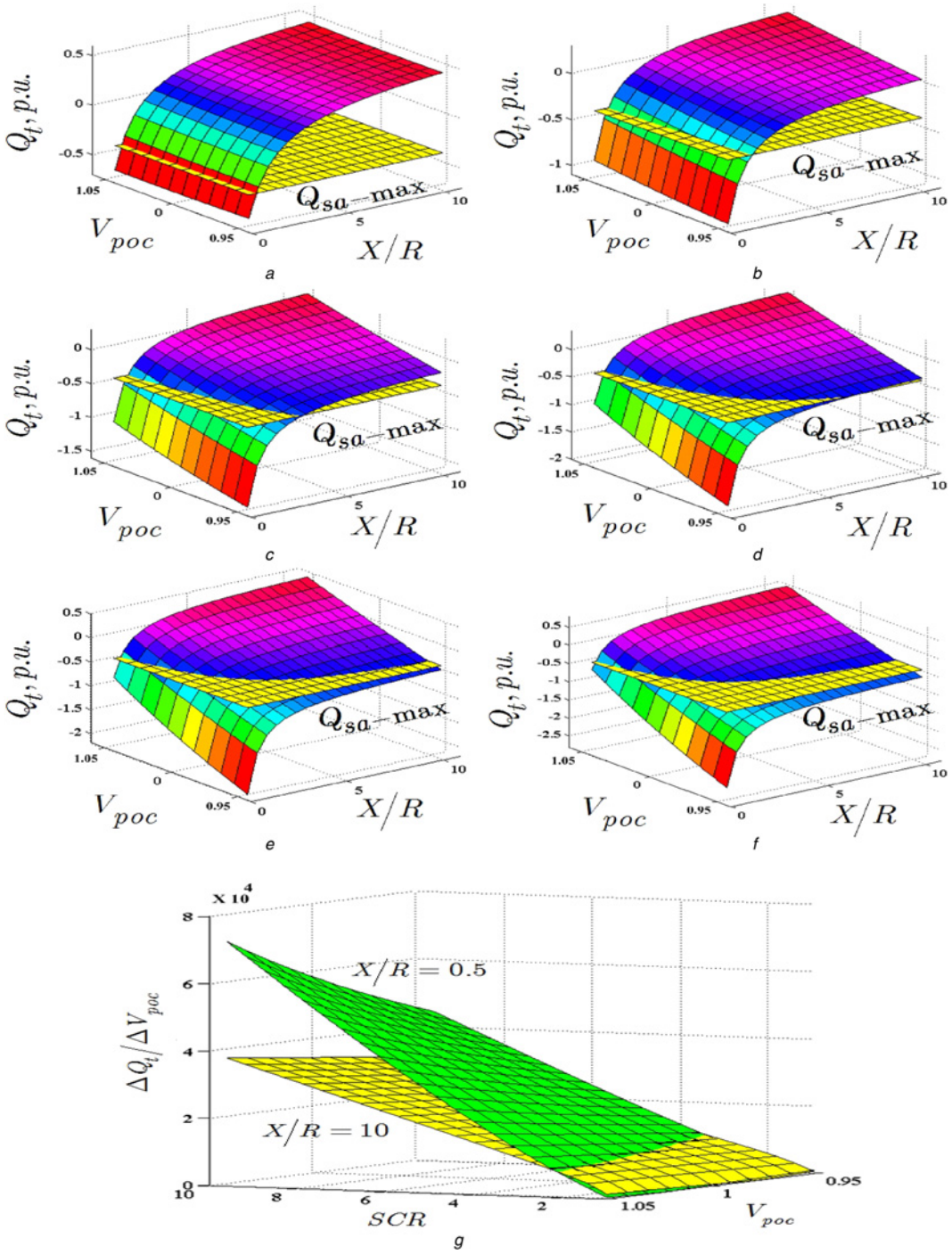

Fig. 4 *Reactive power regulation for ±5% POC voltage deviation SCR = 1*

b SCR = 2
c SCR = 4
d SCR = 6
e SCR = 8
f SCR = 10
g Sensitivity of Q_t for ±5% POC voltage deviation

order to ensure the optimal tip speed ratio λ_{opt}. Normally, grid-side and stator side reactive power set-points $Q_{g\text{-ref}}$, , $Q_{s\text{-ref}}$ are fixed to zero to achieve UPF operation. However, in this paper these reference values are dispatched through the proposed AVC scheme to continually regulate the POC voltage.

4.2 Adaptive voltage control AVC

In contrast to the operating point, variation of network parameters can adversely impact system dynamics. Few papers address VC issue of WTs attached to weak networks with remarkably changing parameters. More specifically, Strachan *et al.* in [5] conducted an analytical eigenvalues stability study for a VSWT, with back-to-back full power converter attached to a weak network. Additionally, VC with modified fixed open-loop gain was suggested to improve the system stability under lower SCRs. Despite the modified control showed enhanced voltage response for lower SCR (10–4), system robustness to further network parameters deteriorated. Besides, the impact of variable X/R ratio was not investigated.

As a continuation of the work of Strachan and Jovcic [5], a proposed AVC approach reliant on operating condition and

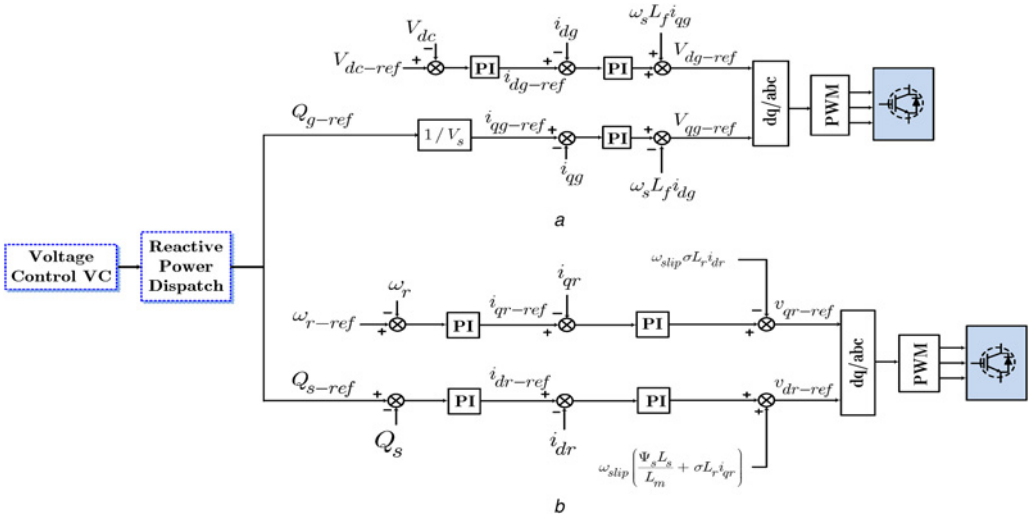

Fig. 5 *DFIG converters controllers*

a GSC controller
b RSC controller

network parameters is implemented in this paper. Although AVC is a pure control method which will not increase the system cost compared with conventional control techniques, however, its technical performance is superior. The latter can be attributed to the fact that AVC can adjust controller performance according to the grid strength and WT output power which assures keeping the POC voltage within allowable limits especially during very weak conditions. The proposed AVC scheme is demonstrated in Fig. 6*a*. The reference reactive power demand $Q_{\text{t-ref}}$ is derived via the deviation from a reference voltage set-point $V_{\text{poc-ref}}$. Basically, the priority of the RPC is devoted to the DFIG Q_{s} followed by the GSC contribution Q_{g} when Q_{s} attains the operational limit. Furthermore, the DFIG Q_{s} and GSC Q_{g} are dispatched according to $Q_{\text{t-ref}}$ and the DFIG capacity limit which will be discussed later. The system parameters are assumed to be measurable. The reactive power distribution of the whole DFIG system with the over-sized GSC under entire range of network parameters is explored here. Moreover, the significance of the proposed AVC under variable wind speed is also presented.

To increase the system stability and enhance the VC performance especially for very weak conditions, the open-loop gain k_{s} will be constantly adjusted in order to optimise the VC. To ensure that the overall system performance is compromised for the typical range of network parameters, the rewarded AVC would mimic the latent behaviour of the system.

The AVC open-loop gain k_{s} would thus be scheduled according to the formula

$$k_{\text{s}} = k_0 \sqrt{P_{\text{t}} \left(\frac{X_{\text{eq}}}{R_{\text{eq}}} + \frac{R_{\text{eq}}}{X_{\text{eq}}} \right)} (\text{pu}) \tag{23}$$

where k_0 is a design factor which can be selected to optimise the AVC. The significance of the selected adaptive gain k_{s} formula can be inferred from (18), (19) where the VC can be reluctant to the change of the system variants, that is P_{t}, R_{eq}, X_{eq} (which significantly affect the performance of the VC) through adjusting the reference compensated reactive power Q_{t} in such a way to minimise the impacts of the terms $P_{\text{t}}R_{\text{eq}} + Q_{\text{t}}X_{\text{eq}}$, $P_{\text{t}}X_{\text{eq}} - Q_{\text{t}}R_{\text{eq}}$ for the entire range of network parameters so that the level of POC voltage variation is minimised, viz.

$$A \simeq 0.5V_{\text{n}}^2 \text{ and } V_{\text{poc}} \simeq V_{\text{n}} \tag{24}$$

In this sense, the reactive power set-point $Q_{\text{t-ref}}$ constantly responds according to these variations to smooth the POC voltage under all conceivable operating conditions. To further increase the system robustness against system parameters change, a differential gain k_{d} is adaptively designed as

$$k_{\text{d}} = k\, k_{\text{s}} \tag{25}$$

where k is a design factor. Additionally, the differential term includes filtering in order to suppress high-frequency noise extension [5].

4.3 Reactive power dispatch

A proposed reactive power dispatch strategy to manage reactive power coordination between the DFIG Q_{s} and the GSC Q_{g} is illustrated in the flowchart shown in Fig. 6*b*. Have the POC voltage deviated from the reference set-point; the VC correspondingly adapts the reactive power $Q_{\text{t-ref}}$ to regulate the voltage. This reactive power is compensated through the DFIG Q_{s} which is processed via the RSC Q-control as long as it lies within DFIG reactive power capacity, that is $Q_{sa\text{-max}} \leq Q_{\text{t-ref}} \leq Q_{\text{sg-max}}$. On the other hand, if the POC voltage overtakes the allowable margins % $-5\% \sim +5\%$ and meanwhile $Q_{\text{t-ref}}$ exceeds the DFIG Q_{s} limits identified in Section 2, the excess reactive power is dictated by the GSC Q_{g} while the DFIG Q_{s} is accordingly set to the maximum absorption or injection capacity, $Q_{sa\text{-max}}$, $Q_{\text{sg-max}}$, respectively, to benefit the DFIG reactive power and optimise the GSC size.

To verify the effectiveness of the adaptive control terms embedded in the AVC scheme, the system of Fig. 1*a* is simulated at a very weak grid condition, that is SCR of 1 and X/R of 0.5 with sporadically wind speed profile. A 10 m/s average wind speed with 0.1 turbulence intensity is used here which is the highest one given by WT manufacturer International Electrotechnical Commission (IEC) flicker test [8]. The 3p oscillation model of [6] is also employed. As the WT rotational speed varies, the 3p oscillations frequency would correspondingly change. Fig. 7 shows the POC voltage response under three distinct control aspects, 'CVC' for conventional (PI) VC, 'AVC-WOD' for adaptive VC without differential (WOD) term (k_{s} only) while 'AVC' signifies adaptive VC (k_{s}, k_{d}).

Compared with conventional voltage control (CVC), the AVC scheme with two adaptive parts effectively alleviates the POC voltage fluctuations particularly at higher wind speed conditions (higher WT output power). Moreover, for low to moderate wind speeds, the AVC satisfactorily suppresses 3p voltage oscillations. Furthermore, the adaptive differential term contributes to further damped performance.

IET Renew. Power Gener., 2016, Vol. 10, Iss. 2, pp. 238–249

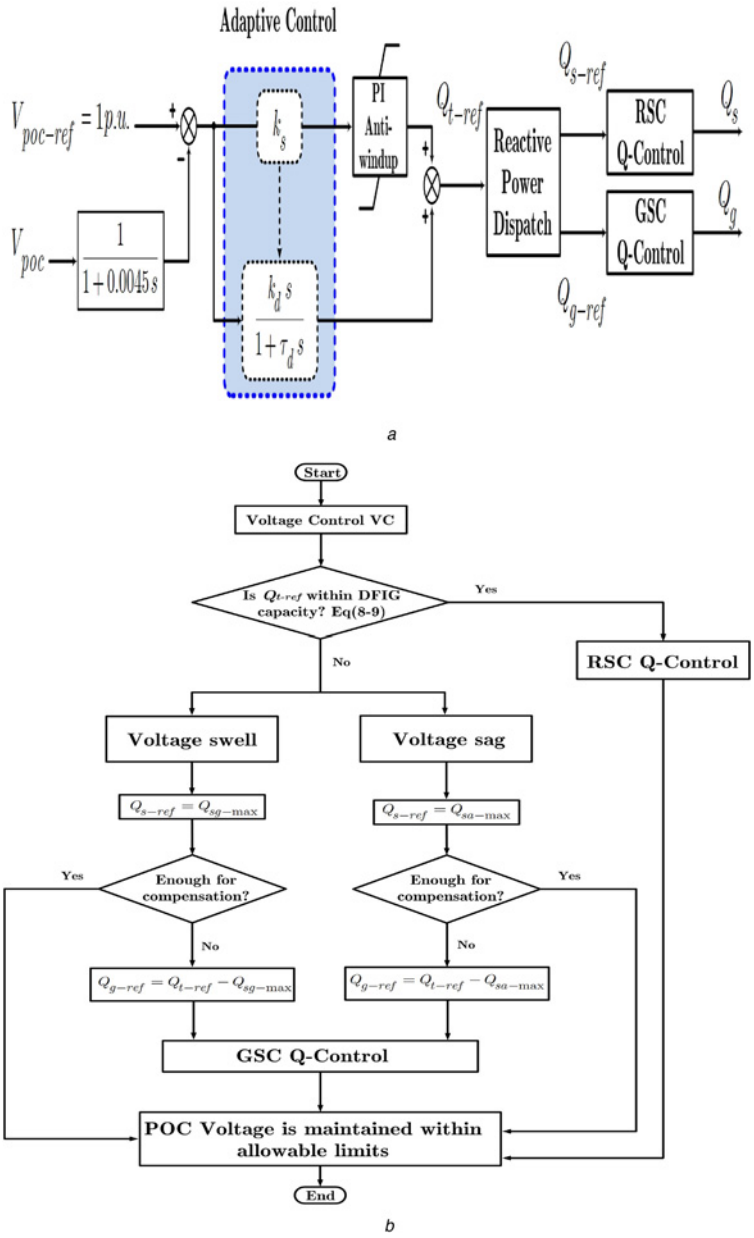

Fig. 6 *Proposed adaptive voltage control and reactive power dispatch strategy to manage reactive power coordination*

a Proposed AVC control strategy
b Flowchart for reactive power dispatch

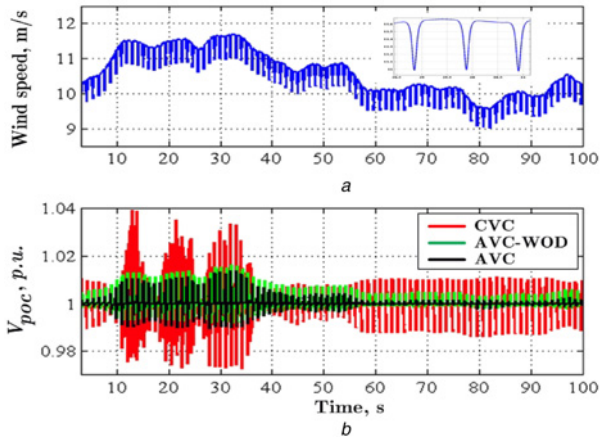

Fig. 7 *POC voltage response under three distinct control aspects*

a Wind speed
b POC voltage with and without AVC

5 Simulation results and discussions

5.1 Effectiveness of AVC strategy

To verify the significance and robustness of the proposed AVC, a detailed system model in MATLAB/SIMULINK software environment is implemented while the test system is examined at wide range of SCR and X/R variations. The hardware specifications of the computer used to conduct the study is Intel (*R*) Xeon (*R*) CPU E5–2650 v2@2.6 GHz with 64 GB installed memory. The 2 MW DFIG WT test system parameters are listed in appendix 1. Fig. 8*a* illustrates a long-term system response to a very weak grid condition which corresponds to SCR of 1 and X/R of 0.5. As it shows, POC voltage fluctuations are induced due to higher network impedance, wind speed variations and also 3p oscillations. Consequently, higher reactive power absorption Q_t is required in this case to compensate the voltage as seen in Fig. 8*a*. Being over the DFIG Q_s capacity, Q_t can be fully compensated by virtue of an over-sized GSC which can absorb a maximum Q_g of 0.17 pu to regulate the voltage while the DFIG Q_s is attaining the

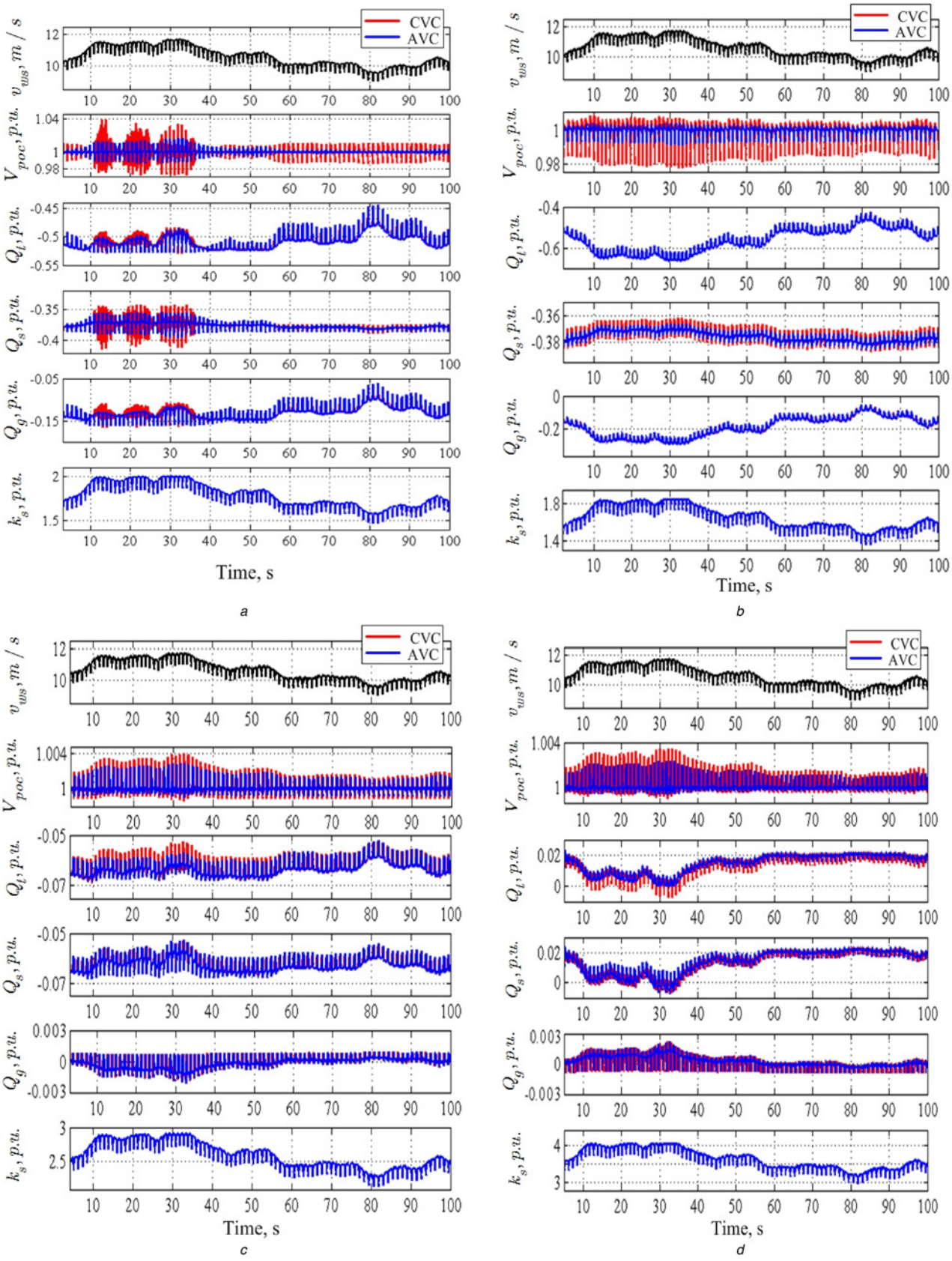

Fig. 8 *Long-term view of system response*

a SCR = 1, X/R = 0.5
b SCR = 2, X/R = 0.7
c SCR = 7, X/R = 5
d SCR = X/R = 10

IET Renew. Power Gener., 2016, Vol. 10, Iss. 2, pp. 238–249

maximum permissible absorption capacity $Q_{sa\text{-}max}$ defined by (10). Normally, GSC is rated at 25% of the DFIG rated power (0.5 MVA). Yet, 6% overrated GSC (0.53 MVA rating) is adequate in this case to drive the POC voltage within safe limits.

Being acting on minifying the impact of system variants change to counteract voltage variations, the AVC scheme causes minimal voltage oscillations with better damped performance compared with CVC as depicted in Fig. 8*a* particularly for high-wind speed due to high-WT output power which contributes to higher voltage fluctuations. The significant CVC oscillations are accordingly reflected on the system reactive power as depicted from Q_t, Q_s and Q_g waveforms. Besides, the system is examined at another weak network condition with SCR of 2 and X/R of 0.7 and the relevant results are demonstrated in Fig. 8*b*. As mentioned before in Section 3, the demanded reactive power Q_t becomes more sensitive to the voltage deviation the higher the SCR (see Fig. 4*g*). Therefore, $Q_t = 0.63$ pu is essential to adjust the voltage which is beyond the DFIG Q_s capability. Hence, a GSC with $Q_g = 0.26$ pu (0.66 MVA rating) can absorb the deficit reactive power, as seen in Fig. 8*b*. Moreover, the AVC provides higher voltage fluctuation mitigation capability which is also reflected on the DFIG Q_s signal as seen in the depicted figure. Fig. 8*c* shows the system response for SCR of 7 and X/R of 5. As the network features an inductive characteristic (higher X/R), less amount of reactive power can regulate the voltage which can be fully dictated by the DFIG Q_s.

Compared with the former case, the system requires less Q_t in case of SCR and X/R of 10 (relatively strong network) as depicted in Fig. 8*d*. In this manner, DFIG releases $Q_s = 0.022$ pu to ensure voltage constancy. Despite, the relatively strong network conditions (Figs. 8*c*,*d*), the AVC preserves satisfactory performance and enhanced POC voltage profile.

5.2 Safe operation zones

To further evaluate the effectiveness of the proposed AVC strategy, the safe operation zones are investigated under various conditions, as shown in Fig. 9*a*. The safe operation zones are examined under variable wind speed profile as such in Fig. 7*a*. Furthermore, the examination is carried out for the entire range of SCR and X/R variations. Note that the safe regions are shown only for X/R from 0.5 to 1.0 which denotes the worst conditions whilst, the study has been carried out for the X/R range from 0.5 to 10. In the shown figures, the white-coloured regions refer to scenarios with safe operation, that is the POC voltage is maintained within acceptable limits, ±5% while the grey-coloured ones signify the voltage violation scenarios.

The obtained results are carried out by executing numerous simulations to the system of Fig. 1*a* using the proposed AVC strategy. Besides, for the shown figure, the adopted X/R ratio step change is 0.1. As it shows, at a given SCR, the operation regions

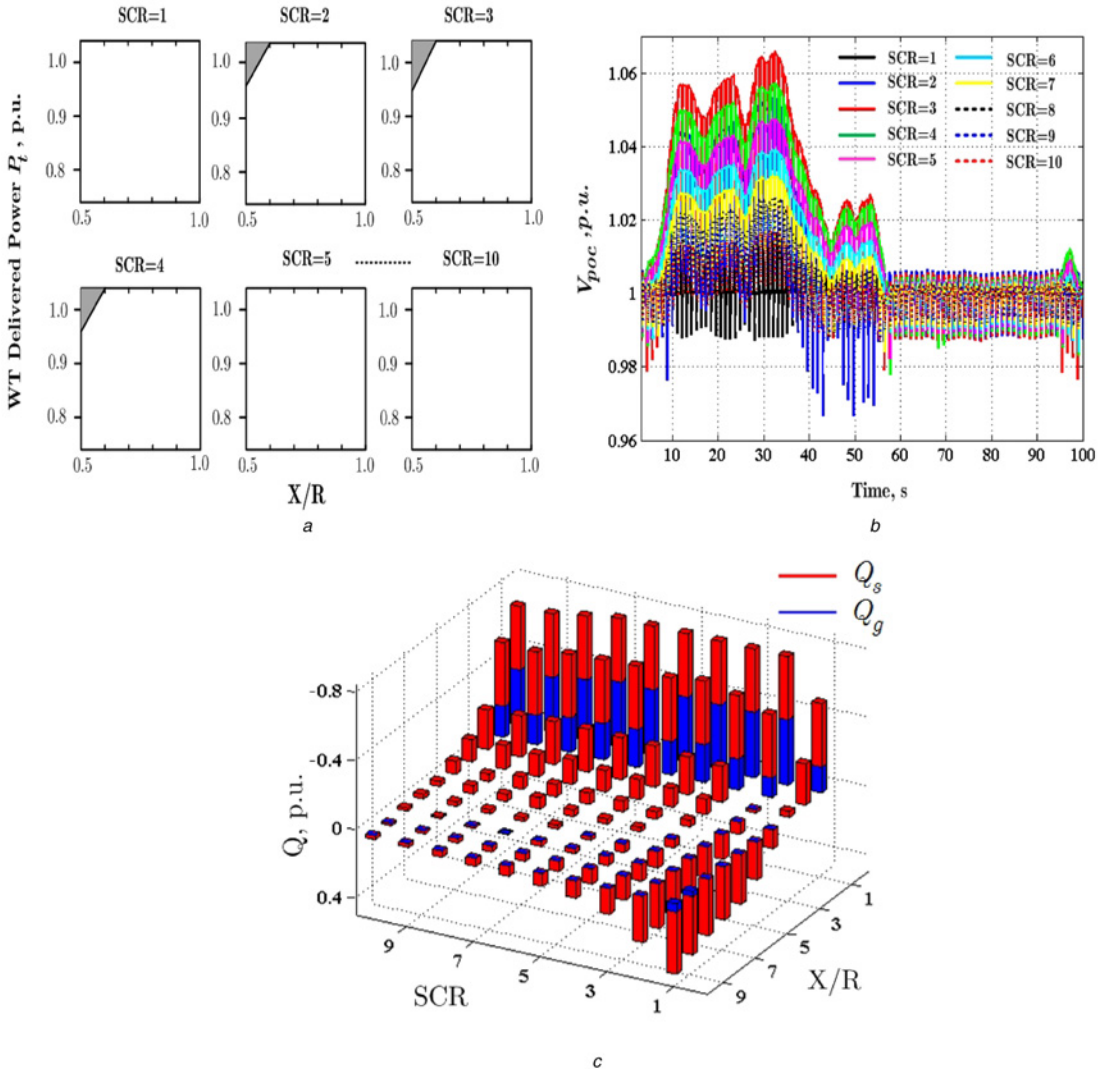

Fig. 9 *Safe operation zones are investigated under various conditions*

a Safe operation zones for the entire range of network parameters
b POC voltage response with the eventual GSC rating for X/R of 0.5
c Reactive power contribution of the DFIG and GSC for the entire range of network parameters

Table 1 Maximum detected POC voltage

SCR	2	3	4	5
V_{max}, pu	1.054	1.066	1.057	1.048

incur insecure areas particularly at very low X/R ratio and higher output power. This is because the higher output power provoke larger voltage deviations which makes the demanded reactive power more vulnerable to the voltage variations especially at very low X/R ratios. It is worth to mentioning that the GSC is additionally overrated to $Q_g = 0.38$ pu (0.86 MVA rating) to tackle the voltage swell for the entire range of SCR with the lowest X/R ratio of 0.5. Subsequently, the POC voltage profile associated with this investigation with the eventual GSC rating is demonstrated in Fig. 9*b*. At SCR = 1 'high-network impedance', a significant reactive power drawn by the WT ensures safe operation. However, due to the system sensitivity to higher SCRs, the voltage exceeds the allowable margin for $2 \leq SCR \leq 4$ as a result of the DFIG and GSC reactive power limitation with maximum voltage detected of 1.066 pu at SCR of 3. Furthermore, the voltage swell decreases again with higher SCR 'lower impedance' as the network with higher SCR is unlikely cause larger voltage perturbations. Therefore, for $SCR \geq 5$ even with X/R = 0.5, safe operation is ensured. The corresponding maximum voltage values are tabulated in Table 1.

5.3 Reactive power sharing

To demonstrate the actual reactive power demand to regulate the voltage for the entire range of network parameters and also sharing among the DFIG Q_s and the GSC Q_g with the AVC scheme, Fig. 9*c* is presented. The figure depicts the maximum reactive power dictated by Q_s and/or Q_g to compensate the voltage in response to the reactive power dispatch under different network parameters and wind speed. The results conform to that in Fig. 4 of the analytical study, as larger reactive power is essential to compensate the voltage at very low X/R ratios which necessitates additional GSC Q_g contribution. Except for some specific conditions such as very low X/R ratios (0.5 to 1), the DFIG can effectively regulate the voltage with the inherent reactive power. Accordingly, the GSC effectively manipulates the reactive power deficit at very low X/R ratios to maintain the voltage as can be seen from the figure.

6 Conclusions

This paper presents an AVC strategy for a DFIG VSWT connected to widely varying weak network parameters. As a basis of investigation, an equivalent system model is utilised to realise the voltage and active/reactive power constraints raised by integration of a wind generator to a weak host network. The associated interactions between the wind generator and the host network under different network strengths are presented. Intensive simulation case studies have been carried out to verify the effectiveness of the proposed AVC scheme. The AVC strategy showed pronounced mitigation capability with better damped performance particularly at very weak grid condition.

7 References

1 Lo, S., Wu, C.: 'Evaluating the performance of wind farms in China: an empirical review', *Electr. Power Energy Syst.*, 2015, **69**, (1), pp. 58–66
2 Ejdemo, T., Söderholm, P.: 'Wind power, regional development and benefit-sharing: the case of Northern Sweden', *Renew. Sustain. Energy Rev.*, 2015, **47**, (7), pp. 476–485
3 Mokryani, G., Siano, P., Piccolo, A., *et al.*: 'Improving fault ride-through capability of variable speed wind turbines in distribution networks', *IEEE Syst. J.*, 2013, **7**, (4), pp. 713–722
4 Zhao, Z., Yan, H., Zuo, J., *et al.*: 'A critical review of factors affecting the wind power generation industry in China', *Renew. Sustain. Energy Rev.*, 2013, **19**, (7), pp. 499–508
5 Strachan, N.P.W., Jovcic, D.: 'Stability of a variable-speed permanent magnet wind generator with weak AC grids', *IEEE Trans. Power Deliv.*, 2010, **25**, (4), pp. 2779–2788
6 Hu, W., Chen, Z., Wang, Y., *et al.*: 'Flicker mitigation by active power control of variable-speed wind turbines with full-scale back-to-back power converters', *IEEE Trans. Energy Convers.*, 2009, **24**, (3), pp. 640–649
7 Zhang, Y., Chen, Z., Hu, W., *et al.* 'Flicker mitigation by individual pitch control of variable speed wind turbines with DFIG', *IEEE Trans. Energy Convers.*, 2014, **29**, (1), pp. 20–28
8 Ammar, M., Joos, G.: 'Impact of distributed wind generators reactive power behavior on flicker severity', *IEEE Trans. Energy Convers.*, 2013, **28**, (2), pp. 425–433
9 Zhang, Y., Hu, W., Chen, Z., *et al.*: 'Flicker mitigation strategy for a doubly fed induction generator by torque control', *IET Renew. Power Gener.*, 2014, **8**, (2), pp. 91–99
10 Chen, X., Kang, C., O'Malley, M., *et al.*: 'Increasing the flexibility of combined heat and power for wind power integration in china: modeling and implications', *IEEE Trans. Power Syst.*, 2015, **30**, (4), pp. 1848–1857
11 Strategy Plan Energinet.dk, 2012, Available at: http://www.energinet.dk/SiteCollectionDocuments/Engelske%20dokumenter/Om%20os/Strategy%20Plan%202012.pdf
12 Kayıkcı, M., Milanovic, J.V.: 'Reactive power control strategies for DFIG-based plants', *IEEE Trans. Energy Convers.*, 2007, **22**, (2), pp. 389–396
13 Yang, L., Xu, Z., Østergaard, J., *et al.*: 'Advanced control strategy of DFIG wind turbines for power system fault ride through', *IEEE Trans. Power Syst.*, 2012, **27**, (2), pp. 713–722
14 Montilla-DJesus, M.E., Santos-Martin, D., Arnaltes, S., *et al.*: 'Optimal operation of offshore wind farms with line-commutated HVDC link connection', *IEEE Trans. Energy Convers.*, 2010, **25**, (2), pp. 504513–504528
15 Mohseni, M., Islam, S.M.: 'Review of international grid codes for wind power integration: diversity, technology and a case for global standard', *Renew. Sustain. Energy Rev.*, 2012, **16**, (6), pp. 3876–3890
16 Girbau-Llistuella, F., Sumper, A., Díaz-González, F., *et al.*: 'Flicker mitigation by reactive power control in wind farm with doubly fed induction generators', *Electr. Power Energy Syst.*, 2014, **55**, (1), pp. 285–296
17 Tande, J.O., Di Marzio, G., Uhlen, K.: 'System requirements for wind power plants', SINTEF energy res., 2007. Available at: http://www.sintef.no/upload/ENERGI/pdf/Vind/TR%20A6586.pdf
18 European Standard. EN 50160, voltage characteristics of electricity supplied by public electricity networks; 2011
19 Energinet. Technical regulation 3.2.5 for wind power plants with a power output greater than 11 kW; September 2010. Available at: http://www.energinet.dk
20 Han, C., Huang, A.Q., Baran, M.E., *et al.*: 'STATCOM impact study on the integration of a large wind farm into a weak loop power system', *IEEE Trans. Energy Convers.*, 2008, **23**, (1), pp. 226–133
21 Olav, J., Tande, G.: 'Exploitation of wind-energy resources in proximity to weak electric grids', *Appl. Energy*, 2000, **65**, (1–4), pp. 395–401

8 Appendices

8.1 Appendix 1

See Table 2.

Table 2 Parameters of the DFIG VSWT

Parameter	Value
rated power	2 MW
rated voltage	0.69 kV
rated frequency	50 Hz
stator resistance	0.00488 pu
stator leakage inductance	0.1656 pu
rotor resistance	0.00549 pu
rotor leakage inductance	0.1763 pu
magnetising inductance	3.9257 pu
number of pole pairs	2
lumped inertia constant	4.5 s
gear box ratio	87
rated DC-link voltage	1200 V
DC-link capacitor	16,000 μF
rotor hub elevation	80 m
WT rotor radius	40 m
wind shear empirical component (α)	0.3
tower radius (a)	2 m
distance from the blade origin to the tower midline (x)	5 m
turbulence intensity	10%
transformer rated power	2.5 MVA
primary winding rated voltage	11 kV
secondary winding rated voltage	0.69 kV
short circuit impedance	0.0033 + j0.039 pu

8.2 Appendix 2: derivation of POC voltage equation

The voltage V_{poc} is defined as

$$V_{\text{poc}} = \left|V_{\text{poc}}\right| e^{j\varphi} \tag{26}$$

Substituting (26) into (15) results in

$$\left|V_{\text{poc}}\right|^2 = \left|V_{\text{poc}}\right| V_{\text{n}} \cos\varphi + P_{\text{t}} R_{\text{eq}} + Q_{\text{t}} X_{\text{eq}} + j\left(P_{\text{t}} X_{\text{eq}} - Q_{\text{t}} R_{\text{eq}} - \left|V_{\text{poc}}\right| V \sin\varphi\right) \tag{27}$$

As the LHS of (27) is real, it follows that the R.H.S is also real which yields

$$P_{\text{t}} X_{\text{eq}} - Q_{\text{t}} R_{\text{eq}} - \left|V_{\text{poc}}\right| V \sin\varphi = 0 \tag{28}$$

From (28), and using trigonometric identity, we obtain

$$\left|V_{\text{poc}}\right| V_{\text{n}} \cos\varphi = \sqrt{\left(\left|V_{\text{poc}}\right| V_{\text{n}}\right)^2 - \left(P_{\text{t}} X_{\text{eq}} - Q_{\text{t}} R_{\text{eq}}\right)^2} \tag{29}$$

By combining (27) and (29), (13) can be derived.

ISSN (online): 2246-1248
ISBN (online): 978-87-7112-708-9

AALBORG UNIVERSITY PRESS